



Numerical Studies of Longitudinal Dispersion in Duct-Flows

Mohammad Mahmudur Rahman

A thesis submitted in fulfilment of the requirements for the degree of

Doctor of Philosophy

Centre for Environmental Safety and Risk Engineering

College of Engineering and Science

Victoria University

August 2016

Dedicated to my elder brother, MD RAHMAT ULLAH RUMI

The one has inspired me throughout my higher study period

DECLARATION

I, *Mohammad Mahmudur Rahman*, declare that the PhD thesis entitled “Numerical Studies of Longitudinal Dispersion in Duct-Flows” is no more than 100,000 words in length including quotes and exclusive of tables, figures, appendices, bibliography, references and footnotes. This thesis contains no material that has been submitted previously, in whole or in part, for the award of any other academic degree or diploma. Except where otherwise indicated, this thesis is my own work.

Signed: 

Date: 31/08/2016

Mohammad Mahmudur Rahman

Melbourne, Australia

Acknowledgements

At first I would like to thank the Almighty Allah for granting me the ability to complete my PhD Studies.

After that I would like to express my sincere and heartiest gratitude to the person who have been supporting, encouraging guiding towards this last stage of my PhD study. He is my principal supervisor- Professor Graham Thorpe, College of Engineering and Science, Victoria University. It could not be possible for me to reach at this stage today without the motivation, advice and inspiration from him. His intellectual support enabled me to sharpen my skills and to become an independent researcher. It was a great opportunity and experience to work with him. I look forward to be nourished from his magnanimous affiliation and collaboration in future.

I am extremely grateful to Associate Professor Khalid Moinuddin, Centre for Environmental Safety and Risk Engineering, Victoria University who had been directing me in my project as associate supervisor. I had received uncountable valuable feedback and suggestions regarding my project as well as my writing during the entire tenure. It had been a great feeling to work with him and would like to carry on this experience in future.

I would like to acknowledge the financial support from College of Engineering and Science, Victoria University through Victoria University Post Graduate Research Award. My gratitude also goes to Prof. Chris Perera, Dean College of Engineering and Science for his kind support and understanding. Special thanks to Elizabeth Smith from Graduate Research Centre for her continuous support throughout this journey.

I would like to thank support staff from Edward HPC in Melbourne University for their cooperation during early years.

Special thanks to my friends and colleagues both in College of Engineering and Science and CESARE. The support, inspiration and direction from Iqbal Mahmud, Mahfuz Sarwar, Kamal Uddin, Andrew Antiohos, and Prasad Inamdar are always memorable. Very special thanks to Mohammad Abul Monsur for his continuous support from every perspectives since the very early days that I came to Australia. His support can never be forgotten.

I am deeply grateful to my beloved parents who have been consistently supporting me emotionally throughout my entire life. The love and affection of my siblings can never be compensated.

Last but not least, I would like to express my deepest appreciation and love to my dear wife and beloved daughter. Their support and smile kept me moving through this expedition to accomplish my degree.

Abstract

The dispersion of solutes in fluid flows is ubiquitous in natural as well as in many manufactured systems. Detailed analyses of the distribution of solutes in fluid flow help us to quantify the performance of chemical reactors, water networks, pollutant dispersion in channels and rivers and so on. This thesis presents numerical studies of solute dispersion in laminar and turbulent flows.

Numerical solutions are inherently approximations of the continuous governing equations and they are often confounded by artificial diffusion. This is a matter of concern, particularly when the objective of the solution is to quantify dispersion. With a view to this, we have developed higher order differencing schemes to quantify the solute dispersion in laminar flow through circular and rectangular ducts. Based on the one-dimensional Quadratic Upwind Interpolation for Convective Kinematics with Estimated Streaming Terms (QUICKEST) scheme, a modified QUICKEST scheme has been developed to accurately solve the problem of three-dimensional solute dispersion. The modified model has been validated against published experimental results and analytical solutions in flows in both circular and rectangular ducts.

Furthermore, a three point Compact Combined Difference (CCD) scheme has been developed to solve the hydrodynamics dispersion in three - dimensions. The unconditionally stable sixth order spatially accurate and second order temporally accurate scheme is found to be extremely promising for estimating longitudinal dispersion coefficients, particularly when the concern is to avoid false diffusion arising from the scheme. Finally, an investigation of the source of secondary flows in turbulent flows through square ducts is reported. These secondary flows play a significant role in the dispersion process in turbulent flow. The schemes developed in this research are anticipated to provide powerful tools for engineers and scientists so that they might obviate the deleterious effects of numerical dispersion and analyse a wide range of fluid flow systems.

Contents

1	Introduction	1
1.1	Introduction	1
1.2	Research Objective	3
1.3	Thesis Contribution	4
1.4	Structure of the Thesis	5
2	Laminar Dispersion in Pipe-flow	7
2.1	Introduction	7
2.2	Literature Review	10
2.2.1	Analytical and Experimental Observations	10
2.2.2	Numerical Approaches	14
2.3	Mathematical Formulation	21
2.4	Numerical Solution	23
2.4.1	Solution Domain and Grid Generation	24
2.4.2	Discretization Scheme	25
2.4.3	QUICKEST Scheme for Laminar Dispersion in Pipes	26
2.4.4	Calculation of the Dispersion Coefficient	39
2.4.5	Grid Sensitivity Analysis	40
2.5	Results	44
2.5.1	Validation	44
2.5.2	Evolution of Concentration Profiles for Small Times	46
2.6	Relative Effect of Convection to Diffusion in Mass Transport	47
2.6.1	Convection Dominated Flows: - High Peclet Number	48

2.6.2	Diffusion Dominated Flows: - Low Peclet Number	49
2.7	Summary and Conclusions	52
3	Dispersion in Laminar Flow through Rectangular Ducts	55
3.1	Introduction	55
3.2	Modified-QUICKEST Scheme	59
3.2.1	Development of the Scheme	60
3.3	Stability Analysis	68
3.4	Numerical Example	76
3.5	Estimating Dispersion Using a Modified QUICKEST Scheme	79
3.5.1	Velocity Profile	79
3.5.2	Grid Sensitivity Analysis	80
3.5.3	Validation of the Model	83
3.6	Results	83
3.6.1	Evolution of Mean Concentration Profile	83
3.6.2	Comparison of Spreading in Square and Circular Ducts	87
3.6.3	Effect of Peclet Number	87
3.6.4	Rate of Dispersion	90
3.7	Conclusions	91
4	A High Order Combined Compact Differencing Scheme to Estimate the Hydrodynamic Dispersion Rate in Laminar Flow through Non- Circular Ducts	93
4.1	Introduction	93
4.2	Three point CCD Scheme	98
4.2.1	One Dimensional Case	98
4.2.2	CCD-ADI Method to Solve a Two-Dimensional Problem	102
4.2.3	CCD-ADI Method in Three Dimensional Case	107
4.3	Stability Analysis	109
4.4	Numerical Experiments	116
4.4.1	Two Dimensional Case	116

4.4.2	Three Dimensional Case	117
4.5	Shear Flow Dispersion in a Rectangular Duct Using the CCD-ADI Scheme	119
4.5.1	Grid Sensitivity Analysis	122
4.5.1.1	Lateral grid independence	124
4.5.1.2	Axial grid independence study	125
4.5.1.3	Temporal grid independence study	127
4.5.2	CCD Scheme in Calculating Solute Spreading	128
4.6	Summary and Conclusions	129
5	Dispersion of a Solute in Turbulent Flow through Circular Pipes	131
5.1	Background	131
5.2	Turbulence	132
5.3	Mathematical Formulation of Turbulence	133
5.4	The Turbulent Advection Diffusion Equation	135
5.5	Modelling the Flow Field	137
5.6	Previous work on Dispersion in Turbulent Flow through Pipes	144
5.7	Simulation of the Turbulent Flow Field in Circular Pipes	146
5.7.1	Grid Sensitivity Analysis	147
5.7.2	Velocity Profile	149
5.8	Modelling Dispersion	151
5.8.1	Analytical Approach	151
5.8.2	Numerical Approach	157
5.8.3	Concentration Profile	159
5.8.4	Dispersion Coefficient	160
5.9	Summary and Conclusions	161
6	A Critical Review of Turbulent Flow in Non-circular Ducts: An Examination of Secondary Flows and Some New Numerical Results	163
6.1	Introduction	163
6.2	Mathematical Formulation of Flow System	165

6.2.1	Reynolds Averaged Navier-Stokes Equation	166
6.2.2	Vorticity Equation	168
6.2.3	Reynolds Stress Transport Equations	171
6.3	Experimental Studies	174
6.4	Numerical Calculations	181
6.4.1	Linear Eddy Viscosity Models	183
6.4.2	Algebraic Stress Models (ASM)	184
6.4.3	Non-Linear Eddy Viscosity Models (NLEVM)	194
6.4.4	Large Eddy Simulation	199
6.4.5	Mathematical Formulation of Turbulence	199
6.4.6	Direct Numerical Simulation	203
6.5	Performance of Various Turbulence Model to Predict Secondary Flow in Square Ducts	208
6.5.1	Flow Regime	209
6.5.2	Outlet Velocity Contours	211
6.5.3	Secondary Flow Velocity Contours	211
6.5.4	Secondary Velocity Vector	214
6.6	Conclusions	217
7	Conclusions and Recommendations for Further Work	222
7.1	Summary of the Work	222
7.2	Major Contributions	224
7.3	Scope, Limitations and Recommendations	226
A	Artificial Diffusion in Numerical Schemes	250
A.1	Preamble	250
A.2	Finite Difference Method	251
A.3	Numerical Diffusion in Linear Convection Equation	253
A.3.1	Modified Equation	254
A.3.2	Von-Neumann Stability Analysis	259

B	A Matlab Script for Simulation of Laminar Dispersion Flow through Pipes	267
B.1	Main Program	267
B.2	Function area_average.m	272
B.3	Function dispersion_coeff.m	272
C	High order Non-periodic Boundary Condition for CCD Method	274
C.1	Preamble	274
C.2	Development of the Boundary Equations	274
C.3	Conclusions and Scope	276
D	Solving a Twin-Tridiagonal Matrix	277
D.1	Solving Algorithm	277
D.2	Conclusions and Scope	289
E	A Twin Tridiagonal Matrix Solver in MATLAB	290
E.1	Main Program	290
F	A MATLAB Script to Solve 3D Convection Diffusion Equation by CCD-ADI Method	297
F.1	Main Program	297
F.2	Function area_average_rect.m	304
F.3	Function coefficients_triple.m	305
G	Dispersion of a Solute in a Square Conduit in Which the Flow is Turbulent	308
G.1	Background	308
G.2	Mathematical Formulation of Flow System	309
G.3	Conclusion	318

List of Figures

2.1	Demonstration of dispersion due to the combined action of convection and molecular diffusion in a shear flow in a pipe. The x -axis moves with the average velocity of the fluid.	9
2.2	Axi-symmetric Solution domain for dispersion of scalar in laminar flow through pipes	24
2.3	Initial condition of the solute for grid independence study	41
2.4	Effect of axial grid size in the mean concentration profile for solute dispersion in a pipe that is 0.152 m long and that has an internal radius of $2.52 \times 10^{-4}m$. The legend shows the variation of the number of axial grid points for a fixed radial grid size.	42
2.5	Grid independence study in radial direction for dispersion of solute in laminar flow through circular pipes. Legend represents the number of radial grid for a 15.2 cm pipe with 200 axial grid points.	42
2.6	Effect of time step refinement in mean concentration of solute dispersion in a laminar flow. The legend indicates the time steps used in the simulation	43
2.7	Comparison of present study with Taylor (1953)work	45
2.8	Comparison of present study with Bournia et al. (1961) results for the longitudinal dispersion of 1,3- butadiene in 1-butadyne.	46
2.9	Comparisons between area-averaged concentration profiles of the solute for Peclet number (Pe) = 10000 at short durations of dimensionless time (τ). (a) $\tau = 1 \times 10^{-8}$ (b) $\tau = 1 \times 10^{-5}$ (c) $\tau = 1 \times 10^{-3}$	50

2.10	Comparison between area-averaged concentration profiles of the solute for Peclet number (Pe) = 10000 at extended periods of dimensionless time (τ). (a) $\tau = 0.02$, (b) $\tau = 0.1$, (c) $\tau = 1$	51
2.11	Comparison between area-averaged concentration profiles of the solute at low Peclet number $Pe = 10$; dimensionless time $\tau = 0.001$	52
2.12	Comparison between area-averaged concentration profiles of the solute for dimensionless time $\tau = 0.02$ at different Peclet numbers (Pe) - (a) $Pe = 1000$, (b) $Pe = 100$, (c) $Pe = 10$	53
3.1	Amplification factor as a function of phase angle in axial direction for the modified QUICKEST scheme developed in this work	74
3.2	Enlarged view of diffusion error in the low frequency regions for the modified QUICKEST scheme developed in this work	75
3.3	Enlarged view of diffusion error in the low frequency regions for the first order upwind scheme	75
3.4	Convection of two different pulses using FOU, QUICKEST numerical scheme and the exact solution	76
3.5	Comparison of the different numerical solution of 1D Convection-Diffusion equation. (a) FTCS, (b) Lax-Wendroff, (c) McCormack, (d) Upwind, (e) Finite Volume Scheme with Sweby flux limiter, (f) Present work-modified QUICKEST scheme.	78
3.6	Solution domain with mesh representation	81
3.7	Axial grid sensitivity to dimensionless mean concentration at outlet of the square ductt	82
3.8	Radial grid sensitivity to dimensionless mean concentration at outlet of the square duct	82
3.9	Time step sensitivity analysis for simulation of axial dispersion in laminar flow through square duct	83

3.10	Comparison of mean concentration profile generated by the modified-QUICKEST scheme at early time (breakthrough curve at a dimensionless axial distance, $X = 0.01$) in a square duct with the analytical solution	84
3.11	Comparison of mean concentration profile obtained from modified-QUICKEST scheme at later time (breakthrough curve at a dimensionless axial distance, $X = 0.1$) in a square duct with the analytical solution	84
3.12	Initial Development of the mean concentration profile of the solute at different axial positions close to the initial plug.	85
3.13	Development of the mean concentration profile of the solute at different axial positions from the initial plug	86
3.14	The evolution of the concentration profile with dimensionless time, τ	86
3.15	Spreading of the dimensionless mean concentration profile in axial direction 660s after an initial plug released at the inlet of a square and circular duct	88
3.16	Breakthrough curve at dimensionless axial distance $X=0.017$	88
3.17	Breakthrough curve at dimensionless axial distance $X=0.01$	89
3.18	Breakthrough curve at dimensionless axial distance $X=0.098$	90
3.19	Dimensionless effective dispersion coefficient in a square duct over a range of dimensionless times.	91
4.1	Diffusion error of the CCD-ADI method as a function of phase angle for different Courant numbers	114
4.2	Comparison between the exact and the numerical solutions using the method presented in this thesis, $Pe=2, 20, 200, 2000$	118
4.3	Comparison between exact solution and the CCD method for linear convection diffusion equation in two dimensional space with Dirichlet boundary condition, , (a) $Pe = 2$, (b) $Pe = 20$, (c) $Pe = 200$, (d) $Pe = 2000$ at $z=1.0$	120

4.4	Comparison of the CCD-ADI solution with the exact solution $0 \leq x, y \leq 2, t = 1.25, Pe = 2$; (a) $z = 0.2$, (b) $z = 1.2$	121
4.5	Lateral grid independence test for the CCD Scheme,	125
4.6	Axial grid independence test for the CCD scheme	126
4.7	Time step independence test for the CCD Scheme	128
4.8	Solute distribution at dimensionless distance $X = 0.1$ in a square channel using CCD-ADI scheme in laminar flow	129
5.1	Schematic representation of the turbulent fluctuating velocity and the mean velocity	134
5.2	Grid sensitivity test for the flow field simulation. Magnitude of the area averaged velocity profile at outlet.	148
5.3	Comparison of Laminar, transitional and turbulent mean velocity profiles for pipe flow as calculated in this work.	150
5.4	Comparison of velocity profile at Reynolds number 91,000 from the simulation carried out in this work with the experimental data of Durst et al. (1995), Laminar profile, Log profile and the velocity profile used in Taylor (1954b)	150
5.5	Comparison of velocity profiles computed in this work at various Reynolds number from the simulation with the experimental data of Durst et al. (1995)	151
5.6	A comparison of the same velocity profile depicted in a stationary reference coordinate (a) and coordinate that translate with the mean velocity of the fluid, (b).	152
5.7	Grid sensitivity analysis for the simulation of solute dispersion in turbulent flow through pipes.	158
5.8	Comparison of dimensionless mean concentration profile at the outlet from breakthrough curve from present work with the experimental data of Flint and Eisenklam (1969) at $Re = 3810$ and $Sc = 0.27$	159

6.8	Grid sensitivity test for the simulation of turbulent flow through rectangular ducts	210
6.9	Simulation results of outlet velocity contour for turbulent flow in rectangular duct using various turbulent models	212
6.10	Simulation results of outlet velocity contour for turbulent flow in rectangular duct using various turbulent models	213
6.11	Simulation results of contour of secondary velocity at outlet of a rectangular duct in turbulent flow using various turbulent models	215
6.12	Simulation results of contour of secondary velocity at outlet of a rectangular duct in turbulent flow using various turbulent models	216
6.13	DNS results (Pinelli et al., 2010) for secondary flow vector in a square duct at $Re = 3500$	217
6.14	Simulation results of contour of secondary velocity at outlet of a rectangular duct in turbulent flow using various turbulent models	218
6.15	Simulation results of contour of secondary velocity at outlet of a rectangular duct in turbulent flow using various turbulent models,	219
A.1	Illustration of artificial diffusion generated by the first order upwind scheme	255
A.2	Diffusion error for a first order upwind scheme for the linear convection equation	264
A.3	Enlarged view of diffusion error for a first order upwind scheme for the linear convection equation in low frequency region	264
A.4	Artificial diffusion in the first order upwind Scheme for convection of a pulse with $\phi = \pi/15$, simulation carried out with $C_r = 0.3$	265

Nomenclatures

Symbols

i	Imaginary number	
C	Concentration of the solute,	[kmol]
C_0	Initial Concentration of the solute,	[kmol]
C_{mean}	Area averaged concentration of the solute,	[kmol]
\mathcal{G}	Amplification factor	
$\mathcal{L}_x, \mathcal{L}_y, \mathcal{L}_z$	Finite difference operator	
\mathcal{P}	Turbulence production rate,	[m ² /s ³]
\bar{t}	Mean Residence Time,	[s]
a, b, c	Diffusion coefficient in x, y, z directions in Equation (4.35),	[m ² /s]
d	Diameter,	[m]
D_L	Longitudinal dispersion coefficient,	[m ² /s]
D_m	Molecular diffusivity,	[m ² /s]
D_{eff}	Effective diffusivity,	[m ² /s]
k	Turbulent kinetic energy,	[m ² /s ²]
L	Length,	[m]

L_K	Kolmogorov length Scale,	[m]
N	Number of meshes	
P	Pressure,	[Pa]
p, q, r	Convection velocity in x, y, z directions in Equation (4.35)	[m/s]
q_m	Mass flux,	[kmol/m ²]
R	Friction velocity,	[m/s]
r	Radial distance variable,	[m]
T	Total time,	[s]
t	Time variable,	[s]
u	Flow velocity,	[m/s]
u^*	Friction velocity,	[m/s]
U_{avg}	Mean velocity,	[m/s]
u_0	Centerline velocity,	[m/s]

Dimensionless Variables

$\gamma_x, \gamma_y, \gamma_z$	Dimensionless diffusion number
c	Dimensionless concentration
C_r	Courant number
Pe	Peclet number
Re	Reynolds number
Sc	Schmidt number
Sc_t	Turbulent Schmidt number

X	Dimensionless axial distance variable
y	Dimensionless radial distance variable
y^+	Dimensionless wall distance

Greek Symbols

ϵ	Turbulent kinetic energy dissipation rate,	$[\text{m}^2/\text{s}^3]$
κ	Wave number	
λ	Wavelength,	$[\text{m}]$
μ	Dynamic viscosity,	$[\text{N}\cdot\text{s}/\text{m}^2]$
ν	Kinematic viscosity,	$[\text{m}^2/\text{s}]$
ν_t	Turbulent viscosity,	$[\text{m}^2/\text{s}]$
Φ	Amplitude of error in fourier domain	
ϕ	A scalar	
ψ	Phase angle of error in fourier domain,	$[\text{°}]$
ρ	Density,	$[\text{kg}/\text{m}^3]$
σ	Variance of the breakthrough curve,	$[\text{s}^2]$
σ_θ	Dimensionless Variance of the breakthrough curve	
τ	Dimensionless time	
τ_w	Wall shear stress,	$[\text{Pa}]$
φ	Phase angle of amplification error in fourier domain,	$[\text{°}]$
ξ	Distance variable in a moving frame of reference,	$[\text{m}]$

Subscripts

eff	Effective value
i, j, k	Indices in x,y,z directions
x, y, z	Coordinate directions
p, q, r	Coordinate directions

Acronyms

ADI	Alternate Direction Implicit
CCD	Combined Compact Differencing
CFD	Computational Fluid Dynamics
DES	Detached Eddy Simulation
DNS	Direct Numerical Simulation
FCTA	Flux Corrected Transport Algorithm
FDM	Finite Difference Method
FEM	Finite Element Method
FOU	First Order Upwind
FTCS	Forward difference in Time and Central difference in Space
FVM	Finite Volume Method
HOC	Higher Order Compact
HOT	Higher Order Terms
HWA	Hot Wire Anemometry
LDA	Laser Doppler Anemometry
LES	Large Eddy Simulation

QUICKEST Quadratic Upwind Interpolation for Convective Kinematics with Estimated Streaming Terms

RANS Reynolds Averaged Navier Stokes

RSM Reynolds Stress Model

SAS Scale Adaptive Simulation

SGS Sub-grid Scale

TE Truncation Error

TSDIA Two Scale Direct Interaction Approximation

Chapter 1

Introduction

1.1 Introduction

Scalar quantities such as dissolved chemicals and internal energy are transported by fluids by two principal mechanisms, namely advection and diffusion. Advection arises as a result of bulk motion, whilst diffusion occurs as the result of the random motion of molecules. The random movement of turbulently flowing fluids also gives rise to behavior that is diffusion-like.

If we consider a chemical species dissolved in a flowing fluid, such as occurs in a river, the chemical will be swept down the river by advection. There is a non-uniform mean velocity distribution in the plane normal to the direction of the flow of the river. As a result, the chemical species will be transported more quickly in some region of the flow, and left behind in other regions. This gives rise to lateral concentration gradients in the plane normal to the flow, and dispersive effects tend to lessen these gradients. These phenomena reduce the spread of the chemical in the direction of the flow, and it makes the concentration in a plane normal the flow more uniform.

Dispersion phenomena of passive scalars in fluid streams are omnipresent in many natural and man-made systems. For example the dispersion of passive scalar take place in thermal and material pollution, sediment transport in rivers, effluents flow in channels, chemical reactors, transport of slurries and polymers, liquid and gas chromatography, biological and physiological transport, etc. In the design of tubular reactors, axial dispersion plays an important role in reducing the driving forces of the reactants. In many naturally occurring and industrial processes the action of advection and dispersion are inextricably linked and they determine the performance of the system. Although dispersion has significant impact on many technological and natural processes, sometimes it is desired to limit the magnitude of the dispersion. For instance, in many analytical instruments, dispersion significantly reduces the resolution of the apparatus and impairs the effectiveness of separation and purification processes. Particularly in chromatographic separation process, it is desired to minimize the rate of dispersion.

Estimation of the rate of dispersion and the spreading of the solute concentration helps scientist and engineers to understand natural phenomena and design industrial systems. However, the physical complexity that may arise from the geometry of the flow domain renders analytical expressions for the rate of dispersion infeasible. Often fluid motions are not very orderly but they are rather chaotic and random. This adds additional complexity to calculating the rate of dispersion and the nature of the concentration profile of the solute since the transport mechanism governed by not only convection and diffusion but also the random fluctuations of the fluid particles. Furthermore, conducting experiments in these scenarios are not always convenient, and sometimes infeasible.

An alternative approach is to perform numerical simulations based on the laws

of physics and using the power of computation to solve the governing equations of the physical phenomena. This technique, broadly known as computational fluid dynamics, has been used for over half a century in the past to solve many complex physical problems. The continuous equations that governs the physical phenomena are transformed into a set of discrete equations followed by solving the set of equations with the help of a computer. The flexibility to adapt almost any type of solution domain would have made this technique of numerical simulation versatile. However computational and mathematical barriers inhibit its accuracy.

Among many factors, one of the major issues with numerical simulations of a physical problem is the artefact of false diffusion in the solution arising from the discretization scheme. Particularly, when diffusion is the prime subject of interest, such as estimating rate of dispersion, it is essential to minimize the effects of false diffusion. In this research we have focused on this issue and developed new techniques to control the degree of false diffusion that arises in the computation process.

1.2 Research Objective

The ubiquitous nature of dispersion motivates us to accurately estimate the rate of spreading of solutes in flowing fluids using numerical methods that do not contaminate the solution with false diffusion in both laminar and turbulent flows. The overall objectives can be summarized as:

1. Development of diffusion-free numerical schemes for the simulation of solute dispersion in laminar flow through circular ducts.
2. Extend the schemes to simulate three-dimensional dispersion in rectangular coordinates.

3. Simulate dispersion in turbulent flow through circular pipes
4. Elucidate the origins of secondary flows in turbulent flow through non-circular ducts which influence dispersion.
5. Investigating a range of turbulent models that capture secondary flow in non-circular ducts.

1.3 Thesis Contribution

This thesis contributes to some general aspects of computational fluid dynamics. It enhances multiple avenues for further research on many physical phenomena relevant to fluid dynamics. The major outcomes from this thesis can be briefly stated as-

- Development of a third order modified QUICKEST scheme that accurately estimates dispersion in laminar and turbulent flow through circular pipes
- Development of the modified QUICKEST scheme for accurately simulating the dispersion of solute in three-dimensional rectangular ducts.
- Development of a novel sixth order combined compact difference scheme for solving three dimensional hydrodynamics dispersion in rectangular ducts. The method and its applications are reported in detail.
- Elucidation of the origin of the turbulent secondary flows in non-circular ducts.
- Calculation of secondary flow through non-circular ducts. A wide variety of turbulent models has been evaluated.

1.4 Structure of the Thesis

The key objective of this research is to devise numerical techniques to quantify dispersion in laminar and turbulent flows in ducts. This has been achieved by developing high order finite difference schemes for solving the governing equations in two and three-dimensional coordinate systems. The achievements have been organized into a total of seven chapters that comprise this thesis.

The nature of the problem has been introduced in Chapter 1 with a brief description of the significance and objective of the present research. In Chapter 2, attention given to the development of a third order accurate numerical scheme to simulate the shear flow dispersion in laminar flow through circular pipes. The scheme developed in this chapter is based on a one-dimensional quadratic upwind interpolation for convective kinematics with estimated streaming terms (QUICKEST) scheme. The existing scheme has been re-derived to account for the axi-symmetric geometry of the pipe. The superiority of the scheme is demonstrated in terms of stability, accuracy and negligible artificial diffusion. These results motivated the further development of a scheme that applies to three-dimensional domains in Chapter 3. A stability analysis of this new scheme that applies to three-dimensional systems and its ability to counteract numerical dispersion is discussed in Chapter 3.

Following the trend of development of higher order numerical schemes for the simulation of dispersion, a sixth order combined compact finite difference scheme has been developed in Chapter 4. The merits and superiority of the developed scheme are reported in detail by performing a stability analysis and numerical experiments.

In chapter 5, the scheme developed in Chapter 3 has been used to simulate dispersion in turbulent flow through circular pipes. It is believed that the dispersion in

turbulent flow through non-circular ducts will be more intense than that in a circular flow. The reasoning based on the understanding that the secondary flow developed in the non-circular duct due to turbulence will greatly affect the dispersion process. With that motivation, a detailed study of the origin of the turbulent secondary flows has been presented in chapter 6. Moreover, we have also carried out original work on the modelling of secondary flows and the results are also presented in Chapter 6.

Chapter 7 provides a summary of this work and highlights some limitations and suggestions regarding future work. An area of pressing concern is the need to develop method that simulates longitudinal dispersion in turbulent flows in non-circular ducts.

Chapter 2

Laminar Dispersion in Pipe-flow

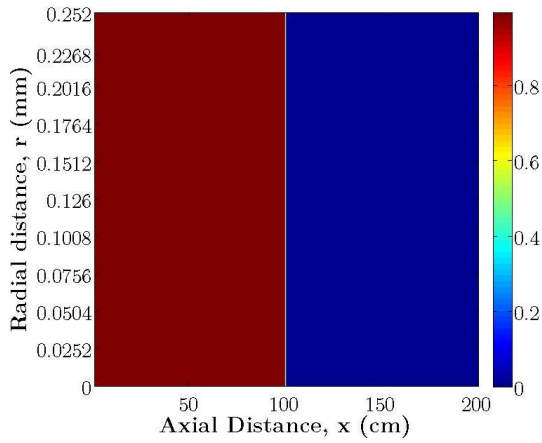
2.1 Introduction

When a passive scalar is introduced into a fluid flowing in a pipe it disperses by the simultaneous effects of molecular diffusion and velocity gradients that arise as a result of bulk motion. For instance, if a plug of non-reacting material, such as a dye, is introduced into a stream of water flowing through a circular tube, the non-uniform velocity profile strongly influences the spreading of the dye. In laminar flow the velocity profile is parabolic. As a result the scalar is distributed in such a way that material close to the center line travels faster than material in proximity to the wall, and a concentration gradient develops in the radial direction. As a result, some material diffuses radially by molecular diffusion which slows the overall longitudinal transport process. These phenomena can be observed by considering axi-symmetric section of a pipe that is subjected to a step change in concentration of a passive scalar as shown in Figure 2.1 (a). If the flow is pressure driven, the velocity profile of the carrier fluid will be parabolic. As a result of the parabolic velocity profile, a scalar

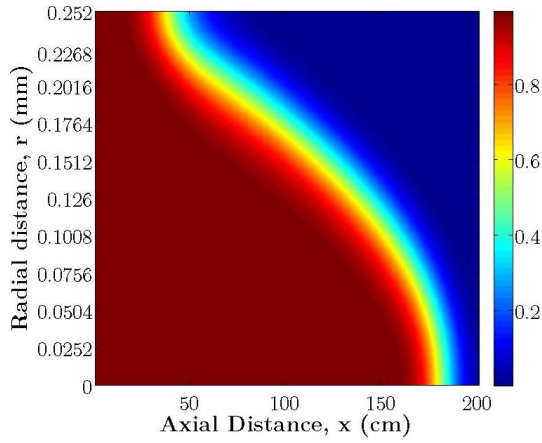
near to the center of the pipe will move faster than that in the vicinity of the wall. This can be observed after a short time (as in Figure 2.1 (b)); the scalar concentration resembles the velocity profile.

Subsequently as the material keeps moving forward, concentration gradients drive some of the material towards the wall (given that the solute diffuse down concentration gradients) (Figure 2.1(c) and Figure 2.1 (d)) until the entire solute stream resembles a longitudinally dispersed plug as seen in Figure 2.1(c). The concentration of the scalar in the axial direction can be modelled by means of a Fickian diffusion equation.

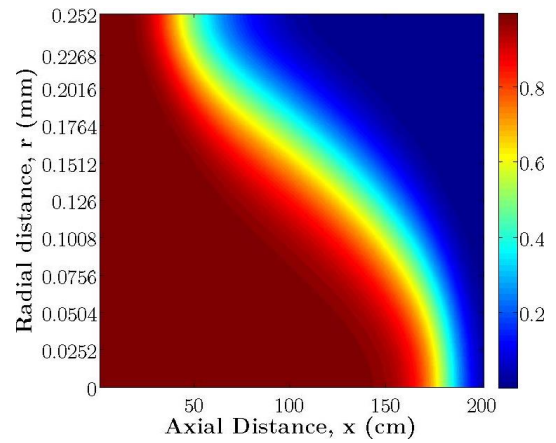
Shear flow dispersion is of great significance in many natural as well as man-made systems such as chemical reactors, pollute transport through rivers, estuaries, passive substance transport through open and closed channels, heat and mass transfer in ducts, etc. Due to its manifestation in many natural and engineering processes, the topic of solute dispersion in laminar flow through pipes has been an active theme of research for over half a century. Experimental observations, analytical solutions and numerical approximations have been brought to bear on the elucidation of the mechanism of solute dispersion and estimate the effective dispersion coefficient. Due to the limitation, and perhaps difficulties, of experimental studies, analytical methods of determining the effective dispersion coefficients have received considerable attention in the literature. However, analytical approaches often contain simplifying assumptions; hence a universal solution might not be obtained from such studies. Therefore, one has to apply the power of numerical methods to study the dispersion phenomena and estimate the dispersion coefficient under arbitrary conditions. Recent developments in numerical techniques combined with the exploitation of computing capability has made computational methods an effective alternative for studying many physical processes. However there is certain challenge with implementation



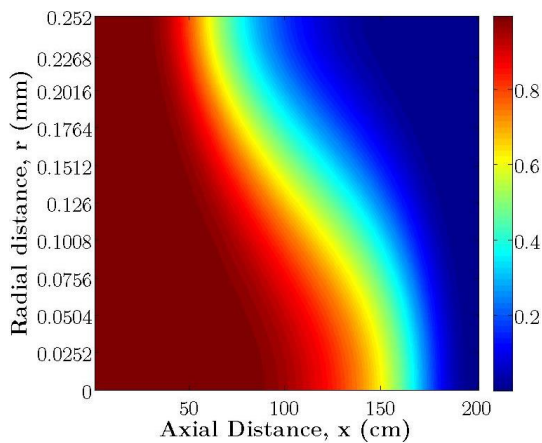
(a) Step input function - Initial Condition, $t = 0$



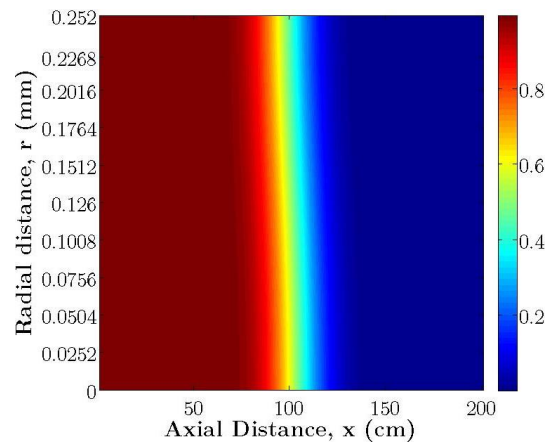
(b) Solute distribution, $t = 1.5s$



(c) Solute distribution, $t = 4s$



(d) Solute distribution, $t = 12s$



(e) Solute distribution, $t = 240s$

Figure 2.1: Demonstration of dispersion due to the combined action of convection and molecular diffusion in a shear flow in a pipe. The x -axis moves with the average velocity of the fluid.

of numerical methods which needs to be addressed fully to exploit the methods.

In this chapter, we investigate dispersion processes in laminar flow through circular duct by adopting the methods of computational fluid dynamics. One of the great challenges in such an approach is to avoid the artificial diffusion that usually arises from a poor selection of the discretising scheme (a method of converting continuous differential equations into set of discrete algebraic equation). To overcome this challenge we adapt a third order Quadratic Upwind Interpolation for Convective Kinematics with Estimated Streaming Terms (QUICKEST) scheme and develop a modified version of the scheme to take the advantage of axi-symmetric geometry for dispersion in laminar flow through pipes.

2.2 Literature Review

2.2.1 Analytical and Experimental Observations

The phenomenon of axial dispersion has been investigated analytically, experimentally and numerically over the last six decades. Taylor (1953) was perhaps the first person to address the issue. Taylors's pioneering work to establish the degree of axial dispersion in laminar flows through circular pipes was essentially an analytical approach. The elegance of such an approach leads to a closed form expression for the axial dispersion coefficient. Taylor's work required deep insights into the factors that affect axial dispersion in laminar flows. Although it could be argued that his insights could have been stated somewhat more explicitly, they led him to develop a profoundly important result. It was reported that the spreading of solute in a fluid flowing slowly through a circular cross sectioned capillary tube can be characterized by a time dependent diffusion process and the mean concentration of the solute can

be approximated by means of an effective longitudinal dispersion coefficient, D_L , given by

$$D_L = \frac{R^2 U^2}{48 D_m} = \frac{Pe^2 D_m}{48} \quad (2.1)$$

Here R is the pipe radius, U_{avg} is mean velocity of the flow, D_m is the molecular diffusivity of the solute and Pe ($= RU_{avg}/D_m$) is the Peclet number, a dimensionless number defining the relative effect of convection to diffusion in the transport process. Inspired by the consistency of the solution with the assumptions made during the solution, Taylor performed an experimental investigation for a dye-water system in a capillary tube. It was concluded that the analytical expression for dispersion coefficient concur with the experimental observation under the limiting conditions, (Taylor, 1954a)

$$\frac{4L}{R} \gg \frac{RU_{avg}}{D_m} \gg 6.9 \quad (2.2)$$

Although this analysis of scalar transport provides useful insight and guidance, it is based on several simplifying assumptions. For example, only radial diffusion is taken into account and axial diffusion is neglected. By an order-of-magnitude analysis (or scale analysis), it was claimed that the solute transport by axial diffusion is very small compared to transport by the convection and radial diffusion. However, in certain cases, such as at low Reynolds number, this may be an erroneous assumption. Nevertheless, Taylor's work established a niche for further investigation in the field, and inspired a series of researchers to apply the techniques of applied mathematics to relax some of the constraints on the original solution and to improve its accuracy and range of applicability. For example, to seek a solution which includes axial diffusion,

Aris (1956) incorporated the method of moment analysis as a modification to Taylor's work. He suggested that the effective dispersion coefficient can be expressed as

$$D_L = D_m + \frac{R^2 U_{avg}^2}{48 D_m} \quad (2.3)$$

Evans and Kenney (1965) have verified this result with their experimental observations of several gas-liquid systems. Although this solution relaxed the restriction of high Peclet number (Pe) in Taylor's work, it failed to estimate the dispersion coefficient for highly diffusion dominated flows with Peclet number of the order of less than 10. To increase the accuracy of the solution developed by Aris, Andersson and Berglin (1981) extended his work by calculating the first four moments instead of calculating only the first moment, and approximating the second moment as in the original work. These methods have been widely used to determine the diffusion coefficient of substances because of its simple and straightforward technique.

Reejhsinghani et al. (1966) reported the effect of wider range of Peclet number, Pe (12-50000) and dimensionless time, τ ($D_m t / R^2$) (0.01-60) by conducting an experimental study of a dye and water system. Their study suggests that at small values of τ (7.45×10^{-3}) and high Pe (36.4×10^3), pure convection dominates the transport process, however as τ increases, diffusion also contributes to the overall dispersion process.

Other techniques from applied mathematics have been used for the solution of laminar dispersion for the flow through circular pipes. For instance, a series solution method for transient shear dispersion phenomena reported by Gill and Ananthakrishnan (1967) and this has been later extended to develop a representation of the dispersion coefficient as a function of time (Gill and Sankarasubramanian, 1970). Furthermore, they analyzed the effect of arbitrary and non-uniform initial conditions

on the solute that is being dispersed and concluded that the value of the peak mean concentration is proportional to the slug length Gill and Sankarasubramanian (1971). Likewise, Tseng and Besant (1970) developed a solution to the convection diffusion equation from the linear combination of the eigenvalues and eigenvectors of the matrix form of the equation for fully developed laminar flow. This solution was found to be in good agreement with the experimental results of Reejhsinghani et al. (1966) at high Peclet number and high dimensionless time. However this solution failed to be applicable for low Peclet numbers and short dimensionless times. Similarly De Gance and Johns (1978) calculated solute concentration profiles using a Hermite polynomial and they developed an expression for the time dependent dispersion coefficient for chemically active solute in rectilinear domain.

The criteria for the validity of Taylor's solution have been examined by Yu (1976) who developed a series solution in terms of zero-order Bessel functions and claimed that Taylor's analysis is valid when $\tau > 0.7$. Furthermore, the solution has been extended by Yu (1979) to include the non-uniform injection of solute who concluded that the position of local maxima of the mean concentration depends on dimensionless time τ for different Peclet numbers. Although the solution proposed by Yu (1979) has a wider range of applicability, its computational complexity prevents the solution from converging towards quick and accurate solutions. Considering the fact that most of the previous solutions are applicable only at large times, Vrentas and Vrentas (1988) developed a perturbation solution for small values of τ and low Pe which exhibits superior convergence. However, the narrow range of applicability limits the approach from being a complete complementary version of the exact solution. Nevertheless, this study highlighted the limitation of Taylor's theory at small times and eliminated the limitation by providing solutions applicable to short times. In addition, they have

developed an alternative approach to study dispersion during its initial development using an exponential Fourier transform (Vrentas and Vrentas, 2000) which provides an asymptotic solution at short times. Other studies on dispersion for short periods of time and low Peclet numbers have been proposed by Shankar and Lenhoff (1989), Lighthill (1966) and Yu (1981). Additionally, a few analytical studies have been reported on dispersion in pulsed systems Paine et al. (1983) and dispersion in short tubes by Shankar and Lenhoff (1989).

Most of the studies mentioned above are concerned with the dispersion in straight circular pipes. However, in practice, pipes may not always be straight and they often contain bends and curved sections. Flow through pipes with bends sometimes gives rise to secondary flows in the radial direction which enhances lateral transport of solute. As a consequence dispersion is usually smaller in curved tubes than straight tubes Daskopoulos and Lenhoff (1988). This effect of secondary flow in reducing dispersion has been utilized in chromatographic separation and purification process where it is desired to minimize dispersion to increase instrumental effectiveness Zhao and Bau (2007). Apart from in curved tubes, secondary flows can be generated by turbulence, particularly in non-circular shaped ducts. Hence, dispersion is usually expected to be reduced in turbulent flow in non-circular ducts. This topic is discussed in detail in forthcoming chapters of this thesis.

2.2.2 Numerical Approaches

It is highly desirable to obtain closed form expressions for the rate of axial dispersion; however, the analyses on which they are based have several limitations. For example, such expressions are generally restricted to systems that have simple geometries. Furthermore, secondary phenomena, such as chemical reactions cannot be readily

accounted for, particularly at the initial stage when the distribution of the scalar is developing. Such details can only be elucidated by harnessing the power of numerical methods. Numerical methods offer flexibility by being able to adapt almost any geometry with arbitrary initial and boundary conditions. Moreover, with the advent of modern computers, computational efficiency has reached an unprecedented level which allows numerical solutions to be fast and robust. Despite these advantages, numerical solutions are inherently approximations of the solution. Hence without proper care, unwanted diffusion and oscillations can occur which ultimately renders the solutions unacceptable. When calculating the degree of dispersion numerically, particular care must be taken not to confound physical and numerical dispersion. This issue is perhaps a leitmotif that pervades this work.

Although there has been plethora of published works on the mathematical analysis of solute dispersion in slowly moving fluids through circular tubes, very limited approaches to the use of numerical techniques have been reported in literature. One of the very early numerical solutions of the dispersion of solute flowing in laminar flow through a circular tube was provided by Bailey and Gogarty (1962). The dimensionless convection diffusion equation was transformed into a finite difference equation using the FTCS (forward difference in time and central difference in space) method which is first order accurate in time and second order accurate in space. Neglecting axial diffusion in the governing equation, they suggest an effective dispersion coefficient as

$$D_L = \frac{t^{0.082} R^{1.836} U_{avg}^2}{48 D_m^{0.918}} \quad (2.4)$$

In addition to the numerical work, they also performed experimental investigations to observe the spreading of a scalar and the dispersion coefficient at a range of

dimensionless times (τ) from 0.1 to 100. It was concluded that, for a constant fluid velocity, the dispersion coefficient increases with time. A similar method was followed by Takahashi et al. (1990) in which the effect of axial diffusion has been taken into account in the numerical solution. A drawback of finite difference methods for estimating accurate concentration distributions becomes apparent when performing a mass balance on the solution. This limitation primarily arises when lower order approximations of the derivative terms in the governing equation are used. This critical issue, which contaminates the solution by overestimating the degree of dispersion if it is not properly treated, can be overcome by implementing higher order discretization schemes.

Further contributions to the numerical solution of the convection diffusion equation have been made by Ananthakrishnan et al. (1965) who employed a finite difference technique for discretising the governing equation and solved the resulting linear algebraic equations using the alternate direction implicit (ADI) method proposed by Peaceman and Rachford (1955). Their work provided results that cover wide ranges of τ (0.01-30) and Pe (1-23,000). They noted that at high Pe (> 500), axial molecular diffusion effects are almost negligible whereas at lower Pe it significantly increases and dominates the transport process at very low Pe , as might be expected. Furthermore, their work concurs with the analytical solution given by Aris (1956), however implying the condition that Aris's work is valid only for large dimensionless time (τ).

A more elegant numerical approach associated with the solution of solute dispersion phenomena in laminar flow through pipes has been proposed by Mayock et al. (1980) in which a flux corrected transport algorithm developed by Boris and Book (1973) was used to reduce the effect of artificial diffusion in the solution. Although

no quantitative validation of the numerical work was presented, it was claimed that the numerical results are in good agreement with the experimental work of Golay and Atwood (1979).

For a better approximation and to cover a wider range of Peclet number and dimensionless time in the solution of solute dispersion in laminar flow through pipes, numerical solutions have been provided by employing finite volume method. However, the second order upwind discretization scheme used to the solution method which is not entirely free from unwanted diffusion. Nevertheless, the solution can be improved further by adopting higher order discretization schemes.

Work on the dispersion of a passive scalar in laminar flow through circular pipe can be classified as being analytical, experimental, and numerical. A comprehensive summary of this research is presented in the following tables. The assumptions that have been considered in these studies are

- 1: Fully developed flow,
- 2: Negligible radial diffusion,
- 3: Negligible axial diffusion,
- 4: No chemical reactions between the carrier fluid and the solute,
- 5: Negligible density difference between fluid and the solute,
- 6: Uniform initial distribution across the cross section of pipe at inlet,
- 7: Constant molecular diffusivity of solute.

Although there have been many solutions of the equation that governs dispersion of solutes in fluids flowing slowly through circular pipes, most of these solutions are based on the assumptions listed Tables 2.2 and 2.3. These solutions lack versatility, particularly in their application to complex geometries. Numerical solutions obviate this limitation in complex shaped geometries. However, care must be taken to avoid

Table 2.1: Experimental investigations on dispersion in laminar flow through circular tubes

Author(s)	Geometry	Medium	Scalar / tracer	Method of Measurement	Ranges of Parameter			
					u_0 mm/s	Re	Pe	τ
Taylor (1953)	(0.5,1.0) × 1520	Water	$KMnO_4$	Colour detection	165 – 1.6×10^3	1 - 800	$50 - 1 \times 10^5$	
Bourmia et al. (1961)	21.7 × 2500	1, 3 - butadiene	1, 3 - butadiene	Ultra-violet detection	1 - 150	5 - 855	$100 - 1 \times 10^4$	0.5 - 100
		1, 3 - butadiene	1, butadiene					
		1,3 - butadiene	Helium					
Bailey and Gogarty (1962)	1.0×762	Water	$KMnO_4$	Spectro-photometry	0.75 - 233	1 - 300	$600 - 15 \times 10^3$	0.1 - 30
Evans and Kenney (1965)	6.35×1769	Nitrogen	Methane	Katharo-meter (Conductivity detector)	10 - 160	3 - 100		
		Argon	Hydrogen					
		Nitrogen	SF_6					
		Hydrogen	SF_6					
		Argon	SF_6					
Helium	SF_6							
Reejisinghani et al. (1966)	(1.5,5.0) × 850	Water		Optical detector			$12 - 50 \times 10^3$	0.01 - 60
Korenaga et al. (1989)								
Romero-Gomez and Choi (2011)								

Table 2.2: Mathematical analyses of dispersion in laminar flow through circular tubes

Author	Assumptions	Ranges of parameters	
		Pe	τ
Taylor (1953, 1954a)	1, 3,4, 5, 6, 7	>500	>0.5
Aris (1956)	1, 4,5, 6, 7	>100	>0.2
Bailey and Gogarty (1962)	1, 3, 4, 5, 6, 7	>600	>0.1
Ananthkrishnan et al. (1965)	1, 4, 5, 6, 7	1 - 23e3	0.01 - 30
Lighthill (1966)	1, 3, 4, 5, 6, 7	>500	>0.1
Gill and Ananthkrishnan (1967)	1, 4, 5, 6, 7	2.0 - 1e3	>0.05
Gill and Sankarasubramanian (1970)	1, 4, 5, 6, 7	>500	$>1e-3$
Tseng and Besant (1970)	1, 4, 5, 6, 7	10 - 60e3	7.45e-3 - 10
Gill and Sankarasubramanian (1971)	1, 4, 5, 7	>500	$>1e-3$
Yu (1976, 1979, 1981)	1, 4, 5, 6, 7	>5	>0.01
Vrentas and Vrentas (1988)	1, 4, 5, 6, 7	5 - 10e3	5e-6 - 1.0
Shankar and Lenhoff (1989)	1, 3, 4, 5, 6, 7	∞	$>2e-3$
Mansour (1989)	1, 3, 4, 5, 6, 7		
Phillips and Kaye (1997)	1, 3, 4, 5, 6, 7	∞	>10 1e-8 - 1e-3
Vrentas and Vrentas (2000)	1, 2, 4, 5, 6, 7	>10	1e-8 - 1e-3

Table 2.3: Numerical methods used to solve dispersion in laminar flow through circular tubes

Author	Assumptions	Method	Ranges of parameters	
			Pe	τ
Bailey and Gogarty (1962)	1, 3,4, 5, 6, 7	FDM	> 600	> 0.1
Ananthakrishnan et al. (1965)	1, 4,5, 6, 7	FDM, ADI	1 - 23e3	0.01 - 30
Gill and Ananthakrishnan (1967)	1, 3, 4, 5, 6, 7	FDM	2.0 - 1e3	> 0.05
Mayock et al. (1980)	1, 4, 5, 6, 7	FCTA		
Takahashi and GILL (1980)	1, 4,5, 6, 7	FDM		
Ekambara and Joshi (2004)	1, 4,5, 6, 7	FVM		

the effects of artificial diffusion arising from the numerical scheme because the dispersion is the object of this study. This is particularly so when the objective is to quantify dispersion in the flow. With a view to this, in this work, we adapt a third order accurate Quadratic Upwind Interpolation for Convective Kinematics with Estimated Streaming Terms (or briefly QUICKEST) scheme to solve the convection diffusion equation in laminar flow through pipes for estimating the dispersion of the scalar. The scheme was originally developed by Leonard (1979) for one dimensional flow. Laminar flows through a circular tube is axi-symmetric, therefore the QUICKEST schemes require a modification to suit with this axi-symmetric domain. Importantly, we shall subsequently modify the approach to ensure that it applies to three-dimensional systems. The justification of using third order QUICKEST method has been discussed in Appendix A.

The remainder of the chapter has been organized in the following sequence. Firstly, a mathematical description of the dispersion phenomena for a solute flowing in laminar flow through circular duct has been reported followed by the different approaches

applied to the solution particularly focusing the numerical solution. This is followed by a grid sensitivity analysis for the proposed QUICKEST method which has been validated against previously reported experimental results. The effects of dimensionless time and Peclet numbers are outlined prior to the result are summarized.

2.3 Mathematical Formulation

The equation that governs dispersion in a laminar flow through circular pipes can be described by the convection diffusion equation in an axi-symmetric geometry, i.e.

$$\frac{\partial \mathcal{C}}{\partial t} + \frac{\partial}{\partial x} (u\mathcal{C}) = \frac{1}{r} \frac{\partial}{\partial r} \left(r D_m \frac{\partial \mathcal{C}}{\partial r} \right) + \frac{\partial}{\partial x} \left(D_m \frac{\partial \mathcal{C}}{\partial x} \right) \quad (2.5)$$

It is well established that in the case of fully developed laminar flow through pipes, the velocity, u , is given by

$$u = u_0 \left(1 - \frac{r^2}{R^2} \right) \quad (2.6)$$

Here u_0 is the center line velocity and R is the radius of the pipe. Considering that in fully developed flow, u becomes independent of axial location and taking molecular diffusivity as being isotropic, equation (2.5) can be rewritten as

$$\frac{\partial \mathcal{C}}{\partial t} + u_0 \left(1 - \frac{r^2}{R^2} \right) \frac{\partial \mathcal{C}}{\partial x} = \frac{1}{r} \left(D_m \frac{\partial \mathcal{C}}{\partial r} \right) + D_m \frac{\partial^2 \mathcal{C}}{\partial r^2} + D_m \frac{\partial^2 \mathcal{C}}{\partial x^2} \quad (2.7)$$

This equation is subjected to the following initial and boundary conditions

The initial concentration of the solute entering the pipe, $\mathcal{C}(r, 0, 0)$

$$\mathcal{C}(r, 0, 0) = \mathcal{C}_0; \quad \mathcal{C}(r, x, 0) = 0 \quad (2.8)$$

There is no mass flux at the wall and we impose axial symmetry

$$\frac{\partial \mathcal{C}}{\partial r}(0, x, t) = \frac{\partial \mathcal{C}}{\partial r}(R, x, t) = 0 \quad (2.9)$$

It is often useful to represent the governing equation in a dimensionless form for the purpose of parametric studies. We therefore introduce following dimensionless variables

$$c = \frac{\mathcal{C}}{\mathcal{C}_0}; \quad \tau = \frac{D_m t}{R^2}; \quad Pe = \frac{Ru_0}{D_m}; \quad y = \frac{r}{R}; \quad X = \frac{x}{R} \quad (2.10)$$

Here, c is a dimensionless concentration of the scalar, τ is dimensionless time, Pe is the Peclet number and y is a dimensionless radial distance. Incorporating these expressions in the equation (2.7) we get

$$\frac{D_m \mathcal{C}_0}{R^2} \frac{\partial c}{\partial \tau} + u_0 (1 - y^2) \frac{\mathcal{C}_0}{R} \frac{\partial c}{\partial X} = \frac{1}{Ry} \left(D_m \frac{\mathcal{C}_0}{R} \frac{\partial c}{\partial y} \right) + D_m \frac{\mathcal{C}_0}{R^2} \frac{\partial^2 c}{\partial y^2} + D_m \frac{\mathcal{C}_0}{R^2} \frac{\partial^2 c}{\partial X^2} \quad (2.11)$$

Collecting terms

$$\frac{\partial c}{\partial \tau} + Pe (1 - y^2) \frac{\partial c}{\partial X} = \frac{1}{y} \left(\frac{\partial c}{\partial y} \right) + \frac{\partial^2 c}{\partial y^2} + \frac{\partial^2 c}{\partial X^2} \quad (2.12)$$

Subject to the initial and boundary conditions

$$c(y, 0, 0) = 1; \quad c(y, X, 0) = 0 \quad (2.13)$$

$$\frac{\partial c}{\partial y}(0, X, \tau) = \frac{\partial c}{\partial y}(1, X, \tau) = 0 \quad (2.14)$$

2.4 Numerical Solution

There have been significant developments in numerical solution techniques over the last century, particularly with the advent of the digital computers in last six decades. Finite difference (FDM), finite volume (FVM) and finite element methods (FEM), the basic tools for the numerical solution of partial differential equations, are widely used in many engineering applications. Among these three techniques, the first two are frequently applied for computational fluid dynamics. Finite difference methods are the simple to apply, perhaps because they retain the form of their progenitor continuous equation. However, its applicability is limited to regular shaped geometries. On the other hand, the finite volume method is more suitable for geometries with irregular and much complex shapes Tannehill et al. (1997).

Finite difference methods consist of rewriting the derivatives in the partial differential equation in terms of discrete quantities of dependent and independent variables. This results in the development of systems of simultaneous algebraic equations with all unknowns at discrete grid point for the entire domain. Finally the systems of linear equations are solved by an iterative scheme to obtain values of the variables at discrete mesh points giving the solution for the entire domain.

For computational fluid dynamics application, it is crucial to choose an appropriate differencing scheme and suitable iterative method of solution based on the physics of the flows. In particular for dispersion of passive scalar in pipe, which is governed by the convection diffusion equation (2.7), it is very important to choose a differencing scheme which will not only reduce numerical diffusion in the solution but also ensures the solution is stable.

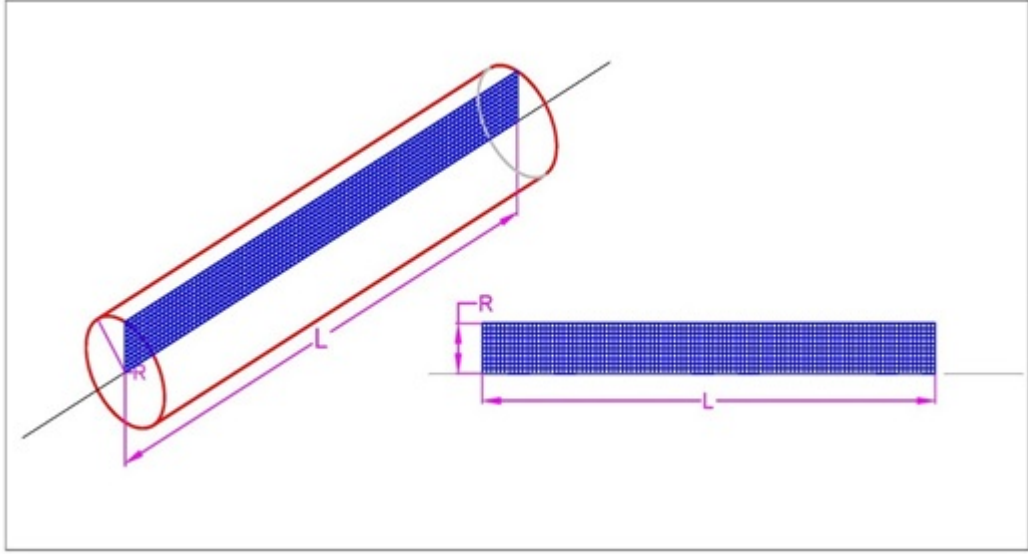


Figure 2.2: Axi-symmetric Solution domain for dispersion of scalar in laminar flow through pipes

2.4.1 Solution Domain and Grid Generation

The solution domain is a three dimensional circular pipe, however we exploit the axi-symmetric geometry to reduce the number of dimensions by one. This allows us to reduce the computational domain to a simple rectangular mesh as shown in Figure 2.2

The total length of the pipe is L and R is the radius of the pipe. Hence the axi-symmetric solution domain becomes $[0, L] \times [0, R]$ and it can be divided into N_{x+1} uniform grids as $0 = x_1 < x_2 \dots < x_{N_x} < x_{N_{x+1}} = L$ in axial direction representing $x_1 = 0$ as the inlet of the pipe and $x_{N_{x+1}} = L$ as the outlet of the pipe. Similarly, the radial locations are divided into N_{r+1} uniform grids as $0 = r_1 < r_2 \dots < r_{N_r} < r_{N_{r+1}} = R$ in the radial direction representing $r_1 = 0$ as the centreline of the pipe and $x_{N_{x+1}} = R$ as the pipe wall. These grids are divided with a uniform spacing of $\Delta x = L/N_x$ and $\Delta r = R/N_r$ along the axial and radial directions respectively. Furthermore the total time interval $[0, T]$ has been divided into N_t time

steps with a step size $\Delta t = T/N_t$. These notations have been used in the development of the scheme as well as in the solution methods

2.4.2 Discretization Scheme

There has been a plethora of discretization schemes developed in last six decades to approximate the governing equation of transport of scalar by combined action of convection and diffusion. However, none of these schemes is known to be completely exact or fully satisfactory (Chung, 2010). This is because the convection diffusion equation combines hyperbolic and parabolic terms which give rise to problems in its solution. When the initial concentration distribution of the solute, has steep or infinite gradient, the numerical schemes have to be well conditioned about the solution stability and accuracy. The diffusion term can be overcome by finite difference methods such as central difference scheme; however the advection term renders the solution unstable if the same scheme is adapted although it is second order accurate in space. This difficulty is usually treated by incorporating upwind effects into the discretization schemes so that the space coordinate is discretized in such a way that it is biased towards the direction of the flow. Although this scheme stabilizes the solution, it suffers a lot of demerits because the addition of false or artificial diffusion in the solution which is unacceptable in many kinds of physical problems. This is particularly the case for solutions that seek to determine the dispersion coefficient of solutes. Furthermore the scheme is accurate to only first order which limits the order of accuracy of the solution as well. A detailed study of issues with upwind scheme is presented in Appendix A.

In order to mitigate the issue of poor accuracy of numerical solutions arising from lower order discretization schemes, we adapt the third order accurate Quadratic

Upstream Interpolation for Convective Kinematics with Estimated Streaming Terms (or in short QUICKEST) difference scheme developed by Leonard (1979) for the solution of one dimensional convection diffusion equation. In the present study, this scheme has been extended by discretising equation (2.7) so that the axi-symmetric case of pipe can be adapted in the scheme. The following section describes the development of the QUICKEST scheme that has been revised for present situation of dispersion phenomena. This scheme is presented here as a propaedeutic to more sophisticated CCD methods we develop in Chapter 4.

2.4.3 QUICKEST Scheme for Laminar Dispersion in Pipes

The QUICKEST scheme developed by Leonard (1979) is a third order finite difference scheme that has been widely used by researchers for dealing with environmental modelling, turbulence modelling and similar fields where the governing equation has the form of convection-diffusion equation. The widespread adoption of this scheme lies in the fact that the scheme considerably reduces the oscillations that often appear with central difference schemes while discretising the convective terms. In addition, the QUICKEST scheme reduces numerical diffusion which is a common feature of lower order schemes such as first order upwinding methods (Patankar, 1980). The idea of the QUICKEST scheme is to cancel out the truncation error up to third order in both space and time derivatives using the governing equation itself. By doing so, the oscillations, which mostly appear because of truncating third order terms from the Taylor series expansion of derivatives, tend to be eliminated in the solution. The governing equation (equation (2.7)) is discretized by means of a forward differencing scheme in time and a central differencing scheme in space, thus

$$\begin{aligned} \frac{\mathcal{C}_{i,j}^{n+1} - \mathcal{C}_{i,j}^n}{\Delta t} + u \frac{\mathcal{C}_{i+1,j}^n - \mathcal{C}_{i-1,j}^n}{2\Delta x} = \\ D_m \left[\frac{1}{r_j} \left(\frac{\mathcal{C}_{i,j+1}^n - \mathcal{C}_{i,j-1}^n}{2\Delta r} \right) + \frac{\mathcal{C}_{i,j+1}^n - 2\mathcal{C}_{i,j}^n + \mathcal{C}_{i,j-1}^n}{(\Delta r)^2} \right. \\ \left. + \frac{\mathcal{C}_{i+1,j}^n - 2\mathcal{C}_{i,j}^n + \mathcal{C}_{i-1,j}^n}{(\Delta x)^2} \right] + \text{TE} \quad (2.15) \end{aligned}$$

Where the truncation error, TE is

$$\text{TE} = \frac{\Delta t}{2} \frac{\partial^2 \mathcal{C}}{\partial t^2} + \frac{\Delta t^2}{6} \frac{\partial^3 \mathcal{C}}{\partial t^3} + u \frac{\Delta x^2}{6} \frac{\partial^3 \mathcal{C}}{\partial x^3} + \frac{D_m}{r} \frac{\Delta r^2}{6} \frac{\partial^3 \mathcal{C}}{\partial r^3} + \text{HOT} \quad (2.16)$$

Where, the higher order terms (HOT) contain all fourth and above order terms. The above equation can be simplified by neglecting these higher order terms in the equation followed by converting all time derivatives into space derivatives. Differentiating equation (2.7) with respect to time gives

$$\frac{\partial^2 \mathcal{C}}{\partial t^2} + u \frac{\partial}{\partial x} \left(\frac{\partial \mathcal{C}}{\partial t} \right) = D_m \left[\frac{1}{r} \left(\frac{\partial}{\partial r} \left(\frac{\partial \mathcal{C}}{\partial t} \right) \right) + \frac{\partial^2}{\partial r^2} \left(\frac{\partial \mathcal{C}}{\partial t} \right) + \frac{\partial^2}{\partial x^2} \left(\frac{\partial \mathcal{C}}{\partial t} \right) \right] \quad (2.17)$$

Inserting the expression for $\left(\frac{\partial \mathcal{C}}{\partial t} \right)$ from equation (2.7) into the above equation and again neglecting fourth order and higher terms gives

$$\begin{aligned}
\frac{\partial^2 \mathcal{C}}{\partial t^2} + u \frac{\partial}{\partial x} \left(-u \frac{\partial \mathcal{C}}{\partial x} + D_m \left[\frac{1}{r} \left(\frac{\partial \mathcal{C}}{\partial r} \right) + \frac{\partial^2 \mathcal{C}}{\partial r^2} + \frac{\partial^2 \mathcal{C}}{\partial x^2} \right] \right) = \\
D_m \left[\frac{1}{r} \left(\frac{\partial}{\partial r} \left(-u \frac{\partial \mathcal{C}}{\partial x} + D_m \left[\frac{1}{r} \left(\frac{\partial \mathcal{C}}{\partial r} \right) + \frac{\partial^2 \mathcal{C}}{\partial r^2} + \frac{\partial^2 \mathcal{C}}{\partial x^2} \right] \right) \right) \right. \\
+ \frac{\partial^2}{\partial r^2} \left(-u \frac{\partial \mathcal{C}}{\partial x} + D_m \left[\frac{1}{r} \left(\frac{\partial \mathcal{C}}{\partial r} \right) + \frac{\partial^2 \mathcal{C}}{\partial r^2} + \frac{\partial^2 \mathcal{C}}{\partial x^2} \right] \right) \\
\left. + \frac{\partial^2}{\partial x^2} \left(-u \frac{\partial \mathcal{C}}{\partial x} + D_m \left[\frac{1}{r} \left(\frac{\partial \mathcal{C}}{\partial r} \right) + \frac{\partial^2 \mathcal{C}}{\partial r^2} + \frac{\partial^2 \mathcal{C}}{\partial x^2} \right] \right) \right] \quad (2.18)
\end{aligned}$$

$$\begin{aligned}
\frac{\partial^2 \mathcal{C}}{\partial t^2} + \left(-u^2 \frac{\partial^2 \mathcal{C}}{\partial x^2} + u D_m \left[\frac{1}{r} \left(\frac{\partial^2 \mathcal{C}}{\partial x \partial r} \right) + \frac{\partial^3 \mathcal{C}}{\partial x \partial r^2} + \frac{\partial^3 \mathcal{C}}{\partial x^3} \right] \right) = \\
D_m \left[\frac{1}{r} \left(\left(-u \frac{\partial^2 \mathcal{C}}{\partial x \partial r} + D_m \left[\frac{1}{r} \left(\frac{\partial^2 \mathcal{C}}{\partial r^2} \right) + \frac{\partial^3 \mathcal{C}}{\partial r^3} + \frac{\partial^3 \mathcal{C}}{\partial x^2 \partial r} \right] \right) \right) \right. \\
+ \left(-u \frac{\partial^3 \mathcal{C}}{\partial x \partial r^2} + D_m \left[\frac{1}{r} \left(\frac{\partial^3 \mathcal{C}}{\partial r^3} \right) \right] \right) \\
\left. + \left(-u \frac{\partial^3 \mathcal{C}}{\partial x^3} + D_m \left[\frac{1}{r} \left(\frac{\partial^3 \mathcal{C}}{\partial r \partial x^2} \right) \right] \right) \right]
\end{aligned}$$

Rearranging terms gives,

$$\begin{aligned}
\frac{\partial^2 \mathcal{C}}{\partial t^2} = u^2 \frac{\partial^2 \mathcal{C}}{\partial x^2} - 2 \frac{u D_m}{r} \frac{\partial^2 \mathcal{C}}{\partial x \partial r} + 2 \frac{D_m^2}{r} \left(\frac{\partial^3 \mathcal{C}}{\partial r^3} + \frac{\partial^3 \mathcal{C}}{\partial x^2 \partial r} \right) \\
+ \frac{D_m^2}{r^2} \left(\frac{\partial^2 \mathcal{C}}{\partial r^2} \right) - 2u D_m \left[\frac{\partial^3 \mathcal{C}}{\partial x^3} + \frac{\partial^3 \mathcal{C}}{\partial x \partial r^2} \right] \quad (2.19)
\end{aligned}$$

Again differentiating equation (2.19) with respect to time and omitting fourth order terms, we obtain

$$\frac{\partial^3 \mathcal{C}}{\partial t^3} = u^2 \frac{\partial^2}{\partial x^2} \left(\frac{\partial \mathcal{C}}{\partial t} \right) - 2 \frac{uD_m}{r} \frac{\partial^2}{\partial x \partial r} \left(\frac{\partial \mathcal{C}}{\partial t} \right) + \frac{D_m^2}{r^2} \frac{\partial^2}{\partial r^2} \left(\frac{\partial \mathcal{C}}{\partial t} \right) \quad (2.20)$$

Substituting the expression for $\left(\frac{\partial \mathcal{C}}{\partial t}\right)$ from equation (2.7) in the above equation (2.20),

$$\begin{aligned} \frac{\partial^3 \mathcal{C}}{\partial t^3} = & u^2 \frac{\partial^2}{\partial x^2} \left(-u \frac{\partial \mathcal{C}}{\partial x} + D_m \left[\frac{1}{r} \left(\frac{\partial \mathcal{C}}{\partial r} \right) + \frac{\partial^2 \mathcal{C}}{\partial r^2} + \frac{\partial^2 \mathcal{C}}{\partial x^2} \right] \right) - \\ & 2 \frac{uD_m}{r} \frac{\partial^2}{\partial x \partial r} \left(-u \frac{\partial \mathcal{C}}{\partial x} + D_m \left[\frac{1}{r} \left(\frac{\partial \mathcal{C}}{\partial r} \right) + \frac{\partial^2 \mathcal{C}}{\partial r^2} + \frac{\partial^2 \mathcal{C}}{\partial x^2} \right] \right) \\ & + \frac{D_m^2}{r^2} \frac{\partial^2}{\partial r^2} \left(-u \frac{\partial \mathcal{C}}{\partial x} + D_m \left[\frac{1}{r} \left(\frac{\partial \mathcal{C}}{\partial r} \right) + \frac{\partial^2 \mathcal{C}}{\partial r^2} + \frac{\partial^2 \mathcal{C}}{\partial x^2} \right] \right) \end{aligned} \quad (2.21)$$

The above expression can be simplified, with result

$$\frac{\partial^3 \mathcal{C}}{\partial t^3} = -u^3 \frac{\partial^3 \mathcal{C}}{\partial x^3} + 3 \frac{u^2 D_m}{r} \frac{\partial^3 \mathcal{C}}{\partial x^2 \partial r} - 3 \frac{uD_m^2}{r^2} \frac{\partial^3 \mathcal{C}}{\partial x \partial r^2} + \frac{D_m^3}{r^3} \frac{\partial^3 \mathcal{C}}{\partial r^3} \quad (2.22)$$

Substituting expressions from equation (2.19) and (2.22) into (2.16), the expression for truncation error term becomes

$$\begin{aligned} TE = & \frac{\Delta t}{2} \left\{ u^2 \frac{\partial^2 \mathcal{C}}{\partial x^2} - 2 \frac{uD_m}{r} \frac{\partial^2 \mathcal{C}}{\partial x \partial r} + 2 \frac{D_m^2}{r} \left(\frac{\partial^3 \mathcal{C}}{\partial r^3} + \frac{\partial^3 \mathcal{C}}{\partial x^2 \partial r} \right) \right. \\ & \left. - 2uD_m \left[\frac{\partial^3 \mathcal{C}}{\partial x^3} + \frac{\partial^3 \mathcal{C}}{\partial x \partial r^2} \right] + \frac{D_m^2}{r^2} \frac{\partial^2 \mathcal{C}}{\partial r^2} \right\} \\ & + \frac{\Delta t^2}{6} \left(-u^3 \frac{\partial^3 \mathcal{C}}{\partial x^3} + 3 \frac{u^2 D_m}{r} \frac{\partial^3 \mathcal{C}}{\partial x^2 \partial r} - 3 \frac{uD_m^2}{r^2} \frac{\partial^3 \mathcal{C}}{\partial x \partial r^2} + \frac{D_m^3}{r^3} \frac{\partial^3 \mathcal{C}}{\partial r^3} \right) + \\ & u \frac{\Delta x^2}{6} \frac{\partial^3 \mathcal{C}}{\partial x^3} + \frac{D_m}{r} \frac{\Delta r^2}{6} \frac{\partial^3 \mathcal{C}}{\partial r^3} + HOT \end{aligned} \quad (2.23)$$

Rearranging and accumulating terms in equation (2.23),

$$\begin{aligned}
TE = & \frac{u^2 \Delta t}{2} \frac{\partial^2 \mathcal{C}}{\partial x^2} - \frac{uD_m \Delta t}{r} \frac{\partial^2 \mathcal{C}}{\partial x \partial r} + \frac{D_m^2 \Delta t}{2r^2} \frac{\partial^2 \mathcal{C}}{\partial r^2} \\
& + \left(u \frac{\Delta x^2}{6} - u^3 \frac{\Delta t^2}{6} - uD_m \Delta t \right) \frac{\partial^3 \mathcal{C}}{\partial x^3} \\
& \left(\frac{u^2 D_m \Delta t^2}{2r} + \frac{D_m^2 \Delta t}{r} \right) \frac{\partial^3 \mathcal{C}}{\partial x^2 \partial r} \\
& + \left(-uD_m \Delta t - \frac{uD_m^2 \Delta t^2}{2r^2} \right) \frac{\partial^3 \mathcal{C}}{\partial x \partial r^2} \\
& + \left(\frac{D_m^2 \Delta t}{r} + \frac{D_m \Delta r^2}{6r} + \frac{D_m^3 \Delta t^2}{6r^3} \right) \frac{\partial^3 \mathcal{C}}{\partial r^3} \quad (2.24)
\end{aligned}$$

Discretising the first, second and third derivatives, we get

$$\begin{aligned}
TE = & u^2 \frac{\Delta t}{2(\Delta x)^2} (\mathcal{C}_{i+1,j}^n - 2\mathcal{C}_{i,j}^n + \mathcal{C}_{i-1,j}^n) \\
& - \frac{uD_m\Delta t}{r\Delta x\Delta r} (\mathcal{C}_{i,j}^n - \mathcal{C}_{i-1,j}^n - \mathcal{C}_{i,j-1}^n + \mathcal{C}_{i-1,j-1}^n) \\
& + \frac{D_m^2\Delta t}{2r^2\Delta r^2} (\mathcal{C}_{i,j+1}^n - 2\mathcal{C}_{i,j}^n + \mathcal{C}_{i,j-1}^n) \\
& + \left(-uD_m\Delta t - u^3\frac{\Delta t^2}{6} + u\frac{\Delta x^2}{6} \right) \frac{1}{(\Delta x)^3} \\
& \left\{ (\mathcal{C}_{i+1,j}^n - 2\mathcal{C}_{i,j}^n + \mathcal{C}_{i-1,j}^n) - (\mathcal{C}_{i,j}^n - 2\mathcal{C}_{i-1,j}^n + \mathcal{C}_{i-2,j}^n) \right\} \\
& + \left(\frac{u^2D_m\Delta t^2}{2r_j\Delta x^2\Delta r} + \frac{D_m^2\Delta t}{r_j\Delta x^2\Delta r} \right) \left[(\mathcal{C}_{i+1,j}^n - 2\mathcal{C}_{i,j}^n + \mathcal{C}_{i-1,j}^n) \right. \\
& \quad \left. - (\mathcal{C}_{i+1,j-1}^n - 2\mathcal{C}_{i,j-1}^n + \mathcal{C}_{i-1,j-1}^n) \right] \\
& + \left(-\frac{uD_m\Delta t}{\Delta x\Delta r^2} - \frac{uD_m^2\Delta t^2}{2r_j^2\Delta x\Delta r^2} \right) \left[(\mathcal{C}_{i,j+1}^n - 2\mathcal{C}_{i,j}^n + \mathcal{C}_{i,j-1}^n) \right. \\
& \quad \left. - (\mathcal{C}_{i-1,j+1}^n - 2\mathcal{C}_{i-1,j}^n + \mathcal{C}_{i-1,j-1}^n) \right] \\
& + \left(\frac{\Delta t D_m^2}{r_j} + \frac{D_m\Delta r^2}{6r_j} + \frac{D_m^3\Delta t^2}{6r^3} \right) \frac{1}{(\Delta r)^3} \left\{ (\mathcal{C}_{i,j+1}^n - 2\mathcal{C}_{i,j}^n + \mathcal{C}_{i,j-1}^n) \right. \\
& \quad \left. - (\mathcal{C}_{i,j}^n - 2\mathcal{C}_{i,j-1}^n + \mathcal{C}_{i,j-2}^n) \right\} \quad (2.25)
\end{aligned}$$

Let us define Courant number, $C_r = \frac{u\Delta t}{\Delta x}$ and $\gamma_x = \frac{D_m\Delta t}{(\Delta x)^2}$, and $\gamma_r = \frac{D_m\Delta t}{(\Delta r)^2}$, which enables us to express equation (2.25) in a concise form as

$$\begin{aligned}
TE = & \frac{1}{\Delta t} \left[\frac{C_r^2}{2} (\mathcal{C}_{i+1,j}^n - 2\mathcal{C}_{i,j}^n + \mathcal{C}_{i-1,j}^n) \right. & (2.26) \\
& - \frac{\Delta r}{r_j} C_r \gamma_r (\mathcal{C}_{i,j}^n - \mathcal{C}_{i-1,j}^n - \mathcal{C}_{i,j-1}^n + \mathcal{C}_{i-1,j-1}^n) \\
& + \frac{1}{2} \left(\frac{\Delta r}{r_j} \gamma_r \right)^2 (\mathcal{C}_{i,j+1}^n - 2\mathcal{C}_{i,j}^n + \mathcal{C}_{i,j-1}^n) \\
& + \left(-C_r \gamma_x - \frac{C_r^3}{6} + \frac{C_r}{6} \right) \{ (\mathcal{C}_{i+1,j}^n - 2\mathcal{C}_{i,j}^n + \mathcal{C}_{i-1,j}^n) - (\mathcal{C}_{i,j,k}^n - 2\mathcal{C}_{i-1,j,k}^n + \mathcal{C}_{i-2,j,k}^n) \} \\
& + \left(\frac{\Delta r}{2r_j} C_r^2 \gamma_r + \frac{\Delta r}{r_j} \gamma_x \gamma_r \right) \{ (\mathcal{C}_{i+1,j}^n - 2\mathcal{C}_{i,j}^n + \mathcal{C}_{i-1,j}^n) - (\mathcal{C}_{i+1,j-1}^n - 2\mathcal{C}_{i,j-1}^n + \mathcal{C}_{i-1,j-1}^n) \} \\
& + \left(-C_r \gamma_r - \frac{C_r}{2} \left(\frac{\Delta r}{r_j} \gamma_r \right)^2 \right) \{ (\mathcal{C}_{i,j+1}^n - 2\mathcal{C}_{i,j}^n + \mathcal{C}_{i,j-1}^n) - (\mathcal{C}_{i-1,j+1}^n - 2\mathcal{C}_{i-1,j}^n + \mathcal{C}_{i-1,j-1}^n) \} \\
& \left. + \left(\frac{\Delta r}{r_j} \gamma_r^2 + \frac{\Delta r}{6r_j} \gamma_r + \frac{1}{6} \left(\frac{\Delta r}{r_j} \gamma_r \right)^3 \right) \{ (\mathcal{C}_{i,j+1}^n - 2\mathcal{C}_{i,j}^n + \mathcal{C}_{i,j-1}^n) - (\mathcal{C}_{i,j}^n - 2\mathcal{C}_{i,j-1}^n + \mathcal{C}_{i,j-2}^n) \} \right]
\end{aligned}$$

Recalling equation (2.15), which after some rearrangements may be expressed as

$$\begin{aligned}
\mathcal{C}_{i,j}^{n+1} - \mathcal{C}_{i,j}^n + \frac{u\Delta t}{2\Delta x} (\mathcal{C}_{i+1,j}^n - \mathcal{C}_{i-1,j}^n) = & \\
& \frac{\Delta r}{2r_j} \frac{D_m \Delta t}{(\Delta r)^2} (\mathcal{C}_{i,j+1}^n - \mathcal{C}_{i,j-1}^n) \\
& + \frac{D_m \Delta t}{(\Delta r)^2} (\mathcal{C}_{i,j+1}^n - 2\mathcal{C}_{i,j}^n + \mathcal{C}_{i,j-1}^n) \\
& + \frac{D_m \Delta t}{(\Delta x)^2} (\mathcal{C}_{i+1,j}^n - 2\mathcal{C}_{i,j}^n + \mathcal{C}_{i-1,j}^n) + \Delta t (TE)
\end{aligned}$$

If we substitute expression for the TE from equation (2.26) into the above equation, we obtain

$$\begin{aligned}
\mathcal{C}_{i,j}^{n+1} = & \mathcal{C}_{i,j}^n - \frac{C_r}{2} (\mathcal{C}_{i+1,j}^n - \mathcal{C}_{i-1,j}^n) \\
& + \frac{\Delta r}{2r_j} \gamma_r (\mathcal{C}_{i,j+1}^n - \mathcal{C}_{i,j-1}^n) + \gamma_r (\mathcal{C}_{i,j+1}^n - 2\mathcal{C}_{i,j}^n + \mathcal{C}_{i,j-1}^n) \\
& + \gamma_x (\mathcal{C}_{i+1,j}^n - 2\mathcal{C}_{i,j}^n + \mathcal{C}_{i-1,j}^n) + \frac{C_r^2}{2} (\mathcal{C}_{i+1,j}^n - 2\mathcal{C}_{i,j}^n + \mathcal{C}_{i-1,j}^n) \\
& - \frac{\Delta r}{r_j} C_r \gamma_r (\mathcal{C}_{i,j}^n - \mathcal{C}_{i-1,j}^n - \mathcal{C}_{i,j-1}^n + \mathcal{C}_{i-1,j-1}^n) \\
& + \frac{1}{2} \left(\frac{\Delta r}{r_j} \gamma_r \right)^2 (\mathcal{C}_{i,j+1}^n - 2\mathcal{C}_{i,j}^n + \mathcal{C}_{i,j-1}^n) \\
& + \left(-C_r \gamma_x - \frac{C_r^3}{6} + \frac{C_r}{6} \right) \{ (\mathcal{C}_{i+1,j}^n - 2\mathcal{C}_{i,j}^n + \mathcal{C}_{i-1,j}^n) - (\mathcal{C}_{i,j}^n - 2\mathcal{C}_{i-1,j}^n + \mathcal{C}_{i-2,j}^n) \} \\
& + \left(\frac{\Delta r}{2r_j} C_r^2 \gamma + \frac{\Delta r}{r_j} \gamma_x \gamma_r \right) [(\mathcal{C}_{i+1,j}^n - 2\mathcal{C}_{i,j}^n + \mathcal{C}_{i-1,j}^n) - (\mathcal{C}_{i+1,j-1}^n - 2\mathcal{C}_{i,j-1}^n + \mathcal{C}_{i-1,j-1}^n)] \\
& + \left(-C_r \gamma_r - \frac{C_r}{2} \left(\frac{\Delta r}{r_j} \gamma_r \right)^2 \right) [(\mathcal{C}_{i,j+1}^n - 2\mathcal{C}_{i,j}^n + \mathcal{C}_{i,j-1}^n) - (\mathcal{C}_{i-1,j+1}^n - 2\mathcal{C}_{i-1,j}^n + \mathcal{C}_{i-1,j-1}^n)] \\
& + \left(\frac{\Delta r}{r_j} \gamma_r^2 + \frac{\Delta r}{6r_j} \gamma_r + \frac{1}{6} \left(\frac{\Delta r}{r_j} \gamma_r \right)^3 \right) \{ (\mathcal{C}_{i,j+1}^n - 2\mathcal{C}_{i,j}^n + \mathcal{C}_{i,j-1}^n) - (\mathcal{C}_{i,j}^n - 2\mathcal{C}_{i,j-1}^n + \mathcal{C}_{i,j-2}^n) \}
\end{aligned}$$

We are now in a position to obtain our ultimate goal, namely an expression for the concentration of solute, $\mathcal{C}_{i,j}^{n+1}$, at the next time step, $n+1$. It is

$$\begin{aligned}
\mathcal{C}_{i,j}^{n+1} = & \\
& \mathcal{C}_{i+1,j}^n \left[-\frac{C_r}{2} + \gamma_x + \frac{C_r^2}{2} + \left(-C_r \gamma_x - \frac{C_r^3}{6} + \frac{C_r}{6} \right) + \left(\frac{\Delta r}{2r_j} C_r^2 \gamma_r + \frac{\Delta r}{r_j} \gamma_x \gamma_r \right) \right] \\
& + \mathcal{C}_{i,j}^n \left[1 - 2\gamma_r - 2\gamma_x - C_r^2 - \frac{\Delta r}{r_j} C_r \gamma_r - 3 \left(-C_r \gamma_x - \frac{C_r^3}{6} + \frac{C_r}{6} \right) \right. \\
& - 2 \left(\frac{\Delta r}{2r_j} C_r^2 \gamma_r + \frac{\Delta r}{r_j} \gamma_x \gamma_r \right) - 2 \left(-C_r \gamma_r - \frac{\Delta x \Delta t}{3r_j^2} \gamma_r \gamma_x \right) \\
& \left. - \left(\frac{\Delta r}{r_j} \gamma_r \right)^2 - 3 \left(\frac{\Delta r}{r_j} \gamma_r^2 + \frac{\Delta r}{6r_j} \gamma_r + \frac{1}{6} \left(\frac{\Delta r}{r_j} \gamma_r \right)^3 \right) \right] \\
& + \mathcal{C}_{i-1,j}^n \left[\frac{C_r}{2} + \gamma_x + \frac{C_r^2}{2} + \frac{\Delta r}{r_j} C_r \gamma_r + 3 \left(-C_r \gamma_x - \frac{C_r^3}{6} + \frac{C_r}{6} \right) \right. \\
& \left. + 2 \left(-C_r \gamma_r - \frac{C_r}{2} \left(\frac{\Delta r}{r_j} \gamma_r \right)^2 \right) \right] \\
& + \mathcal{C}_{i,j+1}^n \left[\frac{\Delta r}{2r_j} \gamma_r + \gamma_r + \left(-C_r \gamma_r - \frac{C_r}{2} \left(\frac{\Delta r}{r_j} \gamma_r \right)^2 \right) \right. \\
& \left. + \frac{1}{2} \left(\frac{\Delta r}{r_j} \gamma_r \right)^2 + \left(\frac{\Delta r}{r_j} \gamma_r^2 + \frac{\Delta r}{6r_j} \gamma_r + \frac{1}{6} \left(\frac{\Delta r}{r_j} \gamma_r \right)^3 \right) \right] \\
& + \mathcal{C}_{i,j-1}^n \left[-\frac{\Delta r}{2r_j} \gamma_r + \gamma_r + \frac{\Delta r}{r_j} C_r \gamma_r + 2 \left(\frac{\Delta r}{2r_j} C_r^2 \gamma_r + \frac{\Delta r}{r_j} \gamma_x \gamma_r \right) \right. \\
& \left. + \left(-C_r \gamma_r - \frac{C_r}{2} \left(\frac{\Delta r}{r_j} \gamma_r \right)^2 \right) + \frac{1}{2} \left(\frac{\Delta r}{r_j} \gamma_r \right)^2 + 3 \left(\frac{\Delta r}{r_j} \gamma_r^2 + \frac{\Delta r}{6r_j} \gamma_r + \frac{1}{6} \left(\frac{\Delta r}{r_j} \gamma_r \right)^3 \right) \right] \\
& + \mathcal{C}_{i-1,j-1}^n \left[-\frac{\Delta r}{r_j} C_r \gamma_r - \left(\frac{\Delta r}{2r_j} C_r^2 \gamma_r + \frac{\Delta r}{r_j} \gamma_x \gamma_r \right) - \left(-C_r \gamma_r - \frac{C_r}{2} \left(\frac{\Delta r}{r_j} \gamma_r \right)^2 \right) \right] \\
& + \mathcal{C}_{i-1,j+1}^n \left[- \left(-C_r \gamma_r - \frac{C_r}{2} \left(\frac{\Delta r}{r_j} \gamma_r \right)^2 \right) \right] \\
& + \mathcal{C}_{i+1,j-1}^n \left[- \left(\frac{\Delta r}{2r_j} C_r^2 \gamma_r + \frac{\Delta r}{r_j} \gamma_x \gamma_r \right) \right] \\
& + \mathcal{C}_{i-2,j}^n \left[\left(-C_r \gamma_x - \frac{C_r^3}{6} + \frac{C_r}{6} \right) \right] \\
& + \mathcal{C}_{i,j-2}^n \left[\left(\frac{\Delta r}{r_j} \gamma_r^2 + \frac{\Delta r}{6r_j} \gamma_r \right) \right]
\end{aligned} \tag{2.27}$$

Equation (2.27) is somewhat cumbersome and it may be simplified by defining the following variables. These definitions also ease the programming for computation.

$$P = \left(-C_r \gamma_x - \frac{C_r^3}{6} + \frac{C_r}{6} \right) \quad (2.28)$$

$$Q = \left(\frac{\Delta r}{2r_j} C_r^2 \gamma_r + \frac{\Delta r}{r_j} \gamma_x \gamma_r \right) \quad (2.29)$$

$$R = \left(-C_r \gamma_r - \frac{C_r}{2} \left(\frac{\Delta r}{r_j} \gamma_r \right)^2 \right) \quad (2.30)$$

$$S = \left(\frac{\Delta r}{r_j} \gamma_r^2 + \frac{\Delta r}{6r_j} \gamma_r + \frac{1}{6} \left(\frac{\Delta r}{r_j} \gamma_r \right)^3 \right) \quad (2.31)$$

$$T = \frac{\Delta r}{r_j} C_r \gamma_r \quad (2.32)$$

$$A_1 = \left[-\frac{C_r}{2} + \gamma_x + \frac{C_r^2}{2} + P + Q \right] \quad (2.33)$$

$$B_1 = \left[1 - 2\gamma_r - 2\gamma_x - C_r^2 - T - \left(\frac{\Delta r}{r_j} \gamma_r \right)^2 - 3P - 2Q - 2R - 3S \right] \quad (2.34)$$

$$C_1 = \left[\frac{C_r}{2} + \gamma_x + \frac{C_r^2}{2} + T + 3P + 2R \right] \quad (2.35)$$

$$D_1 = \left[\frac{\Delta r}{2r_j} \gamma_r + \gamma_r + \frac{1}{2} \left(\frac{\Delta r}{r_j} \gamma_r \right)^2 + R + S \right] \quad (2.36)$$

$$E_1 = \left[-\frac{\Delta r}{2r_j} \gamma_r + \gamma_r + \frac{1}{2} \left(\frac{\Delta r}{r_j} \gamma_r \right)^2 + T + 2Q + R + 3S \right] \quad (2.37)$$

$$F_1 = [-T - Q - R] \quad (2.38)$$

$$\begin{aligned} C_{i,j}^{n+1} = & [A_1] C_{i+1,j}^n + [B_1] C_{i,j}^n + [C_1] C_{i-1,j}^n + [D_1] C_{i,j+1}^n + [E_1] C_{i,j-1}^n + [F_1] C_{i-1,j-1}^n \quad (2.39) \\ & + [-R] C_{i-1,j+1}^n + [-Q] C_{i+1,j-1}^n + [-P] C_{i-2,j}^n + [-S] C_{i,j-2}^n \end{aligned}$$

The scheme represented by equation (2.39) applies to every grid point in the axial and radial directions except for $i = 1, 2, nx$ and $j = 1, 2, ny$. An inlet boundary condition is applied at $i = 1, 2$ and outlet boundary condition is incorporated at $i = nx$. Moreover, a no slip boundary condition is applied at $j = ny$. As the coefficients in the expression (2.39) contains radial coordinate in the denominator, singularity may arise along the centreline where $r_j = 0$. To avoid this singularity, we apply L'Hopital's rule to the derivatives and recalculate the expressions for coefficients for node $j = 1, 2$. For this purpose, we combine the expression of TE from equation (2.24) with equation (2.7)

$$\begin{aligned}
\frac{\partial \mathcal{C}}{\partial t} + u \frac{\partial \mathcal{C}}{\partial x} = & \\
& \frac{1}{r} \left(D_m \frac{\partial \mathcal{C}}{\partial r} \right) + D_m \frac{\partial^2 \mathcal{C}}{\partial r^2} + D_m \frac{\partial^2 \mathcal{C}}{\partial x^2} + \frac{u^2 \Delta t}{2} \frac{\partial^2 \mathcal{C}}{\partial x^2} \\
& - \frac{uD_m \Delta t}{r} \frac{\partial^2 \mathcal{C}}{\partial x \partial r} + \frac{D_m^2 \Delta t}{2r^2} \frac{\partial^2 \mathcal{C}}{\partial r^2} \\
& + \left(u \frac{\Delta x^2}{6} - u^3 \frac{\Delta t^2}{6} - u D_m \Delta t \right) \frac{\partial^3 \mathcal{C}}{\partial x^3} \\
& + \left(\frac{u^2 D_m \Delta t^2}{2r} + \frac{D_m^2 \Delta t}{r} \right) \frac{\partial^3 \mathcal{C}}{\partial x^2 \partial r} \\
& + \left(-u D_m \Delta t - \frac{u D_m^2 \Delta t^2}{2r^2} \right) \frac{\partial^3 \mathcal{C}}{\partial x \partial r^2} \\
& + \left(\frac{D_m^2 \Delta t}{r} + \frac{D_m \Delta r^2}{6r} + \frac{D_m^3 \Delta t^2}{6r^3} \right) \frac{\partial^3 \mathcal{C}}{\partial r^3}
\end{aligned} \tag{2.40}$$

Applying L'Hopital's rule to the above equation,

$$\begin{aligned}
\frac{\partial \mathcal{C}}{\partial t} + u \frac{\partial \mathcal{C}}{\partial x} = & \\
& D_m \frac{\partial^2 \mathcal{C}}{\partial r^2} + D_m \frac{\partial^2 \mathcal{C}}{\partial r^2} + D_m \frac{\partial^2 \mathcal{C}}{\partial x^2} + \frac{u^2 \Delta t}{2} \frac{\partial^2 \mathcal{C}}{\partial x^2} \\
& - u D_m \Delta t \frac{\partial^3 \mathcal{C}}{\partial x \partial r^2} + \frac{D_m^2 \Delta t}{4} \frac{\partial^4 \mathcal{C}}{\partial r^4} \\
& + \left(u \frac{\Delta x^2}{6} - u^3 \frac{\Delta t^2}{6} - u D_m \Delta t \right) \frac{\partial^3 \mathcal{C}}{\partial x^3} \\
& + \left(\frac{u^2 D_m \Delta t^2}{2} + D_m^2 \Delta t \right) \frac{\partial^4 \mathcal{C}}{\partial x^2 \partial r^2} \\
& - u D_m \Delta t \frac{\partial^3 \mathcal{C}}{\partial x \partial r^2} - \frac{u D_m^2 \Delta t^2}{4r} \frac{\partial^4 \mathcal{C}}{\partial x \partial r^3} \\
& + \left(D_m^2 \Delta t + \frac{D_m \Delta r^2}{6} + \frac{D_m^3 \Delta t^2}{18r^2} \right) \frac{\partial^4 \mathcal{C}}{\partial r^4}
\end{aligned} \tag{2.41}$$

Again neglecting fourth order terms we find

$$\begin{aligned} \frac{\partial \mathcal{C}}{\partial t} + u \frac{\partial \mathcal{C}}{\partial x} &= 2D_m \frac{\partial^2 \mathcal{C}}{\partial r^2} + \left(D_m + \frac{u^2 \Delta t}{2} \right) \frac{\partial^2 \mathcal{C}}{\partial x^2} \\ &+ \left(u \frac{\Delta x^2}{6} - u^3 \frac{\Delta t^2}{6} - u D_m \Delta t \right) \frac{\partial^3 \mathcal{C}}{\partial x^3} - 2u D_m \Delta t \frac{\partial^3 \mathcal{C}}{\partial x \partial r^2} \quad (2.42) \end{aligned}$$

Discretising the derivatives in space and time, (for $j \leq 2$)

$$\begin{aligned} \mathcal{C}_{i,j}^{n+1} &= \\ &\mathcal{C}_{i,j}^n - \frac{u \Delta t}{2 \Delta x} (\mathcal{C}_{i+1,j}^n - \mathcal{C}_{i-1,j}^n) + \frac{2D_m \Delta t}{\Delta r^2} (\mathcal{C}_{i,j+1}^n - 2\mathcal{C}_{i,j}^n + \mathcal{C}_{i,j-1}^n) \\ &+ \left(\frac{D_m \Delta t}{\Delta x^2} + \frac{u^2 \Delta t^2}{2 \Delta x^2} \right) (\mathcal{C}_{i+1,j}^n - 2\mathcal{C}_{i,j}^n + \mathcal{C}_{i-1,j}^n) \\ &+ \left(\frac{u \Delta t}{6 \Delta x} - \frac{u^3 \Delta t^3}{6 \Delta x^3} - \frac{u \Delta t}{\Delta x} \frac{D_m \Delta t}{\Delta x^2} \right) (\mathcal{C}_{i+1,j}^n - 3\mathcal{C}_{i,j}^n + 3\mathcal{C}_{i-1,j}^n - \mathcal{C}_{i-2,j}^n) \\ &- 2 \frac{u \Delta t}{\Delta x} \frac{D_m \Delta t}{\Delta r^2} [(\mathcal{C}_{i,j+1}^n - 2\mathcal{C}_{i,j}^n + \mathcal{C}_{i,j-1}^n) - (\mathcal{C}_{i-1,j+1}^n - 2\mathcal{C}_{i-1,j}^n + \mathcal{C}_{i-1,j-1}^n)] \end{aligned}$$

Making use of the definition of Courant number and dimensionless diffusion coefficients as defined earlier, the above expression becomes,

$$\begin{aligned} \mathcal{C}_{i,j}^{n+1} &= \\ &\mathcal{C}_{i,j}^n - \frac{C_r}{2} (\mathcal{C}_{i+1,j}^n - \mathcal{C}_{i-1,j}^n) + 2\gamma_r (\mathcal{C}_{i,j+1}^n - 2\mathcal{C}_{i,j}^n + \mathcal{C}_{i,j-1}^n) \\ &+ \left(\gamma_x + \frac{C_r^2}{2} \right) (\mathcal{C}_{i+1,j}^n - 2\mathcal{C}_{i,j}^n + \mathcal{C}_{i-1,j}^n) \\ &+ \left(\frac{C_r}{6} - \frac{C_r^3}{6} - C_r \gamma_x \right) (\mathcal{C}_{i+1,j}^n - 3\mathcal{C}_{i,j}^n + 3\mathcal{C}_{i-1,j}^n - \mathcal{C}_{i-2,j}^n) \\ &- 2C_r \gamma_r [(\mathcal{C}_{i,j+1}^n - 2\mathcal{C}_{i,j}^n + \mathcal{C}_{i,j-1}^n) - (\mathcal{C}_{i-1,j+1}^n - 2\mathcal{C}_{i-1,j}^n + \mathcal{C}_{i-1,j-1}^n)] \end{aligned}$$

Accumulating terms, we obtain the complementary expression of concentration the next time level along the centreline as,

$$\begin{aligned}
\mathcal{C}_{i,j}^{n+1} = & \left(-\frac{C_r}{2} + \gamma_x + \frac{C_r^2}{2} + \frac{C_r}{6} - \frac{C_r^3}{6} - C_r\gamma_x \right) \mathcal{C}_{i+1,j}^n \\
& + \left(1 - 4\gamma_r - 2\gamma_x - C_r^2 - \frac{C_r}{2} + \frac{C_r^3}{2} + 3C_r\gamma_x + 4C_r\gamma_r \right) \mathcal{C}_{i,j}^n \\
& + \left(\frac{C_r}{2} + \gamma_x + \frac{C_r^2}{2} + \frac{C_r}{2} - \frac{C_r^3}{2} - 3C_r\gamma_x - 4C_r\gamma_r \right) \mathcal{C}_{i-1,j}^n \\
& + (2\gamma_r - 2C_r\gamma_r) (\mathcal{C}_{i,j-1}^n + \mathcal{C}_{i,j+1}^n) \\
& 2C_r\gamma_r (\mathcal{C}_{i-1,j-1}^n + \mathcal{C}_{i-1,j+1}^n) - \left(\frac{C_r}{6} - \frac{C_r^3}{6} - C_r\gamma_x \right) \mathcal{C}_{i-2,j}^n
\end{aligned} \tag{2.43}$$

2.4.4 Calculation of the Dispersion Coefficient

The Fickian description of the scalar dispersion in shear flow is viable after dimensionless time of 0.7. As a result, the solute transport can be characterized by an effective dispersion coefficient. The numeric value of this dispersion coefficient can be calculated from the concentration profile by fitting dispersion models of open and closed vessels developed by Levenspiel (2011). From the solution of the convection diffusion equation, we record the distribution of mean concentration (\mathcal{C}_{mean}) for the entire duration of the flow at the outlet. This curve is known as breakthrough curve which represents the concentration of the solute at a particular axial position as a function of time. Using the following numerical computation, we obtain the effective dispersion coefficient.

The mean concentration profile is calculated over the cross sectional area at a particular axial point as

$$\mathcal{C}_{mean} = \frac{1}{\pi R^2} \int_0^R 2\pi r \mathcal{C}(r) dr \quad (2.44)$$

The mean travel time or mean residence time of the solute and the variance in the solute distribution profile is calculated from

$$\bar{t} = \frac{\sum_{n=1}^{nt} t_n (\mathcal{C}_{mean})_n \Delta t_n}{\sum_{n=1}^{nt} (\mathcal{C}_{mean})_n \Delta t_n} \quad (2.45)$$

$$\sigma^2 = \frac{\sum_{n=1}^{nt} t_n^2 (\mathcal{C}_{mean})_n \Delta t_n}{\sum_{n=1}^{nt} (\mathcal{C}_{mean})_n \Delta t_n} - \bar{t}^2 \quad (2.46)$$

The dimensionless variance is fitted to the dispersion model for a closed vessel as

$$\sigma_\theta^2 = \frac{\sigma^2}{\bar{t}^2} = 2 \frac{D_L}{u_0 L} - 2 \left(\frac{D_{eff}}{u_0 L} \right) \left(1 - e^{-\frac{u_0 L}{D_L}} \right) \quad (2.47)$$

equation (2.47) provides the approximation for the effective dispersion coefficient, D_{eff} , for the solute

$$D_L \cong \frac{u_0 L}{2} \sigma_\theta^2 \quad (2.48)$$

2.4.5 Grid Sensitivity Analysis

It is essential that the spatial grid spacing and the time step provide a converged solution. Hence, ranges of grid sizes and time steps were investigated to ensure grid converged solutions.

For the grid convergence test and validation of the model, a solute was introduced as triangular shaped pulse to maintain consistency with the work of Taylor (1953). The length of the pipe was taken 15.2 cm to test the grid convergence whereas in

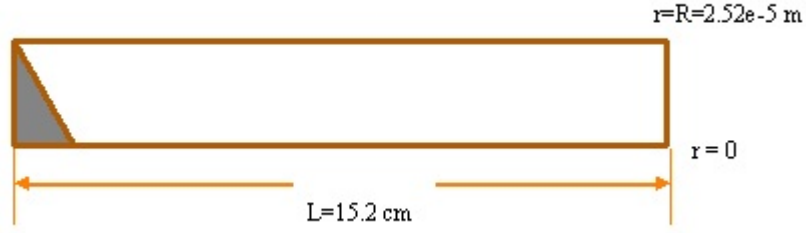


Figure 2.3: Initial condition of the solute for grid independence study

Table 2.4: Peak values of mean concentration as a function of grid points in the axial direction

Grid Resolution	10×10	20×10	40×10	60×10	80×10
Peak value of C_{mean}	0.2628	0.3037	0.3058	0.3048	0.3042
Grid Resolution	100×10	200×10	400×10	800×10	
Peak value of C_{mean}	0.3038	0.3031	0.3027	0.3025	

actual simulation it was taken same 152 cm. The radius of the pipe is 0.0252 cm in both cases.

A series of mesh sizes was tested in both the radial and axial directions to determine a suitable grid size. The final grid size is taken as the finest size of the mesh that does not cause significant variation in the numerical solution upon further refinement. For testing purposes, simulation was carried out with a tube with length 15.2 cm and radius 0.0252 cm with different number of meshes. The concentration profile of the scalar was measured at the outlet for the entire duration of the simulation. This curve is known as the breakthrough curve which represents the distribution of mean concentration of the scalar with respect to time at a particular

Table 2.5: Peak values of mean concentration for different grid resolutions in the radial direction

Grid Resolution	200×10	200×20	200×40	200×60
Peak value of C_{mean}	0.6010	0.5381	0.5105	0.5017
Grid Resolution	200×80	200×100	400×120	800×160
Peak value of C_{mean}	0.4973	0.4947	0.4930	0.4909

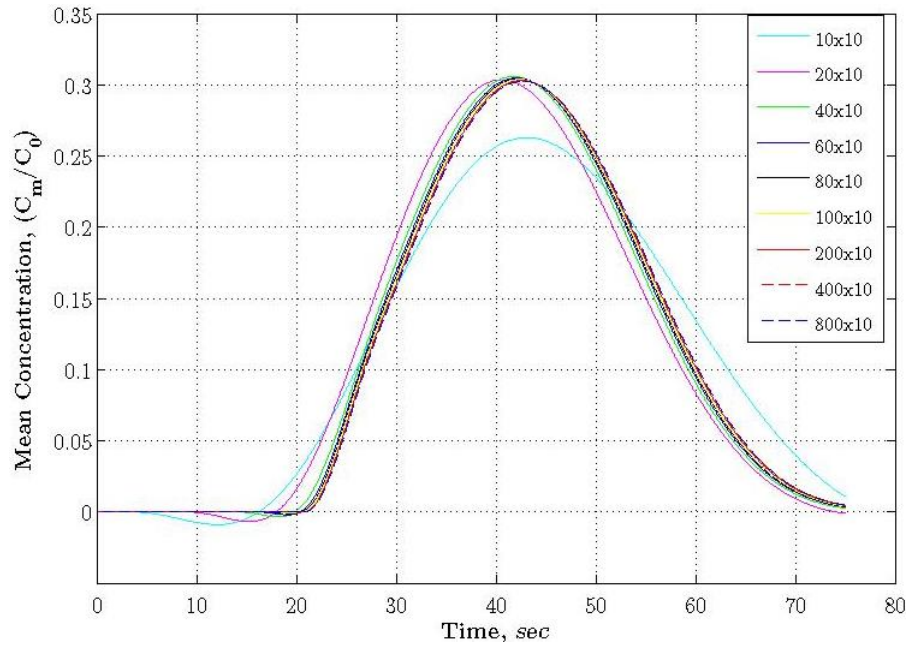


Figure 2.4: Effect of axial grid size in the mean concentration profile for solute dispersion in a pipe that is 0.152 m long and that has an internal radius of $2.52 \times 10^{-4}m$. The legend shows the variation of the number of axial grid points for a fixed radial grid size.

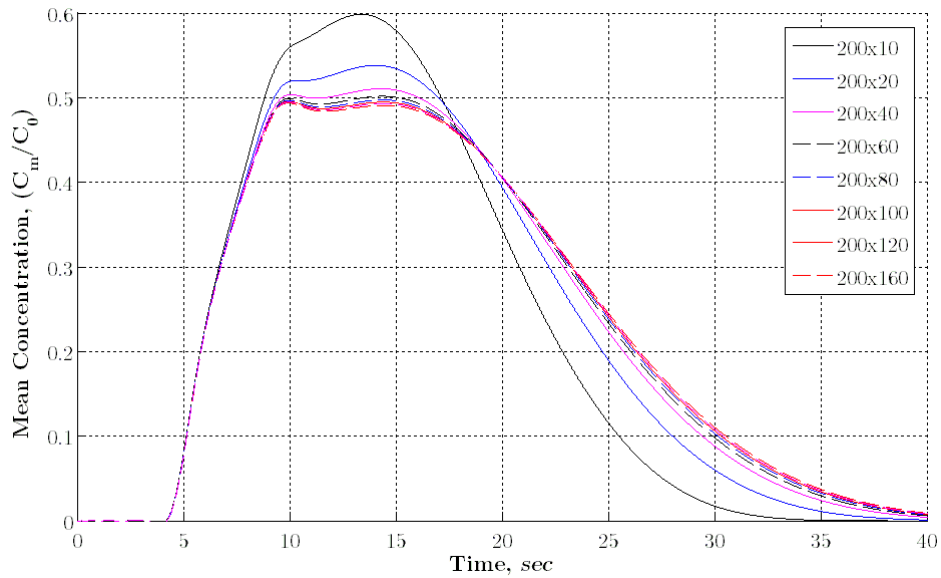


Figure 2.5: Grid independence study in radial direction for dispersion of solute in laminar flow through circular pipes. Legend represents the number of radial grid for a 15.2 cm pipe with 200 axial grid points.

Table 2.6: Peak values of mean concentration for different time step in the solution

Time step	0.005	0.0025	0.001	0.0005	0.00025	0.0001
Peak value of C_{mean}	0.4998	0.4997	0.4997	0.4997	0.4997	0.4996

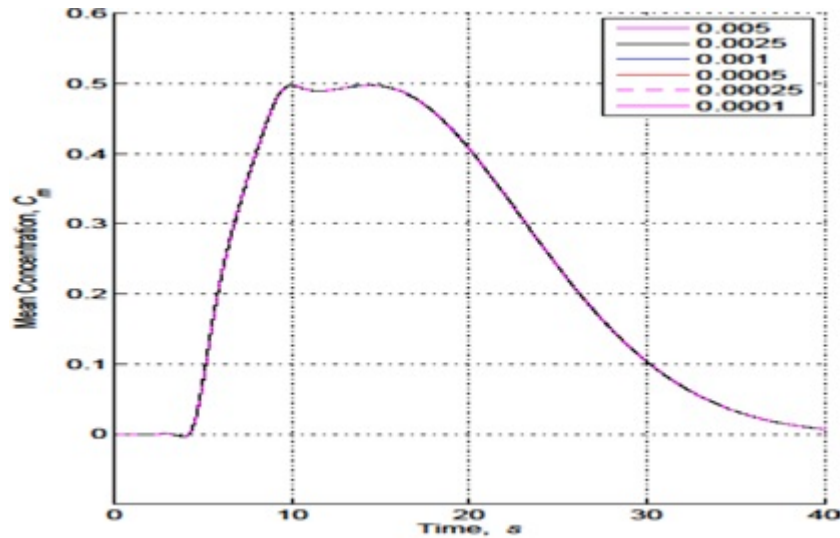


Figure 2.6: Effect of time step refinement in mean concentration of solute dispersion in a laminar flow. The legend indicates the time steps used in the simulation

point along the pipe. Simulations were carried out for various numbers of grid points in axial direction varying from 10 to 800 grids. The corresponding values of maximum mean concentration for each run are presented in Table 2.4 - Table 2.6. From Table 2.4, it can be observed that the peak value of mean concentration of scalar changes from 0.2628 to 0.3037 (a 15.56% decrease) as the mesh number increases from 10 to 20. For a further mesh refinement by increasing number of grids from 20 to 40 results in the maximum value of mean concentration changing from 0.3037 to 0.3058 (0.69% change). This corresponding change in solution reflects that further refining in axial grid size would not cause much difference to the solution. Therefore the 20 mesh points for a length of 15.2 cm will be chosen for the study. This means that the axial grid size for the entire study will be 0.76 cm.

Similarly for choosing a radial grid size, simulation performed by varying number

of meshes in radial direction from 10 to 80 and keeping constant axial grid size. The corresponding peak-mean concentration values are tabulated in Table 2.5. From the table, it is observed that $(C_{mean})_{max}$ is 0.6010 to 0.5381, 0.5105, 0.5017 and 0.4973 for numbers of grid of 10, 20, 40, and 80 showing 10.47%, 5.13%, 1.72%, 0.88% change and it plateaus with further refinement. Therefore, the number of grids taken for the simulation is 80 in the radial direction giving $\Delta r = 3.15 \times 10^{-4}$ cm.

Likewise, the effect of refining the time step was examined by carrying out simulations with time steps and starting from $\Delta t = 0.005$ s and decreasing to $\Delta t = 0.0001$ s. From the tabulated values of $(C_{mean})_{max}$ in Table 2.6, it is clear that decreasing the time step beyond 0.005 makes negligible difference to the solution. Hence Δt was chosen as 0.005s throughout the entire simulation for dispersion in laminar flow through circular pipes.

2.5 Results

2.5.1 Validation

It can be argued that the ultimate test of a numerical model is how well it represents reality. Hence, the numerical model requires validating against available experimental data. It provides confidence in the model for further studying of the evolution of scalars. The experimental result from the laminar dispersion in pipes has been used to compare the model developed with the same parameters. Figure 2.7 shows the concentration distribution of a scalar in laminar flow under the same conditions as in Taylor's experiment. With a centreline velocity of 0.33 cm/s, Taylor measured the concentration distribution along the axis after 660 s. The molecular diffusivity, D_m , was taken to be 6×10^{-6} cm²/s . Using these data, it can be seen

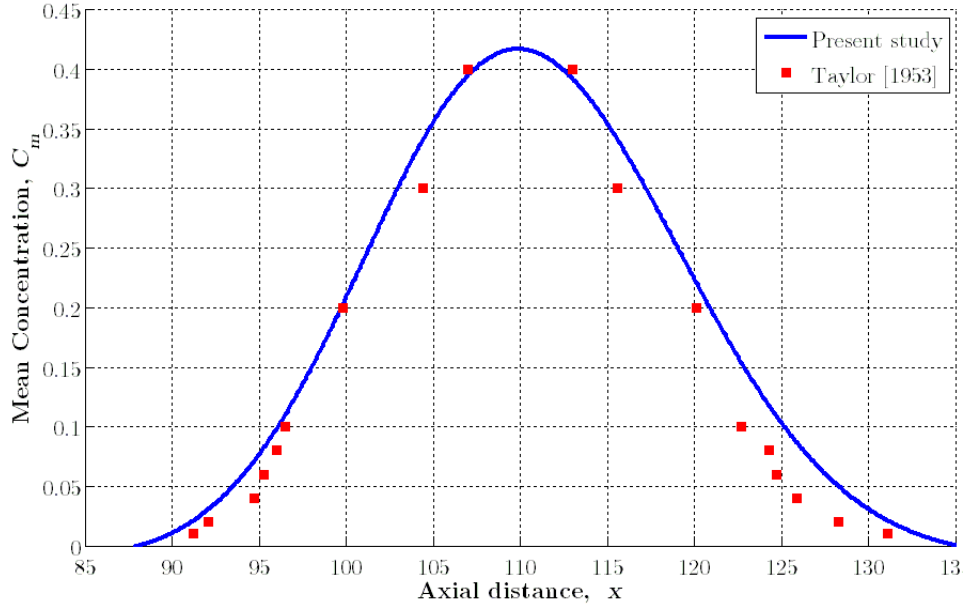


Figure 2.7: Comparison of present study with Taylor (1953)work

from Figure 2.7 that the model produces a concentration profile that concurs closely with experimental results. Importantly, the effective dispersion coefficient from the simulation result was found to $2.4720 \times 10^{-4} \text{ cm}^2/\text{s}$ which was calculated as $2.5931 \times 10^{-4} \text{ cm}^2/\text{s}$ using Taylor's method in equation (2.1)

Taylor carried out his work on a liquid medium in which the scalar was potassium permanganate dissolved in water. However to explore the validity of the model in gaseous medium it was also compared against the experimental work of Bournia et al. (1961) who used a 1,3-butadiene slug in gaseous 1-butadyne with $u_0 = 0.113 \text{ m/s}$. The breakthrough curve for dimensionless mean concentration at the downstream location at $z = 1.25 \text{ m}$ was measured. Figure 2.8 indicates excellent agreement between the results obtained from our work and the experimental results obtained by Bournia et al. (1961).

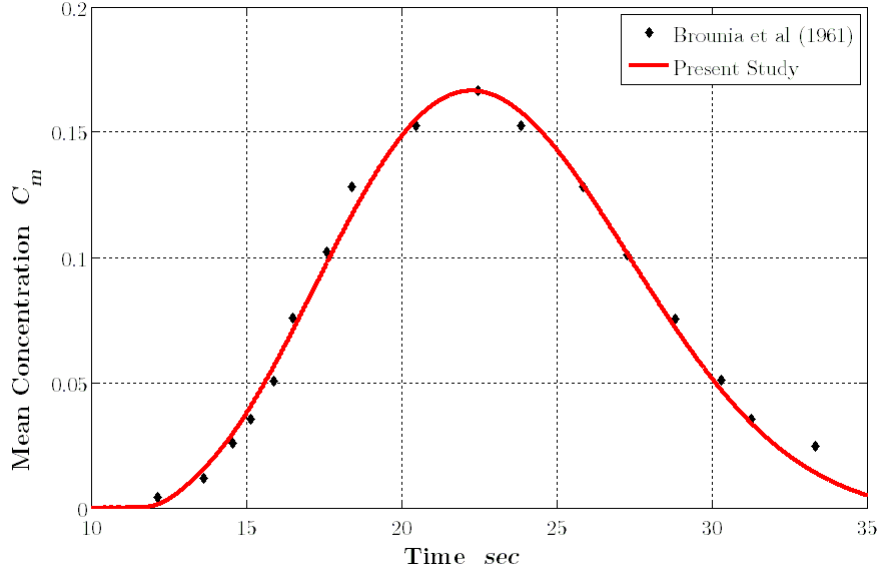


Figure 2.8: Comparison of present study with Bournia et al. (1961) results for the longitudinal dispersion of 1,3-butadiene in 1-butadiene.

2.5.2 Evolution of Concentration Profiles for Small Times

A Fickian description of longitudinal dispersion developed by Taylor does not manifest at short dimensionless times ($\tau \leq 0.7$). From a practical point of view, this condition does not seem to always be applicable. For instance, a gaseous solute typically has a molecular diffusion coefficient (at standard pressure and temperature) $0.1 \text{ cm}^2/\text{s}$. Now for the case of a scalar transport in gaseous medium in a pipe of 0.1 cm radius with a mean flow velocity 10 cm/s , time after which the Fickian description of the dispersion coefficient becomes applicable is $t = \tau R^2/D_m = (0.7 \times 0.1^2)/0.1 = 0.07 \text{ s}$ and the length of pipe after which Taylor's description conforms is $u_m \cdot t = 10 \times 0.07 \text{ cm} = 0.7 \text{ cm}$. This time and length scale where the Fickian description fails is acceptable and can be neglected in the final solution because of their small order of magnitude compared to the total distance and time transported. Therefore Taylor's theory can be readily adapted for gaseous dispersion. However the molecular diffusivity of liquids is usually 10^4 times lower than that of gases. Hence, for the same flow arrangement

mentioned above, the time required after which the Fickian type diffusivity will be able to describe the scalar spreading using an effective dispersion coefficient (in equation (2.1)) will be 700 s and the length of the pipe would be 70 m. Hence it is not practicable to use the dispersion coefficient for dispersion in liquid medium and we need a description of the evolution of concentration profile at short time. In order to present the evolution of concentration profile in early stages of dispersion phenomena, the concentration profile will be presented for various Peclet number. This representation also elucidates the relative effect of convection and diffusion in spreading of scalar at short interval after flow begins.

2.6 Relative Effect of Convection to Diffusion in Mass Transport

The effect of Peclet numbers (Pe) and dimensionless time (τ) is of practical importance when it comes to calculating dispersion. In applications, many transport phenomena are convection dominated (high Peclet number) such as pollutant transport through rivers and channels etc. At the same time many engineering processes are diffusion dominated (low Peclet number), e.g. mixing process in chemical mixing chambers, microfluidic devices etc. Most of the solutions that have been developed analytically are limited to a narrow range of Peclet numbers. These ramifications has been surmounted in the present model which agree with the existing analytical solutions for both high and low Peclet number at short as well as longer dimensionless time after the solute had injected in the flow.

2.6.1 Convection Dominated Flows: - High Peclet Number

The delimitation for high and low Peclet number can be drawn from the consideration of the effect of axial molecular diffusion on the dispersion. In diffusion dominated flow, i.e. low Peclet number, both axial, radial molecular diffusivity of the scalar have an influence on the degree of dispersion whereas in convection dominated flow, axial diffusion has a negligible effect. At high Peclet number, the short time asymptotic solution proposed by Vrentas and Vrentas (2000) is able to accurately calculating the mean concentration profile (Ekambara and Joshi, 2003). It has been demonstrated that even in convection dominated flows with a high Peclet number, diffusion can still be the prevailing mechanism of transport - provided that the duration of the flow is extremely small (Vrentas and Vrentas, 1988). This is observed from Figure 2.9 (a), at dimensionless time $\tau = 1 \times 10^{-8}$, the pure diffusive nature of the mean concentration profile calculated from this short time asymptotic solution is essentially identical with the mean concentration profile obtained from the present computational model. However, at time, $\tau = 1 \times 10^{-5}$, simulation reveals that, the transport mechanism is governed by the convection process with negligible amount of diffusion (Figure 2.9(b)). The mean concentration profile is expected to represent an asymmetric shape prior to approaching the symmetric shape at longer time described by Taylor-Aris solution. It is observed qualitatively from the short time asymptotic solution in Figure 2.9 (c); however the pronounced peak close to the trailing edge should be wider in the mean concentration profile as confirmed by Ekambara and Joshi (2003). Furthermore, the superiority of the present third order scheme over the second order scheme of Ekambara and Joshi (2003) can be observed from the leading edge of the concentration profile Figure 2.9 (c). The lower order scheme produces artificial

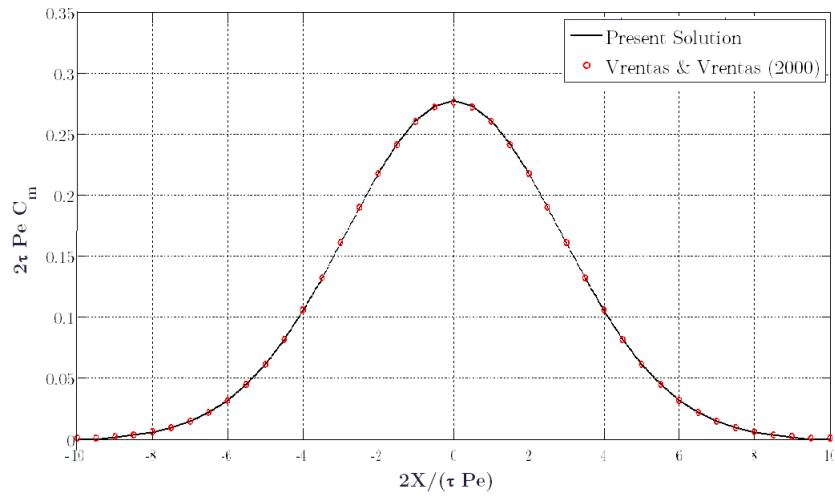
diffusion in the solution which does not exhibit in the present scheme.

The asymmetry of the mean concentration profile is maintained at early times however, the radial diffusion due to non-uniform velocity profile causes the solute to be spread uniformly. It is observed from Figure 2.10 that, at time $\tau = 0.02$ and $\tau = 0.1$ the spreading of the peak increases with time until the entire profile becomes uniform at a larger time. The comparison between existing solutions and the present work are shown for $Pe = 10000$ at $\tau = 0.02$, $\tau = 0.10$ and $\tau = 1.0$. At large time, the most elegant and accurate solution has been provided by Yu (1979). The solution obtained by the present work predicts almost identical mean concentration profile as Yu (1979) as can be seen in Figure 2.10 (a) - (c). This confirms the superiority of the present model over other models at extended time periods.

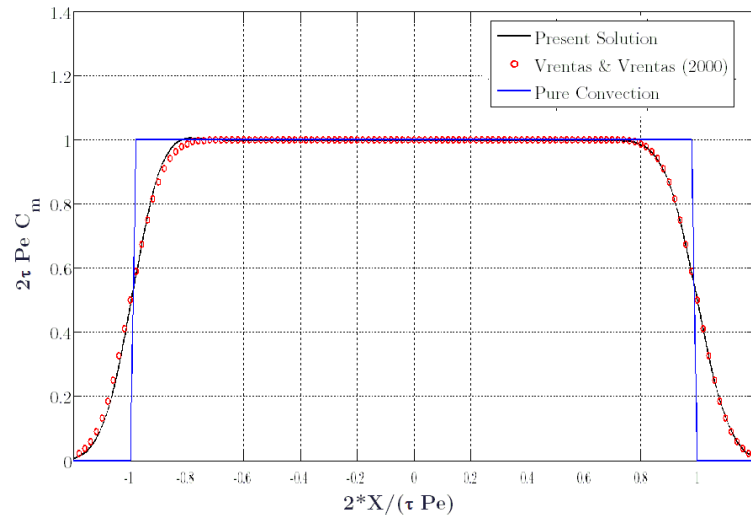
2.6.2 Diffusion Dominated Flows: - Low Peclet Number

At low Peclet numbers, the solute transport is predominated by a diffusion process. It has been shown in Figure 2.9 that at higher Peclet number, diffusion prevails only during early stage of transport process. At $\tau = 0.001$, convection appears to play role in the process. However, at low Peclet number, for example $Pe = 10$, even at this time, the concentration profile exhibits a diffusive nature that corresponds to the pure diffusion solution. From Figure 3.12, it can be observed that the present solution precisely predicts the mean concentration profile at $Pe = 10$ and $\tau = 0.001$ similar to Vrentas's short time solution and pure diffusion solution. Moreover, Taylor's solution appears to overestimate the dispersion at this range of Peclet number and time.

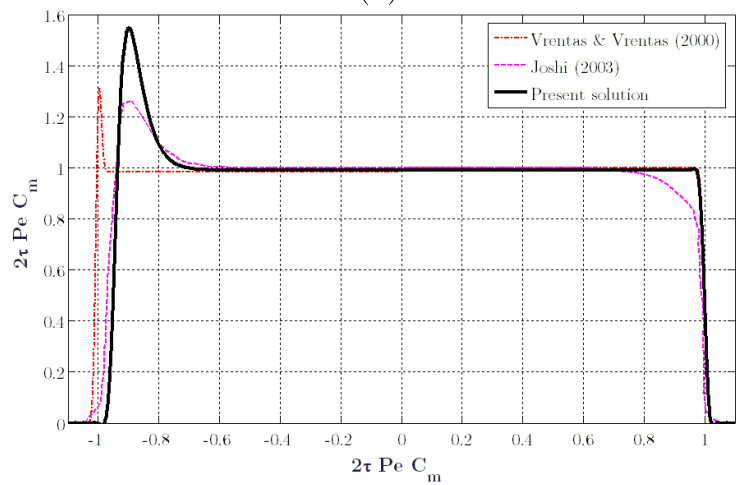
To observe the characteristics of the concentration profile simulation carried out for various low Pe (1000, 100 and 10) at a fixed dimensionless time ($\tau = 0.02$) and compared with the existing numerical and analytical results. As can be seen from



(a)

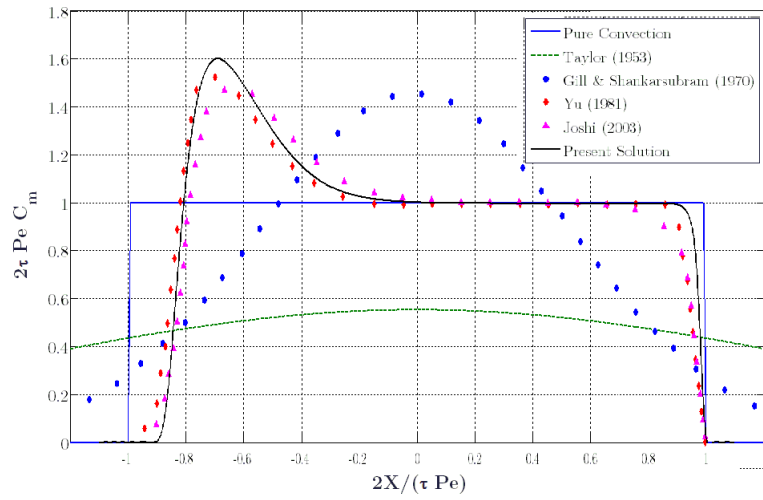


(b)

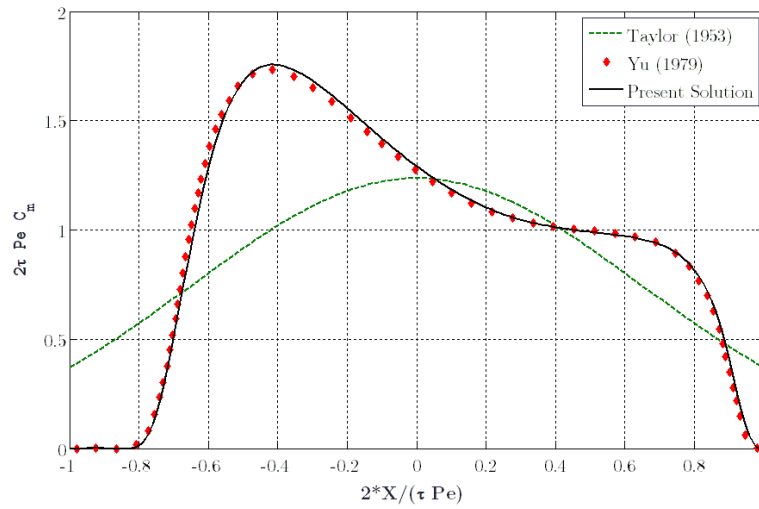


(c)

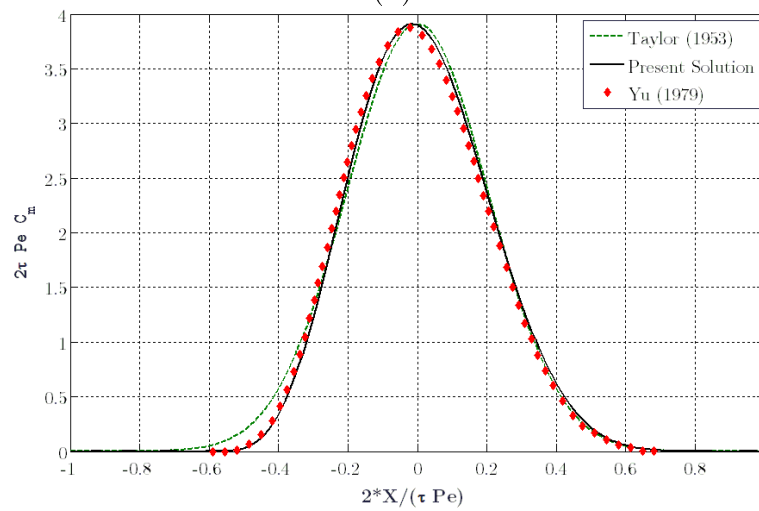
Figure 2.9: Comparisons between area-averaged concentration profiles of the solute for Peclet number (Pe) = 10000 at short durations of dimensionless time (τ). (a) $\tau = 1 \times 10^{-8}$ (b) $\tau = 1 \times 10^{-5}$ (c) $\tau = 1 \times 10^{-3}$



(a)



(b)



(c)

Figure 2.10: Comparison between area-averaged concentration profiles of the solute for Peclet number (Pe) = 10000 at extended periods of dimensionless time (τ). (a) $\tau = 0.02$, (b) $\tau = 0.1$, (c) $\tau = 1$.

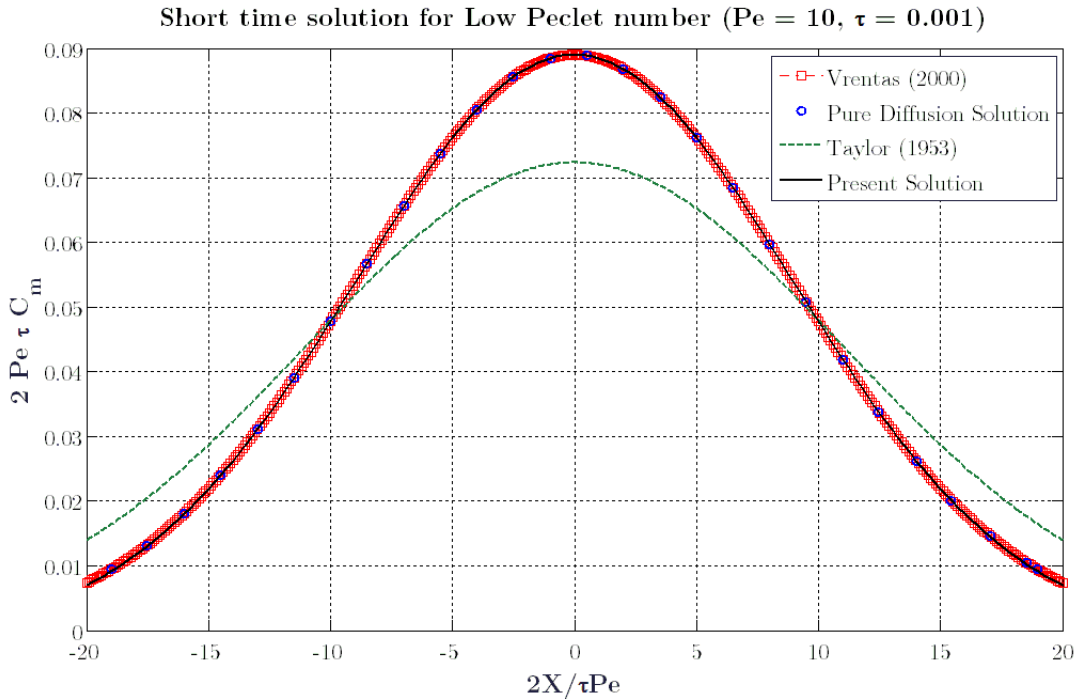


Figure 2.11: Comparison between area-averaged concentration profiles of the solute at low Peclet number $Pe = 10$; dimensionless time $\tau = 0.001$

Figure 3.13 (a) - (c), the present method predicts the distribution of solution across the cross section of the pipe beautifully. Particularly with the solution of Yu (1979), which is widely accepted as being one of the most accurate solutions at long times for solute dispersion, the present work produces essentially indistinguishable solute concentration profiles.

2.7 Summary and Conclusions

The widespread application of the convection diffusion equation in many engineering transport operations demands numerical solutions that are free from artificial diffusion arising from the differencing scheme. In this chapter, a third order spatially accurate finite difference scheme has been developed to solve the hydrodynamics dispersion of a plug of solute in laminar flow through a pipe. The merit of the scheme over

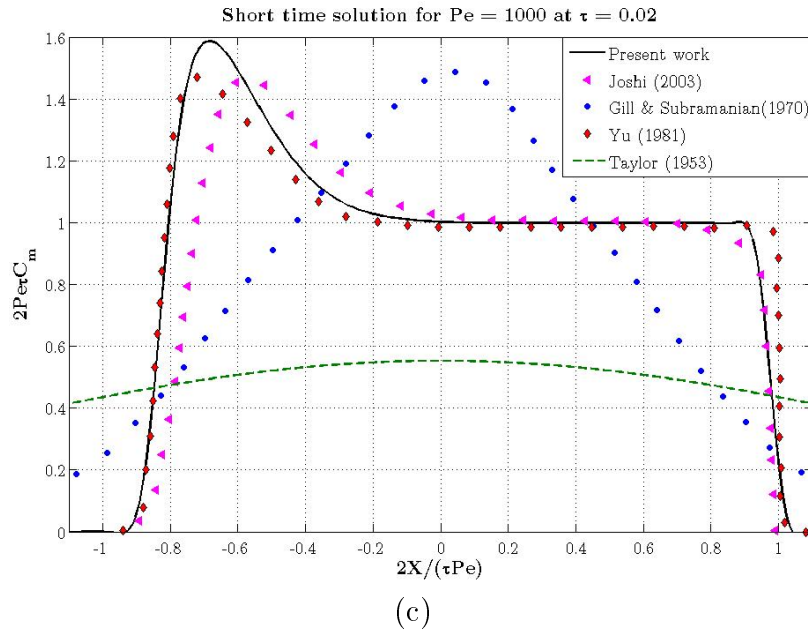
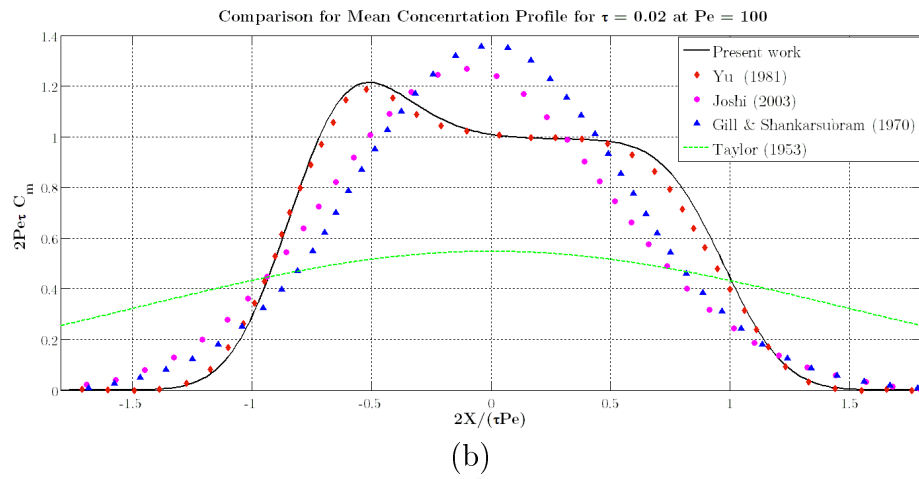
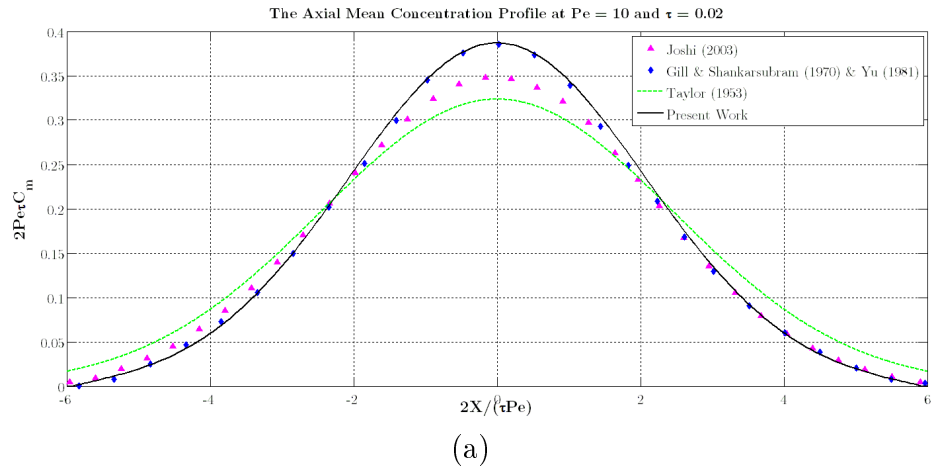


Figure 2.12: Comparison between area-averaged concentration profiles of the solute for dimensionless time $\tau = 0.02$ at different Peclet numbers (Pe) - (a) $Pe = 1000$, (b) $Pe = 100$, (c) $Pe = 10$

lower order schemes has been qualitatively and quantitatively illustrated in Appendix A by performing modified equation analysis and von-Neumann stability analysis respectively.

Numerical simulations are inherently an approximation of the solution. Hence as well as being grid independent, they requires validation. Unless they are checked for a grid independence, numerical solutions may be often unreliable and inaccurate. Therefore, prior to any numerical experiment, the scheme developed in this work was thoroughly checked to obtain a grid independence by refining the grid resolution in spatial and temporal dimension. The grid independent mesh and time resolutions have been used in the succeeding numerical simulations. Furthermore, the validation of the numerical solution has been performed by comparing the concentration profile of the solute flowing through liquids as well as gaseous media. Excellent agreement of the work presented in this chapter with experimental results provides us with confidence with the scheme to pursue further studies of dispersion in flows through pipes and ducts.

The superiority of the numerical model has been demonstrated by performing numerical experiments for the convection dominated (high Peclet number) and diffusion dominated (low Peclet number) flows at short and long times after injection of the solute in the flow. It has been found that the computational model developed in this work can predict the mean concentration profile with a high degree of accuracy over an extremely wide range of Peclet numbers along with wide ranges of time duration after the solute injection. This makes the present scheme a very general model to use for predicting the spreading of passive scalar flowing in a slowing moving fluid though circular pipes.

Chapter 3

Dispersion in Laminar Flow through Rectangular Ducts

3.1 Introduction

Axial dispersion of a passive scalar advected in a laminar flow through duct with a square cross section is governed by two physical processes. One of these processes occurs as a result of the non-uniform velocity distribution of carrier fluid in a plane normal to the direction of the flow. The second process which governs the rate of axial dispersion is molecular diffusion of the solute. Although molecular diffusion is isotropic, it is mostly diffusion in the plane normal to the mean flow direction that determines the effective, Fickian-like axial dispersion coefficient.

The analytical and experimental study of the dispersion phenomena initiated by Taylor (1953), who presented a comprehensive description of asymptotic, area averaged concentration profile for circular ducts. Taylor's work has been extended and modified afterwards for more than half a century. A surprisingly limited number

of papers are found in the literature which deals with dispersion in non-circular ducts. The ubiquitous application of circular pipes in the transport of solute attracted such attention of researchers towards studying the dispersion phenomenon in circular ducts. However, non-circular ducts, particularly square ducts, have broad range of application in heat and mass transfer in which dispersion has a profound effect. For example, pollutants and contaminants transfer in rivers and canals, smoke arising from fire inside buildings spreading by air through air conditioning ducts, effluent transport through drains etc. Therefore, a general solution approach is required to determine the concentration profile as well as effective axial dispersion coefficient in non-circular ducts.

Shear dispersion in pressure driven flow in open and closed rectangular duct with large aspect ratio¹ was analysed by Doshi et al. (1978). They showed that the dispersion coefficient in rectangular ducts with an aspect ratio approaching infinity, instead of being equal in magnitude to the two-dimensional parallel plate case, becomes larger. In fact they have demonstrated that for rectangular cross-sectional duct with arbitrarily high aspect ratio, the dispersion coefficient is 8 times higher than that for two-dimensional parallel plate arrangement where no side wall effects are present. Furthermore, they have presented the effect of aspect ratio in longitudinal dispersion for shear flow in rectangular ducts. These results are verified by Chatwin and Sullivan (1982) who proposed that the discrepancy in diffusion coefficients between high aspect ratio rectangular duct and parallel plate is due to the boundary layer effect of the side walls in rectangular cross-section. This significantly higher dispersion coefficient is a matter of concern when it is required to keep dispersion as low as possible such as in microfluidic separation and purification devices. Hence analytical studies have

¹The ratio of breadth to width of a rectangle

been reported concerning ways to reduce dispersion in rectangular geometries such as inducing transverse flow by electro-osmosis (Zhao and Bau, 2007), modifying the edge of the duct Dutta et al. (2006); Leighton and Dutta (2005), and optimizing the geometry Parks and Romero (2007).

The estimation of time dependent dispersion coefficients in laminar flow through rectangular ducts has been presented by Mauri and Haber (1991). Their analytical expression has been developed by studying the Brownian motion of typical scalar particle in the velocity field. An important observation of this study is that the dispersion coefficient is independent of the initial condition of the scalar. Furthermore, it was stated that the time dependent dispersion coefficient at long times is about 7.95 times higher than two-dimensional dispersivity. This estimation is slightly different from the estimation provided by Doshi et al. (1978). Furthermore, Ajdari et al. (2006) presented simple expression of dispersion coefficient for micro-channels with various cross-sectional shapes. These expressions relate the dispersion coefficient to the inverse aspect ratio and the effect of channel cross section has been mostly accounted by the modifying this value.

A major interest has been observed in estimating dispersion coefficients for open channels such as rivers and estuaries. Chatwin and Allen (1985) presented a comprehensive review of mathematical model developed for estimating dispersion coefficients in rivers and estuaries. Since in such cases, flow is mostly turbulent, most of these studies are reported for dispersion in turbulent flows. These studies will be discussed in forthcoming chapters for dispersion in turbulent flow. An attempt to estimate solute dispersion in using numerical approach has been reported by Wu and Falconer (2000). They developed a QUICKEST scheme combined with ULTIMATE limiter to estimate the solute flux of in estuarine waters. The approach is basically a

two-dimensional scheme in which the authors solved the three-dimensional sediment transport equation in two steps assuming two different length scales in lateral and longitudinal direction. This assumption limits the application of their approach for many engineering phenomena. For example in chemical reactors, the dispersion takes place in all direction.

A substantial study has been observed for estimating dispersion coefficients in open and closed conduits. These studies are mostly concerned with evaluating analytical expressions for estimating the degree of dispersion in non-circular duct. Furthermore, a significant effort has been made to develop expressions for estimating dispersion coefficients for ducts with modified geometries with an objective to reduce dispersion in rectangular and other non-circular ducts. However it is surprisingly noticed that, as to authors knowledge, no effort have made for numerical solution of solute dispersion in flow through non-circular duct so far. Numerical methods have been a widely popular tool for simulating fluid flow phenomena in recent decades.

With the development of modern numerical techniques, Computational Fluid Dynamics has become an indispensable tool in numerical modelling of many physical phenomena that involve fluid motion. The idea is to divide the physical domain into a number of grid points (referred as a mesh or node) and develop a set of discretized algebraic equations from the governing equation at every node using a discretization scheme. This set of linear equations is solved to get an approximate solution of the variable.

In order to discretize governing equations on various grid points, many schemes have been devised in the last few decades. However, satisfactory numerical modelling of fluid flow phenomena have always been a matter of dilemma to the researchers. The development of artificial numerical diffusion during convection of a sharp axial

discontinuity (Roache, 1972) brings a great challenge to the solution of the governing equation. Particularly the use of lower order discretization scheme such as first order upwind, central difference, hybrid differencing, Lax-Wendroff etc give rise to unwanted diffusion in the solution; especially when the initial condition is a pulse of solute across the cross-section having sharp axial concentration gradients. In order to calculate the actual spreading rate, it is very important that one should be very careful about any artificial dispersion so that it does not overestimate the actual dispersion.

The order of a discretization scheme (which, in a sense, represents the order of accuracy of the numerical scheme) is the lowest power of the variable in truncation error. Truncation error evolves as a result of approximation of derivatives from a polynomial expansion. For a discretization scheme, it is the largest truncation error of each individual derivative term in the differential equation that is being discretized. Although truncation error gives an idea of accuracy of any discretization method, it does not represent how much error appears in the solution; rather it tells us about how fast the error decreases with mesh refinement.

A simple example of how lower order discretization scheme leads to the generation artificial diffusion as well as dispersive error in the solution has been illustrated in Appendix A using modified equation representation and spectral analysis of a linear convection equation for the case of first order upwind scheme.

3.2 Modified-QUICKEST Scheme

The QUICKEST scheme was developed by Leonard (1979) originally for one-dimensional flow. In order to cope with this project, the scheme has been modified and extended to three-dimensional flow. In this work, we develop the stability criterion for this scheme and demonstrate its accuracy. This is particularly important in studying of

dispersion. As one might expect the proposed scheme gives rise to considerably less numerical dispersion than first order upwind schemes.

3.2.1 Development of the Scheme

The governing equation for dispersion of a scalar in a fluid flowing through a rectangular duct can be written as

$$\frac{\partial \mathcal{C}}{\partial t} + u(y, z) \frac{\partial \mathcal{C}}{\partial x} = D_m \left(\frac{\partial^2 \mathcal{C}}{\partial x^2} + \frac{\partial^2 \mathcal{C}}{\partial y^2} + \frac{\partial^2 \mathcal{C}}{\partial z^2} \right) \quad (3.1)$$

subject to the following initial and boundary conditions

$$\mathcal{C}(x, y, 0) = C_0 \quad (3.2)$$

$$\left. \frac{\partial \mathcal{C}}{\partial y} \right|_{y=0, L_y} = 0, \quad \left. \frac{\partial \mathcal{C}}{\partial z} \right|_{z=0, L_z} = 0 \quad (3.3)$$

Where, \mathcal{C} is the concentration of the scalar being transported by the fully developed, steady velocity field $u(y, z)$, diffused by isotropic constant diffusivity D_m . It is assumed that the scalar is convected along the axial direction only and diffusion takes place in all direction. Applying a Taylor series expansion for the derivative terms in equation (3.1), the following finite difference equation is obtained

$$\begin{aligned}
\frac{\mathcal{C}_{i,j,k}^{n+1} - \mathcal{C}_{i,j,k}^n}{\Delta t} + u(y, z) \frac{\mathcal{C}_{i+1,j,k}^n - \mathcal{C}_{i-1,j,k}^n}{2\Delta x} = \\
D_m \left(\frac{\mathcal{C}_{i+1,j,k}^n - 2\mathcal{C}_{i,j,k}^n + \mathcal{C}_{i-1,j,k}^n}{(\Delta x)^2} \right) + \\
D_m \left(\frac{\mathcal{C}_{i,j+1,k}^n - 2\mathcal{C}_{i,j,k}^n + \mathcal{C}_{i,j-1,k}^n}{(\Delta y)^2} \right) + \\
D_m \left(\frac{\mathcal{C}_{i,j,k+1}^n - 2\mathcal{C}_{i,j,k}^n + \mathcal{C}_{i,j,k-1}^n}{(\Delta z)^2} \right) + TE \quad (3.4)
\end{aligned}$$

Where, the truncation error is

$$TE = \frac{\Delta t}{2} \frac{\partial^2 \mathcal{C}}{\partial t^2} + \frac{\Delta t^2}{6} \frac{\partial^3 \mathcal{C}}{\partial t^3} + u \frac{\Delta x^2}{6} \frac{\partial^3 \mathcal{C}}{\partial x^3} + HOT \quad (3.5)$$

the *HOT* (higher order terms) contain all fourth and higher order truncation error terms, which can be neglected in this work due to the fact we specify that the scheme is third order accurate.

To eliminate the time derivative appearing in equation (3.5) differentiating equation (3.1) with respect to time gives

$$\frac{\partial^2 \mathcal{C}}{\partial t^2} + u \frac{\partial}{\partial x} \left(\frac{\partial \mathcal{C}}{\partial t} \right) = D_m \left\{ \frac{\partial^2}{\partial x^2} \left(\frac{\partial \mathcal{C}}{\partial t} \right) + \frac{\partial^2}{\partial y^2} \left(\frac{\partial \mathcal{C}}{\partial t} \right) + \frac{\partial^2}{\partial z^2} \left(\frac{\partial \mathcal{C}}{\partial t} \right) \right\} \quad (3.6)$$

Inserting $\left(\frac{\partial \mathcal{C}}{\partial t} \right)$ from equation (3.1) in the above equation and again ignoring fourth and higher order terms gives

$$\begin{aligned}
\frac{\partial^2 \mathcal{C}}{\partial t^2} + u \frac{\partial}{\partial x} \left\{ -u \frac{\partial \mathcal{C}}{\partial x} + D_m \left(\frac{\partial^2 \mathcal{C}}{\partial x^2} + \frac{\partial^2 \mathcal{C}}{\partial y^2} + \frac{\partial^2 \mathcal{C}}{\partial z^2} \right) \right\} = \\
D_m \left[\frac{\partial^2}{\partial x^2} \left\{ -u \frac{\partial \mathcal{C}}{\partial x} + D_m \left(\frac{\partial^2 \mathcal{C}}{\partial x^2} + \frac{\partial^2 \mathcal{C}}{\partial y^2} + \frac{\partial^2 \mathcal{C}}{\partial z^2} \right) \right\} \right. \\
\left. + \frac{\partial^2}{\partial y^2} \left\{ -u \frac{\partial \mathcal{C}}{\partial x} + D_m \left(\frac{\partial^2 \mathcal{C}}{\partial x^2} + \frac{\partial^2 \mathcal{C}}{\partial y^2} + \frac{\partial^2 \mathcal{C}}{\partial z^2} \right) \right\} + \right. \\
\left. \frac{\partial^2}{\partial z^2} \left\{ -u \frac{\partial \mathcal{C}}{\partial x} + D_m \left(\frac{\partial^2 \mathcal{C}}{\partial x^2} + \frac{\partial^2 \mathcal{C}}{\partial y^2} + \frac{\partial^2 \mathcal{C}}{\partial z^2} \right) \right\} \right] \quad (3.7)
\end{aligned}$$

$$\begin{aligned}
\frac{\partial^2 \mathcal{C}}{\partial t^2} + \left\{ -u^2 \frac{\partial^2 \mathcal{C}}{\partial x^2} + D_m u \left(\frac{\partial^3 \mathcal{C}}{\partial x^3} + \frac{\partial^3 \mathcal{C}}{\partial x \partial y^2} + \frac{\partial^3 \mathcal{C}}{\partial z^2 \partial x} \right) \right\} = \\
- D_m u \left(\frac{\partial^3 \mathcal{C}}{\partial x^3} - \frac{\partial^3 \mathcal{C}}{\partial x \partial y^2} - \frac{\partial^3 \mathcal{C}}{\partial z^2 \partial x} \right) + HOT \quad (3.8)
\end{aligned}$$

$$\frac{\partial^2 \mathcal{C}}{\partial t^2} = u^2 \frac{\partial^2 \mathcal{C}}{\partial x^2} - 2D_m u \left(\frac{\partial^3 \mathcal{C}}{\partial x^3} - \frac{\partial^3 \mathcal{C}}{\partial x \partial y^2} - \frac{\partial^3 \mathcal{C}}{\partial z^2 \partial x} \right) + HOT \quad (3.9)$$

$$\begin{aligned}
\frac{\partial^3 \mathcal{C}}{\partial t^3} = u^2 \frac{\partial^2}{\partial x^2} \left(\frac{\partial \mathcal{C}}{\partial t} \right) - \\
2D_m u \left\{ \frac{\partial^3}{\partial x^3} \left(\frac{\partial \mathcal{C}}{\partial t} \right) - \frac{\partial^3}{\partial x \partial y^2} \left(\frac{\partial \mathcal{C}}{\partial t} \right) - \frac{\partial^3}{\partial z^2 \partial x} \left(\frac{\partial \mathcal{C}}{\partial t} \right) \right\} \quad (3.10)
\end{aligned}$$

Further differentiating equation (3.6) with respect to time gives

$$\frac{\partial^3 \mathcal{C}}{\partial t^3} = u^2 \frac{\partial^2}{\partial x^2} \left\{ -u \frac{\partial \mathcal{C}}{\partial x} + D_m \left(\frac{\partial^2 \mathcal{C}}{\partial x^2} + \frac{\partial^2 \mathcal{C}}{\partial y^2} + \frac{\partial^2 \mathcal{C}}{\partial z^2} \right) \right\} \quad (3.11)$$

Neglecting fourth and above order terms

$$\frac{\partial^3 \mathcal{C}}{\partial t^3} = -u^3 \frac{\partial^3 \mathcal{C}}{\partial x^2} + HOT \quad (3.12)$$

Evaluating higher spatial derivatives in equation (3.6) using central differencing

$$\frac{\partial^3 \mathcal{C}}{\partial x^3} = \frac{1}{(\Delta x)^3} \{ (\mathcal{C}_{i+1,j,k}^n - 2\mathcal{C}_{i,j,k}^n + \mathcal{C}_{i-1,j,k}^n) - (\mathcal{C}_{i,j,k}^n - 2\mathcal{C}_{i-1,j,k}^n + \mathcal{C}_{i-2,j,k}^n) \} \quad (3.13)$$

$$\begin{aligned} \frac{\partial^3 \mathcal{C}}{\partial x \partial y^2} = \frac{1}{\Delta x (\Delta y)^2} \{ & (\mathcal{C}_{i,j+1,k}^n - 2\mathcal{C}_{i,j,k}^n + \mathcal{C}_{i,j-1,k}^n) \\ & - (\mathcal{C}_{i-1,j+1,k}^n - 2\mathcal{C}_{i-1,j,k}^n + \mathcal{C}_{i-1,j-1,k}^n) \} \quad (3.14) \end{aligned}$$

$$\begin{aligned} \frac{\partial^3 \mathcal{C}}{\partial x \partial z^2} = \frac{1}{\Delta x (\Delta z)^2} \{ & (\mathcal{C}_{i,k+1}^n - 2\mathcal{C}_{i,j,k}^n + \mathcal{C}_{i,j,k-1}^n) \\ & - (\mathcal{C}_{i-1,j,k+1}^n - 2\mathcal{C}_{i-1,j,k}^n + \mathcal{C}_{i-1,j,k-1}^n) \} \quad (3.15) \end{aligned}$$

Substituting these expressions into equation (3.6) and then inserting the result into equation (3.5) enables us to obtain an expression for the truncation error, TE

$$\begin{aligned} TE = \frac{\Delta t}{2} u^2 \left(\frac{\partial^2 \mathcal{C}}{\partial x^2} \right) - D_m u \Delta t \left(\frac{\partial^3 \mathcal{C}}{\partial x^3} - \frac{\partial^3 \mathcal{C}}{\partial x \partial y^2} - \frac{\partial^3 \mathcal{C}}{\partial z^2 \partial x} \right) \\ - u^3 \frac{\Delta t^2}{6} \left(\frac{\partial^3 \mathcal{C}}{\partial x^2} \right) + u \frac{\Delta x^2}{6} \left(\frac{\partial^3 \mathcal{C}}{\partial x^3} \right) \quad (3.16) \end{aligned}$$

Successive rearrangements of equation (3.16) are made, thus

$$TE = \frac{\Delta t}{2} u^2 \left(\frac{\partial^2 \mathcal{C}}{\partial x^2} \right) - D_m u \Delta t \left(\frac{\partial^3 \mathcal{C}}{\partial x^3} - \frac{\partial^3 \mathcal{C}}{\partial x \partial y^2} - \frac{\partial^3 \mathcal{C}}{\partial z^2 \partial x} \right) - u^3 \frac{\Delta t^2}{6} \left(\frac{\partial^3 \mathcal{C}}{\partial x^2} \right) + u \frac{\Delta x^2}{6} \left(\frac{\partial^3 \mathcal{C}}{\partial x^3} \right) \quad (3.17)$$

$$TE = \frac{\Delta t}{2} u^2 \left(\frac{\partial^2 \mathcal{C}}{\partial x^2} \right) + D_m u \Delta t \left(\frac{\partial^3 \mathcal{C}}{\partial x \partial y^2} + \frac{\partial^3 \mathcal{C}}{\partial z^2 \partial x} \right) + \left(-D_m u \Delta t - u^3 \frac{\Delta t^2}{6} + u \frac{\Delta x^2}{6} \right) \frac{\partial^3 \mathcal{C}}{\partial x^3} \quad (3.18)$$

The discretized for of equation (3.18) can be written as,

$$\begin{aligned} TE = & u^2 \frac{\Delta t}{2 (\Delta x)^2} (\mathcal{C}_{i+1,j,k}^n - 2\mathcal{C}_{i,j,k}^n + \mathcal{C}_{i-1,j,k}^n) - \\ & \frac{uD_m \Delta t}{\Delta x (\Delta y)^2} \{ (\mathcal{C}_{i,j+1,k}^n - 2\mathcal{C}_{i,j,k}^n + \mathcal{C}_{i,j-1,k}^n) \\ & - (\mathcal{C}_{i-1,j+1,k}^n - 2\mathcal{C}_{i-1,j,k}^n + \mathcal{C}_{i-1,j-1,k}^n) \} \\ & + \frac{uD_m \Delta t}{\Delta x (\Delta z)^2} \{ (\mathcal{C}_{i,j,k+1}^n - 2\mathcal{C}_{i,j,k}^n + \mathcal{C}_{i,j,k-1}^n) \\ & - (\mathcal{C}_{i-1,j,k+1}^n - 2\mathcal{C}_{i-1,j,k}^n + \mathcal{C}_{i-1,j,k-1}^n) \} \\ & + \left(-D_m u \Delta t - u^3 \frac{\Delta t^2}{6} + u \frac{\Delta x^2}{6} \right) \frac{1}{(\Delta x)^3} \\ & \{ (\mathcal{C}_{i+1,j,k}^n - 2\mathcal{C}_{i,j,k}^n + \mathcal{C}_{i-1,j,k}^n) \\ & - (\mathcal{C}_{i,j,k}^n - 2\mathcal{C}_{i-1,j,k}^n + \mathcal{C}_{i-2,j,k}^n) \} \quad (3.19) \end{aligned}$$

Let us define the Courant number, $C_r = \frac{u\Delta t}{\Delta x}$ along with dimensionless diffusion coefficient in respective directions $\gamma_x = \frac{D_m\Delta t}{(\Delta x)^2}$, $\gamma_y = \frac{D_m\Delta t}{(\Delta y)^2}$, and $\gamma_z = \frac{D_m\Delta t}{(\Delta z)^2}$. This enables us to write

$$\begin{aligned}
TE = & \frac{1}{\Delta t} \left[\frac{C_r^2}{2} (\mathcal{C}_{i+1,j,k}^n - 2\mathcal{C}_{i,j,k}^n + \mathcal{C}_{i-1,j,k}^n) - \right. \\
& C_r \gamma_y \{ (\mathcal{C}_{i,j+1,k}^n - 2\mathcal{C}_{i,j,k}^n + \mathcal{C}_{i,j-1,k}^n) \\
& \quad - (\mathcal{C}_{i-1,j+1,k}^n - 2\mathcal{C}_{i-1,j,k}^n + \mathcal{C}_{i-1,j-1,k}^n) \} \\
& - C_r \gamma_z \{ (\mathcal{C}_{i,k+1}^n - 2\mathcal{C}_{i,j,k}^n + \mathcal{C}_{i,j,k-1}^n) \\
& \quad - (\mathcal{C}_{i-1,j,k+1}^n - 2\mathcal{C}_{i-1,j,k}^n + \mathcal{C}_{i-1,j,k-1}^n) \} \\
& \left. \left(-C_r \gamma_x - \frac{C_r^3}{6} + \frac{C_r}{6} \right) \{ (\mathcal{C}_{i+1,j,k}^n - 2\mathcal{C}_{i,j,k}^n + \mathcal{C}_{i-1,j,k}^n) \right. \\
& \quad \left. - (\mathcal{C}_{i,j,k}^n - 2\mathcal{C}_{i-1,j,k}^n + \mathcal{C}_{i-2,j,k}^n) \} \right] \tag{3.20}
\end{aligned}$$

Substituting expression of TE from equation (3.20) into equation (3.4) results in

$$\begin{aligned}
& \frac{\mathcal{C}_{i,j,k}^{n+1} - \mathcal{C}_{i,j,k}^n}{\Delta t} + u \frac{\mathcal{C}_{i+1,j,k}^n - \mathcal{C}_{i-1,j,k}^n}{2\Delta x} = \\
& D_m \left\{ \left(\frac{\mathcal{C}_{i+1,j,k}^n - 2\mathcal{C}_{i,j,k}^n + \mathcal{C}_{i-1,j,k}^n}{(\Delta x)^2} \right) \right. \\
& \left(\frac{\mathcal{C}_{i,j+1,k}^n - 2\mathcal{C}_{i,j,k}^n + \mathcal{C}_{i,j-1,k}^n}{(\Delta y)^2} \right) \\
& \left. \left(\frac{\mathcal{C}_{i,j,k+1}^n - 2\mathcal{C}_{i,j,k}^n + \mathcal{C}_{i,j,k-1}^n}{(\Delta z)^2} \right) \right\} \\
& \frac{1}{\Delta t} \left[\frac{C_r^2}{2} (\mathcal{C}_{i+1,j,k}^n - 2\mathcal{C}_{i,j,k}^n + \mathcal{C}_{i-1,j,k}^n) \right. \\
& - C_r \gamma_y (\mathcal{C}_{i,j+1,k}^n - 2\mathcal{C}_{i,j,k}^n + \mathcal{C}_{i,j-1,k}^n \\
& - \mathcal{C}_{i,j,k+1}^n + 2\mathcal{C}_{i,j,k}^n - \mathcal{C}_{i,j,k-1}^n) \\
& - C_r \gamma_z (\mathcal{C}_{i,j,k+1}^n - 2\mathcal{C}_{i,j,k}^n + \mathcal{C}_{i,j,k-1}^n \\
& - \mathcal{C}_{i+1,j,k}^n + 2\mathcal{C}_{i,j,k}^n - \mathcal{C}_{i-1,j,k}^n) \\
& + \left(-C_r \gamma_x - \frac{C_r^3}{6} + \frac{C_r}{6} \right) \{ (\mathcal{C}_{i+1,j,k}^n - 2\mathcal{C}_{i,j,k}^n + \mathcal{C}_{i-1,j,k}^n) \\
& \left. - (\mathcal{C}_{i,j,k}^n - 2\mathcal{C}_{i-1,j,k}^n + \mathcal{C}_{i-2,j,k}^n) \} \right]
\end{aligned}$$

$$\begin{aligned}
\mathcal{C}_{i,j,k}^{n+1} &= \mathcal{C}_{i,j,k}^n - \frac{C_r}{2} (\mathcal{C}_{i+1,j,k}^n - \mathcal{C}_{i-1,j,k}^n) \\
&+ \gamma_x (\mathcal{C}_{i+1,j,k}^n - 2\mathcal{C}_{i,j,k}^n + \mathcal{C}_{i-1,j,k}^n) + \gamma_y (\mathcal{C}_{i,j+1,k}^n - 2\mathcal{C}_{i,j,k}^n + \mathcal{C}_{i,j-1,k}^n) \\
&+ \gamma_z (\mathcal{C}_{i,j,k+1}^n - 2\mathcal{C}_{i,j,k}^n + \mathcal{C}_{i,j,k-1}^n) + \left[\frac{C_r^2}{2} (\mathcal{C}_{i+1,j,k}^n - 2\mathcal{C}_{i,j,k}^n + \mathcal{C}_{i-1,j,k}^n) \right. \\
&- C_r \gamma_y (\mathcal{C}_{i,j+1,k}^n - 2\mathcal{C}_{i,j,k}^n + \mathcal{C}_{i,j-1,k}^n - \mathcal{C}_{i-1,j+1,k}^n + 2\mathcal{C}_{i-1,j,k}^n - \mathcal{C}_{i-1,j-1,k}^n) \\
&- C_r \gamma_z (\mathcal{C}_{i,j,k+1}^n - 2\mathcal{C}_{i,j,k}^n + \mathcal{C}_{i,j,k-1}^n - \mathcal{C}_{i-1,j,k+1}^n + 2\mathcal{C}_{i-1,j,k}^n - \mathcal{C}_{i-1,j,k-1}^n) \\
&+ \left(-C_r \gamma_x - \frac{C_r^3}{6} + \frac{C_r}{6} \right) \left\{ (\mathcal{C}_{i+1,j,k}^n - 2\mathcal{C}_{i,j,k}^n + \mathcal{C}_{i-1,j,k}^n) \right. \\
&\left. - (\mathcal{C}_{i,j,k}^n - 2\mathcal{C}_{i-1,j,k}^n + \mathcal{C}_{i-2,j,k}^n) \right\} \left. \right] \tag{3.21}
\end{aligned}$$

Collecting terms yields

$$\begin{aligned}
\mathcal{C}_{i,j,k}^{n+1} &= \mathcal{C}_{i,j,k}^n + \mathcal{C}_{i+1,j,k}^n \left(-\frac{C_r^3}{6} + \frac{C_r^2}{2} - \frac{C_r}{3} + \gamma_x - C_r \gamma_x \right) \\
&+ \mathcal{C}_{i,j,k}^n \left(\frac{C_r^3}{2} - C_r^2 - \frac{C_r}{2} + 3C_r \gamma_x + 2C_r \gamma_y + 2C_r \gamma_z - 2\gamma_x - 2\gamma_y - 2\gamma_z \right) \\
&+ \mathcal{C}_{i-1,j,k}^n \left(-\frac{C_r^3}{2} + \frac{C_r^2}{2} + C_r - 3C_r \gamma_x - 2C_r \gamma_y - 2C_r \gamma_z + \gamma_x \right) \\
&+ \mathcal{C}_{i-2,j,k}^n \left(-\frac{C_r}{6} + C_r \gamma_x + \frac{C_r^3}{6} \right) + \mathcal{C}_{i,j+1,k}^n (\gamma_y - C_r \gamma_y) \\
&+ \mathcal{C}_{i,j-1,k}^n (\gamma_y - C_r \gamma_y) + \mathcal{C}_{i,j,k+1}^n (-\gamma_z - C_r \gamma_z) \\
&+ \mathcal{C}_{i,j,k-1}^n (-\gamma_z - C_r \gamma_z) + \mathcal{C}_{i-1,j+1,k}^n (C_r \gamma_y) \\
&+ \mathcal{C}_{i-1,j-1,k}^n (C_r \gamma_y) + \mathcal{C}_{i-1,j,k+1}^n (C_r \gamma_z) + \mathcal{C}_{i-1,j,k-1}^n (C_r \gamma_z) \tag{3.22}
\end{aligned}$$

3.3 Stability Analysis

Numerical solutions must be not only accurate but also stable. Stability refers to a condition in the numerical solution which ensures all errors must remain bounded as the iteration process progresses i.e. for finite values of Δt and Δx , the error has to remain bounded when the number of time steps tends to infinity (Hirsch, 2007).

If the error, $\bar{\epsilon}^n = \mathcal{C}_i^n - \overline{\mathcal{C}_i^n}$ is the difference between the computed solution, \mathcal{C}_i^n and the exact solution of the discretized equation, $\overline{\mathcal{C}_i^n}$ the stability condition requires that

$$\lim_{n \rightarrow \infty} |\bar{\epsilon}^n| \leq k \quad \text{at fixed } \Delta t \quad (3.23)$$

Here k is a constant independent of n

In order to establish stability criteria as well as quantify the numerical diffusion arising from the modified QUICKEST scheme developed in this work we use Von Neumann Stability Analysis as discussed in Appendix A. We decompose the solution from a finite mesh into finite Fourier series and then calculate the amplification factor, \mathcal{G} , as follows-

$$\begin{aligned}
\mathcal{G} &= \frac{\Phi_{p,q,r}^{n+1}}{\Phi_{p,q,r}^n} \\
&= \left(1 + 3C_r\gamma_x - 2\gamma_x - 2\gamma_y - 2\gamma_z - \frac{C_r}{2} + 2C_r\gamma_y + 2C_r\gamma_z - C_r^2 + \frac{C_r^3}{2} \right) \\
&\quad + \left(\gamma_x - \frac{C_r}{3} - C_r\gamma_x + \frac{C_r^2}{2} - \frac{C_r^3}{6} \right) e^{i\varphi_x} \\
&\quad + \left(-\frac{C_r^3}{2} + \frac{C_r^2}{2} + Cr - 3C_r\gamma_x - 2C_r\gamma - 2C_r\gamma + \gamma_x \right) e^{-i\varphi_x} \\
&\quad + (\gamma_y - C_r\gamma) (e^{i\varphi_y} + e^{-i\varphi_y}) + (-\gamma_z - C_r\gamma) (e^{i\varphi_z} + e^{-i\varphi_z}) \\
&\quad + C_r\gamma e^{-i\varphi_x} (e^{i\varphi_y} + e^{-i\varphi_y}) + C_r\gamma e^{-i\varphi_x} (e^{i\varphi_z} + e^{-i\varphi_z}) \\
&\quad + \left(-\frac{Cr}{6} + C_r\gamma + \frac{C_r^3}{6} \right) e^{-2i\varphi_x}
\end{aligned}$$

Collecting the coefficients of the exponents and rearranging the leading terms,

$$\begin{aligned}
\mathcal{G} &= \left(1 + \frac{C_r^3}{2} - C_r^2 - \frac{C_r}{2} + 3C_r\gamma_x + 2C_r\gamma_y + 2C_r\gamma_z - 2\gamma_x - 2\gamma_y - 2\gamma_z \right) \\
&\quad + \left(\gamma_x - \frac{C_r}{3} - C_r\gamma_x + \frac{C_r^2}{2} - \frac{C_r^3}{6} \right) e^{i\varphi_x} \\
&\quad + \left(-\frac{Cr^3}{2} + \frac{Cr^2}{2} + Cr - 3C_r\gamma - 2C_r\gamma - 2C_r\gamma_z + \gamma_x \right) e^{-i\varphi_x} \\
&\quad + (\gamma_y - C_r\gamma + C_r\gamma e^{-i\varphi_x}) (e^{i\varphi_y} + e^{-i\varphi_y}) \\
&\quad + (-\gamma_z - C_r + C_r\gamma e^{-i\varphi_x}) (e^{i\varphi_z} + e^{-i\varphi_z}) \\
&\quad + \left(-\frac{Cr}{6} + C_r + \frac{C_r^3}{6} \right) e^{-2i\varphi_x}
\end{aligned}$$

Recognizing from Euler's formula namely $e^{i\theta} = \cos\theta + i\sin\theta$ or $e^{-i\theta} = \cos\theta - i\sin\theta$

and separating the real and imaginary parts of the amplification factor yields

$$\begin{aligned}
\text{Real}(\mathcal{G}) &= 1 + 3C_r\gamma_x - 2\gamma_x - 2\gamma_y - 2\gamma_z - \frac{C_r}{2} + 2C_r\gamma_y + 2C_r\gamma_z \\
&\quad - \cos\varphi_x \left(4C_r\gamma_x - 2\gamma_x - \frac{2C_r}{3} + 2C_r\gamma_y + 2C_r\gamma_z - C_r^2 + \frac{2C_r^3}{3} \right) \\
&\quad + \cos\varphi_y (2\gamma_y - 2C_r\gamma_y) + \cos\varphi_z (2\gamma_z - 2C_r\gamma_z) \\
&\quad + \cos 2\varphi_x \left(C_r\gamma_x - \frac{C_r}{6} + \frac{C_r^3}{6} \right) - C_r^2 + \frac{C_r^3}{2} \\
&\quad + 2C_r\gamma_y \cos\varphi_x \cos\varphi_y + 2C_r\gamma_z \cos\varphi_x \cos\varphi_z
\end{aligned}$$

$$\begin{aligned}
\text{Imaginary}(\mathcal{G}) &= \sin\varphi_x \left(2C_r\gamma_x - \frac{4C_r}{3} + 2C_r\gamma_y + 2C_r\gamma_z + \frac{C_r^3}{3} \right) \\
&\quad - \sin 2\varphi_x \left(C_r\gamma_x - \frac{C_r}{6} + \frac{C_r^3}{6} \right) - \\
&\quad 2C_r\gamma_y \cos\varphi_y \sin\varphi_x - 2C_r\gamma_z \cos\varphi_z \sin\varphi_x
\end{aligned}$$

Therefore the magnitude of the modulus of amplification factor becomes

$$\begin{aligned}
|\mathcal{G}| = & \left[\left\{ 3C_r\gamma_x - 2\gamma_x - 2\gamma_y - 2\gamma_z - \frac{C_r}{2} + 2C_r\gamma_y + 2C_r\gamma_z \right. \right. \\
& - \cos\varphi_x \left(4C_r\gamma_x - 2\gamma_x - \frac{2C_r}{3} + 2C_r\gamma_y + 2C_r\gamma_z - C_r^2 + \frac{2C_r^3}{3} \right) \\
& + \cos\varphi_y (2\gamma_y - 2C_r\gamma_y) + \cos\varphi_z (2\gamma_z - 2C_r\gamma_z) \\
& + \cos 2\varphi_x \left(C_r\gamma_x - \frac{C_r}{6} + \frac{C_r^3}{6} \right) - C_r^2 + \frac{C_r^3}{2} \\
& \left. \left. + 2C_r\gamma_y \cos\varphi_x \cos\varphi_y + 2C_r\gamma_z \cos\varphi_x \cos\varphi_z + 1 \right\}^2 \right. \\
& \left. - \left(\sin 2\varphi_x C_r\gamma_x - \frac{C_r}{6} + \frac{C_r^3}{6} \right) \right. \\
& - \sin\varphi_x \left(2C_r\gamma_x - \frac{4C_r}{3} + 2C_r\gamma_y + 2C_r\gamma_z + \frac{C_r^3}{3} \right) \\
& \left. \left. + 2C_r\gamma_y \cos\varphi_y \sin\varphi_x + 2C_r\gamma_z \cos\varphi_z \sin\varphi_x \right\}^2 \right]^{\frac{1}{2}} \quad (3.24)
\end{aligned}$$

Considering the highest resolvable wave, for which the phase angles in corresponding directions are $\varphi_x = \varphi_y = \varphi_z = \pi$, the amplification factor becomes after simplifying

$$\begin{aligned}
|\mathcal{G}| = \frac{1}{3} & \left[16C_r^6 - 48C_r^5 + 192C_r^4\gamma_x + 192C_r^4\gamma_y + 192C_r^4\gamma_z + 4C_r^4 \right. \\
& - 384C_r^3\gamma_x - 384C_r^3\gamma_y - 384C_r^3\gamma_z + 72C_r^3 + 576C_r^2\gamma_x^2 + 1152C_r^2\gamma_x\gamma_y \\
& + 1152C_r^2\gamma_x\gamma_z - 48C_r^2\gamma_x + 576C_r^2\gamma_y^2 + 1152C_r^2\gamma_y\gamma_z - 48C_r^2\gamma_y \\
& + 576C_r^2\gamma_z^2 - 48C_r^2\gamma_z - 20C_r^2 - 576C_r\gamma_x^2 - 1152C_r\gamma_x\gamma_y \\
& - 1152C_r\gamma_x\gamma_z + 240C_r\gamma_x - 576C_r\gamma_y^2 - 1152C_r\gamma_y\gamma_z \\
& + 240C_r\gamma_y - 576C_r\gamma_z^2 + 240C_r\gamma_z - 24C_r \\
& + 144\gamma_x^2 + 288\gamma_x\gamma_y + 288\gamma_x\gamma_z - 72\gamma_x + 144\gamma_y^2 \\
& \left. + 288\gamma_y\gamma_z - 72\gamma_y + 144\gamma_z^2 - 72\gamma_z + 9 \right]^{\frac{1}{2}}
\end{aligned}$$

Further simplification results in the following expression

$$|\mathcal{G}| = 1 + 8C_r\gamma_x + 8C_r\gamma_y + 8C_r\gamma_z - \frac{4C_r}{3} - 2C_r^2 + \frac{4C_r^3}{3} - 4\gamma_x - 4\gamma_y - 4\gamma_z \quad (3.25)$$

For $\gamma_x = \gamma_y = \gamma_z = \gamma$

$$|\mathcal{G}| = 1 + 24C_r\gamma - \frac{4C_r}{3} - 2C_r^2 + \frac{4C_r^3}{3} - 12\gamma \quad (3.26)$$

For stability, $|\mathcal{G}| \leq 1$ hence

$$24C_r\gamma - \frac{4C_r}{3} - 2C_r^2 + \frac{4C_r^3}{3} - 12\gamma < 0 \quad (3.27)$$

or

$$24C_r\gamma - 12\gamma \leq \frac{4C_r}{3} + \frac{6C_r^2}{3} - \frac{4C_r^3}{3} \quad (3.28)$$

Hence

$$\gamma \leq \frac{2C_r + 3C_r^2 - 2C_r^3}{36C_r - 18} \quad (3.29)$$

Or

$$\gamma \leq \frac{1}{12} \left(1 + \frac{1}{2C_r - 1} \right) + \frac{1}{18} (C_r - C_r^2) \quad (3.30)$$

In order to compare this with the first order upwind scheme for linear convection with no diffusion, (i.e. $\gamma = 0$), the stability requires

$$0 \leq 2C_r + 3C_r^2 - 2C_r^3 \quad (3.31)$$

or

$$C_r \leq \frac{1}{2} \quad (3.32)$$

To observe the diffusion error for the above scheme, we plot equation (3.24), $|\mathcal{G}| = f(\varphi_x)$ for constant $\gamma_x = \gamma_y = \gamma_z = 0.02$ and $\varphi_y = \varphi_z = \pi$ for different Courant numbers in Figure 3.1. In order to have accurate solution with no artificial diffusion error, the amplification factor $|\mathcal{G}|$ has to be as close as possible to unity. From Figure 3.1, it can be observed that the developed scheme possesses this characteristic in the low frequency region.

A closer inspection to the diffusion error for first order upwind scheme and modified QUICKEST developed scheme at the low frequency region in Figure 3.2 and

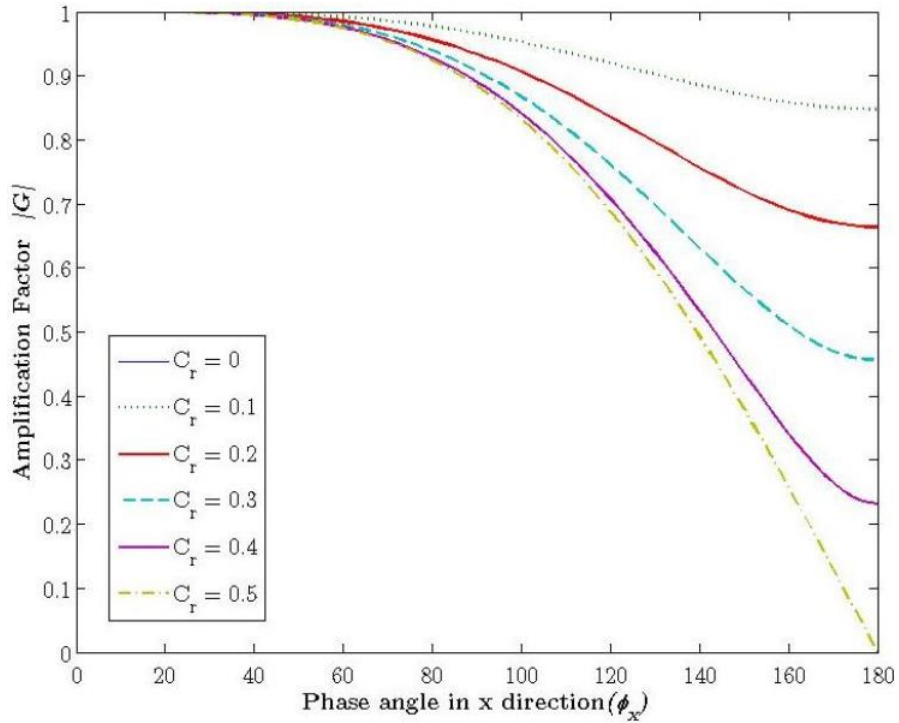


Figure 3.1: Amplification factor as a function of phase angle in axial direction for the modified QUICKEST scheme developed in this work

Figure 3.3 reveals that the diffusion is significantly higher in first order upwind in compare to the modified QUICKEST scheme developed in this work. The amplitude of the initial harmonic can be quantified by $|G|^n$ after n time steps. Hence, as time progresses, the first order upwind scheme tends to contribute significant numerical diffusion to the solution whereas the proposed scheme generates comparatively less artificial diffusion, particularly for small Courant numbers

Finally from a numerical simulation of linear convection of two different pulses in a one dimensional domain of length 1 m with Courant number $C_r = \frac{1}{3}$ and periodic boundary conditions, the comparative representation of the solution from first order upwind (FOU), QUICKEST and exact solution is illustrated in Figure 3.4.

The simulation after one complete cycle in the periodic boundary condition will bring both initial pulses at their original position because it is a linear convection phe-

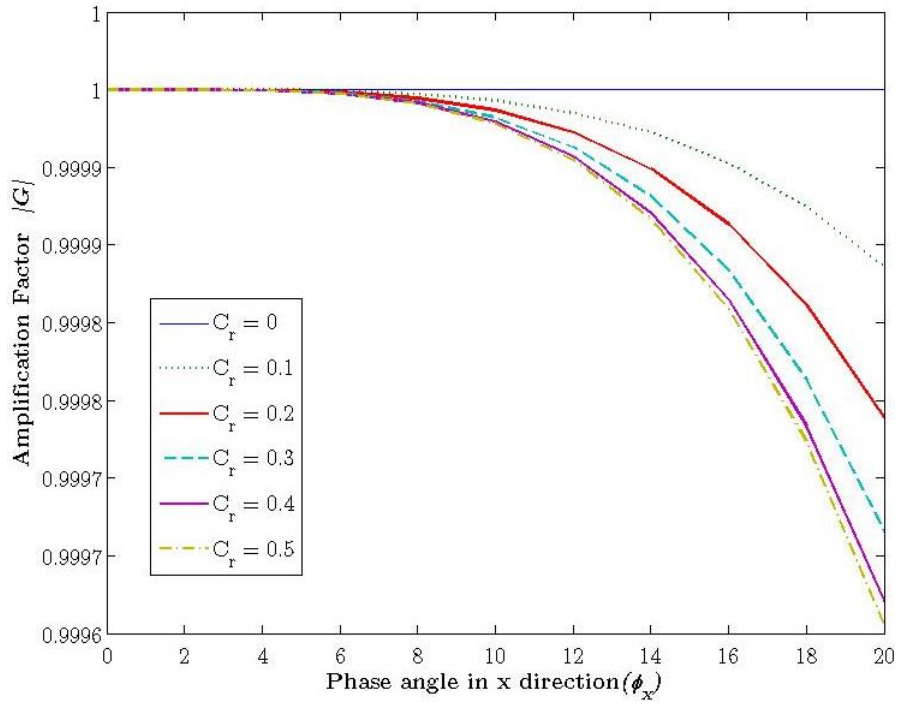


Figure 3.2: Enlarged view of diffusion error in the low frequency regions for the modified QUICKEST scheme developed in this work

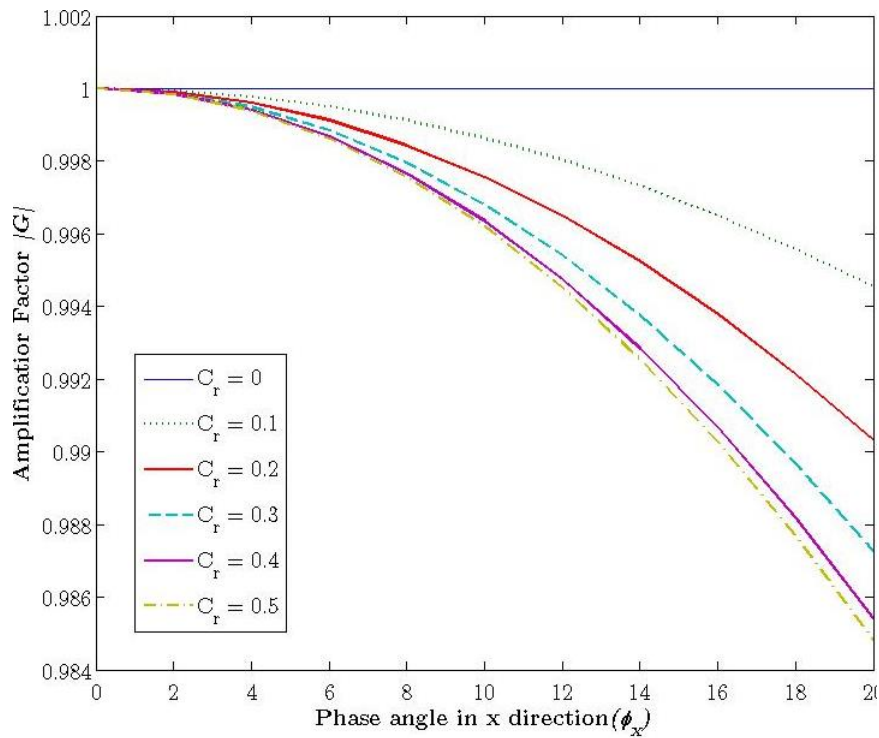


Figure 3.3: Enlarged view of diffusion error in the low frequency regions for the first order upwind scheme

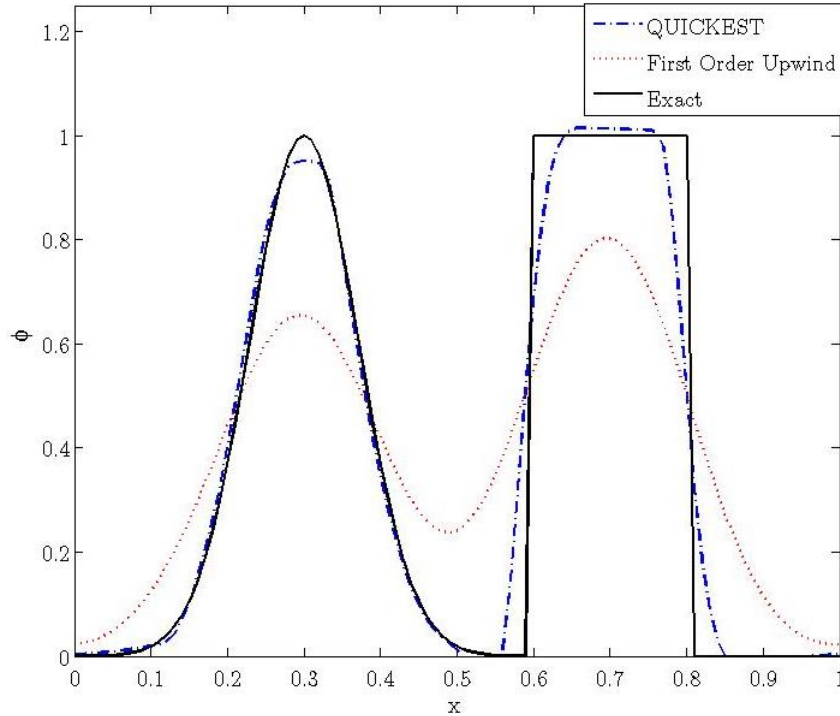


Figure 3.4: Convection of two different pulses using FOU, QUICKEST numerical scheme and the exact solution

nomenon with constant velocity. However, as seen in the Figure 3.4 the FOU scheme produces significant diffusion in the solution thus spreading both pulses whereas QUICKEST scheme produces almost negligible diffusion maintaining the shape of the pulses almost identical with the exact solution. This gives suggests the superiority of the higher order scheme such as QUICKEST particularly when physical dispersion is the object of study.

3.4 Numerical Example

In order to test the developed scheme, we consider a simplified one dimensional convection diffusion equation with a sharp front gradient,

$$\frac{\partial C}{\partial t} + p \frac{\partial C}{\partial x} = a \frac{\partial^2 C}{\partial x^2} \quad 0 < x < 1, t > 0 \quad (3.33)$$

with initial and boundary conditions as

$$C(x, 0) = \begin{cases} 1 & 0.0905 \leq x \leq 0.205 \\ 0 & \textit{otherwise} \end{cases} \quad (3.34)$$

$$C(0, t) = C(1, t) = 0 \quad (3.35)$$

The analytical solution of the above set of equations is given by (Tian and Yu, 2011)

$$C(x, t) = \frac{1}{2} \left[\operatorname{erf} \left(\frac{0.205 - x + pt}{2\sqrt{at}} \right) + \operatorname{erf} \left(\frac{-0.9005 + x - pt}{2\sqrt{at}} \right) \right] \quad (3.36)$$

where the error function is given by

$$\operatorname{erf}(x) = \frac{2}{\sqrt{\pi}} \int_0^x \exp(-\eta^2) d\eta \quad (3.37)$$

Simulations were carried out with different finite difference schemes to demonstrate the capability of the present scheme. The diffusion term in all schemes except the present work has been discretized by FTCS (Forward in Time and Centered in Space) method. In the test the advective velocity u set as unity, the diffusion coefficient set as $0.001 \text{ m}^2/\text{s}$. The unit length domain is divided into 100 nodes ($\Delta x = 0.01\text{m}$). The time step was set such a way so that it satisfies the CFL condition. The concentration profile of a passive scalar has been plotted along the axial distance after time $T = 0.2$ s in figure 3.5

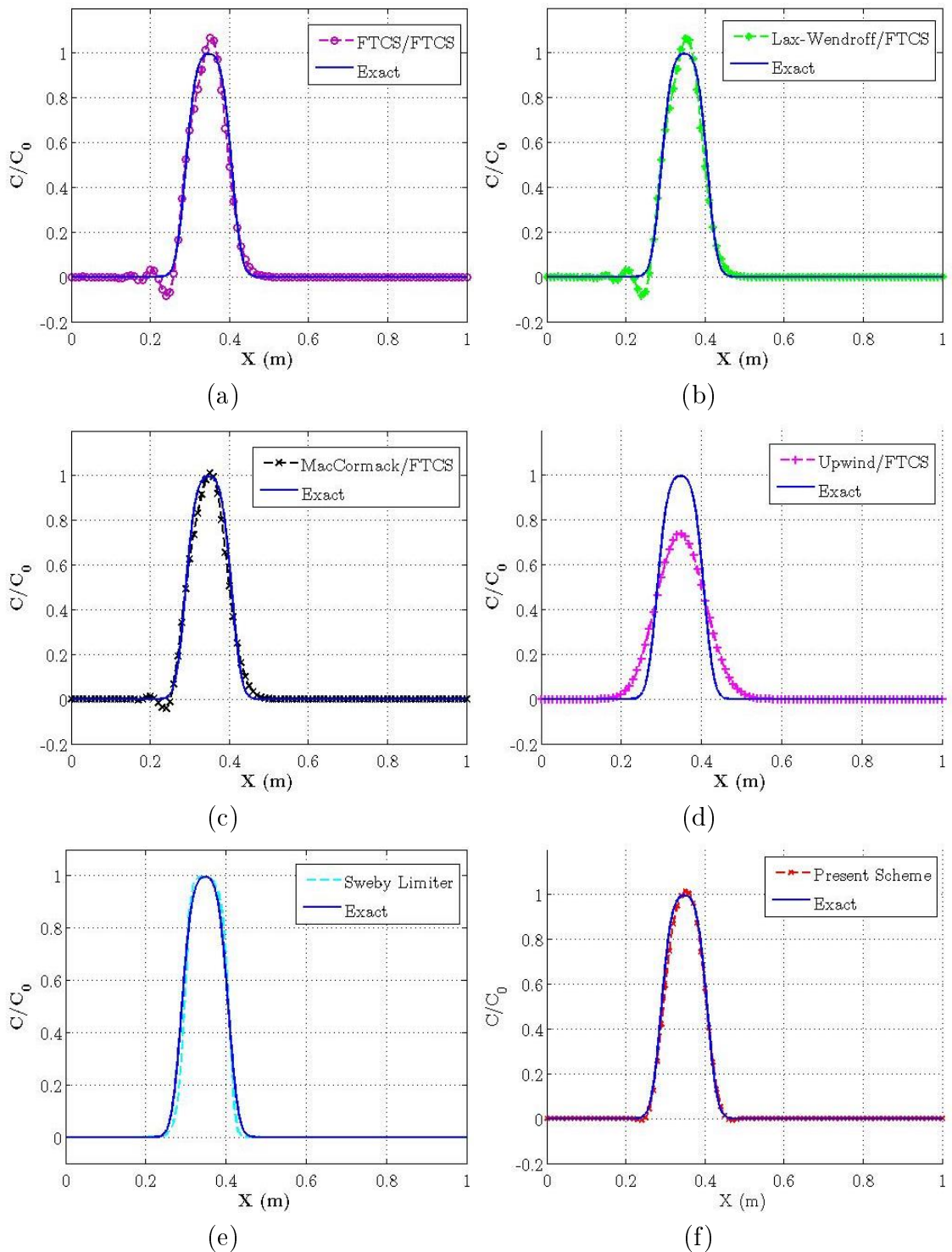


Figure 3.5: Comparison of the different numerical solution of 1D Convection-Diffusion equation. (a) FTCS, (b) Lax-Wendroff, (c) McCormack, (d) Upwind, (e) Finite Volume Scheme with Sweby flux limiter, (f) Present work-modified QUICKEST scheme.

From the results shown in figure 3.5, it is observed that the first order schemes such as FTCS (Forward in Time Centered in Space), upwind schemes as well as second order schemes such as the Lax-Wendroff and McCormack schemes give rise to excessive artificial diffusion and unwanted wiggles. The scheme developed in this work (modified QUICKEST scheme) shows excellent agreement with the analytical solution. The Finite Volume scheme with flux limiters has been widely used to suppress the oscillations of the solution and make it stable. The Sweby limiter function performs very well. However when compared with the analytical solution, the flux limiter estimates the concentration profile less accurately than the scheme presented in this thesis as seen in figure 3.5 (e) and figure 3.5(f)

3.5 Estimating Dispersion Using a Modified QUICKEST Scheme

3.5.1 Velocity Profile

It has been argued that the accuracy of estimating dispersion coefficient for a scalar flowing through closed channel significantly depends on the velocity profile. Although, the velocity profile in laminar flows through rectangular ducts can be calculated analytically from the Navier-Stokes equation, many forms of solutions have been reported in the literature (Johnson, 2016; Straub et al., 1958; Owen, 1954; Spiga and Morino, 1994) and experimental velocity profile have also been measured (Holmes and Vermeulen, 1968). Furthermore, the velocity profile in non-circular ducts can be calculated by solving Navier Stokes equation numerically (Seibold, 2008). Among these, we use an analytical solution derived from using Fourier analysis giving a final

expression for pressure driven axial velocity profile in a rectangular duct as

$$u(y, z) = (y^2 - L_y^2) + \sum_{n=0}^{\infty} \left(\frac{4(-1)^n \cosh(\alpha_n z)}{L_y \alpha_n^3 \cosh(\alpha_n L_z)} \cos(\alpha_n y) \right) \quad (3.38)$$

Where, L_y and L_z are the width and breadth of the ducts and $\alpha_n = (n + \frac{1}{2})$, with $n = 0, 1, 2, \dots$

3.5.2 Grid Sensitivity Analysis

The acceptability and reliability of numerical solutions depend on obtaining grid independence. Hence selecting appropriate spatial grid spacing for the domain and choosing an appropriate time step is crucial for any numerical solution. Keeping this in mind, a wide range of mesh sizes was tested in both the transverse and axial directions to choose the grid size for grid independent solution. A grid independent solution is the solution of the numerical scheme with a grid size that result in a predetermined variation in the numerical solution upon further refinement in grid size. For a grid convergence test of the model, the domain of simulation was chosen as shown in Figure 3.6. The solute was introduced at $x = 0.01\text{m}$ up to $x = 0.03\text{m}$. The length of the pipe was taken as 0.10 m . The breadth and width of the duct was taken $a = b = 2 \times 10^{-3}\text{m}$. The cross-sectional area averaged value of solute concentration is recorded for each simulation at the outlet of the duct.

Figures 3.7 and 3.8 reveal that a significant amount of change in the breakthrough curve is observed while changing number of grid points from 10 up to 70 in the lateral direction and from 25 up to 400 in the axial direction. Further mesh refinement after 40 and 150 in the corresponding directions results in a negligible difference in the solution. Hence, grid sizes were chosen as $5 \times 10^{-4}\text{ cm}$ in the radial direction and 0.1 cm in the axial direction. In order to account for the temporal grid independence

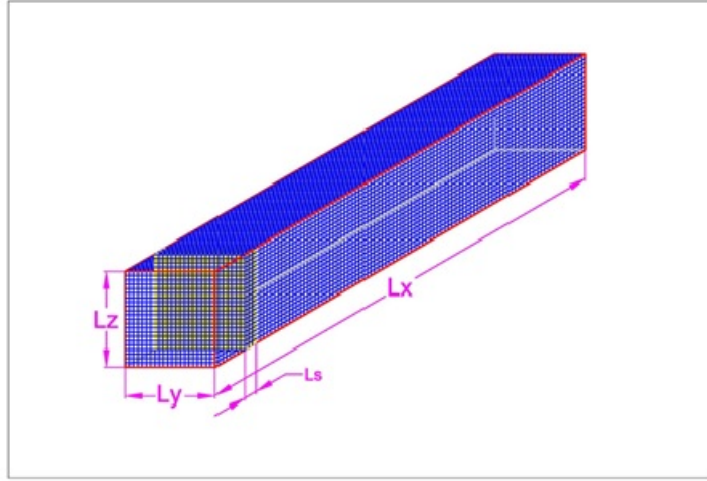


Figure 3.6: Solution domain with mesh representation

Table 3.1: Peak values of mean concentration for different grid resolutions in the axial direction

Grid Resolution	25	50	100	150	200	300	400
$max(C_{mean})$	0.4521	0.3548	0.3306	0.3093	0.3088	0.3027	0.3013

test, the simulations were carried out with time steps ranging from $\Delta t = 0.01$ s and decreasing to $\Delta t = 0.0001$ s. A time step greater than 0.0075 s cause instability of the scheme in the second situation considered (Figure 3.9(b), $Pe = 1000$). Hence a separate setup with $Pe = 100000$ (Figure 3.9(a)) is considered to inspect the effect of greater time step. It is clear from both Figures in 3.9 that further decreasing in time step beyond 0.01 s makes negligible difference to the solution.

Table 3.2: Peak values of mean concentration for different grid resolutions in the radial direction

Grid Resolution	10	20	30	40	50	60	70
$max(C_{mean})$	0.3940	0.3382	0.3281	0.3248	0.3232	0.3220	0.3217

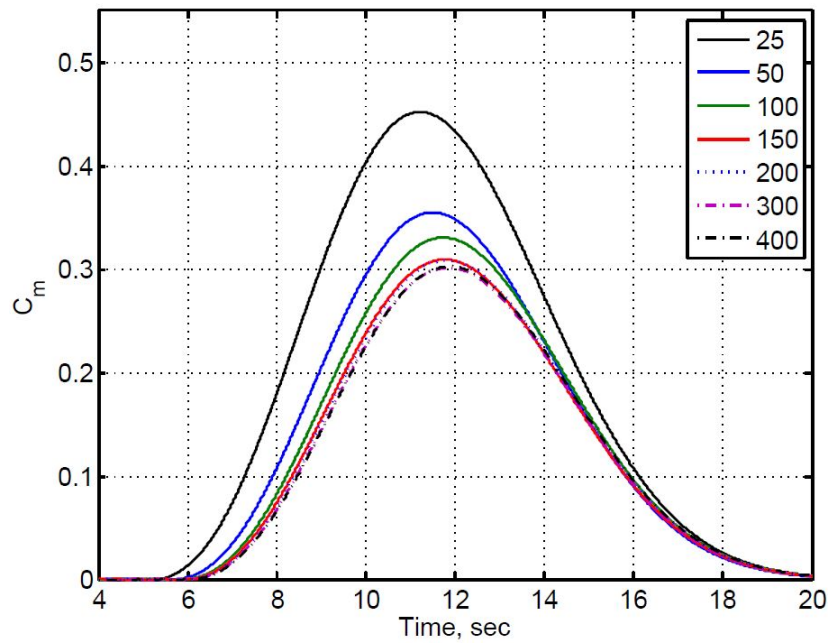


Figure 3.7: Axial grid sensitivity to dimensionless mean concentration at outlet of the square duct

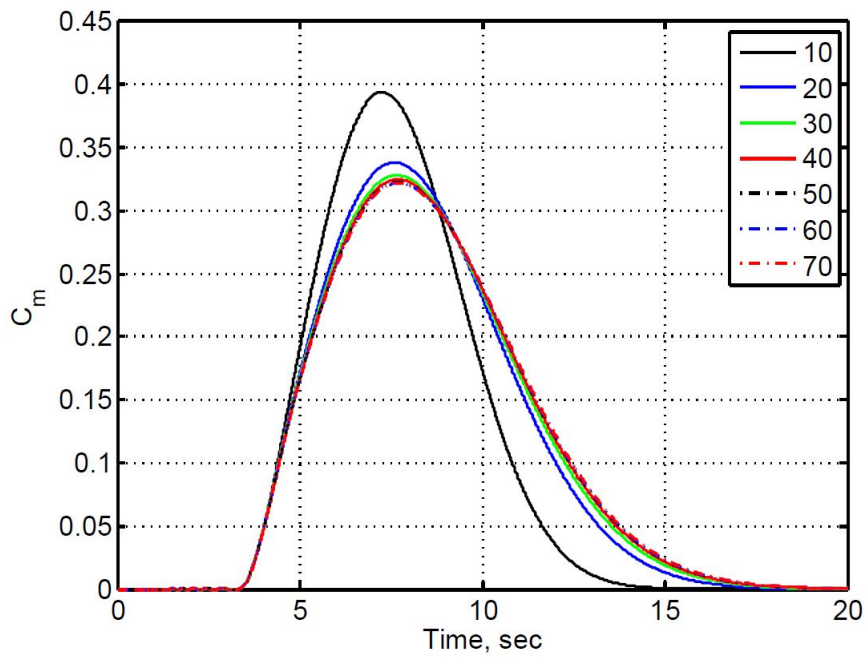


Figure 3.8: Radial grid sensitivity to dimensionless mean concentration at outlet of the square duct

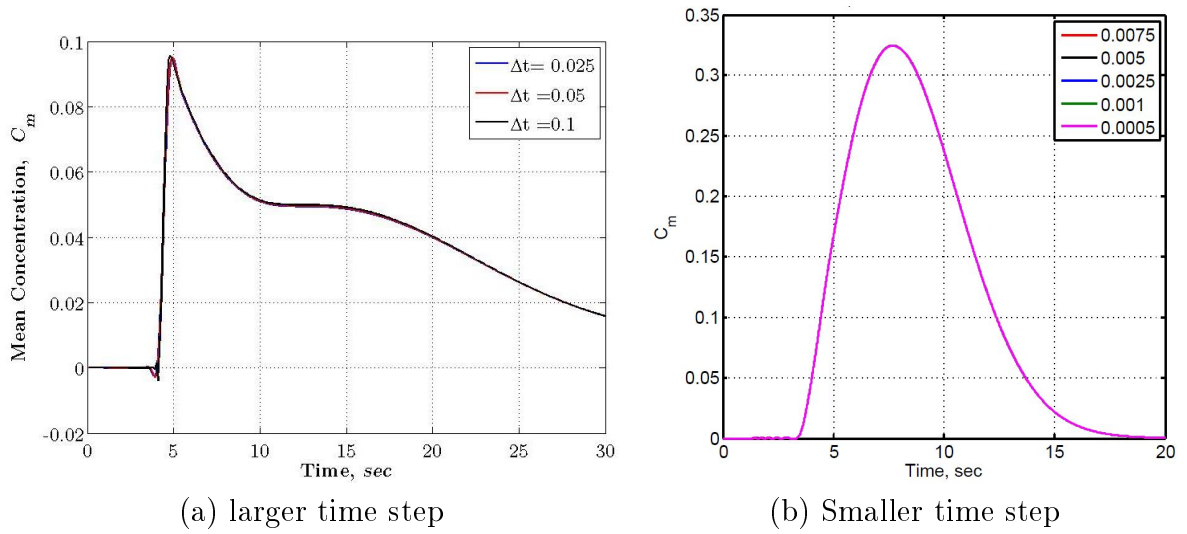


Figure 3.9: Time step sensitivity analysis for simulation of axial dispersion in laminar flow through square duct

3.5.3 Validation of the Model

It is essential for a numerical scheme to be consistent with established results. Hence the present model has been validated against the work of Doshi et al. (1978). The evolution of concentration across the cross section at a short dimensionless distance $X (= x/(Pe \times R)) = 0.01$ and long distance $X = 0.1$ is presented in Figure 3.10 and Figure 3.11 to compare the result with the analytical result obtained by Doshi et al. (1978). From the figure it is evident that the simulation results and analytical results are in excellent agreement.

3.6 Results

3.6.1 Evolution of Mean Concentration Profile

To demonstrate the development of the concentration profile, simulation carried out for different short and long periods in square duct. Figure 3.12 shows the mean elution

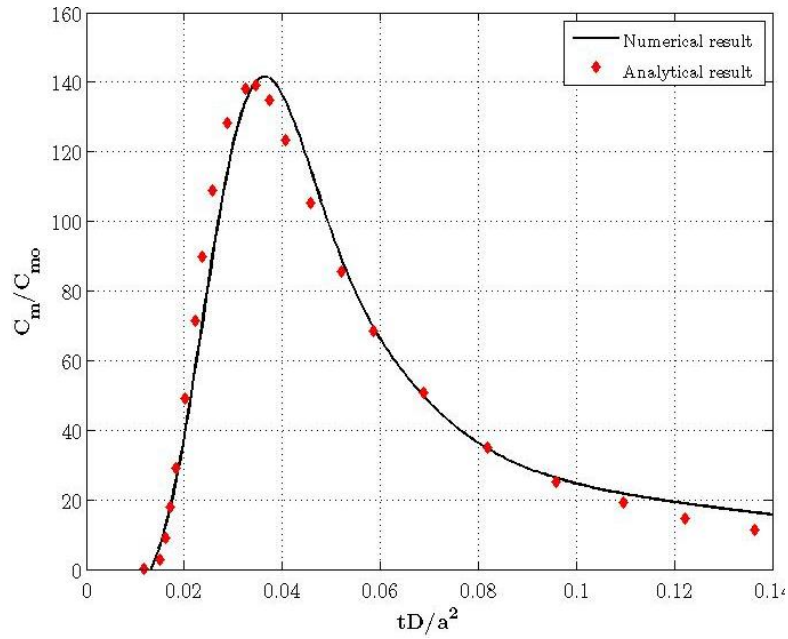


Figure 3.10: Comparison of mean concentration profile generated by the modified-QUICKEST scheme at early time (breakthrough curve at a dimensionless axial distance, $X = 0.01$) in a square duct with the analytical solution

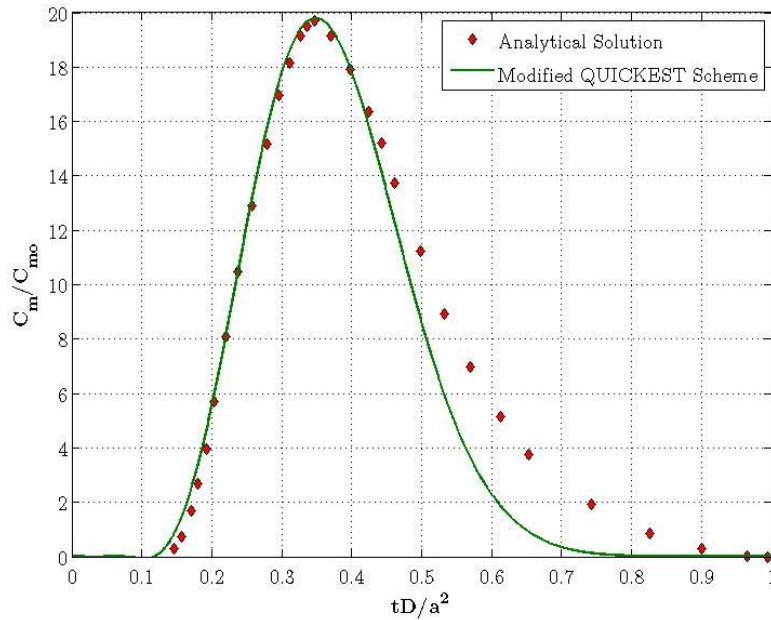


Figure 3.11: Comparison of mean concentration profile obtained from modified-QUICKEST scheme at later time (breakthrough curve at a dimensionless axial distance, $X = 0.1$) in a square duct with the analytical solution

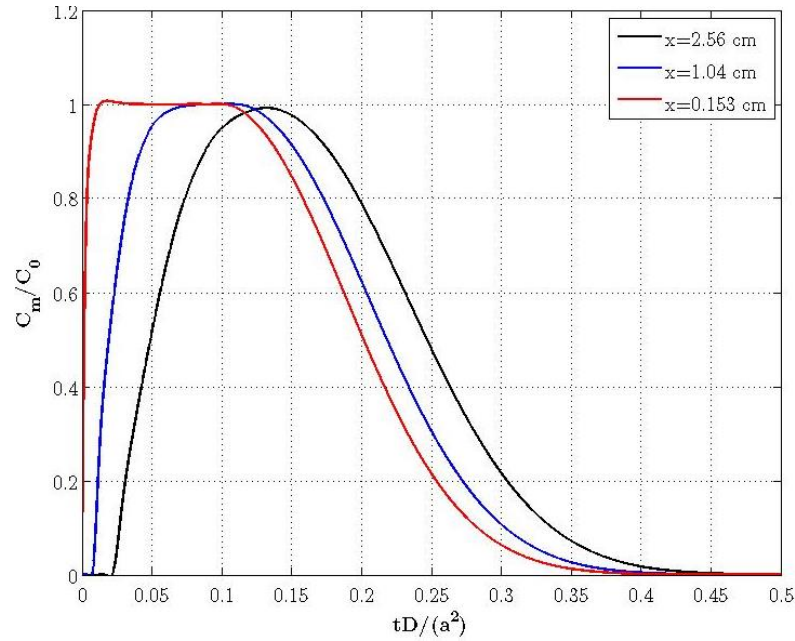


Figure 3.12: Initial Development of the mean concentration profile of the solute at different axial positions close to the initial plug.

curves at an early time at short axial distances (the solute introduced at $x = 0$ up to $x = 10.5$ cm, distances labelled in figure legend are measured from the upstream of the slug). The sharp mean concentration peak in these curves indicates convection domination at the beginning time. Further downstream of the square duct the mean breakthrough curve is single peaked without any shoulders which shows quite similar behaviour as circular case approximated by Taylor (1953) analytically 3.13.

Furthermore, the evolution of the concentration profile can be also observed from the breakthrough curves at the outlets at different dimensionless time. From Figure 3.14 it can be observed that the area averaged concentration spreads with two shoulders indicating that convection dominating at very low time. At higher dimensionless times, the diffusive nature of the solute transport is observed in the flow resembling Fickian diffusion. The distribution exhibits a higher magnitude of the peak concentration at later time whereas it should be less as it diffuses over the time. The reason for such behaviour is that to approximate the later solute distribution at

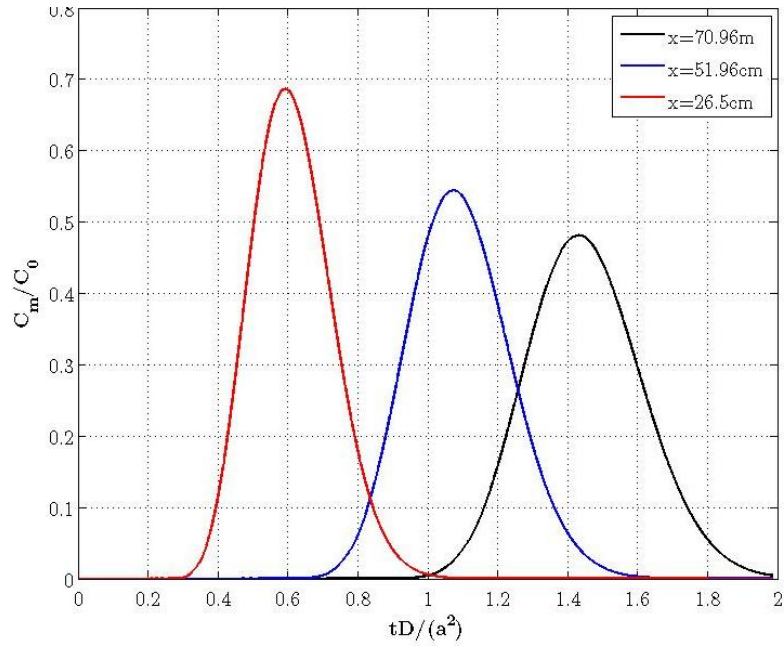


Figure 3.13: Development of the mean concentration profile of the solute at different axial positions from the initial plug

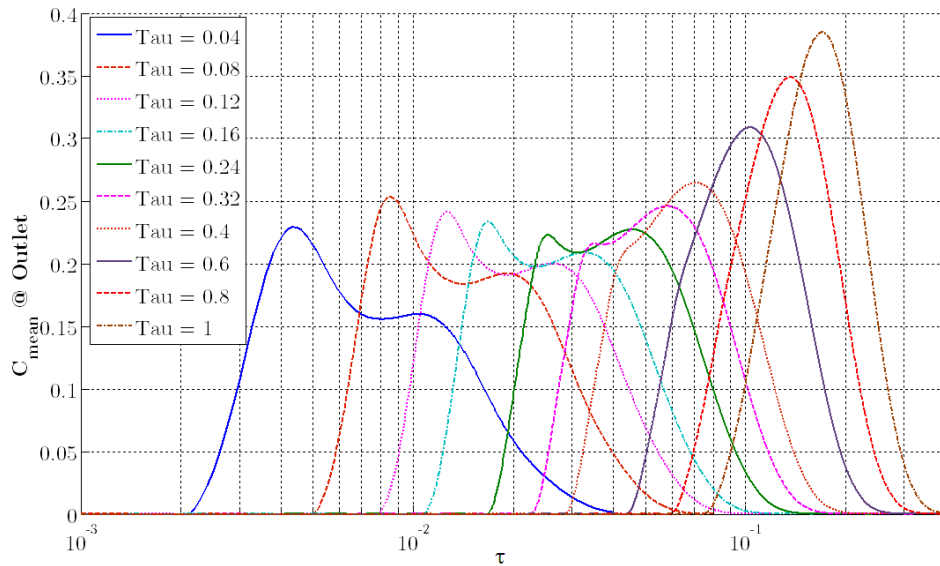


Figure 3.14: The evolution of the concentration profile with dimensionless time, τ

higher dimensionless time, the length of the duct was taken longer in the simulation. In fact, the length was determined from the dimensionless time and the velocity. In addition, the initial plug of solute was also taken proportional to the total length of the duct. Hence the solute distribution curve did not retain the the dimensionless pattern and total mass in each simulation were not kept equal. This was intentionally done to demonstrate the feature of the shape of the concentration distribution curve as one might expect to have a minute peak of the mean concentration at the outlet if the equal mass was used in the simulation of later times.

3.6.2 Comparison of Spreading in Square and Circular Ducts

To compare the longitudinal dispersion in circular and non-circular ducts, all the parameters were kept same as in Taylor's (1953) and study the simulation carried out for the square duct for 660 seconds with the same mass flow rate. The dimensionless mean concentration was plotted along the axis of the duct to observe the spreading of the scalar plotted together in Figure 3.15. It is evident from the figure that the dispersion in square duct is greater than that in the circular duct for the same cross sectional area and mass flow rate. This is probably because the corners of the square duct cause the material to be left behind and increases the amount of dispersion

3.6.3 Effect of Peclet Number

The analytical solution does not demonstrate any significant change due to variation of Peclet number of the system. We used the numerical model to study the effect of changing Peclet number at the same lateral positions.

At a higher Peclet number ($Pe = 10000$) the breakthrough curve (which is the mean concentration curve over the cross section during entire time interval at a

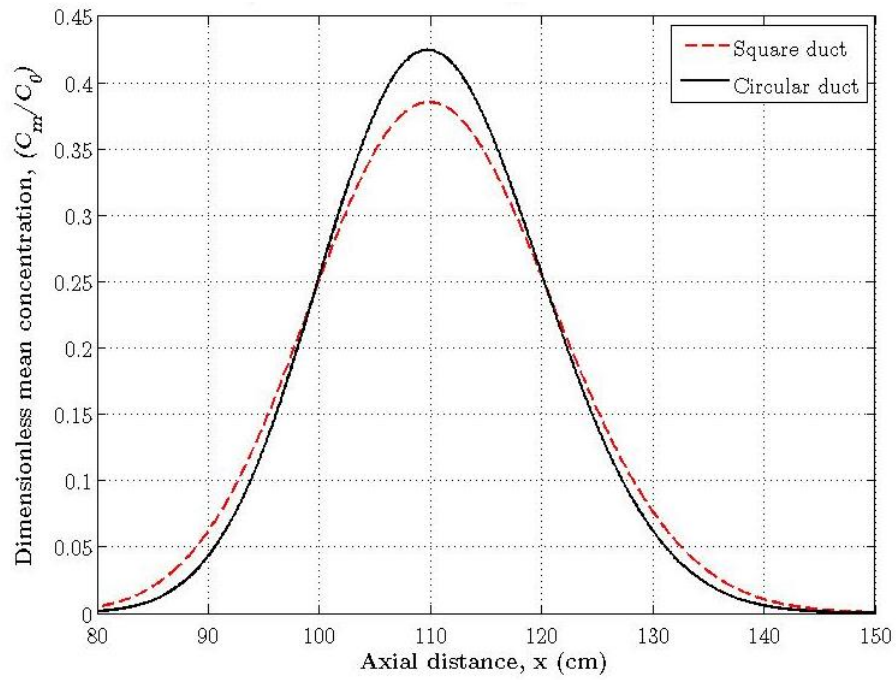


Figure 3.15: Spreading of the dimensionless mean concentration profile in axial direction 660s after an initial plug released at the inlet of a square and circular duct

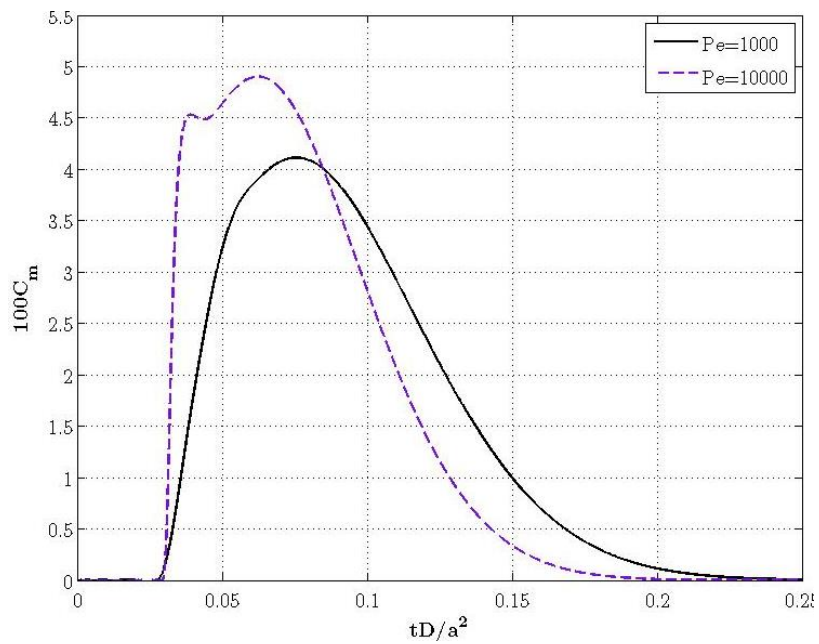


Figure 3.16: Breakthrough curve at dimensionless axial distance $X=0.017$

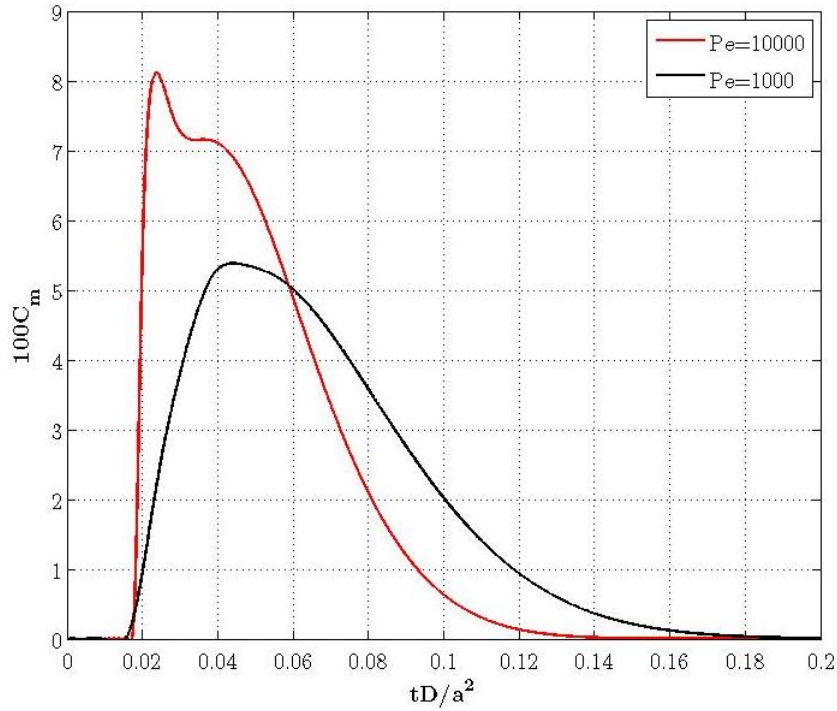


Figure 3.17: Breakthrough curve at dimensionless axial distance $X=0.01$

particular axial position) at $X = 0.01$ is distinguished by a surprising double peak (Figure 3.17). The sharp peak at the beginning demonstrates the domination of convection in the core region of the duct. The smooth second peak is an artefact of the increasing domination of diffusion as the flow proceeds down the pipe as can be also inferred from Figure 3.16. As can be seen from Figure 3.17 and Figure 3.16, at a lower Peclet number the effect of convection domination is neutralized even before $X = 0.01$. After a longer time (at $X = 0.098$) the mean elution curve exhibits a single peak without any shoulder (Figure 3.18) and it is reasonably well approximated by the analytical solution of Doshi et al. (1978) for both cases, high and low Peclet number.

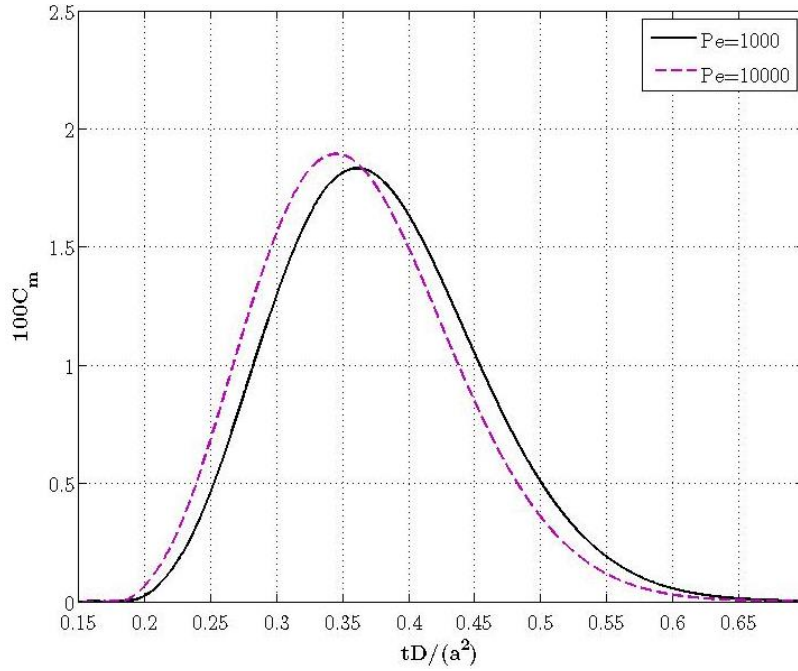


Figure 3.18: Breakthrough curve at dimensionless axial distance $X=0.098$

3.6.4 Rate of Dispersion

One of the important aspect of solute dispersion is to calculate the rate at which the solute is carrying away by the carrier fluid - the effective dispersion coefficient. From the simulation, we obtain the local concentration profile of the solute along the duct as well as the distribution of the mean concentration profile at the outlet. From the distribution of the mean concentration profile at the outlet over time, which is often termed as the breakthrough curve, the effective dispersion coefficient can be evaluated from the open vessel assumption from the C-curve as described in section 2.4.4. To observe the effect of Reynolds number on the dispersion parameter, multiple simulations were carried out. From figure 3.19 it can be observed that the dimensionless dispersion parameter varies at low Reynolds number, however it reaches plateau at higher Reynolds number as indicated in the circular pipe case by Taylor (1953).

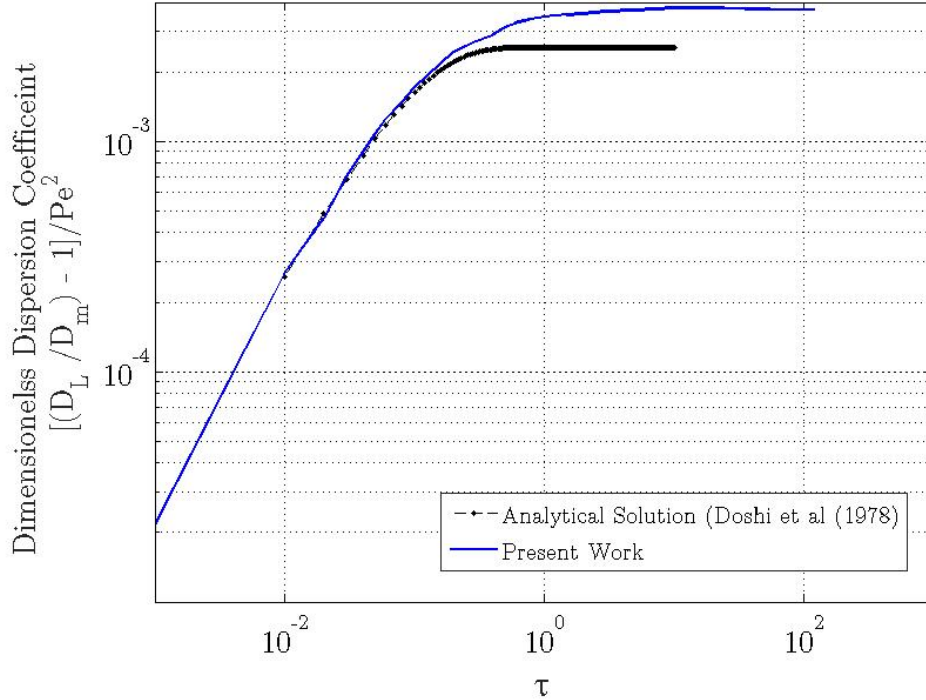


Figure 3.19: Dimensionless effective dispersion coefficient in a square duct over a range of dimensionless times.

Moreover, it can be noted that the analytical solution suggested by Doshi et al. (1978) underestimates the rate of dispersion at higher dimensionless time.

3.7 Conclusions

Predicting the spreading of a passive scalar is vital in many engineering applications. A numerical tool to simulate the phenomena can help to carry on extensive studies provided the tool predicts the spreading accurately without numerical diffusion. With that motivation, a third order spatially accurate Modified Quadratic Upwind Interpolation for Convective Kinematics with Estimated Streaming Terms (modified - QUICKEST) scheme has been developed. The stability criteria for the scheme have been determined using spectral analysis and its ability to produce solution with negligible diffusion has been demonstrated by calculating the amplification factor

using von Neumann analysis.

Furthermore, the newly developed scheme has been used to simulate the solute dispersion in rectilinear coordinate. The outstanding performance of the scheme to predict concentration profile at short and long dimensionless distance provides confidence in its application in future studies. The study of the solute distribution curve for various Peclet number has been presented at various axial distance of the duct. It has been found that at early times, the spreading of the solute manifests a double peak at high Peclet number representing convection domination in the transport mechanism. however, at low Peclet numbers, a single peak in the solute breakthrough curve corresponds to diffusion domination of the solute transport mechanism.

In addition, a comparison of spreading of solute in circular and square duct presented. A similitude analysis reveals that the dispersion in circular duct is less than in a square duct. The reason perhaps remains to the fact that the corner region in a square duct slows down the solute as it moves with the flow axially. Moreover, it was found that the dispersion coefficient increases with the dimensionless time until it becomes steady.

Chapter 4

A High Order Combined Compact Differencing Scheme to Estimate the Hydrodynamic Dispersion Rate in Laminar Flow through Non-Circular Ducts

4.1 Introduction

The hydrodynamic dispersion of scalars being transported by a flowing fluid has great practical significance as the phenomenon appears in many engineering applications. When a solute is being carried in by a fluid flowing through duct in which the velocity profile is non-uniform on a cross-section normal to the flow, some of the

solute advances faster at the center of the duct where the velocity is maximum and a portion of the solute moves more slowly near the wall. Consequently, transverse diffusion comes into action because of lateral concentration gradients of the scalar and this slows down the overall transport process in the direction of the flow. Theoretical and experimental studies have revealed that the overall transport of a solute can be characterized by an effective diffusion coefficient, analogous to the Fickian diffusion process.

Numerical simulation of physical processes enables engineers and scientists to design efficient systems and test them in great detail. By establishing the mechanisms in the real system followed by solving the governing equations approximately using numerical method, it is useful to study any physical phenomena before its practical implementation. The physical phenomena that govern mass dispersion of a scalar with an isotropic diffusion coefficient (i.e. the diffusion coefficient is constant in all directions) in fully developed flow through rectangular duct can be described by the unsteady convection diffusion equation in Cartesian coordinates.

$$\frac{\partial \mathcal{C}}{\partial t} + u(y, z) \frac{\partial \mathcal{C}}{\partial x} = D_m \left(\frac{\partial^2 \mathcal{C}}{\partial x^2} + \frac{\partial^2 \mathcal{C}}{\partial y^2} + \frac{\partial^2 \mathcal{C}}{\partial z^2} \right) \quad (4.1)$$

subject to the initial and boundary conditions

$$\mathcal{C}(x, y, 0) = \mathcal{C}_0 \quad (4.2)$$

$$\left. \frac{\partial \mathcal{C}}{\partial y} \right|_{y=0, L_y} = 0, \quad \left. \frac{\partial \mathcal{C}}{\partial z} \right|_{z=0, L_z} = 0 \quad (4.3)$$

A numerical solution technique involves discretising the governing equation using Taylor's series approximation at a finite number of grid points in the solution domain

and converting the governing equation into a set of algebraic linear equations at every grid point. This set of linear equations is then solved for node values of the variable which provides the solution. Although numerical techniques are an efficient way of solving physical problem because of availability of high computing power, it is an approximate solution. The order of accuracy of a numerical scheme depends on the number of terms being considered in the Taylor series used to approximate the derivatives. Lower order discretization schemes usually approximate the solution with poor accuracy, whereas higher order schemes results in more accurate solutions.

Researchers have invested considerable effort to develop discretization schemes with higher order accuracy. However in most of the cases, the solution involves large stencils which require solution of a denser system of equations causing higher computational cost. In order to overcome this issue, combined compact difference (CCD) schemes have been developed and used in the solution of many partial differential equations in recent years.

Gupta et al. (1984) presented a finite difference scheme with spatial fourth order accuracy for one dimensional convection diffusion equation with variable diffusion coefficient. This scheme has been extended to solve the two-dimensional unsteady convection diffusion equation by Spatz and Carey (2001). Nevertheless, the scheme involved nine nodes in the difference equation which make it computationally inefficient. Furthermore, Noye and Tan (1989) derived a set of higher order compact (HOC) implicit schemes for solving one dimensional steady convection diffusion equation with third order accuracy in space and second order accurate in time.

In pursuance of a computationally effective scheme, Karaa and Zhang (2004) developed a HOC scheme with a standard alternating direction implicit method adapted from Peaceman and Rachford (1955) (PR-ADI) to solve two dimensional time depen-

dent convection diffusion equation with constant diffusion coefficient. It was demonstrated that the HOC-ADI scheme is unconditionally stable and fourth order accurate in space and second order accurate in time. This scheme has been implemented for solving the three-dimensional unsteady convection diffusion equation by Karaa (2006). The computational efficiency of the scheme has made it superior to other fourth order schemes; however the error behaviour cannot retain this superiority. The high order Pade ADI method (PDE-ADI) proposed by You (2006) represents better characteristics of phase and amplitude than PR-ADI and HOC-ADI method maintaining similar order of accuracy. The PDE-ADI method has been modified to develop a hybrid PDE-ADI scheme by Karaa (2010) incorporating a linear multi-step method with approximate factorization developed by Beam and Warming (1976) in the time integration.

Furthermore, a series of HOC exponential finite difference schemes (EHOC-ADI) has been proposed by Tian and Dai (2007) to solve the one dimensional and two dimensional steady state convection diffusion equations. This scheme has been revised to solve the one dimensional unsteady equation adapting pade approximation for temporal discretization by Tian and Yu (2011). Furthermore, Tian and Ge (2007) and Ge et al. (2013) have extended the approach for solving the unsteady convection diffusion equation in two and three-dimensional Cartesian coordinates respectively. These methods have fourth order accuracy in the spatial domain and possess non-oscillatory behaviour.

Tian and Yu (2011) have presented a rational HOC scheme with ADI method (RHOC-ADI) for solving one-dimensional steady convection diffusion equation and extended it for two dimensional steady and unsteady cases. This scheme is temporally second order and spatially fourth order accurate and involves only a three point stencil

in each direction. Moreover, superior accuracy and computational efficiency as well as better phase and amplitude error characteristics have been demonstrated for the scheme compared with the HOC-ADI, EHOC-ADI and PDE-ADI methods.

An alternative approach to solving the unsteady convection diffusion equation with constant coefficients in one and two-dimension has been proposed by Liao (2012). In this work, the unsteady convection diffusion equation has been transformed to a reaction diffusion equation and solved by a fourth order scheme originally developed for a reaction diffusion equation by Liao et al. (2006). The convective term is eliminated from the governing equation by applying an exponential transformation; as a result the scheme constrained to small cell Reynolds numbers.

Most of the schemes discussed above are limited to comparatively low cell Peclet number and do not possess same level of accuracy when convection becomes the dominant mechanism in the flow (Sun and Li, 2014). To overcome this limitation the combined compact difference (CCD) scheme has been proposed by Chu and Fan (1998) for one- and two-dimensional time independent convection diffusion equations. The scheme is a sixth order spatially accurate implicit method. (Sun and Li, 2014) have used the CCD method combined with ADI method for solving two-dimensional unsteady convection diffusion equation. The three point stencil structure of the scheme enables high computational efficiency for the solution. Numerical experiments demonstrate that the CCD-ADI scheme provides excellent results for high Peclet number i.e. for highly convective flows. In this work we develop a CCD-ADI scheme to solve the unsteady convection diffusion equation in three dimensional Cartesian coordinates.

4.2 Three point CCD Scheme

4.2.1 One Dimensional Case

To visualize the development of three point CCD scheme, we consider following one dimensional differential equation

$$\alpha(x) \frac{d^2\phi}{dx^2} + \beta(x) \frac{d\phi}{dx} + \gamma(x) \phi = f(x), \quad 0 \leq x < L \quad (4.4)$$

with boundary conditions

$$\zeta_1(x) \phi(x) + \zeta_2(x) \frac{d\phi(x)}{dx} = g(x), \quad x = 0, L \quad (4.5)$$

where α , β , γ , f , ζ_1 , ζ_2 and g are given functions.

We discretise the one dimensional domain into a uniform grid $0 = x_1 < x_2 < \dots < x_{N-1} < x_N = L$ with grid spacing $h = L/(N - 1)$. Expanding any arbitrary function $\phi(x)$ and x_i , $i = 1, 2, \dots, N$ using Taylor series with up to the sixth derivative, we obtain

$$\begin{aligned} \phi(x_{i\pm 1}) = \phi(x_i) \pm h\phi'(x_i) + \frac{h^2}{2}\phi''(x_i) \pm \frac{h^3}{6}\phi'''(x_i) + \frac{h^4}{24}\phi^{(4)}(x_i) \pm \frac{h^5}{120}\phi^{(5)}(x_i) \\ + \frac{h^6}{720}\phi^{(6)}(x_i) + \mathcal{O}(h^7) \end{aligned} \quad (4.6)$$

Similar expressions can be obtained by replacing $\phi(x_i)$ with $\phi'(x_i)$ and $\phi''(x_i)$

$$\begin{aligned}\phi'(x_{i\pm 1}) = \phi'(x_i) \pm h\phi''(x_i) + \frac{h^2}{2}\phi'''(x_i) \pm \frac{h^3}{6}\phi^{(4)}(x_i) + \frac{h^4}{24}\phi^{(5)}(x_i) \\ \pm \frac{h^5}{120}\phi^{(6)}(x_i) + \mathcal{O}(h^7)\end{aligned}\quad (4.7)$$

and

$$\phi''(x_{i\pm 1}) = \phi''(x_i) \pm h\phi'''(x_i) + \frac{h^2}{2}\phi^{(4)}(x_i) \pm \frac{h^3}{6}\phi^{(5)}(x_i) + \frac{h^4}{24}\phi^{(6)}(x_i) + \mathcal{O}(h^7)\quad (4.8)$$

In order to express the variable with a higher order truncation term, equations (4.6) - (4.8) can be manipulated to develop combined expression of the variable with its first and second derivatives as follows.

$$\begin{aligned}\frac{\phi(x_{i+1}) - \phi(x_{i-1})}{2h} &= \phi'(x_i) + \frac{h^2}{6}\phi'''(x_i) + \frac{h^4}{120}\phi^{(5)}(x_i) + \mathcal{O}(h^6) \\ \frac{\phi'(x_{i+1}) + \phi'(x_{i-1})}{2} &= \phi'(x_i) + \frac{h^2}{2}\phi'''(x_i) + \frac{h^4}{24}\phi^{(5)}(x_i) + \mathcal{O}(h^6) \\ \phi''(x_{i+1}) - \phi''(x_{i-1}) &= 2h\phi'''(x_i) + \frac{h^3}{3}\phi^{(5)}(x_i) + \mathcal{O}(h^5)\end{aligned}\quad (4.9)$$

$$\begin{aligned}\frac{\phi(x_{i+1}) - 2\phi(x_i) + \phi(x_{i-1}))}{h^2} &= \phi''(x_i) + \frac{h^2}{12}\phi^{(4)}(x_i) + \frac{h^4}{360}\phi^{(6)}(x_i) + \mathcal{O}(h^6) \\ \frac{\phi'(x_{i+1}) - \phi'(x_{i-1}))}{2h} &= \phi''(x_i) + \frac{h^2}{6}\phi^{(4)}(x_i) + \frac{h^4}{120}\phi^{(6)}(x_i) + \mathcal{O}(h^6) \\ \frac{\phi''(x_{i+1}) + \phi''(x_{i-1}))}{2} &= \phi''(x_i) + \frac{h^2}{2}\phi^{(4)}(x_i) + \frac{h^4}{24}\phi^{(6)}(x_i) + \mathcal{O}(h^6)\end{aligned}\quad (4.10)$$

From equations (4.9) and (4.10), writing $\phi(x_i) = \phi_i$, the first and second derivative at point i can be expressed as

$$\phi'_i = \frac{15}{16h} [\phi_{i+1} - \phi_{i-1}] - \frac{7}{16} [\phi'_{i+1} + \phi'_{i-1}] + \frac{h}{16} [\phi''_{i+1} - \phi''_{i-1}] + \mathcal{O}(h^6) \quad (4.11)$$

and

$$\phi''_i = \frac{3}{h^2} [\phi_{i+1} - 2\phi_i + \phi_{i-1}] - \frac{9}{8h} [\phi'_{i+1} - \phi'_{i-1}] + \frac{1}{8} [\phi''_{i+1} + \phi''_{i-1}] + \mathcal{O}(h^6) \quad (4.12)$$

Furthermore, equations (4.11) and (4.12) can be rearranged into the following form and dropping the truncation errors

$$\frac{15}{16h}\phi_{i-1} - \frac{15}{16h}3\phi_{i+1} + \frac{7}{16}\phi'_{i-1} + \phi'_i + \frac{7}{16}\phi'_{i+1} + \frac{h}{16}\phi''_{i-1} - \frac{h}{16}\phi''_{i+1} = 0 \quad (4.13)$$

$$-\frac{3}{h^2}\phi_{i-1} + \frac{6}{h^2}\phi_i - \frac{3}{h^2}\phi_{i+1} - \frac{9}{8h}\phi'_{i-1} + \frac{9}{8h}\phi'_{i+1} - \frac{1}{8}\phi''_{i-1} + \phi''_i - \frac{1}{8}\phi''_{i+1} = 0 \quad (4.14)$$

These equations are applicable at nodes $i = 2, 3, \dots, N - 1$ resulting in a total $2(N - 1)$ equations. For periodic boundaries ($\phi_1 = \phi_N$, $\phi'_1 = \phi'_N$, and $\phi''_1 = \phi''_N$) the above equations (4.13) and (4.14) apply to $i = 1$. However, for non-periodic boundaries, to maintain the three point structure at the boundaries, a pair of fifth order one sided CCD schemes is introduced as follows at x_1 and x_N

$$\frac{31}{h}\phi_1 - \frac{32}{h}\phi_2 + \phi_3 + 14\phi'_1 + 16\phi'_2 + 2h\phi''_1 - 4h\phi''_2 = 0 \quad (4.15)$$

$$-\frac{31}{h}\phi_N + \frac{32}{h}\phi_{N-1} - \phi_{N-2} + 16\phi'_{N-1} + 14\phi'_N - 4h\phi''_{N-1} + 2h\phi''_N = 0 \quad (4.16)$$

Details of the derivation of these boundary equations are discussed in Appendix C. Furthermore, equations (4.4) and (4.5) can be written in discretized form as

$$\gamma_i\phi_i + \beta_i\phi'_i + \alpha_i\phi''_i = f_i, \quad i = 1, 2, 3, \dots, N \quad (4.17)$$

and

$$\zeta_1(0)\phi_1 + \zeta_2(0)\phi'_1 = g(0) \quad (4.18)$$

$$\zeta_1(L)\phi_N + \zeta_2(L)\phi'_N = g(L)$$

The above system of equations can be organized into a triple tridiagonal system of $3N$ equations (equation (4.13) and (4.14) for $i = 2, 3, \dots, N - 1$ giving $2(N - 2)$ equations, equation (4.15) for $i = 1$ and ((4.16) for $i = N$ giving 2 equations, and equations (4.17) for $i = 1, 2, 3, \dots, N$ and equation (4.18) for $i = 1, N$ providing $N + 2$ equations) with $3N$ unknowns (ϕ_i , ϕ'_i , and ϕ''_i for $i = 1, 2, 3, \dots, N$). This system of linear equations can be solved by triple forward elimination and triple backward substitutions. A simpler version of the algorithm solves a twin tridiagonal system which appears while calculating first and second derivatives from a given function with the CCD method (discussion to appear in later section). An algorithm for efficiently solving a twin tridiagonal matrix system is discussed in the Appendix D

and the solver is presented in Appendix E on a Matlab programming platform. This algorithm can readily be expanded to solve triple tridiagonal matrices.

4.2.2 CCD-ADI Method to Solve a Two-Dimensional Problem

The method described above has been developed for the one dimensional case. However, in most of the cases we have to deal with multidimensional system. Before implementing the three-dimensional case in which we are interested, it is a worthwhile, if somewhat didactic exercise, to discuss the implementation procedure for a two-dimensional case. Consider a two-dimensional convection diffusion equation with constant velocity q and r and constant molecular diffusivity b and c in the y and z directions respectively. The unsteady convection diffusion of any scalar ϕ expressed as

$$\frac{\partial \phi}{\partial t} + q \frac{\partial \phi}{\partial y} + r \frac{\partial \phi}{\partial z} = b \frac{\partial^2 \phi}{\partial y^2} + c \frac{\partial^2 \phi}{\partial z^2} + S, \quad (y, z, t) \in \Omega \times (0, T] \quad (4.19)$$

where Ω is a two dimensional domain in \mathbb{R}^2 in $[L_y \times L_z]$. The above equation is subjected to the initial condition

$$\phi(y, z, 0) = \phi_0(y, z), \quad (y, z) \in \Omega \quad (4.20)$$

and the boundary condition

$$\zeta_1 \phi(y, z, t) + \zeta_2 \frac{\partial \phi}{\partial n}(y, z, t) = g(y, z, t), \quad (y, z) \in \partial \Omega, \quad t \in (0, T] \quad (4.21)$$

In this case $\zeta_1=1$ and $\zeta_2=0$ corresponds to Dirichlet boundary condition and $\zeta_1=0$

and $\zeta_2=1$ corresponds to Neumann boundary condition. n is the outward unit normal vector of the domain

The source term S , ϕ_0 and g are given smooth functions. For convenience, let us define two finite difference operators

$$\mathcal{L}_y \equiv b \frac{\partial^2}{\partial y^2} - q \frac{\partial}{\partial y}, \quad \mathcal{L}_z \equiv c \frac{\partial^2}{\partial z^2} - r \frac{\partial}{\partial z} \quad (4.22)$$

Hence equation (4.19) can be rewritten as

$$\frac{\partial \phi}{\partial t} = (\mathcal{L}_y + \mathcal{L}_z)\phi + S \quad (4.23)$$

Using the Crank-Nicholson scheme, discretising the above equation over the time interval $[0, T]$ with time increment $\Delta t = T/N$ where N is the total number of time steps, we obtain

$$\frac{\phi^{n+1} - \phi^n}{\Delta t} = \frac{1}{2} (\mathcal{L}_y + \mathcal{L}_z) (\phi^{n+1} + \phi^n) + S^{n+\frac{1}{2}} + \mathcal{O}(\Delta t^2) \quad (4.24)$$

Here ϕ^n is the approximation of $\phi(y, z, n\Delta t)$ for an arbitrary function $\phi(y, z, t)$. Collecting terms in ϕ^{n+1} and ϕ^n

$$\left(1 - \frac{\Delta t}{2} \mathcal{L}_y - \frac{\Delta t}{2} \mathcal{L}_z\right) \phi^{n+1} = \left(1 + \frac{\Delta t}{2} \mathcal{L}_y + \frac{\Delta t}{2} \mathcal{L}_z\right) \phi^n + \Delta t S^{n+\frac{1}{2}} + \mathcal{O}(\Delta t^3) \quad (4.25)$$

Further modification by factorization of the above equation gives (assuming all coefficients to be constant)

$$\begin{aligned} \left(1 - \frac{\Delta t}{2} \mathcal{L}_y\right) \left(1 - \frac{\Delta t}{2} \mathcal{L}_z\right) \phi^{n+1} &= \left(1 + \frac{\Delta t}{2} \mathcal{L}_y\right) \left(1 + \frac{\Delta t}{2} \mathcal{L}_z\right) \phi^n \\ &+ \Delta t S^{n+\frac{1}{2}} + \frac{\Delta t^2}{4} \mathcal{L}_y \mathcal{L}_z (\phi^{n+1} - \phi^n) + \mathcal{O}(\Delta t^3) \end{aligned} \quad (4.26)$$

We note that the term $\frac{\Delta t^2}{4} \mathcal{L}_y \mathcal{L}_z (\phi^{n+1} - \phi^n)$ on the right hand side of the above equation has order of accuracy of $\mathcal{O}(\Delta t^3)$ because $\phi^{n+1} - \phi^n \approx \Delta t$. Hence this term can be subsumed in the truncation error

$$\begin{aligned} \left(1 - \frac{\Delta t}{2} \mathcal{L}_y\right) \left(1 - \frac{\Delta t}{2} \mathcal{L}_z\right) \phi^{n+1} &= \left(1 + \frac{\Delta t}{2} \mathcal{L}_y\right) \left(1 + \frac{\Delta t}{2} \mathcal{L}_z\right) \phi^n \\ &+ \Delta t S^{n+\frac{1}{2}} + \mathcal{O}(\Delta t^3) \end{aligned} \quad (4.27)$$

To discretize equation (4.19) we divide the domain Ω into a uniform grid with grid sizes $\Delta y = L_y/(N_y - 1)$ and $\Delta z = L_z/(N_z - 1)$ in the y and z directions respectively. Moreover, if we denote $\phi_{j,k}^n$ as an approximation of $\phi(y_j, z_k, t_n)$ for an arbitrary function $\phi(y, z, t)$ and drop the truncation error the above equation is written as

$$\left(1 - \frac{\Delta t}{2} \mathcal{L}_y\right) \left(1 - \frac{\Delta t}{2} \mathcal{L}_z\right) \phi_{j,k}^{n+1} = \left(1 + \frac{\Delta t}{2} \mathcal{L}_y\right) \left(1 + \frac{\Delta t}{2} \mathcal{L}_z\right) \phi_{j,k}^n + \Delta t S_{j,k}^{n+\frac{1}{2}} \quad (4.28)$$

This equation can be solved by splitting the operators using the D'Yakonov Alternating Directional Implicit scheme (D'yakonov 1963) and introducing an intermediate variable ϕ^*

$$\left(1 - \frac{\Delta t}{2} \mathcal{L}_z\right) \phi_{j,k}^* = \left(1 + \frac{\Delta t}{2} \mathcal{L}_y\right) \left(1 + \frac{\Delta t}{2} \mathcal{L}_z\right) \phi_{j,k}^n + \Delta t S_{j,k}^{n+\frac{1}{2}} \quad (4.29)$$

$$\left(1 - \frac{\Delta t}{2} \mathcal{L}_y\right) \phi_{j,k}^{n+1} = \phi_{j,k}^* \quad (4.30)$$

The above operation creates two one dimensional equations which can be solved by the CCD method. The sixth order accurate CCD formula (4.13) and (4.14) combined with boundary equations (4.15) and (4.16) can be used by replacing h with Δy and Δz to solve equation (4.29) and (4.30) respectively with the accuracy of $\mathcal{O}(\Delta y^6 + \Delta z^6 + \Delta t^2)$

In solving equation (4.29), we have to calculate the right hand side of the equation which requires computing first and second derivative of $\phi_{j,k}^n$ with higher order accuracy beforehand. For periodic boundary conditions, equations (4.13) - (4.16) is sufficient to calculate ϕ_i' and ϕ_i'' provided that ϕ_i are given. However for non-periodic boundary we have $2(N - 1)$ equations with $2N$ unknowns. Therefore we need additional two boundary CCD equations to solve additional two variables in the boundary. [The derivation of these equations are presented in Appendix C]

$$\frac{7}{2h} \phi_1 - \frac{4}{h} \phi_2 + \phi_3 + \phi_1' + 2\phi_2' - h\phi_2'' = 0 \quad (4.31)$$

$$-\phi_{N-2} + \frac{4}{h} \phi_{N-1} - \frac{7}{2h} \phi_N + 2\phi_{N-1}' + \phi_N' + 4h\phi_{N-1}'' = 0 \quad (4.32)$$

The algorithm for implementing the schemes for solving equation (4.19) is as follows

- (1). Do $j = 1, 2, \dots, N_y$ [for all y]

Compute $\frac{\partial\phi}{\partial z}\Big|_{j,k}^0$ and $\frac{\partial^2\phi}{\partial z^2}\Big|_{j,k}^0$ by equation (4.13) - (4.16) and (4.31) - (4.32) for $k = 1, 2, \dots, N_z$

(2) Do $n = 1, 2, \dots, N$ [time marching]

(a) Compute the RHS of equation (4.29) for all $j = 1, 2, \dots, N_y$ and $k = 1, 2, \dots, N_z$

$$(i) g_{j,k}^n = \phi_{j,k}^n + \frac{\Delta t}{2} \left(c \frac{\partial^2\phi}{\partial z^2}\Big|_{j,k}^n - r \frac{\partial\phi}{\partial z}\Big|_{j,k}^n \right)$$

(ii) Calculate $\frac{\partial g}{\partial y}\Big|_{j,k}^n$ and $\frac{\partial^2 g}{\partial y^2}\Big|_{j,k}^n$ by equation (4.13) - (4.16) and (4.31) - (4.32)

$$(ii) f_{j,k}^n = g_{j,k}^n + \frac{\Delta t}{2} \left(b \frac{\partial^2 g}{\partial y^2}\Big|_{j,k}^n - q \frac{\partial g}{\partial y}\Big|_{j,k}^n \right) + \Delta t S^{n+\frac{1}{2}}$$

(b) Compute the boundary condition on $\phi_{j,k}^*$ in equation (4.29) from equation (4.30) for $k = 1, N_z$ and $j = 1, 2, 3, \dots, N_y$ [this step is for the Dirichlet boundary condition, for the Neumann boundary condition we do not have to calculate boundary values of intermediate variable explicitly rather we have to solve for the variable at the boundary with higher order approximation and incorporate it in the triple tridiagonal system]

(i) Compute $\frac{\partial\phi}{\partial z}\Big|_{j,k}^{n+1}$ and $\frac{\partial^2\phi}{\partial z^2}\Big|_{j,k}^{n+1}$ by equation (4.13) - (4.16) and (4.31) - (4.32) for $k = 1, N_z$ and $j = 1, 2, \dots, N_y$ [since for the Dirichlet boundary condition we know the value of ϕ at the boundary for all the time steps we can readily use those equations to calculate first and second derivatives from the known values of the variables at boundary.]

$$(ii) \phi_{j,k}^* = \phi_{j,k}^{n+1} + \frac{\Delta t}{2} \left(c \frac{\partial^2\phi}{\partial z^2}\Big|_{j,k}^{n+1} - r \frac{\partial\phi}{\partial z}\Big|_{j,k}^{n+1} \right)$$

c) Solve equation (4.29) using CCD scheme i.e. equations (4.13) - (4.18)

$$\phi_{j,k}^* - c \frac{\Delta t}{2} \frac{\partial^2\phi_{j,k}^*}{\partial z^2} + r \frac{\Delta t}{2} \frac{\partial\phi_{j,k}^*}{\partial z} = f_{j,k}^n \quad (4.33)$$

d) Solve equation (4.30) using the CCD scheme i.e. equations (4.13) - (4.18)

$$\phi_{j,k}^{n+1} - b \frac{\Delta t}{2} \frac{\partial^2 \phi_{j,k}^{n+1}}{\partial y^2} + q \frac{\Delta t}{2} \frac{\partial \phi_{j,k}^{n+1}}{\partial y} = \phi_{j,k}^* \quad (4.34)$$

Some examples with Dirichlet boundary condition are illustrated in Numerical Experiment section

4.2.3 CCD-ADI Method in Three Dimensional Case

For a three dimensional case, the governing equation is expressed as

$$\frac{\partial \phi}{\partial t} + p \frac{\partial \phi}{\partial x} + q \frac{\partial \phi}{\partial y} + r \frac{\partial \phi}{\partial z} = a \frac{\partial^2 \phi}{\partial x^2} + b \frac{\partial^2 \phi}{\partial y^2} + c \frac{\partial^2 \phi}{\partial z^2} + S \quad (4.35)$$

$$(x, y, z, t) \in \Omega \times (0, T]$$

Where Ω is a three dimensional domain in \mathbb{R}^3 in $[L_x \times L_y \times L_z]$. The initial condition is given by

$$\phi(x, y, z, 0) = \phi_0(x, y, z), \quad (x, y, z) \in \Omega \quad (4.36)$$

and the boundary condition is

$$\zeta_1 \phi(x, y, z, t) + \zeta_2 \frac{\partial \phi}{\partial n}(x, y, z, t) = g(x, y, z, t), \quad (x, y, z) \in \partial\Omega, \quad t \in (0, T] \quad (4.37)$$

Using similar notation presented for one and two-dimensional cases, we can derive the following equation

$$\begin{aligned} \left(1 - \frac{\Delta t}{2} \mathcal{L}_x\right) \left(1 - \frac{\Delta t}{2} \mathcal{L}_y\right) \left(1 - \frac{\Delta t}{2} \mathcal{L}_z\right) \phi_{j,k}^{n+1} = \\ \left(1 + \frac{\Delta t}{2} \mathcal{L}_x\right) \left(1 + \frac{\Delta t}{2} \mathcal{L}_y\right) \left(1 + \frac{\Delta t}{2} \mathcal{L}_z\right) \phi_{j,k}^n + \Delta t S_{j,k}^{n+\frac{1}{2}} \end{aligned} \quad (4.38)$$

By following the same procedure as in or the two dimensional case, the above equation can be readily solved using the to following ADI scheme

$$\left(1 - \frac{\Delta t}{2} \mathcal{L}_z\right) \phi_{i,j,k}^{**} = \left(1 + \frac{\Delta t}{2} \mathcal{L}_x\right) \left(1 + \frac{\Delta t}{2} \mathcal{L}_y\right) \left(1 + \frac{\Delta t}{2} \mathcal{L}_z\right) \phi_{i,j,k}^n + \Delta t S_{i,j,k}^{n+\frac{1}{2}} \quad (4.39)$$

$$\left(1 - \frac{\Delta t}{2} \mathcal{L}_y\right) \phi_{i,j,k}^* = \phi_{i,j,k}^{**} \quad (4.40)$$

$$\left(1 - \frac{\Delta t}{2} \mathcal{L}_x\right) \phi_{i,j,k}^{n+1} = \phi_{i,j,k}^* \quad (4.41)$$

The solution technique is similar with Dirichlet boundary condition. However the boundary-conditions for ϕ^* and ϕ^{**} are calculated from the following equations for Dirichlet type boundaries. .

$$\phi_{i,j,k}^* = \left(1 - \frac{\Delta t}{2} \mathcal{L}_x\right) g_{i,j,k}^{n+1} \quad (4.42)$$

$$\phi_{i,j,k}^{**} = \left(1 - \frac{\Delta t}{2} \mathcal{L}_y\right) \left(1 - \frac{\Delta t}{2} \mathcal{L}_x\right) g_{i,j,k}^{n+1} \quad (4.43)$$

Examples with such boundary condition are given in the Numerical Experiment

section to demonstrate the accuracy of the technique.

4.3 Stability Analysis

A numerical scheme has to be stable as well as accurate. The stability of a numerical scheme can be studied by mean of a von-Neumann stability analysis where the solution or the error of the solution is decomposed into the frequency domain by Fourier transformation. The details of the von Neumann stability analysis procedure has been discussed in Appendix A. Decomposing the solution variable in Fourier nodes as

$$\phi_{i,j,k}^n = \Phi^n e^{i(i\varphi_x + j\varphi_y + k\varphi_z)} \quad (4.44)$$

$$\left. \frac{\partial \phi}{\partial x} \right|_{i,j,k}^n = \Phi_x^n e^{i(i\varphi_x + j\varphi_y + k\varphi_z)} \quad (4.45)$$

$$\left. \frac{\partial^2 \phi}{\partial x^2} \right|_{i,j,k}^n = \Phi_{xx}^n e^{i(i\varphi_x + j\varphi_y + k\varphi_z)} \quad (4.46)$$

$$\left. \frac{\partial \phi}{\partial y} \right|_{i,j,k}^n = \Phi_y^n e^{i(i\varphi_x + j\varphi_y + k\varphi_z)} \quad (4.47)$$

$$\left. \frac{\partial^2 \phi}{\partial y^2} \right|_{i,j,k}^n = \Phi_{yy}^n e^{i(i\varphi_x + j\varphi_y + k\varphi_z)} \quad (4.48)$$

$$\left. \frac{\partial \phi}{\partial z} \right|_{i,j,k}^n = \Phi_z^n e^{i(i\varphi_x + j\varphi_y + k\varphi_z)} \quad (4.49)$$

$$\left. \frac{\partial^2 \phi}{\partial z^2} \right|_{i,j,k}^n = \Phi_{zz}^n e^{i(i\varphi_x + j\varphi_y + k\varphi_z)} \quad (4.50)$$

Substituting equations (4.44) - (4.49) into equations (4.13) and (4.14) and rewriting $h = \Delta x$

$$\begin{aligned} & \frac{15}{16\Delta x} (\Phi^n e^{i((i+1)\varphi_x + j\varphi_y + k\varphi_z)} - \Phi^n e^{i((i-1)\varphi_x + j\varphi_y + k\varphi_z)}) \\ & \quad + \frac{7}{16} (\Phi_x^n e^{i((i-1)\varphi_x + j\varphi_y + k\varphi_z)} + \Phi_x^n e^{i((i+1)\varphi_x + j\varphi_y + k\varphi_z)}) \\ & \quad + \Phi_x^n e^{i(i\varphi_x + j\varphi_y + k\varphi_z)} + \frac{h}{16} (\Phi_{xx}^n e^{i((i-1)\varphi_x + j\varphi_y + k\varphi_z)} - \Phi_{xx}^n e^{i((i+1)\varphi_x + j\varphi_y + k\varphi_z)}) = 0 \end{aligned}$$

$$\begin{aligned} & - \frac{3}{\Delta x^2} (\Phi^n e^{i((i+1)\varphi_x + j\varphi_y + k\varphi_z)} - 2\Phi^n e^{i(i\varphi_x + j\varphi_y + k\varphi_z)} + \Phi^n e^{i((i-1)\varphi_x + j\varphi_y + k\varphi_z)}) \\ & \quad + \frac{9}{8\Delta x} (\Phi_x^n e^{i((i+1)\varphi_x + j\varphi_y + k\varphi_z)} - \Phi_x^n e^{i((i-1)\varphi_x + j\varphi_y + k\varphi_z)}) \\ & \quad - \frac{1}{8} (\Phi_{xx}^n e^{i((i-1)\varphi_x + j\varphi_y + k\varphi_z)} + \Phi_{xx}^n e^{i((i+1)\varphi_x + j\varphi_y + k\varphi_z)}) \\ & \quad \quad \quad + \Phi_{xx}^n e^{i(i\varphi_x + j\varphi_y + k\varphi_z)} = 0 \end{aligned}$$

Collecting terms and rearranging gives

$$\begin{aligned} & \frac{15}{16\Delta x} \Phi^n e^{i(i\varphi_x + j\varphi_y + k\varphi_z)} (e^{i\varphi_x} - e^{-i\varphi_x}) + \frac{7}{16} \Phi_x^n e^{i(i\varphi_x + j\varphi_y + k\varphi_z)} (e^{i\varphi_x} + e^{-i\varphi_x}) \\ & \quad + \Phi_x^n e^{i(i\varphi_x + j\varphi_y + k\varphi_z)} - \frac{h}{16} \Phi_{xx}^n e^{i(i\varphi_x + j\varphi_y + k\varphi_z)} (e^{i\varphi_x} - e^{-i\varphi_x}) = 0 \end{aligned}$$

$$\begin{aligned}
& -\frac{3}{\Delta x^2} \Phi^n e^{i(\varphi_x + j\varphi_y + k\varphi_z)} (e^{i\varphi_x} - 2 + e^{-i\varphi_x}) + \frac{9}{8\Delta x} \Phi_x^n e^{i(\varphi_x + j\varphi_y + k\varphi_z)} (e^{i\varphi_x} - e^{-i\varphi_x}) \\
& - \frac{1}{8} \Phi_{xx}^n e^{i(\varphi_x + j\varphi_y + k\varphi_z)} (e^{i\varphi_x} + e^{-i\varphi_x}) + \Phi_{xx}^n e^{i(\varphi_x + j\varphi_y + k\varphi_z)} = 0
\end{aligned}$$

By the Euler formula, we can write $e^{i\varphi_x} + e^{-i\varphi_x} = 2\cos\varphi_x$ and $e^{i\varphi_x} - e^{-i\varphi_x} = 2i\sin\varphi_x$.

As a result, we obtain

$$\frac{15}{16\Delta x} \Phi^n (2i\sin\varphi_x) + \frac{7}{16} \Phi_x^n (2\cos\varphi_x) + \Phi_x^n - \frac{h}{16} \Phi_{xx}^n (2i\sin\varphi_x) = 0 \quad (4.51)$$

$$-\frac{3}{\Delta x^2} \Phi^n (2\cos\varphi_x - 2) + \frac{9}{8\Delta x} \Phi_x^n (2i\sin\varphi_x) - \frac{1}{8} \Phi_{xx}^n (2\cos\varphi_x) + \Phi_{xx}^n = 0 \quad (4.52)$$

Solving for Φ_x^n and Φ_{xx}^n from above linear equations (4.51) and (4.52)

$$\Phi_x^n = i \frac{9\Phi^n \sin\varphi_x (\cos\varphi_x + 4)}{\Delta x (20\cos\varphi_x + 2\cos^2\varphi_x + 23)} = i \frac{B_x}{\Delta x A_x} \quad (4.53)$$

$$\Phi_{xx}^n = \frac{3\Phi^n (8\cos\varphi_x + 11\cos^2\varphi_x - 19)}{\Delta x^2 (20\cos\varphi_x + 2\cos^2\varphi_x + 23)} = \frac{C_x}{\Delta x^2 A_x} \quad (4.54)$$

With $B_x = 9\Phi^n \sin\varphi_x (\cos\varphi_x + 4)$, $A_x = 20\cos\varphi_x + 2\cos^2\varphi_x + 23$, and $C_x = 3\Phi^n (8\cos\varphi_x + 11\cos^2\varphi_x - 19)$. Analogous expressions can be obtained for Φ_y^n , Φ_{yy}^n , Φ_z^n and Φ_{zz}^n

The stability condition requires that the amplification factor between two harmonics remains less than unity, i.e.

$$\mathcal{G} = \frac{\phi_{i,j,k}^{n+1}}{\phi_{i,j,k}^n} \leq 1 \quad (4.55)$$

Considering the source term in equation (4.38) to be zero and substituting expressions for $\frac{\partial \phi}{\partial x}|_{i,j,k}^n$, $\frac{\partial^2 \phi}{\partial x^2}|_{i,j,k}^n$, $\frac{\partial \phi}{\partial y}|_{i,j,k}^n$, $\frac{\partial^2 \phi}{\partial y^2}|_{i,j,k}^n$, $\frac{\partial \phi}{\partial z}|_{i,j,k}^n$, $\frac{\partial^2 \phi}{\partial z^2}|_{i,j,k}^n$

$$\begin{aligned} \left(1 - \frac{\Delta t}{2} \mathcal{L}_x\right) \left(1 - \frac{\Delta t}{2} \mathcal{L}_y\right) \left(1 - \frac{\Delta t}{2} \mathcal{L}_z\right) \phi_{j,k}^{n+1} = \\ \left(1 + \frac{\Delta t}{2} \mathcal{L}_x\right) \left(1 + \frac{\Delta t}{2} \mathcal{L}_y\right) \left(1 + \frac{\Delta t}{2} \mathcal{L}_z\right) \phi_{j,k}^n + \Delta t S_{j,k}^{n+\frac{1}{2}} \end{aligned} \quad (4.56)$$

$$\begin{aligned} \mathcal{G} &= \frac{\phi_{i,j,k}^{n+1}}{\phi_{i,j,k}^n} \\ &= \left[\frac{1 + \frac{\Delta t}{2} (a\Phi_{xx}^n - p\Phi_x^n)}{1 - \frac{\Delta t}{2} (a\Phi_{xx}^n - p\Phi_x^n)} \right] \left[\frac{1 + \frac{\Delta t}{2} (b\Phi_{yy}^n - q\Phi_y^n)}{1 - \frac{\Delta t}{2} (b\Phi_{yy}^n - q\Phi_y^n)} \right] \left[\frac{1 + \frac{\Delta t}{2} (c\Phi_{zz}^n - r\Phi_z^n)}{1 - \frac{\Delta t}{2} (c\Phi_{zz}^n - r\Phi_z^n)} \right] \\ &= g_x(\varphi_x) g_y(\varphi_y) g_z(\varphi_z) \end{aligned} \quad (4.57)$$

We consider each term on the right hand side of equation (4.57)

$$g_x(\varphi_x) = \frac{1 + \frac{\Delta t}{2} a\Phi_{xx}^n - \frac{\Delta t}{2} p\Phi_x^n}{1 - \frac{\Delta t}{2} a\Phi_{xx}^n + \frac{\Delta t}{2} p\Phi_x^n} \quad (4.58)$$

Substituting expressions from equation (4.53) and (4.54)

$$g_x(\varphi_x) = \frac{1 + \frac{\Delta t}{2} a \left(\frac{C_x}{\Delta x^2 A_x} \right) - \frac{\Delta t}{2} p \left(\iota \frac{B_x}{\Delta x A_x} \right)}{1 - \frac{\Delta t}{2} a \left(\frac{C_x}{\Delta x^2 A_x} \right) + \frac{\Delta t}{2} p \left(\iota \frac{B_x}{\Delta x A_x} \right)} \quad (4.59)$$

Defining the Courant numbers, $(C_r)_x = \frac{p\Delta t}{\Delta x}$, $(C_r)_y = \frac{q\Delta t}{\Delta y}$, $(C_r)_z = \frac{r\Delta t}{\Delta z}$ and $\gamma_x = \frac{a\Delta t}{(\Delta x)^2}$, $\gamma_y = \frac{b\Delta t}{(\Delta y)^2}$, $\gamma_z = \frac{c\Delta t}{(\Delta z)^2}$

$$g_x(\varphi_x) = \frac{1 + \left(\frac{\gamma_x C_x}{2A_x}\right) - \left(i \frac{(C_r)_x B_x}{2A_x}\right)}{1 - \left(\frac{\gamma_x C_x}{A_x}\right) + \left(i \frac{(C_r)_x B_x}{2A_x}\right)} \quad (4.60)$$

The imaginary part of the numerator and denominator are the same, therefore we consider the real part. Since, $A_x > 0$, $A_y > 0$, $A_z > 0$, and $C_x \leq 0$, $C_y \leq 0$, $C_z \leq 0$, hence

$$\left[1 + \left(\frac{\gamma_x C_x}{2A_x}\right)\right] \leq 1 - \left(\frac{\gamma_x C_x}{2A_x}\right) \quad (4.61)$$

and

$$1 + \left(\frac{\gamma_z C_z}{2A_z}\right) \leq 1 - \left(\frac{\gamma_z C_z}{2A_z}\right) \quad (4.62)$$

Which implies that $g_x(\varphi_x) \leq 1$, $g_y(\varphi_y) \leq 1$ and $g_z(\varphi_z) \leq 1$. Thus

$$|\mathcal{G}| = |g_x(\varphi_x)g_y(\varphi_y)g_z(\varphi_z)| \leq 1 \quad (4.63)$$

This indicates that the CCD-ADI scheme is unconditionally stable;

One of the principal motivations of this research project is an investigation of dispersive processes. When we model these processes, it is essential that the results are not oppugned by numerical dispersion. To explore the diffusion error in CCD-ADI scheme, we proceed to find the magnitude of the amplification factor

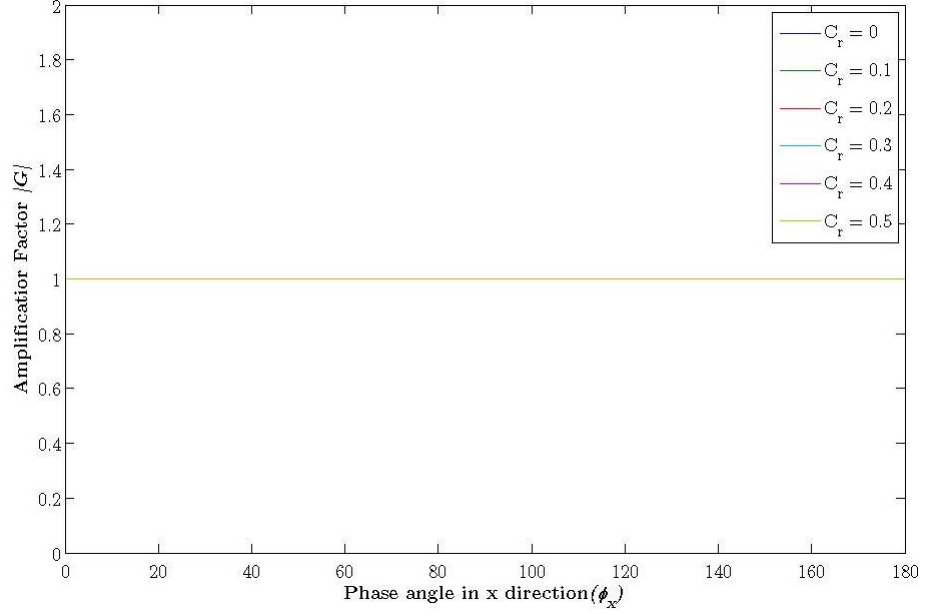


Figure 4.1: Diffusion error of the CCD-ADI method as a function of phase angle for different Courant numbers

$$\begin{aligned}
 |\mathcal{G}| = & \left[\left\{ \left(-4A_x^2 + B_x^2 (C_r)_x^2 + C_x^2 \gamma_x^2 \right)^2 \right. \right. \\
 & + 16A_x^2 B_x^2 (C_r)_x^2 \left. \right\}^{\frac{1}{2}} \left\{ \left(-4A_y^2 + B_y^2 (C_r)_y^2 + C_y^2 \gamma_y^2 \right)^2 \right. \\
 & + 16A_y^2 B_y^2 (C_r)_y^2 \left. \right\}^{\frac{1}{2}} \left\{ \left(-4A_z^2 + B_z^2 (C_r)_z^2 + C_z^2 \gamma_z^2 \right)^2 \right. \\
 & + 16A_z^2 B_z^2 (C_r)_z^2 \left. \right\}^{\frac{1}{2}} \Big] / \left(4A_x^2 - 4A_x C_x \gamma_x + B_x^2 (C_r)_x^2 \right. \\
 & + C_x^2 \gamma_x^2 \Big) \left(4A_y^2 - 4A_y C_y \gamma_y + B_y^2 (C_r)_y^2 \right. \\
 & \left. \left. + C_y^2 \gamma_y^2 \right) \left(4A_z^2 - 4A_z C_z \gamma_z + B_z^2 (C_r)_z^2 + C_z^2 \gamma_z^2 \right)
 \end{aligned}$$

$$\begin{aligned}
|\mathcal{G}| = & \left[\left\{ \left(\gamma_x^2 (8\cos\varphi_x + 11\cos^2\varphi_x - 19)^2 - 4 (20\cos\varphi_x + 2\cos^2\varphi_x + 23)^2 \right. \right. \right. \\
& \left. \left. \left. + (C_r)_x^2 \sin^2\varphi_x (\cos\varphi_x + 4)^2 \right)^2 \right. \right. \\
& \left. \left. + 16 (C_r)_x^2 \sin^2\varphi_x (\cos\varphi_x + 4) (20\cos\varphi_x + 2\cos^2\varphi_x + 23)^2 \right\}^{\frac{1}{2}} \right. \\
& \left. \left\{ \left(\gamma_z^2 (8\cos\varphi_z + 11\cos^2\varphi_z - 19)^2 - 4 (20\cos\varphi_x + 2\cos^2\varphi_x + 23)^2 \right. \right. \right. \\
& \left. \left. \left. + (C_r)_x^2 \sin^2\varphi_x (\cos\varphi_x + 4)^2 \right)^2 \right. \right. \\
& \left. \left. + 16 (C_r)_x^2 \sin^2\varphi_x (\cos\varphi_x + 4)^2 (20\cos\varphi_x + 2\cos^2\varphi_x + 23)^2 \right\}^{\frac{1}{2}} \right] \\
& / \left[4 \left\{ (20\cos\varphi_x + 2\cos^2\varphi_x + 23)^2 + \gamma_x^2 (8\cos\varphi_x + 11\cos^2\varphi_x - 19)^2 \right. \right. \\
& \left. \left. - \gamma_x (8\cos\varphi_x + 11\cos^2\varphi_x - 19)^2 (80\cos\varphi_x + 8\cos^2\varphi_x + 92) \right. \right. \\
& \left. \left. + (C_r)_x^2 \sin^2\varphi_x (\cos\varphi_x + 4)^2 \right\} \right. \\
& 4 \left\{ (20\cos\varphi_y + 2\cos^2\varphi_y + 23)^2 + \gamma_y^2 (8\cos\varphi_y + 11\cos^2\varphi_y - 19)^2 \right. \\
& \left. - \gamma_x (8\cos\varphi_y + 11\cos^2\varphi_y - 19)^2 (80\cos\varphi_y + 8\cos^2\varphi_y + 92) \right. \\
& \left. + (C_r)_y^2 \sin^2\varphi_y (\cos\varphi_y + 4)^2 \right\} \\
& 4 \left\{ (20\cos\varphi_z + 2\cos^2\varphi_z + 23)^2 + \gamma_z^2 (8\cos\varphi_z + 11\cos^2\varphi_z - 19)^2 \right. \\
& \left. - \gamma_z (8\cos\varphi_z + 11\cos^2\varphi_z - 19)^2 (80\cos\varphi_z + 8\cos^2\varphi_z + 92) \right. \\
& \left. \left. + (C_r)_z^2 \sin^2\varphi_z (\cos\varphi_z + 4)^2 \right\} \right] \quad (4.64)
\end{aligned}$$

In order to observe the diffusion error for a linear convection equation, the am-

plification factor has been plotted as a function of φ_x for different Courant number varying from 0 to 0.5 with $\gamma_x = \gamma_y = \gamma_z = 0$ and maximum wavelength in the y and z direction with $\varphi_y = \varphi_z = \pi$. Although the CCD-ADI scheme is unconditionally stable, the range of Courant number has been chosen in accordance with first order upwind and modified QUICKEST scheme. In Figure 4.1, it is observed that the amplification factor is unity for the entire range of Courant numbers and phase angle. This confirms that there is no artificial diffusion in the scheme.

4.4 Numerical Experiments

4.4.1 Two Dimensional Case

We consider the following partial differential equation in two-dimensional square domain $0 \leq x, y \leq 2$

$$\frac{\partial \phi}{\partial t} + p \frac{\partial \phi}{\partial x} + q \frac{\partial \phi}{\partial y} = a \frac{\partial^2 \phi}{\partial x^2} + b \frac{\partial^2 \phi}{\partial y^2} \quad (4.65)$$

The initial condition is

$$\phi(x, y, 0) = \exp\left(-\frac{(x-0.5)^2}{a} - \frac{(y-0.5)^2}{b}\right) \quad (4.66)$$

And the boundary conditions are

$$\phi(0, y, t) = \frac{1}{4t+1} \exp\left(-\frac{(pt-0.5)^2}{a(4t+1)} - \frac{(y-qt-0.5)^2}{b(4t+1)}\right) \quad (4.67)$$

$$\phi(2, y, t) = \frac{1}{4t+1} \exp\left(-\frac{(pt+1.5)^2}{a(4t+1)} - \frac{(y-qt-0.5)^2}{b(4t+1)}\right) \quad (4.68)$$

$$\phi(x, 0, t) = \frac{1}{4t+1} \exp\left(-\frac{(x-pt-0.5)^2}{a(4t+1)} - \frac{(qt-0.5)^2}{b(4t+1)}\right) \quad (4.69)$$

$$\phi(x, 2, t) = \frac{1}{4t+1} \exp\left(-\frac{(x-pt-0.5)^2}{a(4t+1)} - \frac{(qt+1.5)^2}{b(4t+1)}\right) \quad (4.70)$$

For which the analytical solution is

$$\phi(x, y, t) = \frac{1}{4t+1} \exp\left(-\frac{(x-pt-0.5)^2}{a(4t+1)} - \frac{(y-qt-0.5)^2}{b(4t+1)}\right) \quad (4.71)$$

The initial and Dirichlet boundary condition are directly taken from the exact solution. For a uniform grid size ($\Delta x = \Delta y = 0.02$), we maintain the diffusivity constant ($a = b = 0.01$) and vary the convection velocity $p, q = 0.01, 0.1, 1.0, 10$ to investigate the effect of Peclet number ($Pe = p\Delta x/a$).

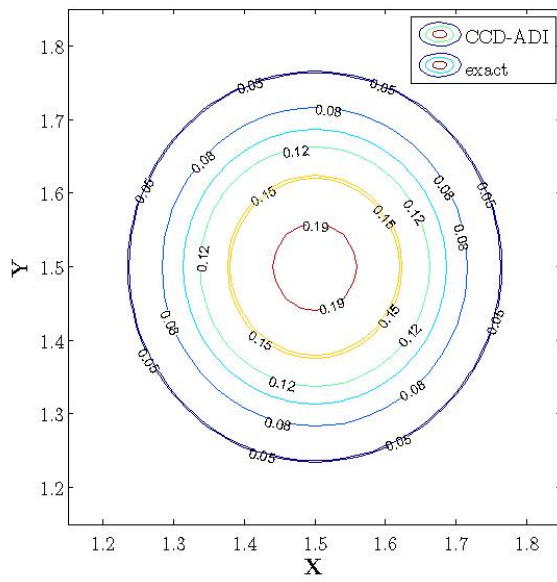
From Figure 4.5 it may be observed that the present scheme very accurately predicts the solution of the equation. This agreement retains a similar degree of accuracy in both high and low Peclet number i. e. in both convection dominated flows and diffusion dominated flows.

4.4.2 Three Dimensional Case

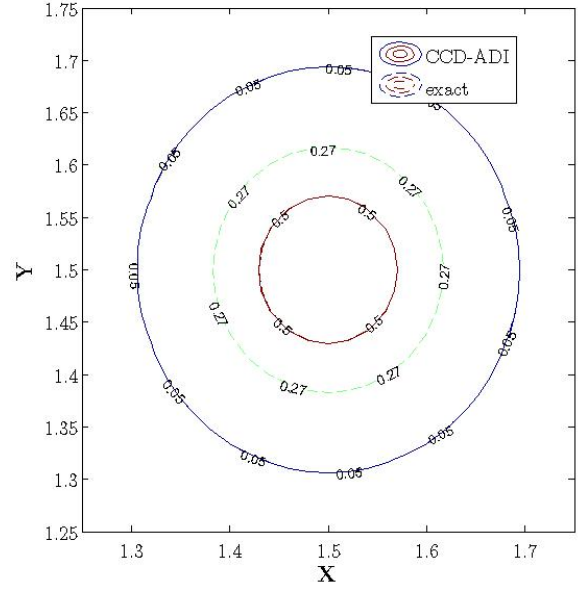
We consider the following partial differential equation in a three-dimensional cubic domain $0 \leq x, y, z \leq 2$

$$\frac{\partial \phi}{\partial t} + p \frac{\partial \phi}{\partial x} + q \frac{\partial \phi}{\partial y} + r \frac{\partial \phi}{\partial z} = a \frac{\partial^2 \phi}{\partial x^2} + b \frac{\partial^2 \phi}{\partial y^2} + c \frac{\partial^2 \phi}{\partial z^2} \quad (4.72)$$

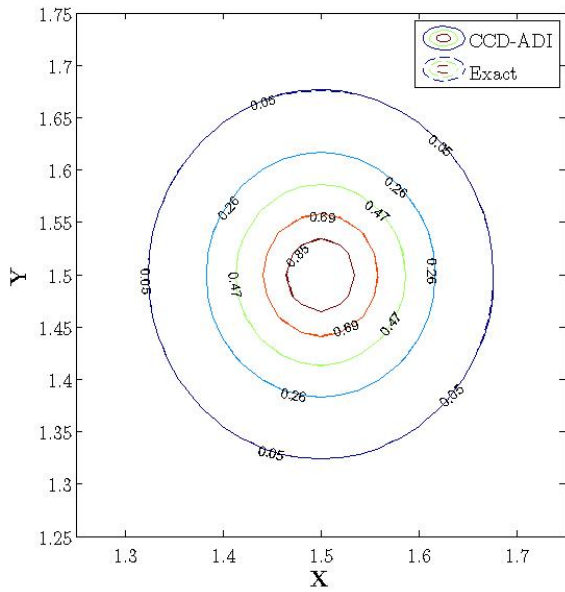
for which the analytical solution is



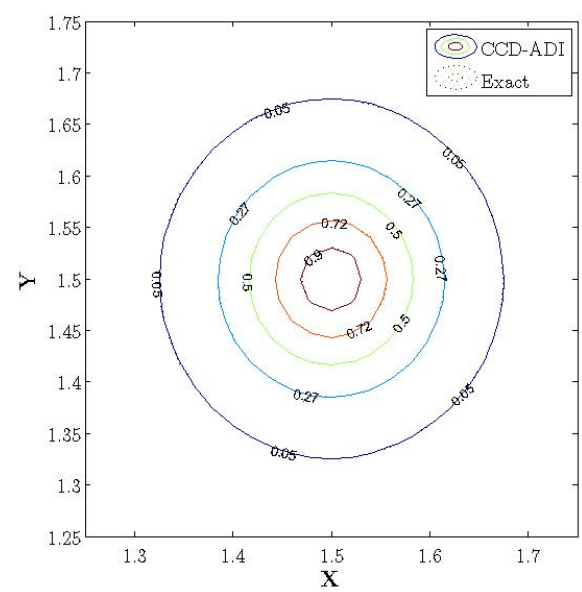
(a)



(b)



(c)



(d)

Figure 4.2: Comparison between the exact and the numerical solutions using the method presented in this thesis, $Pe=2, 20, 200, 2000$

$$\phi(x, y, z, t) = \frac{1}{(4t + 1)^{\frac{3}{2}}} \exp \left(-\frac{(x - pt - 0.5)^2}{a(4t + 1)} - \frac{(y - qt - 0.5)^2}{b(4t + 1)} - \frac{(z - rt - 0.5)^2}{c(4t + 1)} \right) \quad (4.73)$$

The initial and Dirichlet boundary conditions are directly taken from the exact solution. For a uniform grid size ($\Delta x = \Delta y = \Delta z = 0.025$), we maintain the diffusivity constant ($a = b = 0.01$) and vary the convection velocities $p, q, r = 0.8, 8, 80, 800$ to see the effect of Peclet number ($Pe = \frac{p\Delta x}{a}$). The resulting solution after time $t = 1.25$ sec

From the comparison of the solution depicted by the CCD method and the exact solution in Figure 4.3, it can be concluded that the present scheme can be used to solve the hydrodynamics dispersion problem with a high degree of confidence. Furthermore, the solution curves for the pulse at $z = 0.2$ and 1.2 is shown for further comparison with the exact solution. Similarly it can be seen in Figure 4.4 that the profile of the variable at both plane calculated by the present scheme agree very well with the exact solution

4.5 Shear Flow Dispersion in a Rectangular Duct

Using the CCD-ADI Scheme

Recalling the governing equation for solute dispersion in laminar flow through a square duct

$$\frac{\partial \mathcal{C}}{\partial t} + u(y, z) \frac{\partial \mathcal{C}}{\partial x} = D_m \left(\frac{\partial^2 \mathcal{C}}{\partial x^2} + \frac{\partial^2 \mathcal{C}}{\partial y^2} + \frac{\partial^2 \mathcal{C}}{\partial z^2} \right) \quad (4.74)$$

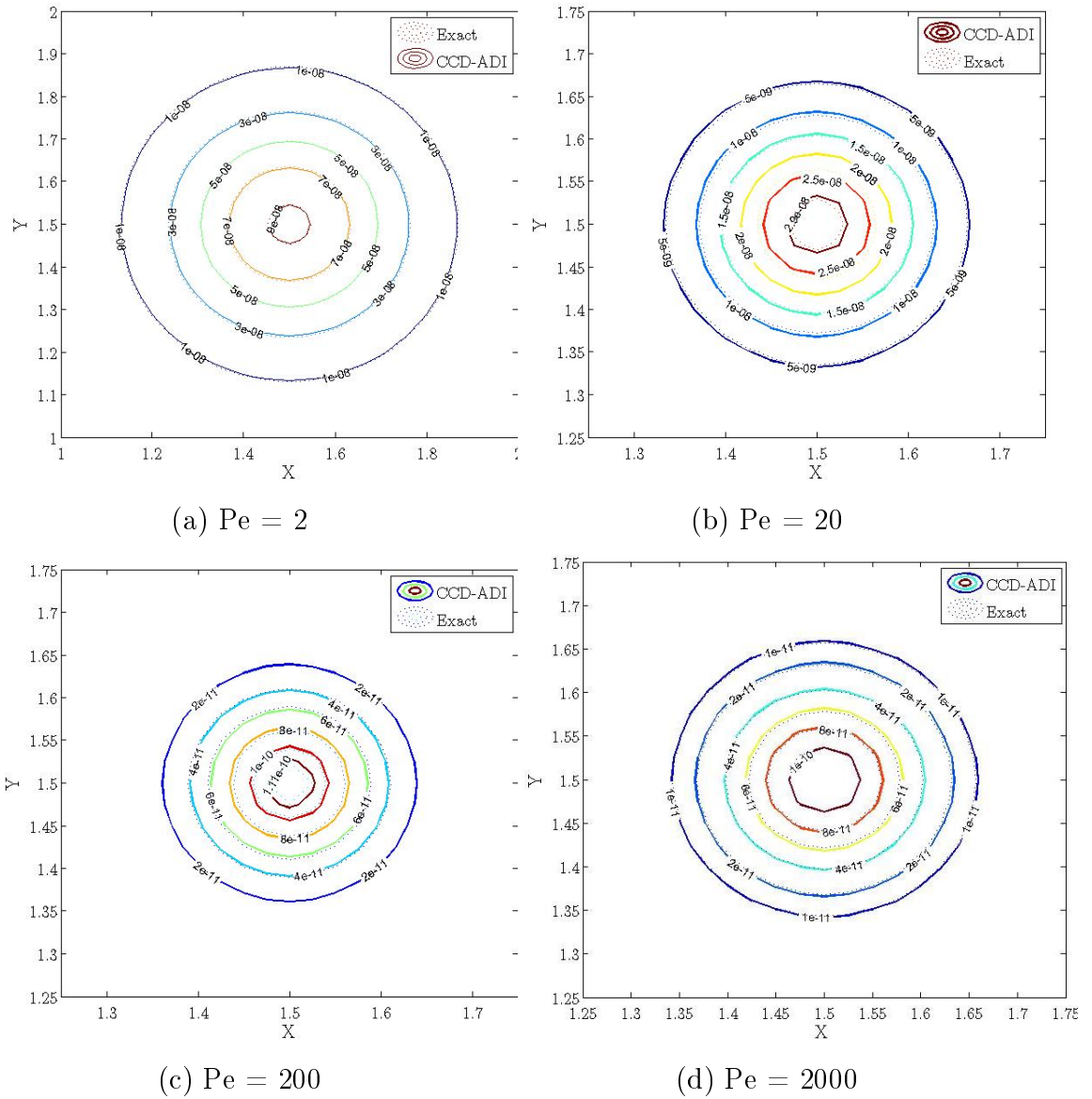
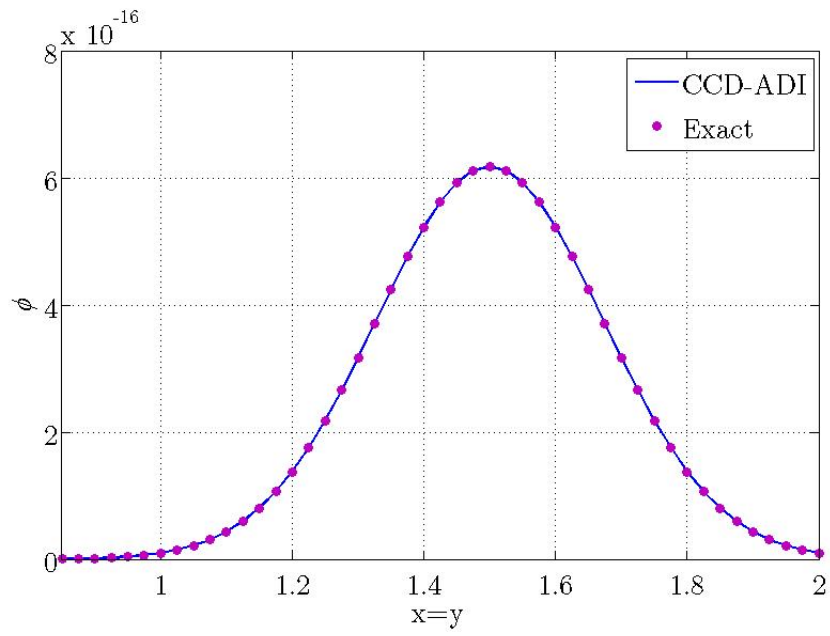
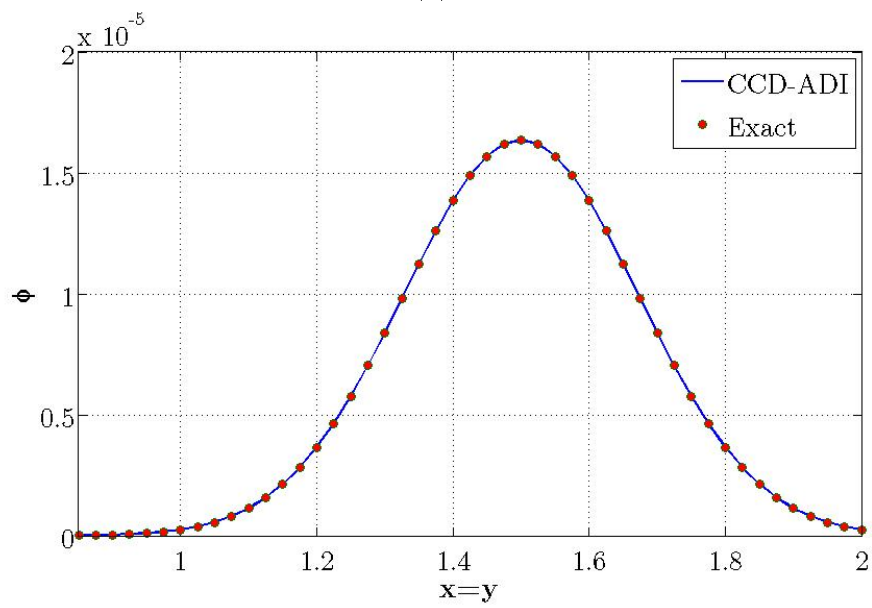


Figure 4.3: Comparison between exact solution and the CCD method for linear convection diffusion equation in two dimensional space with Dirichlet boundary condition, , (a) $Pe = 2$, (b) $Pe = 20$, (c) $Pe = 200$, (d) $Pe = 2000$ at $z=1.0$



(a)



(b)

Figure 4.4: Comparison of the CCD-ADI solution with the exact solution $0 \leq x, y \leq 2$, $t = 1.25$, $Pe = 2$; (a) $z = 0.2$, (b) $z = 1.2$

subject to initial condition $\mathcal{C}(x, y, 0) = \mathcal{C}_0$

since there is no flow across the boundary

$$\left. \frac{\partial \mathcal{C}}{\partial y} \right|_{y=0, L_y} = 0, \quad \left. \frac{\partial \mathcal{C}}{\partial z} \right|_{z=0, L_z} = 0 \quad (4.75)$$

Furthermore, the outflow boundary condition is expressed as

$$\left. \frac{\partial \mathcal{C}}{\partial x} \right|_{x=L_x} = 0 \quad (4.76)$$

We have assumed constant coefficients for the operators while developing the ADI method. Although the velocity is a function of y and z , it is constant in the x direction for fully developed flow in square ducts. Hence we can employ the same method for solving this equation without any major modification.

By setting the variable ϕ as the concentration of a scalar \mathcal{C} , diffusion coefficients $a = b = c = D_m$, which is the isotropic molecular diffusivity of the scalar in the fluid, and $q = r = 0$, $p = u(y, z)$, fully developed convection velocity profile in laminar flow through square duct, the equation (4.35) becomes our study problem for solute dispersion in laminar flow through square ducts with Neumann boundary conditions at the walls and outlet.

4.5.1 Grid Sensitivity Analysis

Numerical solutions of continuous equations are inherently an approximation of the actual solution where the variable is solved at each grid point of a particular domain. The final result strongly depends on the resolution of grid points in the domain. Hence, in order to increase the reliability of the solution, it is important to have a grid independent or grid converged solution. A solution is termed as grid independent

when it does not show significant changes with grid refinement. A grid convergence study is carried out to determine the optimum spatial and temporal grid resolution. Optimal grids show a minimal effect on the solution after further refinement and at the same time reduces computational effort.

For the grid sensitivity analysis, we solve equation (4.64) along with boundary conditions defined by in equation (4.74) and equation (4.75) for a finite domain $\{x, y, z\} \in \{L_x \times L_y \times L_z\}$ and $t \in (0, 0.1)$ s, where $L_x = L_y = L_z = 0.1$. The fully developed velocity profile in axial direction is given by (Johnson, 2016)

$$u(y, z) = \frac{16L_y^2}{\mu\pi^3} \left(-\frac{dp}{dx} \right) \sum_{n=1,3,5,\dots}^{\infty} (-1)^{\frac{(n-1)}{2}} \left[1 - \frac{\cosh\left(\frac{n\pi z}{2L_y}\right)}{\cosh\left(\frac{n\pi L_z}{2L_y}\right)} \right] \frac{\cos\left(\frac{n\pi y}{2L_y}\right)}{n^3} \quad (4.77)$$

in which

μ = kinematic viscosity of the flowing fluid, Pa.s

$-\frac{dp}{dx}$ = axial pressure gradient, Pa/m

The velocity profile is calculated from the above equation and then normalized with the mean velocity (u_0) that we have taken and varied to study the effect of Peclet number. In this study we consider ($u_0 = 0.1$ m/s) and diffusion coefficient $D_m = 1 \times 10^{-4}$ m/s² so that the Peclet number becomes 1 in the lateral and temporal grid independence study.

Furthermore, we solve equation (4.64) with a Gaussian pulse input as the initial condition given by

Table 4.1: Lateral grid convergence test result for the CCD Scheme

$N_y = N_z$	6	11	21	26	31
$\sigma_{\mathcal{C}_{mean}}^2$	0.0403	0.0446	0.0458	0.0460	0.0462
$max(\mathcal{C})_{mean}$	0.5560	0.6059	0.6168	0.6180	0.6185
$N_y = N_z$	41	51	81	101	
$\sigma_{\mathcal{C}_{mean}}^2$	0.0462	0.0462	0.0462	0.0462	
$max(\mathcal{C})_{mean}$	0.6194	0.6197	0.6200	0.6201	

$$\mathcal{C}_0 = \begin{cases} \exp\left(-\left(\frac{x-0.05}{0.009}\right)^2\right); & 0.001 < x < 0.101; y \in \{0, L_y\}; z \in \{0, L_z\}; \\ 0; & x \leq 0.001 \text{ and } x \geq 0.101; \in \{0, L_y\}; z \in \{0, L_z\} \end{cases} \quad (4.78)$$

4.5.1.1 Lateral grid independence

For the lateral grid independence study the axial mesh is considered as 101 for the domain defined above and the time step is taken as 0.001s. With this setup the simulation is run for 0.1 s. The mean velocity is set such that the scalar does not escape through outlet in this time and we can check mass conservation by comparing total mass before and after the simulation. Two parameters are observed after the simulation, firstly the highest value of the cross-sectional area averaged concentration $(\mathcal{C}_{mean})_{max}$, and secondly the spreading of the Gaussian pulse which is indicated by the variance $(\sigma_{\mathcal{C}_{mean}}^2)$ of the mean concentration of the pulse.

For lateral grid sensitivity test the simulation is run with the number of lateral nodes set at 6, 11, 21, 26, 31, 41, 51, 81, and 101.

From Figure 4.5 it is evident that the values of both variance and peak of cross sectional area average concentration converge as the lateral grid is refined. The variation for both parameters is quite significant for number of grids changing from 6 to 21, however further refinement beyond 21 makes a very little change in the

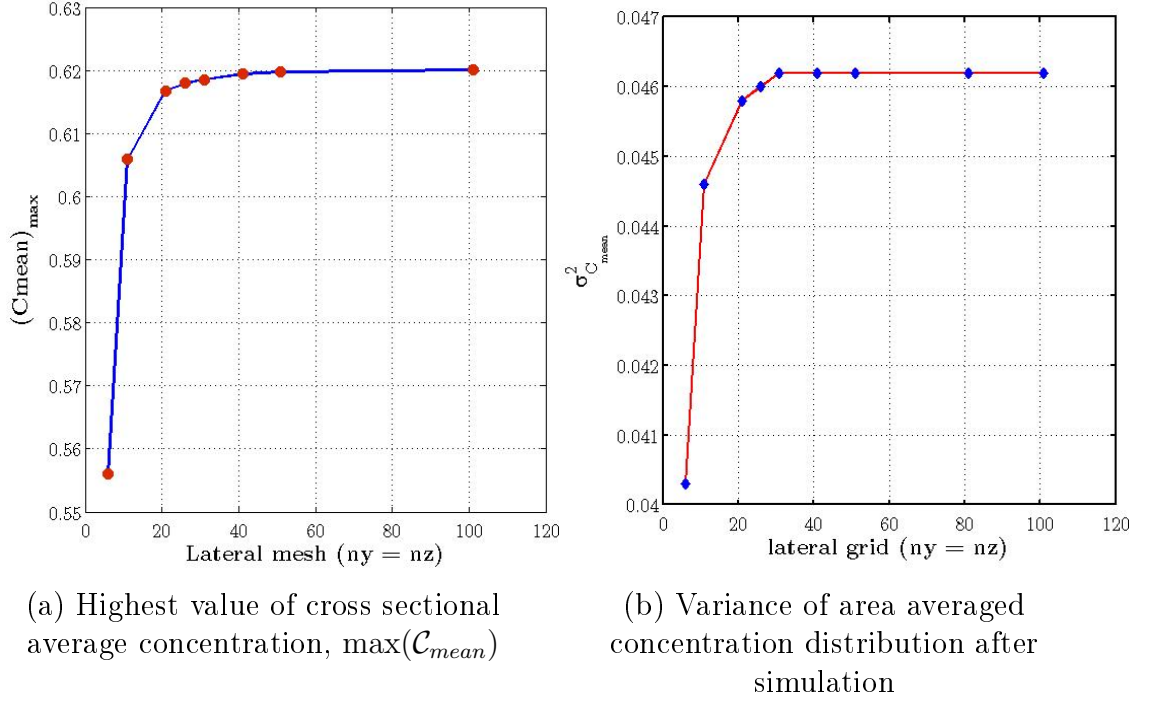


Figure 4.5: Lateral grid independence test for the CCD Scheme,

solution with double, triple and quadruple computational expense. Therefore, we can conclude that for a grid independent result, the number of grid in lateral direction can be considered to be 21; therefore the grid size in lateral direction would be $\Delta y = L_y / (N_y - 1) = 0.1 / 20 = 0.005$.

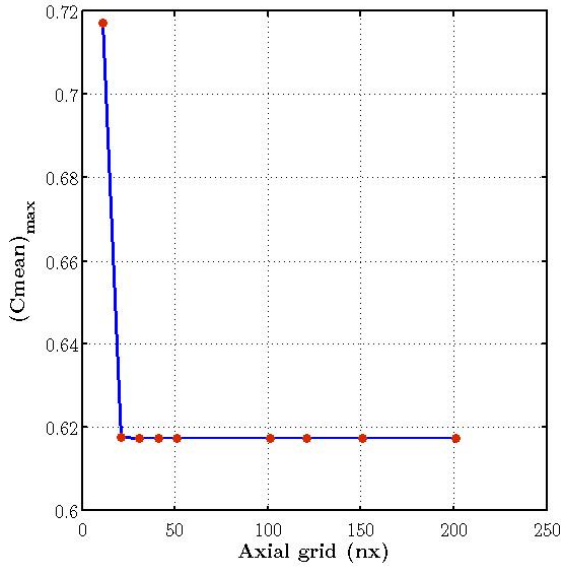
4.5.1.2 Axial grid independence study

In the axial grid independence study the lateral mesh is considered as 21×21 in the y and z directions which we considered in the previous section. Furthermore, the time step remains unchanged at 0.001s and the simulation is run for 0.1 s for similar test setup that used for lateral grid independence test. In the following, Table 4.2 shows the values for $\sigma_{C_{mean}}^2$ and $\max(\mathcal{C}_{mean})$ for corresponding axial grid resolution and Figure 4.6 graphically demonstrates these results.

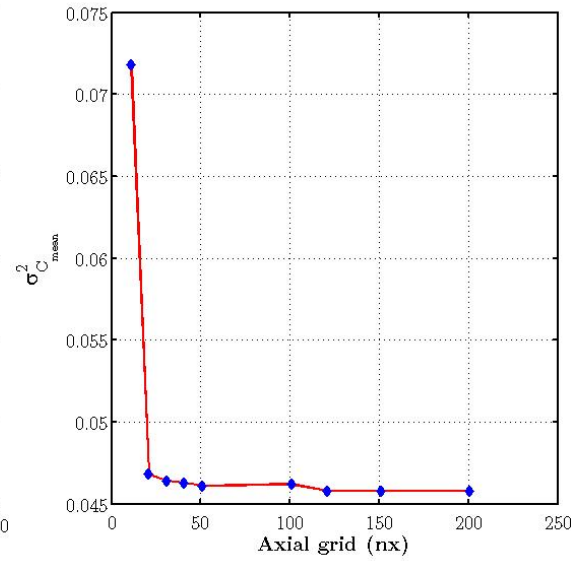
From Figure 4.6, it can be observed that both parameters indicate a converged

Table 4.2: Axial grid convergence test result for the CCD Scheme

$N_y = N_z$	11	21	31	41	51	101	121	151	201
$\sigma_{\mathcal{C}_{mean}}^2$	0.0718	0.0468	0.0464	0.0463	0.0461	0.0462	0.0458	0.0458	0.0458
$\max(\mathcal{C}_{mean})$	0.7172	0.6176	0.6174	0.6174	0.6174	0.6174	0.6174	0.6174	0.6174



(a) Highest value of cross sectional average concentration, $\max(\mathcal{C}_{mean})$



(b) Variance of area averaged concentration distribution after simulation

Figure 4.6: Axial grid independence test for the CCD scheme

Table 4.3: The effect of time step on the solution for the CCD Scheme

dt	0.05	0.01	0.005	0.001	0.0005	0.0001	0.00005	0.00001
$\sigma_{C_{mean}}^2$	0.05	0.046	0.0459	0.0458	0.0458	0.0458	0.0458	0.0458
$max(C_{mean})$	0.6956	0.6196	0.6174	0.6168	0.6167	0.6167	0.6167	0.6167

solution at 21 grids in the axial direction. Further refinement beyond 21 does not change the solution hence at $N_x=21$ (which means $dx = L_x/(N_x - 1) = 0.1/20 = 0.005$ is the largest grid size in the axial direction which do not invoke a considerable change in the solution upon further refinement); the solution can be taken as being a grid independent solution for the given domain.

4.5.1.3 Temporal grid independence study

After ensuring a spatial grid independent solution, it is important to have a solution which will be independent of time step refinement. In order to do so, the problem is setup with the similar initial and boundary condition as before and the axial and lateral grid resolution is considered as $100 \times 21 \times 21$ in x , y and z directions respectively. The time step is varied from 0.05 s to 0.00005 s to observe the effect of refining the time step. The domain remained unchanged and the simulation is run for 0.1 s with all other parameters unchanged. The simulated values of $\sigma_{C_{mean}}^2$ and $max(C_{mean})$ are tabulated corresponding to the the time steps in Table 4.3 and 4.7 graphically demonstrates these results.

It can be concluded that both parameters shows a converge solution for time step $\Delta t = 0.01$. Further refinement beyond 21 represents minor change in the solution. Therefore, $\Delta t = 0.01$ s is used in this study.

Grid independent solutions are vital for the reliability of any numerical simulation. Hence, a grid independence study has been carried out for a confined spatial domain $0.1 \times 0.1 \times 0.1$ in x , y and z directions respectively for 0.1 s with Peclet number 1.

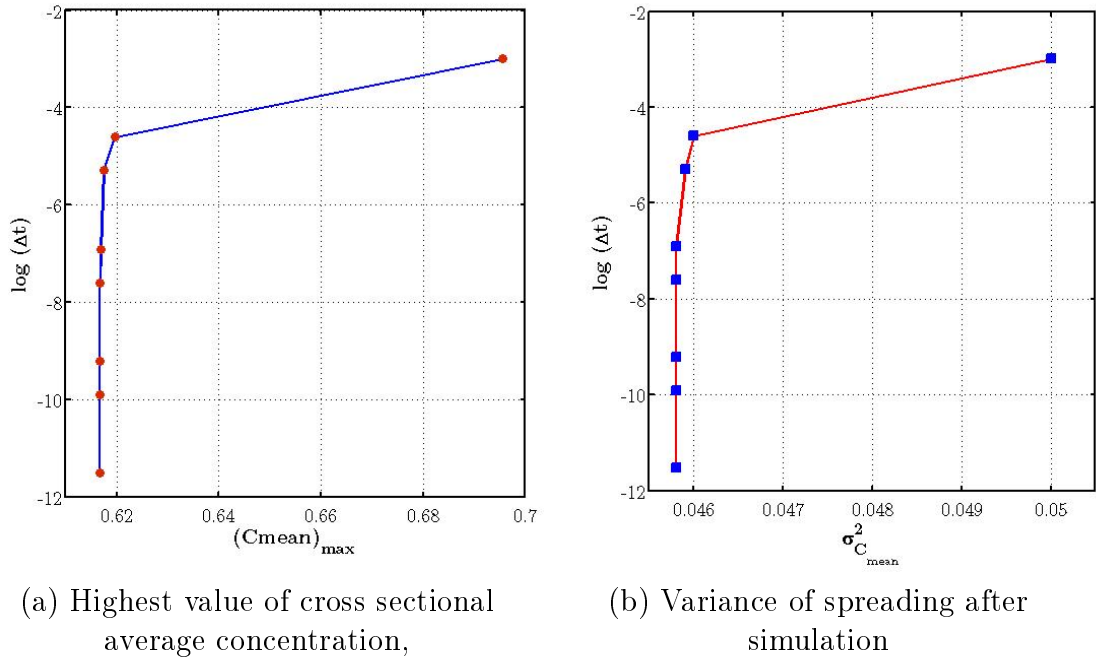


Figure 4.7: Time step independence test for the CCD Scheme

From the analysis, it has been found that a spatial resolution of $21 \times 21 \times 21$ in the x , y and z directions respectively with $\Delta t = 0.01s$ gives a solution which does not pose any significant change in further refinement. Hence the appropriate grid spacing for the numerical simulation is taken to be $\Delta x = 0.005$, $\Delta y = 0.005$, $\Delta z = 0.005$ and $\Delta t = 0.01s$.

4.5.2 CCD Scheme in Calculating Solute Spreading

The acceptability of a numerical scheme relies heavily on the validation accuracy of the scheme with simplified analytical results or experimental observations. The experimental results for dispersion of a solute in laminar flow through rectangular ducts are scant in the literature. Hence we consider the analytical solution of the phenomena as given in Doshi et al. (1978). Using the velocity profile as described by (4.77) in the CCD scheme, the solute distribution is plotted in Figure 4.8. It

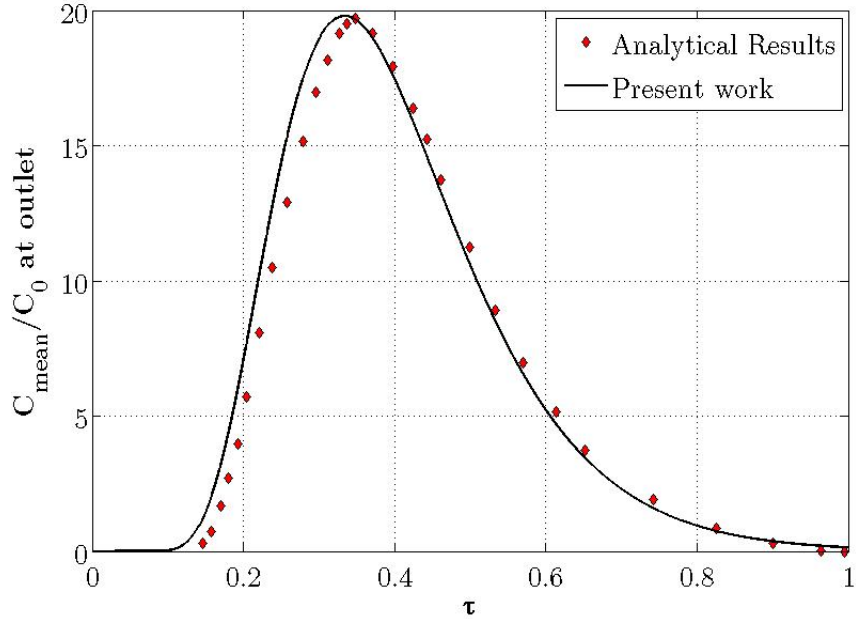


Figure 4.8: Solute distribution at dimensionless distance $X=0.1$ in a square channel using CCD-ADI scheme in laminar flow

is observed that the CCD scheme is well versed in predicting the concentration distribution of the solute in flowing through a square duct.

4.6 Summary and Conclusions

The convection diffusion equation governs many physical phenomena. Numerical solution of this equation is highly desirable in many engineering applications. In this chapter, we have devised a sixth order spatially accurate CCD scheme for solving the convection diffusion equation in two and three-dimensions. The three point stencil of the scheme renders it compact and computationally efficient. A solver for the twin tridiagonal and triple tridiagonal matrix has been developed to solve the simultaneous equations computationally effectively. Furthermore, by means of a Fourier analysis, it is demonstrated that the numerical scheme is unconditionally stable and artificial diffusion in the solution is negligible. Moreover, numerical experiments have been

performed with both Dirichlet and Neumann boundary conditions. Simulation results clearly demonstrate that the scheme developed in this work is capable of solving the convection diffusion equation accurately in high and low Peclet numbers.

Chapter 5

Dispersion of a Solute in Turbulent Flow through Circular Pipes

5.1 Background

Turbulent mixing processes are prevalent in many engineering applications. Such processes take place in pipes and ducts that have circular cross-sections such as water supply networks, oil and gas pipelines and so on. This mixing process has significant impact in many engineering aspects. For instance it can reduce the driving forces in chemical reactors and reduce the effectiveness of signals in tracer experiments in oil and gas flow.

The longitudinal mixing process in turbulent flow through ducts occurs due to molecular motion (diffusion), bulk motion (convection) and random fluctuation of fluid particles (eddies). However in highly turbulent flows, the effect of molecular diffusion is negligible and the governing mechanism of scalar dispersion is the turbulent motion of small regions of the carrier fluid. Hence the elements of turbulence are

discussed as a propaedeutic to discussing dispersion in turbulent flow.

5.2 Turbulence

Turbulence can be characterized as unsteady, apparently random, irregular and chaotic fluid motion in which wide ranges of length and time scales prevail. These characteristics lead to one of the most important aspects of turbulence, namely its ability to enhance dispersion of solute transport compared to laminar flow. This phenomenon was experimentally demonstrated by Reynolds (1883) observing a dye streak through water flowing in glass tubes. In the slow moving flow, described as laminar flow, parallel layers of fluid move along almost perfect straight lines and the disturbances are attenuated by the effect of viscosity. The only mechanism that may spread the dye streak in the experiment is through the action of molecular diffusion which required a much longer pipe to be observed. On the other hand, at higher velocities of the flow, described as turbulent flow, instabilities and flow disturbances appear which give rise to a spectrum of eddies or swirling fluid masses in the flow region. Furthermore, an electric spark in the flow conforms that the pattern of dye, which is essentially following fluid masses passively, forming eddies in the flow regime. The findings from Reynolds experiment established quantitative description flow behavior and showed that laminar and turbulent flow behavior is dependent of the non-dimensionless number, known as Reynolds number $Re = Ud/\nu$ where U and d are cross sectional averaged velocity and diameter of the pipe and ν is the kinematic viscosity of the flowing fluid. A primal consequence of turbulence is that it enhances mass, momentum and energy transport.

5.3 Mathematical Formulation of Turbulence

In a turbulent flow, the continuous formation of large eddies and their breaking down into smaller eddy takes place. As a consequence, there is always a spectrum of eddy size present in the flow. During this process, kinetic energy is transferred from larger eddies to smaller eddies through a cascade of eddy sizes efficiently. Ultimately, all eddies break down to a sufficiently small scale at which viscosity dissipates the kinetic energy into heat. The rate at which the kinetic energy is dissipated as

$$\epsilon = \frac{\text{dissipated kinetic energy}}{\text{time}} \quad (5.1)$$

with dimensions $[L^2/T^3]$. For homogeneous turbulence (i.e. the statistical properties of turbulence remain unchanged with time), the kinetic energy is transferred efficiently through cascading of eddy sizes. In the quasi-steady state, the total rate of production and destruction of kinetic energy are balanced. The smallest length scale of the eddies from which kinetic energy is dissipated into heat is known as the Kolmogorov scale, L_K which can be quantified by dimensional analysis. Since friction converts the energy into heat, the length scale depends on the rate of dissipation or production of kinetic energy (ϵ), and viscosity (ν). Extraction of a length scale from these quantities gives

$$L_K \propto \left(\frac{\nu^3}{\epsilon} \right)^{\frac{1}{4}} \quad (5.2)$$

The difficulties of tracking each fluid particle as in Lagrangian frame of reference leads to express the governing equation in terms of an Eulerian reference frame for accounting for turbulence in which the velocity of fluid is measured at a particular

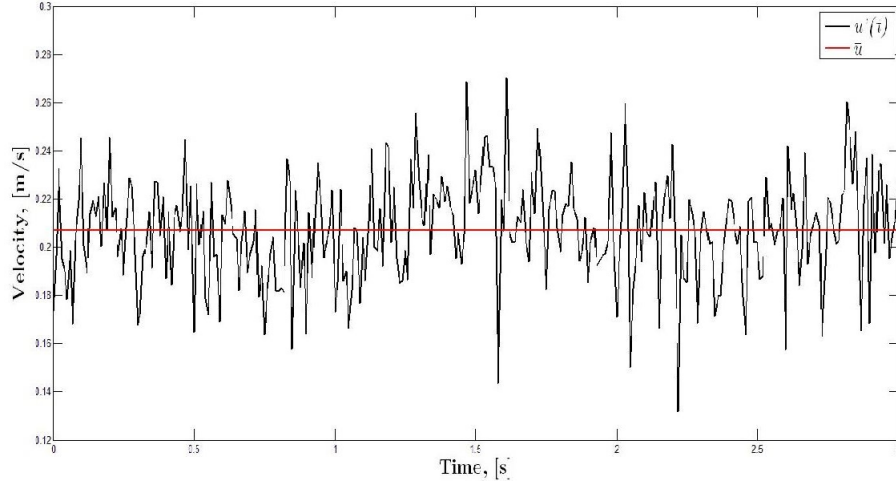


Figure 5.1: Schematic representation of the turbulent fluctuating velocity and the mean velocity

point. In time series data, the period of the velocity fluctuation represent the scale of the eddies.

Figure 5.1 demonstrates the mean and the fluctuating component of a turbulent velocity field at a particular point. In a short time scale, the velocity is orderly and deterministic. However, in a greater time scale, the velocity is completely disordered and random. The time scale which differentiates this orderly and disorderly velocity patterns is termed as integral time scale (t_I) which can be represented as characteristic length (l_I) and velocity (u_I). According to Reynolds suggestion, at a longer time than t_I , the velocity at a point x_i could be decomposed into the mean (\bar{u}) and fluctuating component (u') as

We discretize the one dimensional domain into a uniform grid $0 = x_1 < x_2 < \dots < x_{N-1} < x_N = L$ with grid spacing $h = L/(N_x - 1)$. Expanding any arbitrary function $\phi(x)$ and x_i , $i = 1, 2, \dots, N_x$ using Taylor series with up to sixth derivative, we obtain

$$u_i(x_i, t) = \bar{u}_i(x_i) + u'_i(x_i, t) \quad (5.3)$$

5.4 The Turbulent Advection Diffusion Equation

To achieve a turbulent convection diffusion equation, we apply Reynolds decomposition into the convection diffusion equation. To facilitate calculation, we perform some a priori analysis of Reynolds decomposition for the concentration (\mathcal{C}) and the time averaged concentration flux ($\overline{u\mathcal{C}}$) at a point

The Reynolds decomposition for the concentration is

$$\mathcal{C}(x_i, t) = \overline{\mathcal{C}}(x_i) + \mathcal{C}'_i(x_i, t) \quad (5.4)$$

$$\overline{u\mathcal{C}} = \overline{(\overline{u_i} + u'_i)(\overline{\mathcal{C}_i} + \mathcal{C}'_i)} = \overline{\overline{u_i}\overline{\mathcal{C}_i}} + \overline{\overline{u_i}\mathcal{C}'_i} + \overline{u'_i\overline{\mathcal{C}_i}} + \overline{u'_i\mathcal{C}'_i} \quad (5.5)$$

Here the time averaged quantity represented by over-bar is defined as

$$\overline{u_i} = \frac{1}{t_I} \int_t^{t+t_I} u_i d\tau \quad (5.6)$$

For homogeneous turbulence the mean of the fluctuating component of the quantity in the turbulent field is zero (Pope, 2001), hence $\overline{u'_i} = 0$ and $\overline{\mathcal{C}'_i} = 0$ and the average of the average of a quantity is the averaged quantity itself. Therefore equation (5.5) reduces to

$$\overline{u\mathcal{C}} = \overline{u_i\overline{\mathcal{C}_i}} + \overline{u'_i\mathcal{C}'_i} \quad (5.7)$$

To obtain the turbulent convection diffusion equation, we substitute the velocity and concentration with its decomposed components as follows

$$\frac{\partial \mathcal{C}}{\partial t} + \frac{\partial(u_i \mathcal{C})}{\partial x_i} = \frac{\partial}{\partial x_i} \left(D_m \frac{\partial \mathcal{C}}{\partial x_i} \right) \quad (5.8)$$

$$\frac{\partial(\overline{\mathcal{C}_i} + \overline{\mathcal{C}'_i})}{\partial t} + \frac{\partial\left((\overline{u_i} + \overline{u'_i}) (\overline{\mathcal{C}_i} + \overline{\mathcal{C}'_i})\right)}{\partial x_i} = \frac{\partial}{\partial x_i} \left(D_m \frac{\partial(\overline{\mathcal{C}_i} + \overline{\mathcal{C}'_i})}{\partial x_i} \right) \quad (5.9)$$

Performing time averaging of equation (5.9) and recognizing that $\overline{u_i \mathcal{C}'_i}$, $\overline{u'_i \mathcal{C}_i}$, and $\overline{\mathcal{C}'_i}$ are each zero,

$$\frac{\partial(\overline{\mathcal{C}_i})}{\partial t} + \frac{\partial\left(\overline{u_i \mathcal{C}_i} + \overline{u'_i \mathcal{C}'_i}\right)}{\partial x_i} = \frac{\partial}{\partial x_i} \left(D_m \frac{\partial(\overline{\mathcal{C}_i})}{\partial x_i} \right) \quad (5.10)$$

Rearranging terms in equation (5.10), we obtain

$$\frac{\partial \overline{\mathcal{C}_i}}{\partial t} + \overline{u_i} \frac{\partial \overline{\mathcal{C}_i}}{\partial x_i} = -\frac{\partial\left(\overline{u'_i \mathcal{C}'_i}\right)}{\partial x_i} + \frac{\partial}{\partial x_i} \left(D_m \frac{\partial(\overline{\mathcal{C}_i})}{\partial x_i} \right) \quad (5.11)$$

To solve equation (5.11) we need a model for the term $\overline{u'_i \mathcal{C}'_i}$. The nature of the term confirms that it is a mass flux associated with turbulence as it is a product of fluctuating velocity and fluctuating concentration. The correlation of this term can be made analogous with Fick's law as indicated by Bird et al. (1960), for example

$$\overline{u'_i \mathcal{C}'_i} = -D_t \frac{\partial \overline{\mathcal{C}_i}}{\partial x_i} \quad (5.12)$$

Substituting the analogy with the turbulent diffusivity in equation (5.11)

$$\frac{\partial \overline{\mathcal{C}_i}}{\partial t} + \overline{u_i} \frac{\partial \overline{\mathcal{C}_i}}{\partial x_i} = -\frac{\partial}{\partial x_i} \left(-D_t \frac{\partial \overline{\mathcal{C}_i}}{\partial x_i} \right) + \frac{\partial}{\partial x_i} \left(D_m \frac{\partial \overline{\mathcal{C}_i}}{\partial x_i} \right) \quad (5.13)$$

Collecting terms, we obtain,

$$\frac{\partial \bar{\mathcal{C}}_i}{\partial t} + \bar{u}_i \frac{\partial \bar{\mathcal{C}}_i}{\partial x_i} = \frac{\partial}{\partial x_i} \left(D_{eff} \frac{\partial \bar{\mathcal{C}}_i}{\partial x_i} \right) \quad (5.14)$$

Where, $D_{eff} = D_t + D_m$, the combined effect of molecular and eddy diffusivity

Flow through a pipe could be simulated as one dimensional flow by taking advantage of axi-symmetric flow. For a fully developed flow, change in the radial velocity component can be neglected and for homogeneous turbulence, the eddy diffusivity can be taken as equal in the radial and axial directions. Under these assumptions, equation (5.14) can be re-written for turbulent dispersion in pipe flow as-

$$\frac{\partial \bar{\mathcal{C}}}{\partial t} + \bar{u}_i \frac{\partial \bar{\mathcal{C}}}{\partial x} = \frac{1}{r} \frac{\partial}{\partial r} \left(r D_{eff} \frac{\partial \bar{\mathcal{C}}}{\partial r} \right) + \frac{\partial}{\partial x} \left(D_{eff} \frac{\partial \bar{\mathcal{C}}}{\partial x} \right) \quad (5.15)$$

Here x and r are axial and radial directions respectively. It can be further simplified as

$$\frac{\partial \bar{\mathcal{C}}}{\partial t} + \bar{u}_x \frac{\partial \bar{\mathcal{C}}}{\partial x} = D_{eff} \left(\frac{1}{r} \frac{\partial \bar{\mathcal{C}}}{\partial r} + \frac{\partial^2 \bar{\mathcal{C}}}{\partial r^2} + \frac{\partial^2 \bar{\mathcal{C}}}{\partial x^2} \right) \quad (5.16)$$

5.5 Modelling the Flow Field

Estimation of turbulent dispersion through pipes from the governing equation (5.16) requires a two-step solution procedure. In the first step, the mean axial velocity (\bar{u}_x), and turbulent diffusivity are obtained by solving the continuity and momentum equations (Navier-Stokes equations). However, the random fluctuation of the dependent variable is highly sensitive to the initial condition and the wide spectrum of length and time scale present in the flow field. To smooth the effect of turbulent fluctuation in the solution, these equations require time averaging which in turn gives rise to a closure problem. Therefore further modelling is required to develop additional

equations for the Reynolds stress terms which appear as a result of statistical time averaging of Navier-Stokes Equations. The continuity and momentum equation in the i^{th} direction can be written with the Reynolds decomposition of the dependent variable as

$$\frac{\partial}{\partial x_i} (\bar{u}_i + u'_i) = 0 \quad (5.17)$$

$$\rho \left[\frac{\partial}{\partial t} (\bar{u}_i + u'_i) + (\bar{u}_j + u'_j) \frac{\partial}{\partial x_j} (\bar{u}_i + u'_i) \right] = - \frac{\partial}{\partial x_i} (\bar{p} + p') + \frac{\partial}{\partial x_j} \left(\mu \frac{\partial}{\partial x_j} (\bar{u}_i + u'_i) \right) \quad (5.18)$$

Time averaging to the continuity equation (equation (5.17)) and recognizing that, $\overline{u'_i} = 0$ we find that

$$\frac{\partial}{\partial x_i} (\bar{u}_i) = 0 \quad (5.19)$$

Again, from equation (5.17),

$$\frac{\partial \bar{u}_i}{\partial x_i} + \frac{\partial u'_i}{\partial x_i} = 0 \quad (5.20)$$

From equation(5.19) and (5.20), we get-

$$\frac{\partial u'_i}{\partial x_i} = 0 \quad (5.21)$$

Similarly, performing time averaging to the momentum equation (equation (5.18)) and utilizing the continuity equation, we obtain-

$$\rho \left[\frac{\partial \bar{u}_i}{\partial t} + \frac{\partial}{\partial x_j} (\bar{u}_i \bar{u}_j + \overline{u'_i u'_j}) \right] = -\frac{\partial \bar{p}}{\partial x_i} + \frac{\partial}{\partial x_j} \left(\mu \frac{\partial \bar{u}_i}{\partial x_j} \right) \quad (5.22)$$

Rearranging terms,

$$\rho \left[\frac{\partial \bar{u}_i}{\partial t} + \frac{\partial}{\partial x_j} (\bar{u}_i \bar{u}_j) \right] = -\frac{\partial \bar{p}}{\partial x_i} + \frac{\partial}{\partial x_j} \left(\mu \frac{\partial \bar{u}_i}{\partial x_j} \right) - \frac{\partial}{\partial x_j} (\overline{\rho u'_i u'_j}) \quad (5.23)$$

Equation (5.23) is referred to as Reynolds averaged Navier-Stokes Equations (RANS).

The time averaging process give rise to well behaved solutions. However, it introduces additional terms $\overline{\rho u'_i u'_j}$ which have a similar effect as stress terms; hence it is known as Reynolds stress. These additional six unknowns along with three velocity component and the pressure term (a total of ten unknowns) is impossible to solve from three momentum equations (in each directions) and a continuity equation (total four). This is known as closure problem in RANS. Therefore we need to invoke modelling where the Reynolds stress components are analogically represented in terms of the time averaged velocity components.

Many turbulence models are available which can be classified according to the number of additional equations required to account for the additional terms. These models are highly dependent on their field of applications. For pipe flow the two equation k-epsilon model has been successfully used for many engineering applications (Argyropoulos and Markatos, 2015). The accuracy and robustness of the k-epsilon model for simulating pipe flow motivates us to it use in the present flow simulation case.

Therefore the turbulent kinetic energy can be decomposed into the averaged and fluctuating components as follows

$$k = \bar{k} + k' \quad (5.24)$$

Here the average and fluctuating component of the turbulent kinetic energy is defined as

$$k' = \frac{1}{2} \overline{u'_i u'_i} \quad (5.25)$$

$$\bar{k} = \frac{1}{2} \overline{u_i u_i} \quad (5.26)$$

Moreover, the dissipation rate of turbulent kinetic energy is defined as,

$$\epsilon = \nu \overline{\frac{\partial u_i}{\partial x_j} \frac{\partial u_i}{\partial x_j}} \quad (5.27)$$

To develop a governing equation for turbulent kinetic energy and dissipation rate, we subtract equation (5.23) from equation (5.18) and multiply the result by u'_i

$$u'_i \frac{\partial u'_i}{\partial t} + u'_i \frac{\partial}{\partial x_j} \left(\overline{u_i u'_j} + \overline{u_j u'_i} + u'_i u'_j - \overline{u'_i u'_j} \right) = -\frac{u'_i}{\rho} \frac{\partial p'}{\partial x_i} + u'_i \frac{\partial}{\partial x_j} \left(\mu \frac{\partial u'_i}{\partial x_j} \right) \quad (5.28)$$

Rearranging terms,

$$u'_i \frac{\partial u'_i}{\partial t} + u'_i \frac{\partial}{\partial x_j} \left(\overline{u_i u'_j} \right) + u'_i \frac{\partial}{\partial x_j} \left(\overline{u_j u'_i} \right) + u'_i \frac{\partial}{\partial x_j} \left(u'_i u'_j \right) - u'_i \frac{\partial}{\partial x_j} \left(\overline{u_i u_j} \right) = -\frac{u'_i}{\rho} \frac{\partial p'}{\partial x_i} + u'_i \frac{\partial}{\partial x_j} \left(\mu \frac{\partial u'_i}{\partial x_j} \right) \quad (5.29)$$

Evaluating each term individually,

Part I:

$$u_i' \frac{\partial u_i'}{\partial t} = \frac{\partial}{\partial t} \left(\frac{1}{2} u_i'^2 \right) \quad (5.30)$$

Part II:

$$u_i' \frac{\partial}{\partial x_j} (\bar{u}_i u_j') = \bar{u}_i u_i' \frac{\partial u_j'}{\partial x_j} + u_j' u_i' \frac{\partial \bar{u}_i}{\partial x_j} \quad (5.31)$$

Since, as per continuity, $\frac{\partial u_j'}{\partial x_j} = 0$, therefore

$$u_i' \frac{\partial}{\partial x_j} (\bar{u}_i u_j') = u_j' u_i' \frac{\partial \bar{u}_i}{\partial x_j} \quad (5.32)$$

Part III:

$$u_i' \frac{\partial}{\partial x_j} (\bar{u}_j u_i') = u_i' \bar{u}_j \frac{\partial u_i'}{\partial x_j} + u_i' u_i' \frac{\partial \bar{u}_j}{\partial x_j} = \bar{u}_j \frac{\partial}{\partial x_j} \left(\frac{1}{2} u_i'^2 \right) + u_i' u_i' \frac{\partial \bar{u}_j}{\partial x_j} \quad (5.33)$$

Continuity requires, $\frac{\partial \bar{u}_j}{\partial x_j} = 0$, hence,

$$u_i' \frac{\partial}{\partial x_j} (\bar{u}_j u_i') = \bar{u}_j \frac{\partial}{\partial x_j} \left(\frac{1}{2} u_i'^2 \right) \quad (5.34)$$

Part IV:

$$u_i' \frac{\partial}{\partial x_j} (u_i' u_j') = u_i' u_i' \frac{\partial u_j'}{\partial x_j} + u_j' u_i' \frac{\partial u_i'}{\partial x_j} = u_i' u_i' \frac{\partial u_j'}{\partial x_j} + u_j' \frac{\partial}{\partial x_j} \left(\frac{1}{2} u_i'^2 \right) \quad (5.35)$$

Continuity requires, $\frac{\partial \bar{u}_j}{\partial x_j} = 0$, hence

$$u'_i \frac{\partial}{\partial x_j} (u'_i u'_j) = u'_j \frac{\partial}{\partial x_j} \left(\frac{1}{2} u_i'^2 \right) = \frac{\partial}{\partial x_j} \left(\frac{1}{2} u'_j u_i'^2 \right) + \frac{1}{2} u_i'^2 \frac{\partial u'_j}{\partial x_j} \quad (5.36)$$

Use of the continuity equation again

$$u'_i \frac{\partial}{\partial x_j} (u'_i u'_j) = \frac{\partial}{\partial x_j} \left(\frac{1}{2} u'_j u_i'^2 \right) \quad (5.37)$$

Part V:

$$-u'_i \frac{\partial}{\partial x_j} (\overline{u'_i u'_j}) = u'_i \frac{\partial}{\partial x_j} (-\overline{u'_i u'_j}) \quad (5.38)$$

Part VI:

$$-\frac{u'_i}{\rho} \frac{\partial p'}{\partial x_i} = - \left[\frac{\partial}{\partial x_i} \left(\frac{u'_i p'}{\rho} \right) - \frac{p'}{\rho} \frac{\partial u'_i}{\partial x_i} \right] \quad (5.39)$$

$$\frac{u'_i}{\rho} \frac{\partial p'}{\partial x_i} = \frac{\partial}{\partial x_i} \left(-\frac{u'_i p'}{\rho} \right) \quad (5.40)$$

Part VII:

$$u'_i \frac{\partial}{\partial x_j} \left(\mu \frac{\partial u'_i}{\partial x_j} \right) = \frac{\partial}{\partial x_j} \left(\nu u'_i \frac{\partial u'_i}{\partial x_j} \right) - \nu \frac{\partial u'_i}{\partial x_j} \frac{\partial u'_i}{\partial x_j} \quad (5.41)$$

Substituting all parts in equation (5.29) and performing time averaging we obtain,

$$\begin{aligned} \overline{\frac{\partial}{\partial t} \left(\frac{1}{2} u_i'^2 \right)} + \overline{u'_j u'_i \frac{\partial \overline{u_i}}{\partial x_j}} + \overline{\overline{u_j} \frac{\partial}{\partial x_j} \left(\frac{1}{2} u_i'^2 \right)} + \overline{\frac{\partial}{\partial x_j} \left(\frac{1}{2} u'_j u_i'^2 \right)} + \overline{u'_i \frac{\partial}{\partial x_j} (-\overline{u'_i u'_j})} = \\ \overline{\frac{\partial}{\partial x_i} \left(-\frac{u'_i p'}{\rho} \right)} + \overline{\frac{\partial}{\partial x_j} \left(\nu u'_i \frac{\partial u'_i}{\partial x_j} \right)} - \overline{\nu \frac{\partial u'_i}{\partial x_j} \frac{\partial u'_i}{\partial x_j}} \end{aligned} \quad (5.42)$$

This gives a transport equation for turbulent kinetic energy as follows-

$$\frac{\partial k}{\partial t} + \overline{u_j} \frac{\partial k}{\partial x_j} = - \frac{\partial}{\partial x_j} \left(\overline{\frac{1}{u_j} u_i'^2} + \frac{\overline{u_i'} p'}{\rho} - \overline{\nu u_i' \frac{\partial u_i'}{\partial x_j}} \right) - \overline{u_j' u_i' \frac{\partial \overline{u_i}}{\partial x_j}} - \nu \overline{\frac{\partial u_i'}{\partial x_j} \frac{\partial u_i'}{\partial x_j}} \quad (5.43)$$

The above equation is a convection diffusion equation which governs the transport of turbulent kinetic energy with a source term. The difficulty in solving the equation leads to a modelling approach for the turbulent kinetic energy and energy dissipation rate as follows-

$$\frac{\partial k}{\partial t} + \overline{u_j} \frac{\partial k}{\partial x_j} = \frac{\partial}{\partial x_j} \left[\left(\nu + \frac{\nu_t}{\sigma_k} \right) \frac{\partial k}{\partial x_j} \right] + \mathcal{P} - \epsilon \quad (5.44)$$

Here \mathcal{P} is the rate of production of turbulence and ϵ is the rate of dissipation of turbulent kinetic energy. Again, the model equation for ϵ is obtained by an analogous expression of the transport of ϵ , i.e.

$$\frac{\partial \epsilon}{\partial t} + \overline{u_j} \frac{\partial \epsilon}{\partial x_j} = \frac{\partial}{\partial x_j} \left[\left(\nu + \frac{\nu_t}{\sigma_\epsilon} \right) \frac{\partial \epsilon}{\partial x_j} \right] + C_{\epsilon 1} \frac{\mathcal{P} \epsilon}{k} - C_{\epsilon 2} \frac{\epsilon^2}{k} \quad (5.45)$$

From equation (5.17) and (5.45), k and ϵ are calculated which is used to calculate the Reynolds stress components from Boussinesq approximation

$$\overline{\rho u_i' u_j'} = \frac{2}{3} \rho \delta_{ij} + \mu_t \left(\frac{\partial \overline{u_i}}{\partial x_j} + \frac{\partial \overline{u_j}}{\partial x_i} \right) \quad (5.46)$$

And the eddy viscosity is calculated as

$$\mu_t = \rho C_\mu \frac{k^2}{\epsilon} \quad (5.47)$$

For a standard k-epsilon model the model constants are suggested by Launder and

Sharma (1974) as

$$C_{\epsilon 1} = 1.44, C_{\epsilon 2} = 1.92, C_{\mu} = 0.09, \sigma_k = 1.0 \text{ and } \sigma_{\epsilon} = 1.3 \quad (5.48)$$

5.6 Previous work on Dispersion in Turbulent Flow through Pipes

The pioneering contribution to turbulent dispersion in pipe flow was made by Taylor (1954b) providing experimental observations and an analytical expression for longitudinal dispersion D_L as

$$D_L = GRu^* \quad (5.49)$$

where G is a constant that assumes the value of 10.1, R is the radius of the pipe and $u^*(= \sqrt{\tau_w/\rho})$ is the shear or friction velocity with τ_w being the wall shear stress and ρ is the density of the fluid. The use of a logarithmic velocity profile in the derivation of the analytical solution for longitudinal dispersion restricted the expression for D_L in equation 5.49 to be valid only in high Reynolds number ($Re > 20000$). Moreover, Taylor neglected the role of molecular diffusion in the deduction of the analytical expression of longitudinal dispersion which is consistent only in highly turbulent flow.

Tichacek et al. (1957) followed Taylor's analysis but included the molecular diffusion into the solution and considered experimental velocity profile instead of an analytical expression. Their analysis suggests that the dispersion parameter (D_L/dU) strongly depends on the accuracy of velocity profile and it exhibits a high value in the laminar regime of the flow.

Another correlation for the longitudinal dispersion coefficient with Reynolds num-

ber was provided by Sittel Jr et al. (1968). By performing a set of experiments, they expressed the longitudinal dispersion coefficient at $Re = 40,000$ and Schmidt number¹, $Sc = 1000$ as

$$D_L = 1.13 \times 10^{-6} Re^{0.875} \quad (5.50)$$

Although the Schmidt number barely affects the longitudinal dispersion coefficient in turbulent flow (Davidson et al., 1955), in the gas medium, Flint and Eisenklam (1969) studied longitudinal dispersion in turbulent flow through pipe for Schmidt numbers ranging from 0.27-1.0 providing a similar expression as in equation 5.49 except the value of G is dependent on Sc . These authors have used two different velocity profiles for low and high Reynolds number covering Re range 300-10,000. However, the experimental data observed by the same authors suggest that the analytical expression underestimates the actual dispersion.

Most of the attempts to relate the longitudinal dispersion coefficient were either analytical or experimental. Not much work found to calculate dispersion coefficient in turbulent flow through pipe using numerical technique. Ekambara and Joshi (2003) solved equation (5.16) numerically using a second order upwinding scheme with a low Reynolds number k-epsilon model for the near wall turbulence modelling. More recently Hart et al. (2013) provided experimental data on dispersion in turbulent flow through pipes covering Reynolds numbers ranging 2000-50000. They have developed a simple model based on the Chikwendu (1986) N-zone model. The model does not perform well in the range of Reynolds number reported in the experimental observations.

¹A dimensionless number expressing as the ratio of kinematic diffusivity to the molecular diffusivity

Numerical methods can be a powerful tool if they are utilized properly. One of the major drawback of numerical analysis is generation of false diffusion. The artificial diffusion arising from the scheme should not confound the solution. Particularly when the objective is to determine the rate of dispersion. Therefore, we utilize the QUICKEST scheme developed in this work for estimating solute dispersion (as in Chapter 2) to calculate the rate of dispersion in turbulent flow. In doing so, it is required to solve the flow field prior to solving the convection diffusion equation. Hence we use FLUENT, a commercial CFD software to simulate flow field in axisymmetric pipe. The turbulent viscosity and mean flow velocity is then exported to be utilized in the QUICKEST scheme developed in this work.

5.7 Simulation of the Turbulent Flow Field in Circular Pipes

Turbulent flow in pipe simulation is carried out in commercial CFD software package FLUENT. After defining the axisymmetric geometry, meshes are created in the domain. The standard k-epsilon model has been used to simulate turbulence. The Navier Stokes equations have been solved using QUICK scheme which is embedded into FLUENT and is 3rd order accurate. The obtained velocity profiles and turbulent viscosity profiles are then compared with experimental results to develop confidence in the results. However, to ensure a grid independent solution, prior to simulation, grid sensitivity study performed .

5.7.1 Grid Sensitivity Analysis

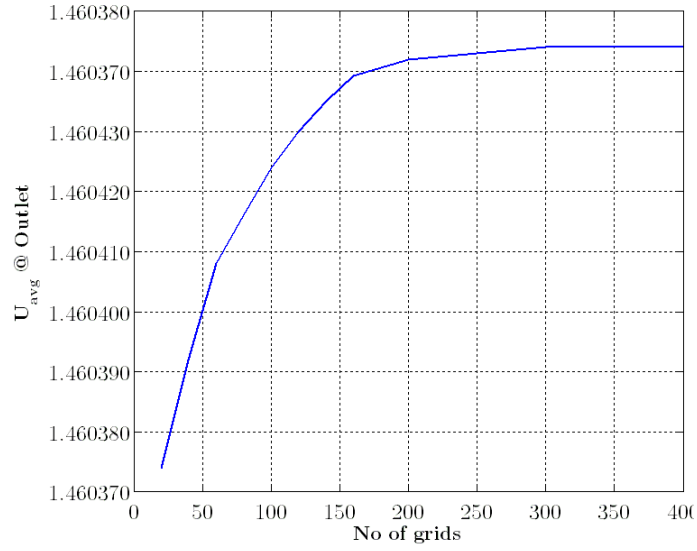
Numerical solutions are inherently an approximation of the exact solution. The discretized equations approach their continuous progenitors as the computational mesh is refined. Therefore, in every step of the simulation, it is required to perform a grid sensitivity test to ensure that the solution obtained becomes effectively independent of the grid size. In the simulation of dispersion of solutes in turbulent flows through pipes, we solve for the flow field (i.e. the averaged velocity and turbulent viscosity) and use the velocity profiles in equation (5.16) to solve for the concentration of the solute using the QUICKEST scheme.

Furthermore, to account for the near wall turbulence, it is important to have extremely fine grids in close proximity to the pipe wall. The dimensionless wall distance (y^+) is a useful measure to ensure resolution of the grids near the wall. It is defined as

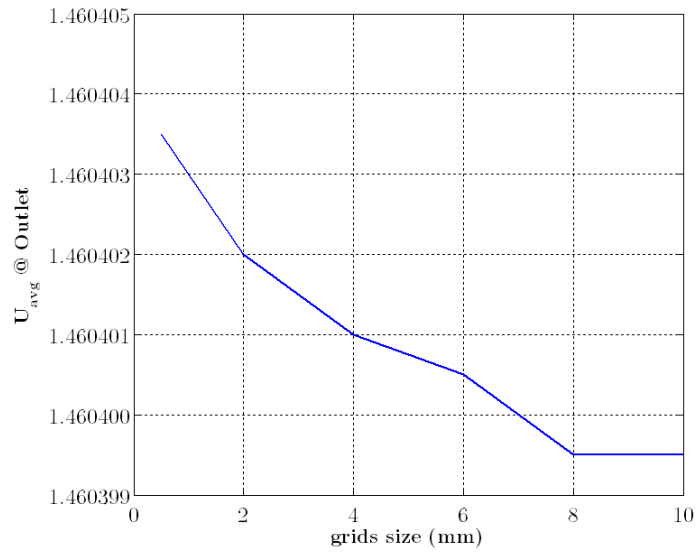
$$y^+ = \frac{yu^*}{\nu} \quad (5.51)$$

in which, u^* is the friction velocity or shear velocity defined as, $u^* = \sqrt{\frac{\tau_w}{\rho}}$ with, τ_w ($= \mu \frac{du}{dy}$) being the wall shear stress. The dimensionless wall distance (y^+) has been maintained less than 5 in the simulation which ensures that the laminar sub-layer of the flow field is accounted for.

Simulations were carried out with different refinements of the mesh in the radial and axial directions. The area averaged velocity (U_{avg}) at the outlet of the pipe is recorded in each simulation and plotted in Figure 5.2. It can be observed that the area averaged velocity hardly varies with the grid refinement in both the axial and radial directions. Therefore we have used 200 grids in the radial direction and the



(a) Radial direction



(b) Axial direction

Figure 5.2: Grid sensitivity test for the flow field simulation. Magnitude of the area averaged velocity profile at outlet.

grid size in the axial direction is 10 mm to obtain an accurate solution of the flow field.

5.7.2 Velocity Profile

The dispersion of a solute in turbulent flow is greatly influenced by the accuracy of the velocity profile (Fischer et al., 2013). In laminar flow, i.e. Reynolds number typically less than 2000 for pipe flow, the spreading of a solute in the flow is due to differential advection arising from the parabolic velocity profile. However, in turbulent flow through pipes, i.e. Reynolds numbers greater than about 4000, the radial velocity distribution is more uniform compared to laminar profile as observed from Figure 5.3. This causes a decrease in the radial differential advection except in the near wall region. Nevertheless, the turbulent boundary layer near the wall significantly contributes to the spreading of solute (Hart et al., 2013). Taylor (1954b) considered a universal velocity profile which does not account for the buffer layer and the laminar sub-layer as observed from Figure 5.5 Therefore the expression for dispersion coefficient is only valid at very high Reynolds number ($Re > 20,000$)

Simulations are carried out for various Reynolds numbers and plotted on a log scale along with the experimental data. From figure 5.5, it can be observed that the simulation results using standard k-epsilon model successfully predicts the turbulent velocity profile in the near wall as well as other radial places in the circular pipe.

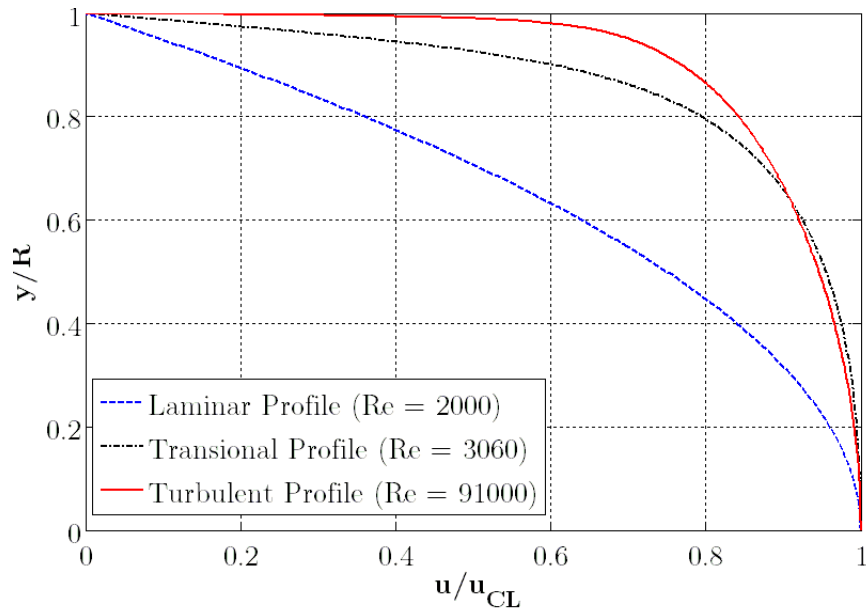


Figure 5.3: Comparison of Laminar, transitional and turbulent mean velocity profiles for pipe flow as calculated in this work.

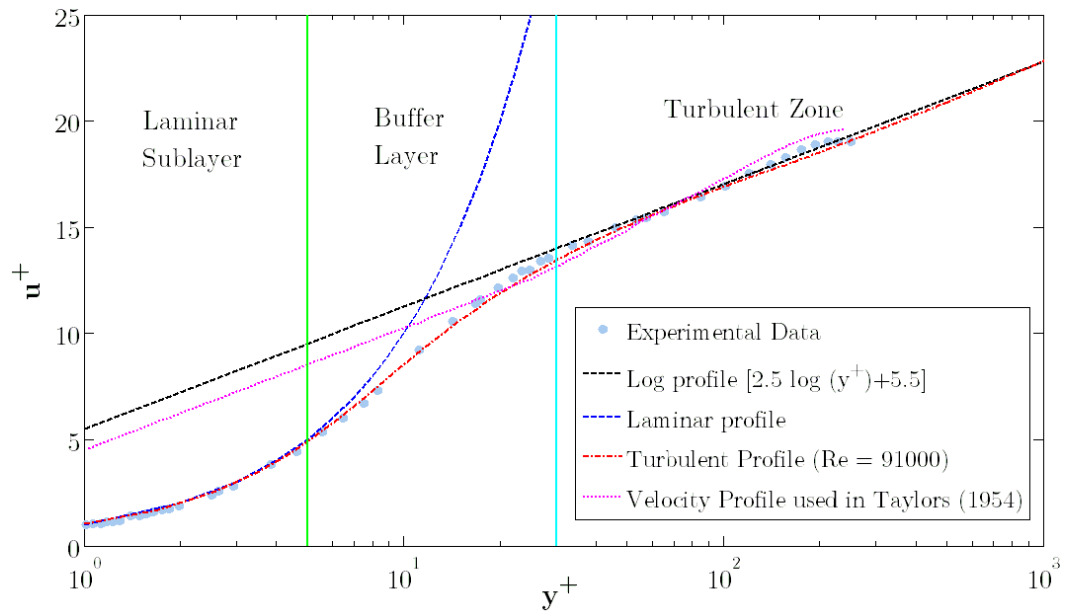


Figure 5.4: Comparison of velocity profile at Reynolds number 91,000 from the simulation carried out in this work with the experimental data of Durst et al. (1995), Laminar profile, Log profile and the velocity profile used in Taylor (1954b)

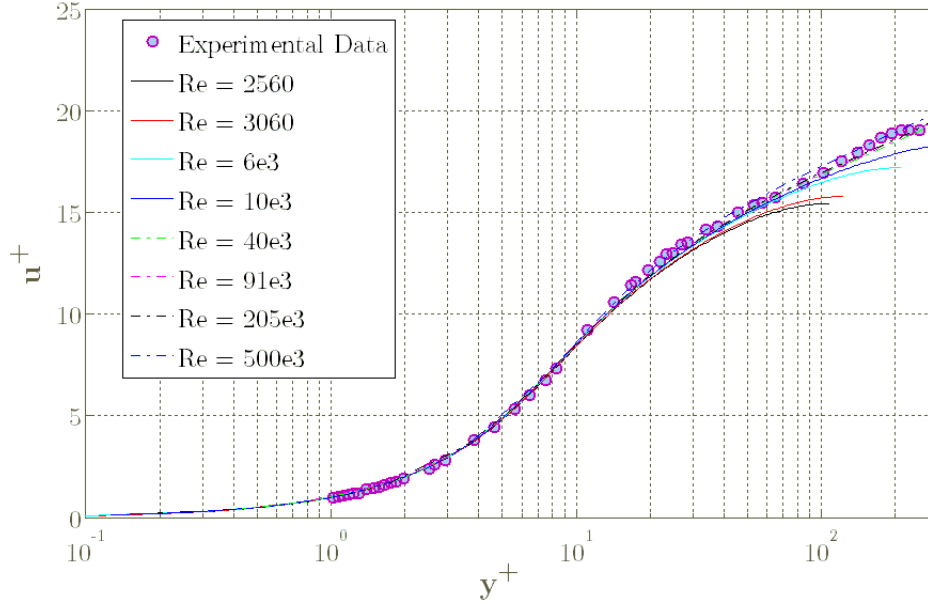


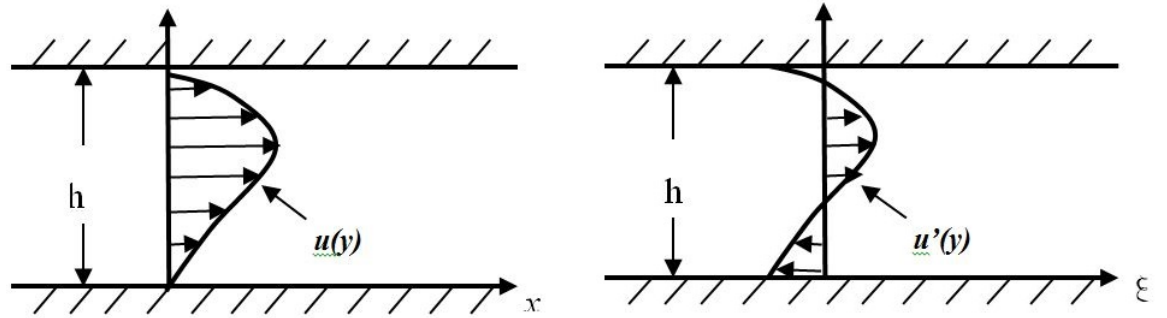
Figure 5.5: Comparison of velocity profiles computed in this work at various Reynolds number from the simulation with the experimental data of Durst et al. (1995)

5.8 Modelling Dispersion

5.8.1 Analytical Approach

The analysis presented by Taylor (1954b) to estimate the longitudinal dispersion coefficient for a solute flowing through turbulent flow from shear velocity profile is an represents an impressive landmark in the study of dispersion in pipes (Fischer, 1973). However, the assumption that the velocity profile corresponds only to a highly turbulent regime limits the work to high Reynolds numbers. Moreover, the molecular diffusion was neglected in his analysis which is justified for the highly turbulent flows. More refined assumptions concerning the turbulent profile along with the inclusion of molecular diffusivity in the analysis is likely to enhance the applicability of Taylor (1954b) analysis of calculating longitudinal dispersion coefficient.

Since the dispersion process occurs as a result of the non-uniform velocity profile of



(a) A non-uniform two dimensional velocity distribution in fixed reference plane,

(b) The same velocity distribution as in (a) but in a new coordinate system that translates with the mean velocity of the flow

Figure 5.6: A comparison of the same velocity profile depicted in a stationary reference coordinate (a) and coordinate that translate with the mean velocity of the fluid, (b).

the carrier fluid, the velocity profile can be decomposed to a mean component as well as fluctuating component. However this decomposition is different from Reynold's decomposition in a way that Reynold's decomposition has a fluctuating component which is aleatoric, the decomposition of shear flow has a known fluctuating component which is better termed as a deviation rather than a fluctuation.

Figure 5.6 shows that the velocity deviation and the concentration deviation in shear flow may be defined in analogous manner as

$$u'(y) = u(y) - \bar{u}; \quad C'(x, y) = C(x, y) - \bar{C} \quad (5.52)$$

Here the area averaged velocity and are averaged concentration of solute can be defined as

$$\bar{u} = \int_0^h u dy \quad \bar{C} = \int_0^h C dy \quad (5.53)$$

Now, the convection diffusion equation can be written with the above decomposi-

tion as

$$\begin{aligned} \frac{\partial}{\partial t}(\bar{C} + C') + (\bar{u} + u') \frac{\partial}{\partial x}(\bar{C} + C') = \\ \frac{\partial}{\partial x} \left(D_m \frac{\partial}{\partial x}(\bar{C} + C') \right) + \frac{\partial}{\partial y} \left(D_m \frac{\partial}{\partial y}(\bar{C} + C') \right) \end{aligned} \quad (5.54)$$

Since the flow is in the x direction only, the mean concentration in the y direction is constant which eliminates the mean term from the second term of right hand side of above equation. Moreover, the diffusion coefficient can be considered as constant in all directions, thus can be taken out from the derivative. Rewriting,

$$\frac{\partial}{\partial t}(\bar{C} + C') + (\bar{u} + u') \frac{\partial}{\partial x}(\bar{C} + C') = D_m \left(\frac{\partial^2}{\partial x^2}(\bar{C} + C') + \frac{\partial^2 C'}{\partial y^2} \right) \quad (5.55)$$

It is convenient to use a moving frame of reference in the analysis. Therefore, to incorporate the new coordinate system, the origin of which travels with the average velocity of the flow, we introduce a new axial coordinate, namely

$$\xi = x - \bar{u}t, \quad \mathcal{T} = t \quad (5.56)$$

Furthermore, using the chain rule of calculus, the following relationships are obtained

$$\begin{aligned} \frac{\partial}{\partial x} &= \frac{\partial \xi}{\partial x} \frac{\partial}{\partial \xi} + \frac{\partial \mathcal{T}}{\partial x} \frac{\partial}{\partial \mathcal{T}} = \frac{\partial}{\partial \xi} \\ \frac{\partial}{\partial t} &= \frac{\partial \xi}{\partial t} \frac{\partial}{\partial \xi} + \frac{\partial \mathcal{T}}{\partial t} \frac{\partial}{\partial \mathcal{T}} = -\bar{u} \frac{\partial}{\partial \xi} + \frac{\partial}{\partial \mathcal{T}} \end{aligned} \quad (5.57)$$

It can be argued that longitudinal dispersion is always greater than axial diffusion; the axial diffusion term can be neglected from equation (5.55) (it can be added as a diffusion term later) which becomes with the coordinate transformation

$$\frac{\partial}{\partial \mathcal{T}}(\bar{c}+c') + u' \frac{\partial}{\partial \xi}(\bar{c}+c') = D_{eff} \left(\frac{\partial^2 c'}{\partial y^2} \right) \quad (5.58)$$

The constant component from equation (5.58) can be eliminated by applying the area average to this equation.

$$\frac{\partial \bar{c}}{\partial \mathcal{T}} + \frac{\partial \overline{u'c'}}{\partial \xi} = 0 \quad (5.59)$$

Subtracting equation (5.59) from equation (5.58) gives

$$\frac{\partial c'}{\partial \mathcal{T}} + u' \frac{\partial}{\partial \xi}(\bar{c}+c') = \frac{\partial \overline{u'c'}}{\partial \xi} + D_{eff} \left(\frac{\partial^2 c'}{\partial y^2} \right) \quad (5.60)$$

This gives us the governing equation for the concentration deviations, c' . Together with the solution of C' from this equation, the solution for depth averaged concentration can be obtained from equation (5.59). Notably, equation (5.60) can be further simplified by considering a scale analysis which enables us to ignore some of the terms from the equation. Of particular note is that the concentration of the solute in a plane to the flow becomes almost uniform, hence

$$c' \ll \bar{c} \quad (5.61)$$

and

$$u' \frac{\partial c'}{\partial \xi} \ll u' \frac{\partial \bar{c}}{\partial \xi} \quad (5.62)$$

Similarly

$$\frac{\partial(\overline{u'c'})}{\partial\xi} \ll u' \frac{\partial\bar{c}}{\partial\xi} \quad (5.63)$$

The dispersion of the solute never reaches a steady state - the further downstream a slug of solute is conveyed, the more it disperses. However empirical evidence suggests that after a sufficiently long time

$$\frac{\partial c'}{\partial\mathcal{T}} \ll u' \frac{\partial\bar{c}}{\partial\xi} \quad (5.64)$$

The transport equation for the solute may be ultimately expressed as

$$u' \frac{\partial\bar{c}}{\partial\xi} = \frac{\partial}{\partial y} \left(D_{eff} \frac{\partial c'}{\partial y} \right) \quad (5.65)$$

Solving for c' by performing double integration in the equation (5.65)

$$c'(y) = \frac{\partial\bar{c}}{\partial\xi} \int_0^y \frac{1}{D_{eff}} \int_0^y u' dy dy \quad (5.66)$$

However, we still have the \bar{c} term in the equation (5.66) which we cannot find directly from this equation. This can be addressed by considering the total mass flux in the longitudinal direction. In the moving coordinate system, since there is only one velocity in the moving reference plane, the advective mass flux should be

$$q_m = u'(c' + \bar{c}) \quad (5.67)$$

And the total mass flux can be determined by taking the area average to the above equation and recalling that the area average of $u'\bar{c}$ is zero

$$\bar{q}_m = \frac{1}{h} \int_0^h u' C' dy = \overline{u' C'} \quad (5.68)$$

Substituting the expression of C' from equation (5.66) into equation (5.68)

$$\bar{q}_m = \frac{1}{h} \int_0^h u' \frac{\partial \bar{C}}{\partial \xi} \int_0^y \frac{1}{D_{eff}} \int_0^y u' dy dy dy \quad (5.69)$$

The term $\frac{\partial \bar{C}}{\partial \xi}$ is independent of y hence can be taken out of the integral leaving with

$$\bar{q}_m = D_L \frac{\partial \bar{C}}{\partial \xi} \quad (5.70)$$

Where,

$$D_L = \frac{1}{h} \int_0^h u' \left(\int_0^y \frac{1}{D_{eff}} \left(\int_0^y u dy \right) dy \right) dy \quad (5.71)$$

It is this analytical expression for longitudinal dispersion coefficient which depends on the velocity profile and the depth and gives a Fickian type flux relationship. Finally this expression can be substituted into the depth average equation (5.59) to get

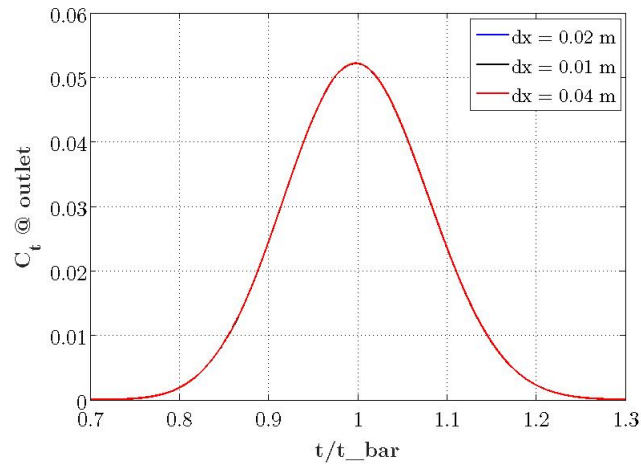
$$\frac{\partial \bar{C}}{\partial \mathcal{T}} = \frac{\partial}{\partial \xi} \left(D_L \frac{\partial \bar{C}}{\partial \xi} \right) \quad (5.72)$$

In the original coordinate system it becomes,

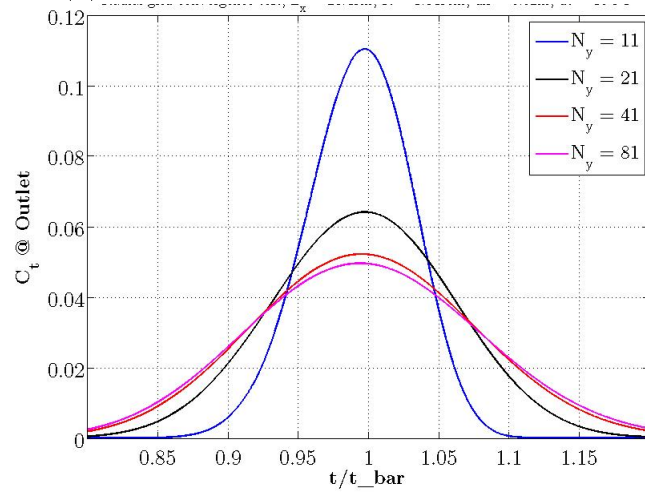
$$\frac{\partial \bar{C}}{\partial t} + \bar{u} \frac{\partial \bar{C}}{\partial x} = \frac{\partial}{\partial x} \left(D_L \frac{\partial \bar{C}}{\partial x} \right) \quad (5.73)$$

5.8.2 Numerical Approach

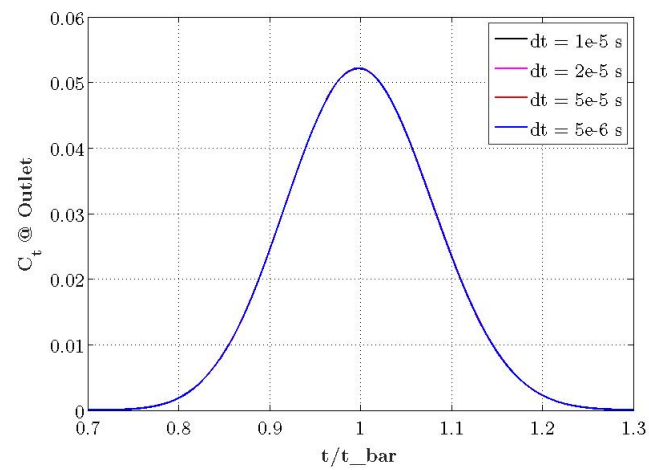
In the numerical modelling of solute dispersion in turbulent flow through a circular cross section, the mean axial velocity profile and the turbulent viscosity obtained from flow field simulation are used in the QUICKEST scheme to as described in Chapter 2. From the distribution of the local concentration profile, the dispersion coefficient is calculated using the method described in section 2.8 of this thesis. Even though a grid sensitivity analysis was conducted while simulating flow field, the grid and time step sensitivity analysis has to be performed again in the numerical simulation of solute dispersion to produce a reliable solution for concentration distribution. Moreover, in the flow field simulation, we have used a non-uniform grid resolution in order to have very fine radial grids near the wall. While importing the velocity profile and turbulent viscosity at corresponding non-uniform grids, we have to interpolate these data to a uniform mesh in order to facilitate programming. This demands a repeat in the grid and time step independence study as well. From Figure 5.7 (a), it can be observed that the number longitudinal grid does not affect the solute concentration distribution when the mesh size varied from 0.01 m to 0.04m. To maintain a stable solution we consider 0.02 m as axial mesh size for the simulation. Moreover in 5.7 (b), it shows that the spreading varies a lot if the number of grids is refined in the radial direction. The reason is on the refined grid, the turbulent viscosity is accounted more precisely which significantly affects the dispersion of the solute. The number of grids was refined from 11 to 81 in the radial direction. We take $N_y = 41$ as refining further cause negligible difference compare to other coarse grids ($N_y=11, 21, \text{ and } 41$). To meet the stability criteria we consider time step size $dt = 5e-5$ s . Further refinement does not cause much difference in solution as seen from 5.7 (c).



(a) Longitudinal grid independence test



(b) Radial grid independence test



(c) Temporal grid independence test

Figure 5.7: Grid sensitivity analysis for the simulation of solute dispersion in turbulent flow through pipes.

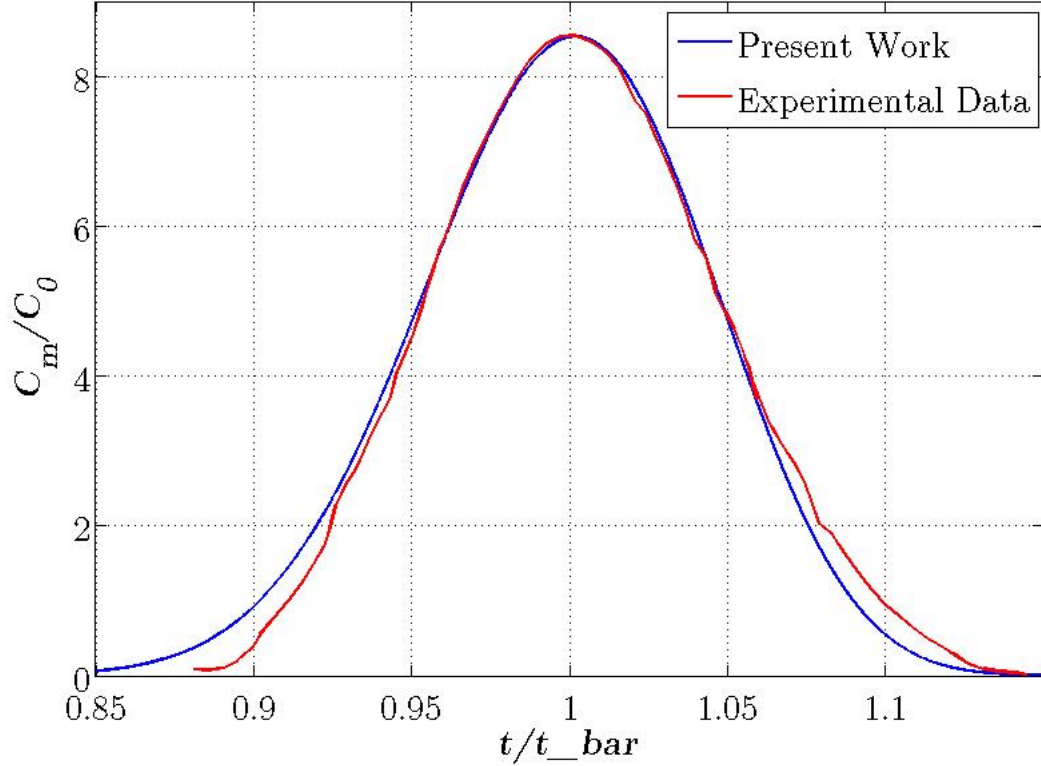


Figure 5.8: Comparison of dimensionless mean concentration profile at the outlet from breakthrough curve from present work with the experimental data of Flint and Eisenklam (1969) at $Re = 3810$ and $Sc = 0.27$

5.8.3 Concentration Profile

With the refined grid determined in the previous section, we perform a simulation to validate against the experimental results of Flint and Eisenklam (1969). A Nitrogen - Helium system at Reynolds number 3810 flowing in a 23.45 m long pipe with radius 1.345 cm was used in the experiment to calculate the dispersion coefficient and breakthrough curve of the system at $Sc = 0.27$. Simulations were carried out reproducing the experiments and it is found that the simulation results for the spreading curve with respect to time at the outlet of the pipe agrees excellently with the experimental data.

It can be observed from the Figure 5.8 that the numerical simulation results almost

identical spreading pattern for the solute dispersion in turbulent flow through circular pipe.

5.8.4 Dispersion Coefficient

The dispersion coefficient can be calculated from the local concentration profile from the break through curve (i.e. the local concentration history at the outlet). The dispersion coefficient is related to the dimensionless variance of the concentration spreading curve. It can be readily calculated by following the procedures mentioned in section 2.4.4. Dispersion coefficient from the simulation results obtained as $D_L/(U_{avg}L) = 0.001038$ which is very close to the value obtained by Flint and Eisenklam (1969) from their experimental data at $Re = 3810$ and $Sc = 0.27$ (5.8) as $D_L/(U_{avg}L) = 0.001085$. Furthermore, the dispersion coefficient can be calculated by the analytical approach mentioned in this chapter. The velocity profile and turbulent viscosity profile obtained from the flow simulation in this work. A comparison between dispersion number ($D_L/(D_m U_{avg})$) calculated and the analytical results presented by Tichacek et al. (1957) is presented in Figure 5.9 at various Reynolds numbers.

The comparison study suggest that the dispersion number calculated using the turbulent velocity profile in this work agrees excellently with the results presented by Tichacek et al. (1957). However at low Reynolds number, the dispersion number calculated by Tichacek et al. (1957) seems to be overestimated . The probable reason the the accuracy of velocity profile at low Reynolds number that it did not capture the detail of the boundary layer in the near wall region. The fineness of grid close to wall in this wall ensures the detail of the boundary later are accounted for in the calculation of dispersion coefficient. The detail of the flow profile in the boundary layer can be observed in Figures 5.4 and 5.5 where the turbulent velocity profile

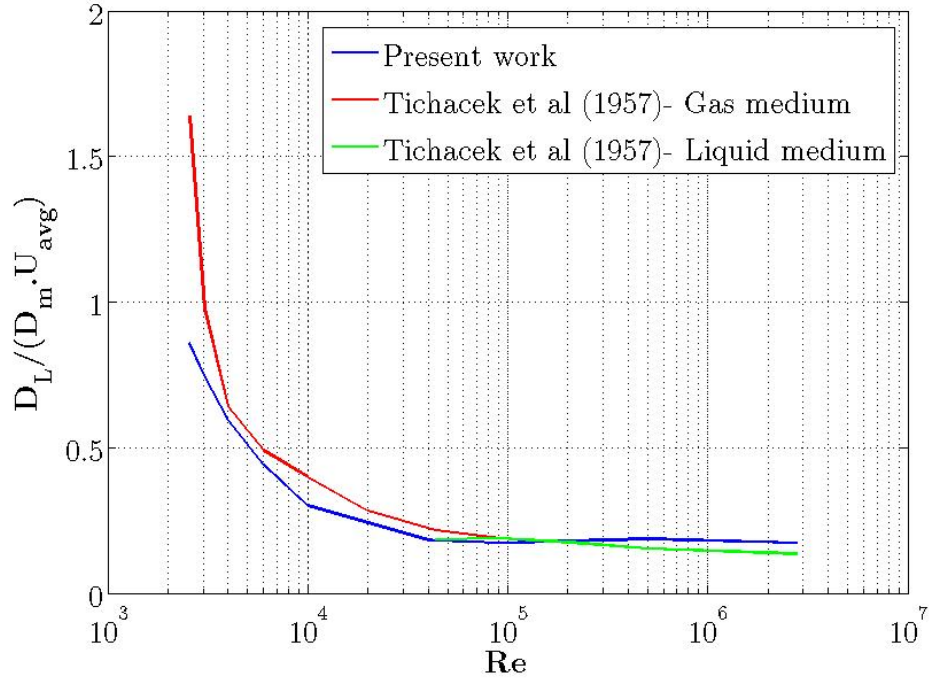


Figure 5.9: Longitudinal dispersion coefficient in turbulent flow through pipe obtained in present work using velocity calculated in this work using k-epsilon model, comparing with the results obtained by Tichacek et al. (1957)

is plotted in log scale and compared with one of the widely accepted experimental results.

5.9 Summary and Conclusions

The accuracy of estimating dispersion is greatly influenced by the precision of the velocity profile, particularly in the near wall region. In this chapter we have demonstrated the effectiveness of the modified QUICKEST scheme developed in Chapter 2 for estimating the dispersion coefficient in turbulent flow through circular ducts. Furthermore an analytical approach based on Taylor's theory is presented to calculate the dispersion coefficient in turbulent flow which indicates the dependence of dispersion coefficient on the turbulent velocity profile. The velocity profile is calculated using a standard k-epsilon turbulence model using a commercial CFD software FLUENT.

From a comparison study with experimental data for velocity profile in log scale, it is found that the simulation result predicts the velocity profile in the near wall region in fine detail. The turbulent velocity profile and the turbulent viscosity are exported and utilized in the analytical solution as well as in the numerical solution . The dispersion coefficient is calculated using analytical and numerical method agrees excellently with the available experimental results at low and high Reynolds numbers.

Chapter 6

A Critical Review of Turbulent Flow in Non-circular Ducts: An Examination of Secondary Flows and Some New Numerical Results

6.1 Introduction

Turbulent flow in ducts with non-circular cross sections is has been a focus for research for almost a century. This phenomenon is encountered in many applications, for example, conditioned air is typically distributed throughout buildings in ducts that have square or rectangular cross sections, rivers have irregular shaped cross sections normal to the mean flow, and the outlets of turbo-machinery may be non-circular. A distinct feature of turbulent flow through non-circular ducts is characterized by

its ever present mean cross stream fluid motion referred as Prandtl's secondary flow which could be of two types (Prandtl 1952). A quasi-inviscid flow arising from the skewness of secondary vorticity, generally named as Prandtl's secondary motion of the first kind, develops in curved ducts where a centrifugal force acts perpendicular to the main stream direction. Such a flow velocity can be significantly large in proportion to free stream velocity of the flow and also exists in circular ducts and in laminar flow (Bradshaw, 1987). The calculation procedure of this motion is relatively simple because it generally contributes to a first - order fluctuation in the mean flow property. On the other hand, secondary motion of Prandtl's second kind appears in turbulent flow in straight non-circular duct which can be present both developing and fully developed flow condition. Since this motion is generated because of turbulence, the estimation and prediction as well as the explanation of origin of this motion challenged the researchers over many years. Although the magnitude of the turbulence-induced secondary motion may be only a few percent of the mean flow, the overall impact of this motion is quite significant in many physical phenomena such as effect on local heat transfer rate, distribution of peripheral wall shear stress and passive scalar transport.

Researchers have investigated turbulent flow experimentally at the beginning of 19th century; however, over time period with the technological advancements, the experimental techniques have been revised and modified in order to measure the flow field, turbulent structure and secondary flow more accurately. In later periods, particularly after the 1970's, with the rapid advancement of computing facilities, this phenomenon has been predicted numerically by modelling the physics of the flow. Particularly, Large Eddy Simulation (LES) and Direct Numerical Simulation (DNS) techniques enabled researchers to predict and describe the turbulent structure, mean

flow characteristics and secondary flow incisively.

Despite the intensity of activity in the investigation of turbulent flow in non-circular cross-sectioned geometries there appears to be no comprehensive review of the corpus of knowledge that has been generated in this field. In this chapter, a review of the previous work that have attempted by researchers for calculating and measuring different flow parameters for turbulent flow through non-circular ducts and particularly findings on the origin of secondary flow has been presented extensively. Initially, a brief description the mathematical formulation of the flow system has been presented which will clarify the understanding of the turbulence modelling. After that, experimental outcomes of the preceding investigators in developing and fully developed flow condition have been discussed with the view of elucidating the origin of secondary flow in incompressible turbulent flow through non-circular ducts. Then the calculated and simulated findings of succeeding researchers have been summarized with a view to discuss various techniques to model secondary flows. Finally we present the result of a study of secondary flows generated in turbulent flows in non-circular ducts. As we anticipated the standard k-epsilon and RNG k-epsilon fail to simulate secondary flows. Non-linear models capture some the detail , but large eddy simulation appears to reproduce the secondary flow with the highest fidelity.

6.2 Mathematical Formulation of Flow System

The governing equation of a fluid flowing in three dimensional Cartesian coordinate can be described by the Navier-Stokes and Continuity Equations, which are given by,

$$\frac{\partial u_i}{\partial t} + u_j \frac{\partial u_i}{\partial x_j} = -\frac{1}{\rho} \frac{\partial p}{\partial x_i} + \nu \nabla^2 u_i \quad (6.1)$$

$$\frac{\partial u_i}{\partial x_i} = 0 \quad (6.2)$$

Here u_i is the velocity vector, the index i represents three orthogonal directional axes, p is the pressure and ν is the kinematic viscosity of the fluid. In the above equations, the Einstein summation convention applies to repeated indices.

In turbulent flow, the velocity and pressure terms can be decomposed into the mean and fluctuating components as follows:

$$u_i = \bar{u}_i + u'_i; \quad p = \bar{p} + p' \quad (6.3)$$

6.2.1 Reynolds Averaged Navier-Stokes Equation

Here it is necessary to introduce Reynolds averaging which assumes a variety of forms either an integral or a summation. In turbulence modelling, three most important forms are often considered namely- time averaging, spatial averaging and ensemble averaging.

For stationary turbulence which is independent of time, an instantaneous flow variable $\phi(x, t)$ is time averaged by means of the following expression

$$\bar{\phi}_T(x) = \lim_{T \rightarrow \infty} \frac{1}{T} \int_t^{t+T} \phi(x, t) dt \quad (6.4)$$

Similarly, for homogeneous turbulence which is uniform in all directions, spatial averaged values of an instantaneous variable $\phi(x, t)$ are expressed as

$$\bar{\phi}_V(t) = \lim_{V \rightarrow \infty} \frac{1}{V} \iiint \phi(x, t) dV \quad (6.5)$$

and the generalized form of averaging is ensemble averaging where the average

$\phi_E(x, t)$ is calculated from N identical measurements as

$$\bar{\phi}_E(x, t) = \lim_{N \rightarrow \infty} \frac{1}{N} \sum_{n=1}^N \phi_n(x, t) \quad (6.6)$$

Notably, the time averaged value of mean quantity is the same quantity as the mean

$$\bar{\bar{\phi}}_i(x) = \lim_{T \rightarrow \infty} \frac{1}{T} \int_t^{t+T} \bar{\phi}_i(x) dt = \bar{\phi}_i(x) \quad (6.7)$$

For the fluctuating component, the time averaging becomes

$$\bar{\phi}'_i = \lim_{T \rightarrow \infty} \frac{1}{T} \int_t^{t+T} [\phi_i(x, t) - \bar{\phi}_i(x)] dt = \bar{\phi}_i(x) - \bar{\bar{\phi}}_i(x) = 0 \quad (6.8)$$

For two flow variables, ϕ and ψ , the time averaged values are correlated as follows

$$\overline{\phi\psi} = \overline{(\bar{\phi} + \phi')(\bar{\psi} + \psi')} = \overline{\bar{\phi}\bar{\psi} + \bar{\phi}\psi' + \bar{\psi}\phi' + \phi'\psi'} = \bar{\phi}\bar{\psi} + \phi'\bar{\psi} \quad (6.9)$$

It is noted that the product of a mean quantity and fluctuation has zero mean, hence $\bar{\phi}\psi'$ and $\bar{\psi}\phi'$ vanishes from the above equation.

$$\bar{\phi}_E(x, t) = \bar{\phi}_T(x) \quad (6.10)$$

And in homogeneous turbulence, it is assumed that

$$\bar{\phi}_E(x, t) = \bar{\phi}_V(t) \quad (6.11)$$

By applying the decomposition from Equation (6.1) and then ensemble averaging along with using the correlations from Equation (6.9) to the Navier Stokes Equation

(6.1) we obtain the Reynolds Averaged Navier Stokes Equation in the following form

$$\frac{\partial \bar{u}_i}{\partial t} + \bar{u}_j \frac{\partial \bar{u}_i}{\partial x_j} = -\frac{1}{\rho} \frac{\partial \bar{p}}{\partial x_i} + \nu \nabla^2 \bar{u}_i - \frac{\partial \tau_{ij}}{\partial x_j} \quad (6.12)$$

The above equation represents the conservation of mean linear momentum of the fluid flow. Here, the Reynolds stress tensor expressed as

$$\tau_{ij} = \overline{u'_i u'_j} \quad (6.13)$$

By carrying out the same procedure on the continuity equation (6.2) the mean continuity equation is

$$\frac{\partial \bar{u}_i}{\partial x_i} = 0 \quad (6.14)$$

The above equations (6.12) - (6.14) represent a system of equation with ten unknowns (six Reynolds stress components, three mean velocity components and pressure) with only four equations (three momentum equations in three directions and the continuity equation). Hence the system is not a closed system of equations for determination of flow variables. This is known as the closure problem of Reynolds Averaged Navier Stokes equation. The problem is to relate six components of Reynolds stress tensor $(\overline{u'_1 u'_2}, \overline{u'_2 u'_3}, \overline{u'_1 u'_3}, \overline{u'^2_1}, \overline{u'^2_2}, \overline{u'^2_3})$ with the mean flow variable in a physically consistent manner.

6.2.2 Vorticity Equation

Since the focus of the present review is in the origin of secondary velocity in non-circular ducts, it is important to examine the mean vorticity transport equation.

Taking curl of equation (6.12)

$$\frac{\partial \Omega_i}{\partial t} + \bar{u}_j \frac{\partial \Omega_i}{\partial x_j} = \Omega_j \frac{\partial \bar{u}_i}{\partial x_j} + \nu \nabla^2 \Omega_i - \Lambda_{ijk} \frac{\partial^2 \tau_{ij}}{\partial x_j \partial x_k} \quad (6.15)$$

Where Λ_{ijk} is the permutation tensor. The pressure term $\left(-\nabla \times \frac{\nabla p}{\rho}\right)$ is eliminated because the density is constant. From the above equation the governing equation for mean stream wise vorticity in steady state can be deduced as

$$\begin{aligned} & \underbrace{\left(\bar{u}_1 \frac{\partial \Omega_1}{\partial x_1} + \bar{u}_2 \frac{\partial \Omega_1}{\partial x_2} + \bar{u}_3 \frac{\partial \Omega_1}{\partial x_3} \right)}_I + \underbrace{\left(\Omega_1 \frac{\partial \bar{u}_1}{\partial x_1} + \Omega_2 \frac{\partial \bar{u}_1}{\partial x_2} + \Omega_3 \frac{\partial \bar{u}_1}{\partial x_3} \right)}_{II} \\ & = \underbrace{\frac{\partial}{\partial x_1} \left(\frac{\partial \bar{u}'_1 \bar{u}'_2}{\partial x_3} - \frac{\partial \bar{u}'_1 \bar{u}'_3}{\partial x_2} \right)}_{III} + \underbrace{\frac{\partial^2}{\partial x_2 \partial x_3} (\bar{u}'_3{}^2 - \bar{u}'_2{}^2)}_{IV} \\ & \quad - \underbrace{\left(\frac{\partial^2}{\partial x_3^2} - \frac{\partial^2}{\partial x_2^2} \right) \bar{u}'_2 \bar{u}'_3}_V + \underbrace{\nu \left(\frac{\partial^2 \Omega_1}{\partial x_1^2} + \frac{\partial^2 \Omega_1}{\partial x_2^2} + \frac{\partial^2 \Omega_1}{\partial x_3^2} \right)}_{VI} \quad (6.16) \end{aligned}$$

Where vorticity components are.

$$\Omega_1 = \frac{\partial \bar{u}_2}{\partial x_3} - \frac{\partial \bar{u}_3}{\partial x_2}, \quad \Omega_2 = \frac{\partial \bar{u}_1}{\partial x_3} - \frac{\partial \bar{u}_3}{\partial x_1}, \quad \Omega_3 = \frac{\partial \bar{u}_2}{\partial x_1} - \frac{\partial \bar{u}_1}{\partial x_2} \quad (6.17)$$

The different terms in equation (6.16) resulting from the flowing phenomena:

I: stream-wise vorticity convection by primary flow which tends to unify the vorticity along the axial direction.

II: vortex stretching and skewing by primary velocity gradient which is the cause of Prandtl's secondary motion of the first kind.

III, IV, V: turbulence effects leading to generation or destruction of vorticity

VI: represents viscous diffusion of vorticity which also responsible for reducing vorticity variation along the cross sectional plane and slows down the rotation of a

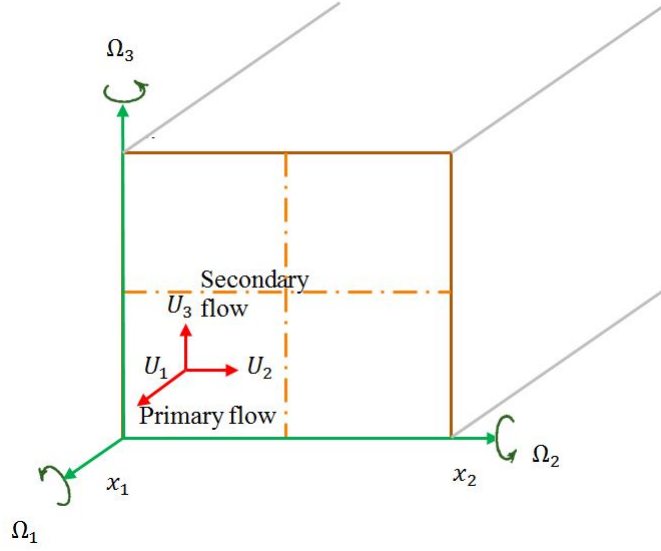


Figure 6.1: Coordinate system for the flow

particle in a straight duct.

It is worthy to note that in laminar flow through straight ducts terms III, IV and V do not exist in equation (6.1) because of absence of Reynolds stresses. Hence secondary flow of Prandtl's second kind does not occur because the mechanism of the flow provides only convection and diffusion of vorticity. On the other hand, in turbulent flow, these terms lead to the production of vorticity consequently developing secondary motions across the plane.

Considering fully developed flow, all of the variations along stream-wise direction (x_1) become zero and thus, equation (6.16) simplifies to

$$\frac{\partial \Omega_1}{\partial x_2} + u_3 \frac{\partial \Omega_1}{\partial x_3} = \frac{\partial^2}{\partial x_2 \partial x_3} (\overline{u_3'^2} - \overline{u_2'^2}) - \left(\frac{\partial^2}{\partial x_3^2} - \frac{\partial^2}{\partial x_2^2} \right) \overline{u_2' u_3'} + \nu \left(\frac{\partial^2 \Omega_1}{\partial x_2^2} + \frac{\partial^2 \Omega_1}{\partial x_3^2} \right) \quad (6.18)$$

6.2.3 Reynolds Stress Transport Equations

To develop more equation from the Navier Stokes (N-S) equation, let us take moment of the equation, i.e. multiply N-S equation by fluctuating property and then take time average of the product. This will lead to a development of the differential equation for the transport of Reynolds Stress tensor

Rewriting equation (6.1) to introduce the Navier Stokes operator

$$\mathcal{N}(u_i) = \frac{\partial u_i}{\partial t} + u_k \frac{\partial u_i}{\partial x_k} + \frac{1}{\rho} \frac{\partial p}{\partial x_i} - \nu \nabla^2 u_i = 0 \quad (6.19)$$

By taking moments of the above equation it becomes as follows

$$\underbrace{\overline{u'_i \frac{\partial u_j}{\partial t} + u'_j \frac{\partial u_i}{\partial t}}}_{\text{Unsteady term}} + \underbrace{\overline{u'_i u_k \frac{\partial u_j}{\partial x_k} + u'_j u_k \frac{\partial u_i}{\partial x_k}}}_{\text{Convection term}} + \underbrace{\frac{1}{\rho} \left(\overline{u'_i \frac{\partial p}{\partial x_j} + u'_j \frac{\partial p}{\partial x_i}} \right)}_{\text{Pressure term}} - \underbrace{\nu \left(\overline{u'_i \nabla^2 u_j + u'_j \nabla^2 u_i} \right)}_{\text{viscous term}} = 0 \quad (6.20)$$

Where the second order moment is defined as

$$\overline{u'_i \mathcal{N}(u_j) + u'_j \mathcal{N}(u_i)} = 0 \quad (6.21)$$

Evaluating each term individually,

$$\begin{aligned}
\overline{u'_i \frac{\partial u_j}{\partial t} + u'_j \frac{\partial u_i}{\partial t}} &= \overline{u'_i \frac{\partial}{\partial t} (\overline{u_j + u'_j}) + u'_j \frac{\partial}{\partial t} (\overline{u_i + u'_i})} \\
&= \overline{u'_i \frac{\partial \overline{u_j}}{\partial t} + u'_i \frac{\partial u'_j}{\partial t} + u'_j \frac{\partial \overline{u_i}}{\partial t} + u'_j \frac{\partial u'_i}{\partial t}} \\
&= \overline{u'_i \frac{\partial u'_j}{\partial t} + u'_j \frac{\partial u'_i}{\partial t}} \\
&= \frac{\partial}{\partial t} \overline{(u'_i u'_j)}
\end{aligned} \tag{6.22}$$

$$\begin{aligned}
\overline{u'_i u'_k \frac{\partial u_j}{\partial x_k} + u'_j u'_k \frac{\partial u_i}{\partial x_k}} &= \\
&= \overline{u'_i (\overline{u_k + u'_k}) \frac{\partial}{\partial x_k} (\overline{u_j + u'_j}) + u'_j (\overline{u_k + u'_k}) \frac{\partial}{\partial x_k} (\overline{u_i + u'_i})} \\
&= \overline{u'_i \overline{u_k} \frac{\partial u'_j}{\partial x_k} + u'_i u'_k \frac{\partial}{\partial x_k} (\overline{u_j + u'_j}) + u'_j \overline{u_k} \frac{\partial u'_i}{\partial x_k} + u'_j u'_k \frac{\partial}{\partial x_k} (\overline{u_i + u'_i})} \\
&= \overline{u_k} \frac{\partial}{\partial x_k} \overline{(u'_i u'_j)} + \overline{u'_i u'_k} \frac{\partial \overline{u_j}}{\partial x_k} + \overline{u'_j u'_k} \frac{\partial \overline{u_i}}{\partial x_k} + \frac{\partial}{\partial x_k} \overline{(u'_i u'_j u'_k)}
\end{aligned} \tag{6.23}$$

The pressure gradient term:

$$\begin{aligned}
\frac{1}{\rho} \left(\overline{u'_i \frac{\partial p}{\partial x_j} + u'_j \frac{\partial p}{\partial x_i}} \right) &= \frac{1}{\rho} \left(\overline{u'_i \frac{\partial}{\partial x_j} (\overline{p + p'}) + u'_j \frac{\partial}{\partial x_i} (\overline{p + p'})} \right) \\
&= \frac{1}{\rho} \text{secodnary} \left(\overline{u'_i \frac{\partial p'}{\partial x_j} + u'_j \frac{\partial p'}{\partial x_i}} \right)
\end{aligned}$$

Finally the viscous term yields

$$\begin{aligned}
\nu \left(\overline{u'_i \nabla^2 u_j + u'_j \nabla^2 u_i} \right) &= \nu \left(\overline{u'_i \nabla^2 (\bar{u}_j + u'_j)} + \overline{u'_j \nabla^2 (\bar{u}_i + u'_i)} \right) \\
&= \nu \left(\overline{u'_i \nabla^2 u'_j + u'_j \nabla^2 u'_i} \right) \\
&= \nu \left(\overline{\frac{\partial}{\partial x_k} \left(u'_i \frac{\partial u'_j}{\partial x_k} \right)} + \overline{\frac{\partial}{\partial x_k} \left(u'_j \frac{\partial u'_i}{\partial x_k} \right)} - 2 \overline{\frac{\partial u'_i}{\partial x_k} \frac{\partial u'_j}{\partial x_k}} \right) \quad (6.24) \\
&= \nu \left(\overline{\frac{\partial^2}{\partial x_k^2} (u'_i u'_j)} - 2 \overline{\frac{\partial u'_i}{\partial x_k} \frac{\partial u'_j}{\partial x_k}} \right)
\end{aligned}$$

Collecting all the terms we get the final version of the equation as follows

$$\begin{aligned}
&\left[\frac{\partial}{\partial t} \overline{(u'_i u'_j)} + \bar{u}_k \frac{\partial}{\partial x_k} \overline{(u'_i u'_j)} \right] \\
&= - \left[\overline{u'_i u'_k} \frac{\partial \bar{u}_j}{\partial x_k} + \overline{u'_j u'_k} \frac{\partial \bar{u}_i}{\partial x_k} \right] + \left[2\nu \overline{\left(\frac{\partial u'_i}{\partial x_k} \right) \left(\frac{\partial u'_j}{\partial x_k} \right)} \right] \\
&\quad + \frac{1}{\rho} \left[\overline{u'_i \frac{\partial p'}{\partial x_j} + u'_j \frac{\partial p'}{\partial x_i}} \right] + \frac{\partial}{\partial x_k} \left[-\nu \frac{\partial}{\partial x_k} \overline{(u'_i u'_j)} + \overline{(u'_i u'_j u'_k)} \right]
\end{aligned}$$

Rearranging terms, we get the transport equation for Reynolds stresses in its most recognizable form;

$$\underbrace{\frac{D}{Dt} \overline{(u'_i u'_j)}}_{\text{Convection}} = - \underbrace{\left[\overline{u'_i u'_k} \frac{\partial \bar{u}_j}{\partial x_k} + \overline{u'_j u'_k} \frac{\partial \bar{u}_i}{\partial x_k} \right]}_{\text{Generation}} - \epsilon_{ij} + \Pi_{ij} - \underbrace{\frac{\partial}{\partial x_k} \left[\nu \frac{\partial}{\partial x_k} \overline{(u'_i u'_j)} + C_{ijk} \right]}_{\text{Diffusion}} \quad (6.25)$$

Where,

$$\epsilon_{ij} \text{ [Destruction]} = 2\nu \overline{\left(\frac{\partial u'_i}{\partial x_k}\right) \left(\frac{\partial u'_j}{\partial x_k}\right)} \quad (6.26)$$

$$\Pi_{ij} \text{ [Redistribution]} = \frac{p'}{\rho} \overline{\left(\frac{\partial u'_i}{\partial x_j} + u'_j\right)} \quad (6.27)$$

$$C_{ijk} = \frac{\partial}{\partial x_k} \left[\overline{(u'_i u'_j u'_k)} + \frac{p'}{\rho} (\delta_{jk} u'_i + \delta_{ik} u'_j) \right] \quad (6.28)$$

6.3 Experimental Studies

The study of turbulent flow in non-circular ducts started with the experimental investigation of Nikuradse (1926) who discovered discrepancies in the axial velocity profile in turbulent flows through straight rectangular and square ducts. He carefully measured the isotach¹ distributions in rectangular duct with various cross sections in order to illustrate the flow profile across the duct. A distortion in the axial mean velocity profile was observed by injecting dye to the flow field which revealed the presence of secondary flows in the duct's cross sectional plane. Prandtl (1926) offered an initial explanation of such phenomena by considering turbulent fluctuation to be the major cause of generating secondary motion in the corner region of a square duct. Particularly, he suggested that, a transverse mean flow is developed because of tangential velocity fluctuation across the region of isotach curvature which subsequently move from the concave towards convex side of the isotach, as shown in Figure 6.2

It was just an indication of the presence of a secondary velocity; however a quantitative description was missing for several decades up until Hoagland (1960)

¹a line of constant axial mean flow velocity in a plane normal to the axial flow direction

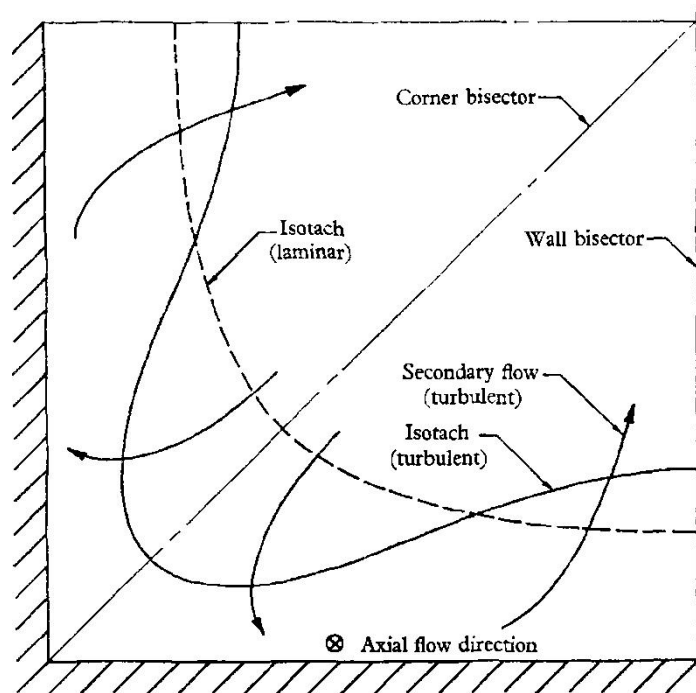


Figure 6.2: Typical isotach patterns in flow along a corner in a square duct.

came up with his experimental techniques for directly measuring secondary velocity profiles in turbulent flows through square ducts. He measured the mean flow velocity of a fully developed turbulent flow in a straight square duct by using hot wire anemometry. Gilbert and Jorgenson (1960) also measured the turbulent velocity profile in a rectangular channel using same technique. Both investigators agreed that the magnitude of the secondary velocity is on the order of 1% of the maximum mean axial flow velocity. Furthermore they have showed that, despite being such small fraction of the mean flow, these secondary velocities have pronounced effect of the overall isotach distribution. Hoagland also evaluated the local wall shear stress by a direct measurement technique using a Preston tube. In spite of the great contribution from Hoagland's data, the accuracy was questionable because of his using a coarse device to measure flow parameters in his study. As the magnitude of the secondary flow compared with axial mean flow is only a few percent at most, a small perturbation

in the flow field will distort the secondary flow pattern significantly. Following Hoagland's work, Leutheusser (1963) calculated the local shear stress distribution in a rectangular channel. However, both of their works were confined to measuring the magnitude of the local wall shear stress. Nevertheless, the directional characteristics of the local wall shear stress should not be omitted from calculation as these vectors are skewed because of the presence of secondary flow.

Townsend (1980) was perhaps the pioneer to formally state the origin of secondary flow in the corner region of fully developed turbulent flow. He postulated that the non-zero value of transverse Reynolds stress difference $(\overline{u_3^2} - \overline{u_2^2})$ give rise to the development of secondary motion. A detailed description of the equation for mean vorticity was presented in his book which was later adopted by many investigators to examine the causes of secondary flow in non-circular ducts.

One of the most rigorous descriptions of turbulent flow through square ducts was provided by Brundrett and Baines (1964), who measured the three axial mean velocity components of the flow as well as all six components of Reynolds stress in their experiment at a distance 260 times hydraulic diameters downstream from the inlet where the flow is most likely fully developed. They simplified the transport equation (equation (6.20)) for mean stream-wise vorticity by considering fully developed flow condition (equation (6.22)) and evaluated each term in this equation in their experiments. From the hot wire measurement data of all six components of the Reynolds stress, they concluded that the origin of secondary velocity is the gradients of Reynolds stress in plane normal to the flow direction. A concluding remark from their work highlighted the normal component of the shear stress gradient as the major contributor to the secondary flow.

In order to explore further the origin of secondary flow, Gessner and Jones (1965)

investigated the effect of Reynolds number in secondary flows and measured the directional characteristics of the local shear stress and orientation of the principal planes of Reynolds shear stress in planes normal to the stream-wise direction. It was found from their experiments that the secondary flow velocities normalized with the bulk velocity decrease for increase in Reynolds number. In addition, they observed that the highest obliquity of the local wall shear-stress occurs at the maximum secondary flow region in the corner. The experimental results were identical for both square and a rectangular channel with 2:1 aspect ratio. Moreover, they determined the forces that are actually responsible for generation of secondary motion by deriving momentum balance equation along a secondary flow streamline in streamline coordinates and experimentally evaluating the each term in the equation. According to author's observations, in contrary to Brundrett and Baines explanation, the viscous terms to be unimportant for the driving mechanism for secondary motion, rather it is the differences in magnitude of opposing forces exerted by Reynolds stresses and static pressure gradients in a plane normal to stream-wise direction. They found that the turbulent normal and shear stress terms, which represented by terms IV and V in equation (6.3), were equal order of magnitude which was later confirmed by Perkins (1970).

Although it provided considerable detail of Reynolds number dependency of the secondary motion, the observation was restricted to a narrow range of Reynolds number because of the limitations of the experimental setup. Furthermore, the authors' failed to explain a discrepancy in mass conservation equation that arose from their experimental observation. In addition, unlike Brundrett and Baines experiment, the flow measurement station was not in a fully developed region. A better approximation to the mass conservation and explanation for such discrepancies was provided by

Launder and Ying (1972) while investigating the effect of internal rough surface on secondary flow. According to the authors' statement, an imprecision of measuring data using hot wire anemometry gives rise to such mass imbalance. In addition, it was concluded that the secondary velocity is independent of Reynolds number and surface roughness provided it is non-dimensionalized with friction velocity u_τ .

Meanwhile many other investigators proposed alternative explanations of the origins of secondary flow. Some of them argued that certain terms in the transverse Reynolds stress equation as responsible for the generation of secondary motion (Townsend (1980); Eichelbrenner and Toan (1969)) while other investigators suggest that, it is rather because of the vorticity along the axial flow direction which develops in the corner region ((Einstein and Li, 1958; Brundrett and Baines, 1964; Perkins, 1970)). All of these foregoing analyses assume that either directly or indirectly, the anisotropy of transverse normal Reynolds stresses is the main cause of the secondary motion. In opposition of this theory, Gessner (1973) argued that it is not the Reynolds stress which dominates rather Reynolds shear stress gradients is the primary factor which develops the secondary flow in the corner region. He examined the mechanism for initialization of secondary flow in developing turbulent flow in a square duct from the energy and vorticity standpoint by applying the energy balance and vorticity balance to the mean axial motion along corner bisector and then evaluated each term in these equations experimentally. A direct influence of the transverse gradients of Reynolds shear stress components to the generation of secondary flow in turbulent flow along a corner revealed from his study. The author postulated that the secondary flow convects momentum, vorticity and the energy of primary flow in planes normal to the axial flow direction.

Other features of the turbulent flow through square ducts such as mean velocity

profiles, peripheral wall shear stress distribution and pressure distribution have been measured by Ahmed and Brundrett (1971) and Thomas et al. (1972). In order to estimate the variation of those parameters, these authors accounted for different Reynolds numbers in the flow. Few more complementary studies have been reported by Po (1975) and Lund (1977) in the entrance region of a turbulent square duct flow as well as developed flow.

The experiments of all the investigators mentioned above were somehow corrupted by the disturbance of flow field because of using probes during the data acquisition. They did not have any alternatives as there were no such instruments available to measure flow parameters without disturbing flow field at their time of research. In order to avoid such error in the experimental data, Melling and Whitelaw (1976) used laser doppler anemometry (LDA) to measure flow field parameters and provided a concise and comprehensive description of the developing flow in square duct. Their work qualitatively agrees with previous researchers; however a quantitative difference was indicated. It was outlined that the developing flow depends on the inlet condition more than fully developed flow. Their measuring stations were at various cross sections across the duct up to $36.8D_h$ (where D_h is the hydraulic diameter) where the flow is not fully developed yet. Despite of not being a fully developed flow description, their works contributed vividly to validate many turbulence models developed afterwards. Figure 6.3 represents the primary velocity profile measured in a square duct by three different authors at different Reynolds number.

Measurement of turbulent flow in non-circular ducts has been reported with many other variant such as flow with one rough surface in square duct (Fujita et al., 1989, 1990), two opposite side roughened in a square duct (Yokosawa et al. 1989), sudden change in smooth to rough surface in the walls (Maeda et al., 2005), flow in equilateral

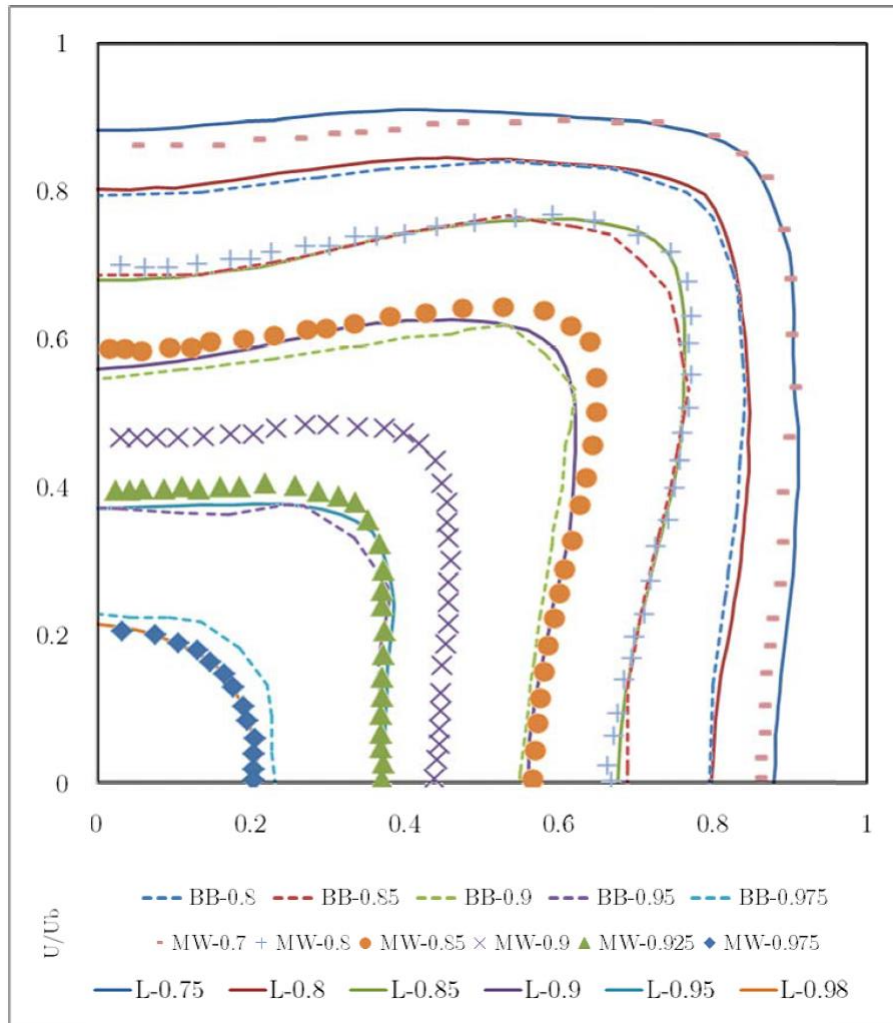


Figure 6.3: Measured primary velocity profile [L- Leutheusser (1963), Re-83,000; MW- Melling and Whitelaw (1976), Re-42,000; BB- Brundrett and Baines (1964) Re-83,000]

triangular ducts Aly et al. (1978) and flow in rectangular duct with large aspect ratio (Hinze, 1973). All these experiments were concerned with the effect of boundary layer in secondary flow and turbulent structure of the flow field.

Most of the experimental investigations involved measuring flow field at high Reynolds numbers whereas a few studies found dealing with low Reynolds number flow. Niederschulte et al. (1990) performed a LDA experiment to rectangular channel at Reynolds number 2777 and 2457 based on channels half width. The experimental data on turbulent structure and flow field mainly obtained to validate the DNS data available at that time. Meanwhile Cheesewright et al. (1990) reported another experimental work in square duct at Reynolds number 4900. These works have been extensively used to validate low Reynolds number model for predicting turbulent flow in square and rectangular channels

6.4 Numerical Calculations

The experimental work carried out by the forgoing researchers disclosed great detail of information on mean flow properties, turbulent characteristics and the development of secondary motion in straight non-circular ducts. However, the exact mechanisms can be more accurately identified by modelling the Reynolds normal stress $\overline{u_3'^2} - \overline{u_2'^2}$ and $\overline{u_2'u_3'}$ in the stream-wise vorticity equation (equation (6.22)). The modelling can be achieved by transporting Reynolds stresses in the stream-wise direction and correlating different terms in equations (6.25) - (6.28) for closure approximation (namely Reynolds stress closure approximation) and solving for these turbulence normal stresses. The form of the Reynolds stresses closure has been proposed using many modelling technique. A brief description of the models used in the past literature along with corresponding investigation on turbulence driven secondary flow

Table 6.1: Summary of Experimental Works

Reference	Medium	Method	Reb	Experimental setup	Channel
Nikuradse (1926)		Dye injection			Square, Rectangular
Hoagland (1960) and Gilbert (1960)	Air	Pitot tube	60,000	12.7 cm \times 12.7 cm \times 9.75 mt 6.35 cm \times 12.7 cm \times 9.75m, 4.22 cm \times 12.7 cm \times 9.75 m	Square
Leutheusser (1963)	Air	Micro-manometer	10,000-100,000	7.62 cm \times 7.62 cm \times 1.59m 7.62 cm \times 22.86 cm \times 1.59m	Rectangular Square
Brundrett & Baines (1964)	Air	HWA	83,000	7.62 cm \times 7.62 cm \times 2.13m	Rectangular
Gessner & Jones (1965)	Air	HWA	75,000; 150,000 & 300,000	20.32 cm \times 20.32 cm section, $L/D_h=40$	Square
Perkins (1970)			50,000; 300,000	20.32 cm \times 10.16 cm, $L/D_h=60$	Square
Ahmed & Brundrett (1971)			88,000	30.5 cm \times 30.5 cm \times 167.64 cm	Square
Launder & Ying (1972)	Air	HWA	215,000, 69,000	50.8 cm \times 50.8 cm \times 182.88 cm	Square, rough surface
(Hinze 1973)	Air	HWA	150,000	45 cm \times 9 cm \times 19m	Rectangular
Melling & Whitelaw (1976)	Water	LDA	42,000	4 cm \times 4.1 cm \times 1.8m	Rectangular
Aly et al. (1978)			53,000-107,000	12.7 cm (each side) \times 7.76 m	Equilateral Triangle
Niederschulte et al. (1990)	Water	LDA	2,457	5.08 cm \times 61 cm \times 10.16 m	rectangular
Cheesewright et al. (1990)	Air	LDA	4,900		Square

will be presented in the following sections.

6.4.1 Linear Eddy Viscosity Models

Linear eddy viscosity models are the simplest types of Reynolds stress modelling where Reynolds stresses are represented by a linear relationship with the turbulent eddy viscosity. Analogously with the molecular viscous stress, the turbulent stress is modelled by decomposing into isotropic and deviatoric part as follows

$$\tau_{ij} = \overline{u'_i u'_j} = \frac{2}{3} k \delta_{ij} + D_{ij} \quad (6.29)$$

The turbulent kinetic energy is expressed as

$$k = \frac{1}{2} \tau_{ii} = \frac{1}{2} \overline{u'_i u'_i} = \frac{1}{2} \left(\overline{u_1'^2} + \overline{u_2'^2} + \overline{u_3'^2} \right) \quad (6.30)$$

The deviatoric component of the turbulent stress D_{ij} is formulated according to Boussinesq hypothesis such that

$$D_{ij} = -\nu_t \left(\frac{\partial \overline{u}_i}{\partial x_j} + \frac{\partial \overline{u}_j}{\partial x_i} \right) \quad (6.31)$$

where ν_t is the turbulent or eddy viscosity which can be expressed as

$$\nu_t = \frac{l_0^2}{t_0} \quad (6.32)$$

and l_0 and t_0 are the turbulent length and time scales respectively. Incorporating these values in equation (6.12) results a compact form of the Reynolds Stress Navier Stokes Equation

$$\frac{\partial \bar{u}_i}{\partial t} + \bar{u}_j \frac{\partial \bar{u}_i}{\partial x_j} = -\frac{1}{\rho} \frac{\partial \bar{p}}{\partial x_i} + \frac{\partial}{\partial x_j} \left[(\nu + \nu_t) \frac{\partial \bar{u}_i}{\partial x_j} \right] \quad (6.33)$$

6.4.2 Algebraic Stress Models (ASM)

In algebraic stress models the turbulent length and time scales l_0 and t_0 are represented by an algebraic expression. The simplest form of representation of this kind is based on Prandtl's mixing length theory (Prandtl, 1926), where the eddy viscosity is represented in terms of turbulent length scale analogous to mean free path in kinetic theory of gases.

$$\nu_t = l_0^2 \left| \frac{du}{dy} \right| \quad (6.34)$$

A more physically consistent representation of eddy viscosity is provided in terms of turbulent intensity of the fluctuations

$$\nu_t \propto \sqrt{k} l_0 \quad (6.35)$$

Despite of gaining a wide acceptance because of its simplicity, the linear representation of eddy viscosity in turbulence modelling has the major shortcoming of being isotropic. This hinders tracking of secondary flows in non-circular ducts. Therefore many modifications to this model have been suggested to adapt it so that it captures the secondary motions. The first modelling of secondary flow in square duct was carried out by Launder and Ying (1972) (hereafter mentioned as LY model) who developed a algebraic stress model coupled with one equation model for the stresses $\overline{u_3'^2} - \overline{u_2'^2}$ and $\overline{u_2' u_3'}$ by adapting a simplified transport equation from the Reynolds stress model of Hanjalic and Launder (1972) where seven coupled non-linear

differential equation in addition to mean flow quantities are suggested to solve for the flow field. In equation (6.25) they neglected convection and diffusion terms in a fully developed flow condition by assuming local equilibrium to obtain an algebraic expression of Reynolds stresses, removing all differential terms of $\overline{u'_i u'_j}$. Moreover, considering the mean velocity gradient in the cross sectional plane much smaller than axial velocity gradient, the generation term omitted from the equation (6.25). The destruction term in equation (6.28) considered to be isotropic at high Reynolds number thereby represented in terms of dissipation rate, ϵ which was ultimately approximated in terms of local kinetic energy and length scale by dimensional analysis

$$\epsilon \propto k^{\frac{2}{3}}/l_0 \quad (6.36)$$

After incorporating these simplifications, the following expressions were obtained for the remaining Reynolds stress terms leading to a simplified algebraic stress model (ASM):

$$\overline{u_3^2} - \overline{u_2^2} = c' \frac{k}{\epsilon} \left(\overline{u_1 u_3} \frac{\partial U_1}{\partial x_3} - \overline{u_1 u_2} \frac{\partial U_1}{\partial x_2} \right) \quad (6.37)$$

$$\overline{u_2 u_3} = c' \frac{k}{\epsilon} \left(\overline{u_1 u_2} \frac{\partial U_1}{\partial x_3} - \overline{u_1 u_3} \frac{\partial U_1}{\partial x_2} \right) \quad (6.38)$$

The kinetic energy appearing in the above equation was calculated by solving a transport equation for k which is formulated by taking the trace of equation (6.25) after incorporating equation (6.30)

$$\frac{\partial k}{\partial t} + \overline{u_j} \frac{\partial k}{\partial x_j} = -\mathcal{P} - \epsilon - \frac{\partial}{\partial x_j} \left(\frac{1}{2} \overline{u'_i u'_i u'_j} + \overline{p' u'_j} \right) + \nu \nabla^2 k \quad (6.39)$$

Where

$$\mathcal{P} [\overline{Turbulence\ production}] = \tau_{ij} \frac{\partial u_i}{\partial x_j} \quad (6.40)$$

The turbulent transport terms is approximated by the gradient transport hypothesis as follows

$$\frac{1}{2} \overline{u'_i u'_i u'_j} + \overline{p' u'_j} = \frac{\nu_t}{\sigma_k} \frac{\partial k}{\partial x_j} \quad (6.41)$$

Finally the transport equation for kinetic energy takes the form of

$$\frac{\partial k}{\partial t} + \overline{u_j} \frac{\partial k}{\partial x_j} = \tau_{ij} \frac{\partial u'_i}{\partial x_j} - \epsilon + \frac{\partial}{\partial x_i} \left[\left(\nu + \frac{\nu_t}{\sigma_k} \right) \frac{\partial k}{\partial x_j} \right] \quad (6.42)$$

The primary stresses $\overline{u'_1 u'_2}$ and $\overline{u'_1 u'_3}$ are approximated from a standard eddy-viscosity model [equation (6.35)] where the distribution of length scale (l_0) determined from algebraic geometrical formula originally provided by Buleev et al. (1963). With this simplified model, the author simulated axial velocity profiles, secondary velocity profile in rough and smooth ducts, kinetic energy contours and friction factors with experimental results. Although the model has its merits for being simple, the prediction of secondary flows cannot be accounted for properly.

Many other investigators have used the LY model to predict turbulent flow in non-circular passages. A slight modification to the algebraic stress model (ASM) has been proposed by Tatchell (1975) where he introduced a transport equation for the dissipation rate ϵ by replacing the algebraic length scale formula [equation (6.36)]. The transport equation is developed by taking moments of the Navier-Stokes equation [equation (6.1)] in the following way

$$2\nu \overline{\frac{\partial u'_i}{\partial x_k} \frac{\partial}{\partial x_k} [\mathcal{N}(u_i)]} = 0 \quad (6.43)$$

This leads to following expression,

$$\frac{\partial \epsilon}{\partial t} + \overline{u_j} \frac{\partial \epsilon}{\partial x_j} = -\mathcal{P}_\epsilon - \Phi_\epsilon - \mathcal{D}_\epsilon - \nu \nabla^2 \epsilon \quad (6.44)$$

Where, the production, destruction and turbulent diffusion of dissipation are defined as,

$$\mathcal{P}_\epsilon = 2\nu \left[\overline{\frac{\partial u'_i}{\partial x_k} \frac{\partial u'_j}{\partial x_k} + \frac{\partial u'_k}{\partial x_i} \frac{\partial u'_k}{\partial x_j}} \right] \frac{\partial \overline{u_i}}{\partial x_j} + 2\nu \overline{u'_k} \frac{\partial u'_i}{\partial x_j} \frac{\partial^2 \overline{u_i}}{\partial x_k \partial x_j} + 2\nu \overline{\frac{\partial u'_k}{\partial x_i} \frac{\partial u'_k}{\partial x_j} \frac{\partial u'_i}{\partial x_j}} \quad (6.45)$$

$$\Phi_\epsilon = 2\nu^2 \overline{\frac{\partial^2 u'_i}{\partial x_j \partial x_k} \frac{\partial^2 u'_i}{\partial x_j \partial x_k}} \quad (6.46)$$

$$\mathcal{D}_\epsilon = 2\nu \frac{\partial}{\partial x_j} \left(\overline{\frac{\partial p'}{\partial x_i} \frac{\partial u'_j}{\partial x_i}} \right) + \nu \frac{\partial}{\partial x_j} \left(\overline{u'_j \frac{\partial u'_i}{\partial x_k} \frac{\partial u'_i}{\partial x_k}} \right) \quad (6.47)$$

The above terms are modelled to obtain a simplified form of transport equation for the rate of dissipation

$$\frac{\partial \epsilon}{\partial t} + \overline{u_j} \frac{\partial \epsilon}{\partial x_j} = C_{\epsilon 1} \frac{\epsilon}{k} \tau_{ij} \frac{\partial \overline{u_i}}{\partial x_j} - C_{\epsilon 2} \frac{\epsilon^2}{k} + \frac{\partial}{\partial x_i} \left[\left(\nu + \frac{\nu_t}{\sigma_\epsilon} \right) \frac{\partial \epsilon}{\partial x_j} \right] \quad (6.48)$$

This modification made the model more generalized and used for many complex geometrical configurations. For instance, Gosman & Rapley (1978; 1980) provided an extensive analysis of fully developed turbulent flow in square, rectangular, elliptic ducts and tube assembly passages with this modified model. They employed

an orthogonal curvilinear coordinate system fitted into an arbitrary cross section. However, a difficulty in convergence with the cross sectional momentum and continuity equations was encountered in the solution. They presented a comprehensive comparison of mean primary and secondary velocity, friction factor and Reynolds stresses components with experimental and previous numerical results. Many other investigators attempted a similar modelling approach focusing on turbulent structure in fully developed flow in arbitrary cross-sectional duct (Nakayama, 1981; Nakayama et al., 1983), equilateral triangular duct (Aly et al., 1978), triangular pitch rod bundles (Carajilescov and Todreas, 1976), developing flow in square duct using different numerical solution techniques ((Nakayama et al., 1984; Nakayama and Chow, 1986)). Neti and Eichhorn (1979) reported a similar work for fully developed flow in square duct at Reynolds number 40,000 for axial distances up to 40 hydraulic diameters. Rapley and Gosman (1984) adapted a simplified approach in the work of Gosman & Rapley(1978; 1980) by ignoring anisotropic effect of the eddy viscosity and considering local equilibrium of convection and diffusion. This simplification eliminated the complexity of the calculation and reduced computational time significantly; however, there was some loss of information in the prediction of flow parameters as observed from detailed comparison for mean flow, secondary flow, and friction factor and wall shear stresses with those of experimental works and numerical results from different turbulent models. Similar work reported by Ramachandra (1979) employed the algebraic stress model successfully with slight modification for determining the heat transfer rate and mean flow characteristics for rod bundle geometries. All these models estimated secondary flow streamlines and isovel patterns in substantial agreement with the experimental results. However, the kinetic energy predicted from these models has shown considerable discrepancies with their experimental counterparts.

Furthermore, the difference between the two transverse normal stresses $\overline{u_3'^2} - \overline{u_2'^2}$, which, according to some authors, is the main mechanism of generating secondary flow, is estimated to be one tenth of its actual magnitude (Kacker, 1973)).

In another study, Naot et al. (1974) proposed a quasi-isotropic two point correlation model developed by the same authors (Naot et al., 1973) for predicting Reynolds stresses in fully developed turbulent flow in square ducts. In addition, the turbulent length scale was prescribed by an algebraic expression, and secondary velocity gradients were retained in the modelled equations. A set of nine governing equations [axial velocity, lateral vorticity and stream function along with six components of Reynolds stresses] were solved simultaneously by using an upwind finite difference technique in a non-uniform mesh and considered the velocity profile near wall to be logarithmic. Although the numerical results from their calculation of the mean flow velocity profile and Reynolds stress yield good agreement with the experimental results of (Leutheusser, 1963), Brundrett and Baines (1964); Gessner and Jones (1965), but an excessively bulging of the isotach contours at the regions of wall bisector appeared in their results. On the other hand, turbulent kinetic energy contours appeared to be less distorted and they agreed with experimental measurements. Moreover, the model is limited to providing a stable solution only up to 2×10^5 because of the strong coupling of mean flow and Reynolds stress equations.

The closure issue of Reynolds stresses modelling has been addressed with significant improvement by Launder et al. (1975) accounting for solid boundary effects by suggesting a systematic model for the pressure-strain correlation. The rest of the correlation terms in the Reynolds stresses transport equation [equation (6.25)] were developed according to Hanjalic and Launder (1972). Unlike Naot et al. (1974), the turbulent length scale was calculated from the dissipation rate which was obtained

from the solution of its transport equation. Good agreement between the predicted and experimental result of the separation of Reynolds normal stresses $\overline{u_2'^2}$ and $\overline{u_3'^2}$ are found from the work. Later on, Reece (1977) applied this model to calculate developing flow in a square ducts without considering local equilibrium of convection and diffusion of Reynolds stresses. The author found good agreement of the predicted distribution of all velocity component and five Reynolds stresses with the experimental data of Melling and Whitelaw (1976).

In a series of papers, a Reynolds stress modelling approach was adopted by Gessner and his co-workers (Gessner and Emery, 1976, 1977) for turbulent flow in internal corner region of non-circular ducts based upon modified Reynolds stress transport equation following Launder et al. (1975). Unlike Reece (1977), convection and diffusion terms were omitted from equation (6.25) assuming local equilibrium to make the approach simpler. Mixing length profile and Reynolds stress distributions were predicted and compared with two sets of experimental data to determine the constants involved in the model. However, the comparison of the model's results are somewhat devaluated as the experimental results chosen for comparison was not satisfactorily accurate (Demuren and Rodi, 1984). Later their work was extended to develop a mixing length scale model for predicting local shear stress in an arbitrary aspect ratio rectangular duct (Gessner and Emery, 1977) and heat transfer in a square duct (Emery et al., 1979) for developing and fully developed flow. Although the model neglects the pressure-strain effect and also convection diffusion terms, it gives a generalized prediction of the local turbulent structure which can also be employed for a 90 degree corner. In a continuation of the work (Gessner and Emery, 1981) employed an explicit (Dufort-Frankel) differencing scheme for the axial momentum equation to solve the flow along with the original mixing length model for the Reynolds stresses.

Detailed comparisons reported between experimental results and numerical predictions of local shear stress distribution at different Reynolds number, friction factor, axial centreline and mean velocity distribution, secondary flow velocity distribution along the wall and corner bisectors, turbulence structure, isotach distribution and secondary flow profiles. To certain extent these results agree with the experimental result, however the secondary flow profile prediction from the calculation shows a large discrepancy with the experimental results.

Gerard (1978) presented a finite difference solution to obtain the mean stream-wise vorticity for evaluating secondary flow in a square duct. The author assumed the Reynolds stresses comprised two superimposed components, namely the background turbulence component which is independent of the primary velocity gradient and the momentum transfer component. Reasonable agreement between the calculated distribution of secondary flow with measured value of Brundrett and Baines experimental data was presented in the paper.

Naot and Rodi (1982) developed a simplified algebraic stress model based on Launder et al. (1975) model to predict secondary motion in fully developed flow in open channels with arbitrary cross sections. The free surface effects are accumulated for by incorporating an additive surface-proximity correction suggested by Shir (1973). A truncated version of equation (6.25) is formulated by neglecting convection and diffusion terms along with the surface correction term and this provides a for the solution of the flow field. In the model equations for individual stresses, they found that omitting secondary velocity gradient equation gives rise to unstable solutions; therefore instead of completely neglecting these term, the authors approximated their influence by an additional eddy viscosity terms. Their simulation assumptions were in line with the assumptions of Cousteix and Arnal (1982) in considering an empirical

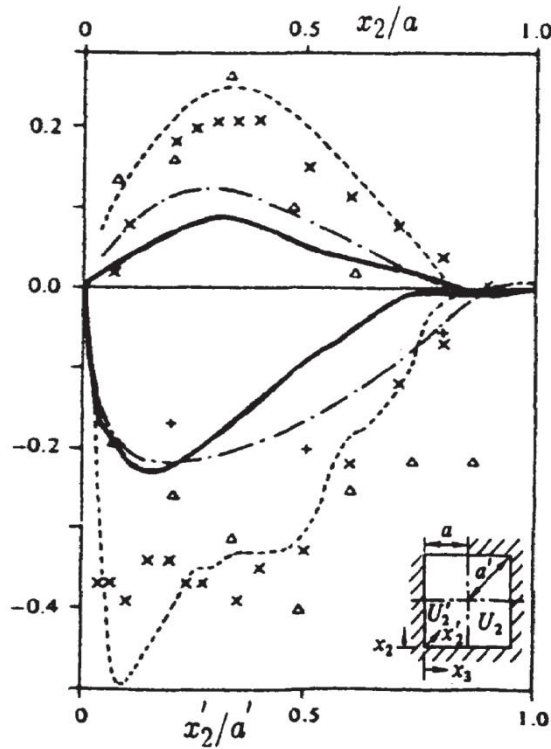


Figure 6.4: Secondary velocities along wall and corner bisectors, - after Breuer and Rodi (1994); Δ , Brundrett and Baines (1964); +, Launder and Ying (1972), \times , Gessner and Emery (1981); $-\cdot-$, Naot and Rodi (1982); $-\cdot-$, Demuren and Rodi (1984) (1984); $-\cdot-$, Breuer and Rodi (1994)

constant \mathcal{C} in equation (6.37) - (6.38). Both of these works attempted a more realistic simulation by including secondary velocity gradient in the Reynolds stress equation instead of assuming an empirical constant value to tune the turbulent structure in the simulation result. Extensive comparison of the predicted flow characteristics with experimental work was presented for both open and closed channel with satisfactory agreement. Furthermore they found that the secondary vortices develops more asymmetrically located near free surface in open channel as opposed to closed channels with similar dimensions. However, due to unavailability of any experimental results for secondary motion in open channel flow, this conclusion could not be verified.

A comprehensive review of the previous work was provided by Demuren and Rodi (1984) where they focused on limitations of all previous simplified algebraic stress

models. These authors argued that in all previous simplified forms of the Reynolds stress models, the secondary velocity gradients in the Reynolds stress equation (particularly $\overline{u'_2 u'_3}$) has been neglected and compensated for by tuning the empirical constant, which in consequence, underestimates the actual driving term $\overline{u'^2_3} - \overline{u'^2_2}$ for secondary flows. In order to eliminate the above limitations, they extended their foregoing work (Naot and Rodi, 1982) by considering secondary velocity gradients in a more realistic way and in a similar fashion of treating primary velocity gradients and observed the effect of secondary velocity gradient in the model quantitatively. Their model predicted the axial velocity fairly well; however a discrepancy in the stream-wise velocities along the corners, and under prediction of secondary motion were observed from their simulation results. The most important conclusion from their review and modelling is to indicate the driving mechanism of secondary motion as to be the difference between turbulent normal stress and shear stress in the cross plane. This argument has been further supported by Wang et al. (1994) who performed an order of magnitude analysis and power-expansion of the governing set of equations to investigate the origin of secondary velocity in a square duct theoretically and computationally. Naimi and Gessner (1995) have demonstrated that a linear wall damping function provides better prediction as opposed to using quadratic formulation of this model. Further extension of the work of Demuren and Rodi (1984) have been reported conforming to duct with non-uniform boundary condition at the inlet Demuren and Rodi (1987) and for duct with arbitrary cross section (Demuren, 1991).

Figure 6.5 represents the calculation and measurements of axial velocity along the centreline of a square duct at different Reynolds numbers as predicted by the previous investigators. A fully developed flow has been found to be established at about $55D_h$.

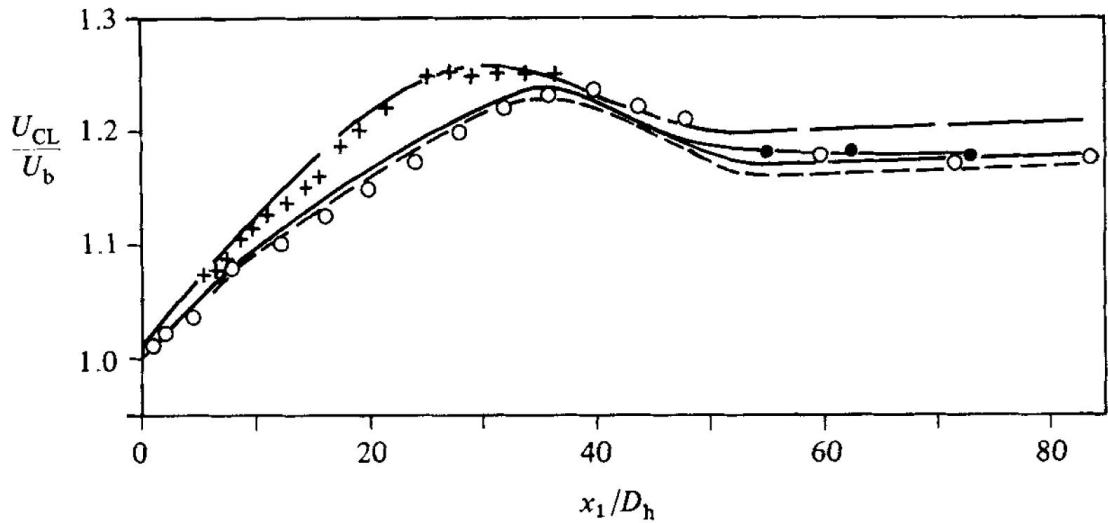


Figure 6.5: Axial velocity profile along the centreline of a square duct, after Demuren and Rodi (1984). Data: + Melling and Whitelaw (1976), $Re=42000$; O, Gessner and Emery (1981), $Re=250,000$; Prediction: — —, Demuren and Rodi (1984), $Re=50,000$; - - -, Demuren and Rodi (1984), $Re=250,000$; - · - ·, Naot and Rodi (1982)

6.4.3 Non-Linear Eddy Viscosity Models (NLEVM)

Despite its widespread adoption in many engineering applications, Boussinesq's hypothesis based models of Reynolds stress closure fails profoundly in predicting the anisotropy of the Reynolds stress and consequently turbulence driven secondary motion (Speziale, 1982). This is because of the closure approximation by a linear representation of the Reynolds stresses tensor with the local strain rate and the ad hoc empiricism included in the modelling (Speziale, 1980). Therefore, further modifications needed to account for the anisotropy of Reynolds stress by additional non-linear functions for the turbulent stress in its governing transport equation (Pope, 1975). This has been achieved by introducing higher order closure correlations for ϵ_{ij} , Π_{ij} and C_{ijk} terms in the Reynolds stresses transport equation (6.29). Unlike eddy viscosity models, second order closure models are capable of capturing effect of the flow history (Speziale, 1990), which helps to describe flow the field more precisely.

The constitutive relationship is developed by nonlinear extension of Boussinesq approximation resulting modified equations for (6.33) and (6.37) (Gatski and Rumsey, 2002)

$$\tau_{ij} = \overline{u'_i u'_j} = \frac{2}{3} k \delta_{ij} + b_{ij} \quad (6.49)$$

The anisotropic component of the Reynolds stress (b_{ij}) is represented by series expansion of tensor bases ($T_{ij}^{(n)}$) and expansion coefficients (A_{ij}).

$$b_{ij} = \sum_{n=1}^N A_{ij} T_{ij}^{(n)} \quad (6.50)$$

A large number of NLEVM have been developed based upon the expansion terms of the above expression which can be categorized as cubic and quadratic models (Argyropoulos and Markatos, 2015). The coupling of the above representation of τ_{ij} results a modified equation of (6.12)

$$\frac{\partial \bar{u}_i}{\partial t} + \bar{u}_j \frac{\partial \bar{u}_i}{\partial x_j} = -\frac{1}{\rho} \frac{\partial \bar{p}}{\partial x_i} + \frac{\partial}{\partial x_j} \left[(\nu + \nu_t) \frac{\partial \bar{u}_i}{\partial x_j} \right] + NLST \quad (6.51)$$

Where NLST is the nonlinear source term arising from the tensor representation in equation (6.50). Speziale (1987) developed a quadratic non-linear $k-l$ and $k-\epsilon$ model for an explicit representation of Reynolds stresses by imposing generalized covariance to an arbitrary coordinate transformation of the Navier-Stokes equation in the limit of two-dimensional turbulence. From a comparison of calculated value of Reynolds normal stresses from linear and non-linear models, the author clearly demonstrated that a more accurate description was obtained along with improved prediction of secondary motion in channels and separated flow. This work has been compared and validated further for a rectangular duct with experimental work and linear models

by Rokni et al. (1998). The author claimed that the “return to isotropy at the duct’s centre” is the main limitation of a nonlinear eddy viscosity model which leads to overestimation of turbulent intensities. Furthermore, this model was successfully used for capturing secondary motion in rotating rectangular duct with various cross-sections Younis (1993).

A similar set of non-linear constitutive relationships for the turbulent stress belongs to quadratic group has been developed from two scale direct interaction approximation (TSDIA) (Yoshizawa 1984), realizability and necessary in-variance requirements (Shih et al., 1993), re-normalization group (RNG) theory (Rubinstein and Barton, 1990; Wang et al., 2011), and explicit solution of algebraic stress models Gatski and Speziale (1993). In a study by Mompean et al. (1996) a quantitative performance analysis of these models and some linear models for applicability at low Reynolds number flow was reported by comparing turbulent structure and secondary vortices with DNS data. The author remarked that the applicability of all these tested linear and nonlinear models is designed for high Reynolds number. Moreover, Rokni and Gatski (2001) have reported the application of an Explicit Algebraic Stress Model (EASM) Gatski and Speziale (1993) for flow and heat transfer through arbitrary cross sectional geometries. Their application shows that the model is capable of predicting turbulent flow in non-circular duct up to Reynolds number 10^5 with minimum requirement of wall functions.

Regardless of the well accepted popularity of models based on the above quadratic nonlinear relationship of anisotropy of Reynolds stress, some authors (Craft and Launder, 1996) argued that in order to extend the range of applicability of nonlinear models, higher order terms need to be included to predict complex flow fields. Craft and Launder (1996) proposed a cubic representation of the anisotropic term in the

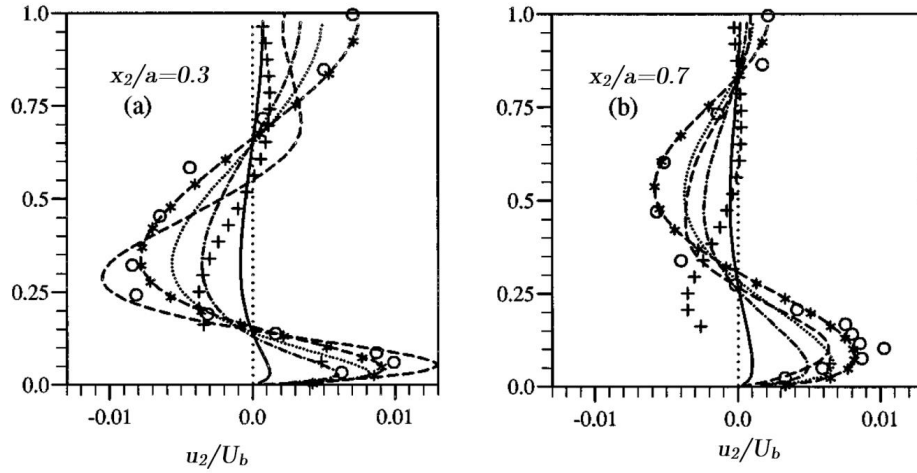


Figure 6.6: Secondary velocity profiles along two sections (a) $x_2/a = 0.3$; and (b) $x_2/a = 0.7$; - after Mompean et al. (1996). $-\cdot-$, Shih et al. (1993); $- \cdot -$, Rubinstein and Barton (1990); \dots , Speziale (1987); $- \cdot - \cdot -$, Gatski and Speziale (1993); \dots , linear model; $+$, RSM; $-$, DNS [Gavrilakis (1992)]; O , Measurement of Cheesewright et al. (1990); x_2 and U_b are the radial coordinate and bulk velocity of the flow respectively.

series expansion to include higher order terms in the model. A few more such models have been proposed by other authors (Wallin and Johansson, 2000; Apsley and Leschziner, 1998).

Myong (1991) introduced a nonlinear low Reynolds number k-epsilon model for wall bounded flow, which has later been used for calculating developing flow structure (Myong, 1991), fully developed flow and heat transfer (Myong and Kasagi, 1990) in square ducts and an improved version for accounting for near wall effects (Myong, 1991). The primary and secondary velocity gradients have been included in their model to capture the mechanisms of secondary motion more realistically. The low Reynolds number consideration enabled the applicability of the model right up to the wall. However, the linear distance representation of wall damping function limits the versatility of the model.

Nisizima and Yoshizawa (1987) developed an anisotropic k-epsilon model based on the Reynolds stresses representation of (Yoshizawa 1984) and applied the model

to channel and Couette flows to demonstrate their capability of capturing Reynolds stresses. This model has been further extended by Nisizima (1990) to predict mean stream-wise velocity, secondary velocity, and turbulent structure in a square duct flow. Near the wall, van Driest's damping function was adapted to stabilize the numerical solution and at the wall, no slip boundary condition considered. A weak and underestimated secondary flow have been observed from the comparison with experimental data; however it predicts most of features better than previous eddy viscosity models.

Internal flows are strongly affected by the presence of solid walls; therefore extra care should be taken during turbulence modelling in these situations. Most of the eddy viscosity models for computing turbulence driven secondary flow in non-circular ducts account this effect by adapting a wall function which has been observed as inadequate for such complex flows Reif and Mortensen (2011). Durbin (1991) introduced an elliptic relaxation approach for near wall treatment (namely $v^2 - f$ model) without any wall damping function. This enabled more physically consistent modelling of near-wall turbulence. However the original $v^2 - f$ model was developed without the accompanying anisotropy of Reynolds stresses therefore it was incapable to capture any turbulence driven secondary flows. Pecnik and Iaccarino (2007) introduced a novel stress strain relationship with the original linear $v^2 - f$ model to capture secondary flow without changing the linearity property of the model. Their modified model demonstrated a qualitative prediction of secondary motion in square and triangular ducts. Nevertheless, the importance of incorporating Reynolds stress anisotropy could not be subsidized. As a consequence many modifications of this model have been suggested to utilize this model for capturing Reynolds stresses properly. Among these models, Reif et al. (2009) suggested a constitutive nonlinear

relationship of Reynolds stresses based on the works of Lien and Durbin (1996) along with the physically appealing near-wall modelling features of an elliptic relaxation method. A comparison study of turbulent structure and secondary flow field with experimental measurement and DNS data shows that the model can predict mean flow velocity and friction factors reasonably well (Reif and Andersson, 2002). However, the turbulent intensity, normal stresses, shear stresses and secondary velocity profile were inaccurately calculated by the model.

The centreline velocity normalized with bulk velocity shows constant behaviour at higher Reynolds number where as the friction velocity normalized with bulk velocity appeared to decrease as Reynolds number increases. This has been established from the experimental work of Lund (1977) and models of Reif and Andersson (2002); Demuren and Rodi (1984).

6.4.4 Large Eddy Simulation

6.4.5 Mathematical Formulation of Turbulence

A more accurate and promising method of turbulent modelling is Large Eddy Simulation (LES) where the important and larger eddies are resolved completely and smaller eddies are modelled with a sub-grid scale (SGS) models. This separation of the scale of eddies is achieved by applying a spatial filtering process to the Navier Stokes Equation. The basic steps of a LES technique comprise (Berselli et al., 2005; Pope, 2001)

- (i) Filtering of the Navier Stokes equation
- (ii) Modelling of sub-grid scale stresses
- (iii) Boundary layer consideration with an accurate near wall treatment

(iv) Solving the filtered Navier Stokes equation with an appropriate numerical scheme and testing the solution for performance

A filtering operation to Navier Stokes Equation, unlike time averaging, is defined by a general convolution integral as (Leonard, 1975)

$$\overline{u_i}(x, t) = u_i - u'_i = \int \int \int G(x - \xi; \Delta) u_i(\xi, t) d^3\xi \quad (6.52)$$

Where G is the filter function, $\overline{u_i}$ is the resolvable-scale filtered velocity, u'_i is the sub-grid scale velocity and $\Delta \left(= (\Delta x_1 \Delta x_2 \Delta x_3)^{\frac{1}{3}} \right)$ is the filter width which accounts for the size of smallest eddy that is resolved.

The filtered Navier Stokes equation and continuity equation therefore stands as,

$$\frac{\partial \overline{u_i}}{\partial t} + \frac{\partial}{\partial x_j} (\overline{u_i u_j}) = -\frac{1}{\rho} \frac{\partial \overline{p}}{\partial x_i} + \nu \nabla^2 \overline{u_i} - \frac{\partial \tau_{ij}}{\partial x_j} \quad (6.53)$$

$$\frac{\partial \overline{u_i}}{\partial x_i} = 0 \quad (6.54)$$

Where the sub-grid scale tensor τ_{ij} defined as

$$\tau_{ij} = \overline{u_i u_j} - \overline{u_i} \overline{u_j} = \underbrace{\overline{u_i u_j} - \overline{u_i} \overline{u_j}}_{L_{ij}} + \underbrace{\overline{u_i u'_j} + \overline{u'_j u_i}}_{C_{ij}} + \underbrace{\overline{u'_i u'_j}}_{R_{ij}} \quad (6.55)$$

The terms in the above equation are known as the Leonard, Cross and Reynolds terms respectively. Equations (6.53) - (6.55) can be organized to following form (Wilcox et al., 1998)

$$\frac{\partial \overline{u_i}}{\partial t} + \frac{\partial}{\partial x_j} (\overline{u_i u_j}) = -\frac{1}{\rho} \frac{\partial P}{\partial x_i} + \frac{\partial}{\partial x_j} \left[\nu \frac{\partial \overline{u_i}}{\partial x_j} + \tau_{ij} \right] \quad (6.56)$$

With

$$\left. \begin{aligned} \tau_{ij} &= - \left(Q_{ij} - \frac{1}{3} Q_{kk} \delta_{ij} \right) \\ P &= \bar{p} + \frac{1}{3} Q_{kk} \delta_{ij} \\ Q_{ij} &= R_{ij} + C_{ij} \end{aligned} \right\} \quad (6.57)$$

A large number of sub-grid scale (SGS) models have been proposed over the last half century to model the SGS stresses represented by the tensor Q_{ij} . The first SGS model postulated by Smagorinsky (1963)) by assuming gradient diffusion hypothesis, representing τ_{ij} as

$$\tau_{ij} = 2\nu_t S_{ij} \quad (6.58)$$

Where the mean strain rate tensor, S_{ij} and Smagorinsky eddy viscosity ν_t are given by

$$S_{ij} = \frac{1}{2} \left(\frac{\partial \bar{u}_i}{\partial x_j} + \frac{\partial \bar{u}_j}{\partial x_i} \right) \quad \text{and,} \quad \nu_t = (C_s \Delta)^2 \sqrt{S_{ij} S_{ij}} \quad (6.59)$$

Here C_s is the Smagorinsky coefficient, a value that depends upon the flow characteristics.

The first large eddy simulations of turbulent flow through square duct were carried out by Miyake and Kajishima (1991) at two different Reynolds numbers ($Re = 6200, 67400$). They have reinforced the fact that the secondary flow originates from the difference of Reynolds stress gradient and corresponding pressure gradient in the corner region. In a separate discussion (Kajishima and Miyake, 1992), the authors have commented on the validity of existing eddy viscosity models based on their LES computation. However, due to lack of sufficient spatial resolution, this work does not

give comprehensive description of the flow physics.

Madabhushi and Vanka (1991) performed an LES study of secondary motion in square ducts using the Smagorinsky (1963) SGS model for a low Reynolds number ($Re = 5810$) flow. They have employed a length scale proposed by Piomelli et al. (1988). An improved prediction observed from the model. However while comparing with experimental data of high Reynolds number, only a qualitative similarity was found from the analysis.

Breuer and Rodi (1994) applied a dynamic SGS model developed by Germano et al. (1991) in inhomogeneous turbulent flow through a square straight and 180 degree bend duct to calculate flow structure at low and high Reynolds numbers ($Re = 4410, 56690$). It was observed that, at the low Reynolds number the dynamic SGS prediction was more accurate result than a Smagorinsky model. However at high Reynolds number, this does not remain true.

A more general description of turbulent secondary flow in fully developed flow through straight square ducts using LES has been provided by Germano et al. (1991); Su and Friedrich (1993). A modified version of SGS model of Schumann (1975) was used to resolve the sub-grid scale stresses. The filtered Navier Stokes equations were solved on a staggered mesh with explicit Leap-frog finite differencing scheme. Three different sets of mesh settings used to check that grid independency had been attained. Good agreement of the simulation and experimental data from the model was obtained and the authors attempted to examine and adjust some of the conceptual models prescribed in the past for secondary flow modelling.

Large eddy simulation have been used in more complex flow condition where internal and external corners affect the flow simultaneously a square annular duct Xu and Pollard (2001). The authors used Smagorinsky (1963) SGS model along with

a wall damping function as suggested by Kajishima and Miyake (1992). Reasonable agreement found with the DNS data for the mean stream wise flow field. Their work suggested the existence of symmetrically located strong counter rotating vortex near the convex 90° corner and a weak counter spinning symmetric vortex pair around the concave 90° corner.

A different approach to the large eddy simulation of Navier Stokes equation proposed by Pattison et al. (2009) using generalized lattice Boltzmann equation (GLBE) with a forcing term for turbulent flow through square duct at Reynolds number 300 based on friction velocity. The GLBE was solved in conjunction with Smagorinsky SGS model aided with van Driest damping function. The result from the simulation appeared to be more promising than other LES studies when compared with DNS data.

Furthermore, Vázquez and Métais (2002) reported a LES study of turbulent flow through a heated square duct where they computed flow structure through heated and isothermal duct to investigate the effect of heated wall on the secondary flow structure. They resolved the larger eddies by incorporating selective structure function sub-grid scale stress model proposed by Métais and Lesieur (1992). Excellent agreement between predicted result and DNS data was reported for a high resolution simulation.

6.4.6 Direct Numerical Simulation

In Direct Numerical Simulation (DNS), all scales are resolved in the solution of Navier Stokes equation with appropriate initial and boundary conditions. Although conceptually it is the easiest method of solving turbulent flow, but it is the most computationally expensive as the flow domain must be sufficiently refined to accommodate the largest eddies at the same time, it must be fine enough to capture the

Table 6.2: Summary of Large Eddy Simulation for turbulent flow through square channels

Reference	Mesh	Re_b	Geometry	Domain	Sub-grid Scale model
Miyake and Kajishima (1991)	$100 \times 127 \times 127$	6200, 67400	Square duct	$20\pi \times 2 \times 2$	Smagorinsky
Madabhushi and Vanka (1991)	$96 \times 101 \times 101$	5810	Square duct	$4\pi \times 2 \times 2$	Smagorinsky
Breuer and Rodi (1994)	$64 \times 41 \times 41$; $63 \times 63 \times 63$; $101 \times 101 \times 101$	4410, 56690	Square duct, 180° bend	$2\pi \times 1 \times 1$, $4\pi \times 1 \times 1$	Smagorinsky & Dynamic (Germano et al., 1991)
Su and Friedrich (1993)	$256 \times 64 \times 64$	49000			Modified Schumann (1975)
Xu and Pollard (2001)	$130 \times 66 \times 66$; $130 \times 130 \times 130$	3650, 3349	Square annular duct	$16\pi \times 4 \times 4$, $8\pi \times 4 \times 4$	Smagorinsky
Pattison et al. (2009)	$432 \times 74 \times 74$	4410	Square duct	$6 \times 1 \times 1$	Smagorinsky
Vázquez and Métais (2002)	$120 \times 60 \times 60$; $64 \times 50 \times 50$	6000	Heated square duct	$4.074\pi \times 1 \times 1$	Structure function (Métais and Lesieur, 1992)

Table 6.3: Summary of Direct Numerical Simulation of turbulent flow through square ducts

Reference	Mesh	Re_b	Geometry	Domain
Gavrilakis (1992)	$1000 \times 127 \times 127$	4410	Square duct	$20\pi \times 2 \times 2$
Huser and Birnigen (1993)	$96 \times 101 \times 101$	10320	Square duct	$2.037\pi \times 1 \times 1$
Uhlmann et al. (2007)		3500	Square duct	
Joung et al. (2007)	$64 \times 96 \times 96$	4440	Square duct	$3\pi \times 1 \times 1$
Zhu et al. (2009)	$121 \times 101 \times 101$	9960	Square duct	$4.082\pi \times 2 \times 2$
Xu (2009)	$256 \times 258 \times 258$	3058	Square annular	$4\pi \times 4 \times 4$
Pinelli et al. (2010)		3500	Square duct	$10.97h < L_x < 12.57$

smallest eddies of the flow. Furthermore, the time step should be small enough to capture smallest perturbation in the flow. However, as computational technologies advances over time, many DNS studies in simple flow geometries have been reported in the literature.

In a square duct, Gavrilakis (1992) first reported DNS of turbulent flow for Reynolds number 4410. The low Reynolds number DNS study provided a detailed description of mean flow in normal plane and turbulent statistics along the wall bisectors. The simulation agreed well with the low Reynolds number experimental data of Niederschulte et al. (1990) and Cheesewright et al. (1990).

Direct Numerical Simulation of a more established turbulent flow in square duct is provided by Huser and Biringen (1993). The authors investigated turbulent flow of Reynolds number 10320 in a shorter flow domain with a periodic boundary condition. Two different sets of mesh size set up for simulation in order to check for grid independent solution. Details of the mean flow characteristics, secondary velocity and turbulent structure reported after verifying with experimental data. The author postulated that the mechanism for secondary motion in the corner region is due to the ejection structure that generates during bursting events consequently originates two stream wise counter rotating vortices. Based upon this DNS data, Huser et al. (1994) evaluated different terms in Reynolds stress transport equation. It seems that the anisotropy of Reynolds stress is developed from the exchange between the two primary shear stresses through production and velocity pressure gradient terms. Moreover, the incapability of modelling vorticity source term (as seen from Figure 6.7) has been indicated as the major cause of failure of nonlinear k-epsilon model to capture anisotropy of Reynolds stress.

Another low Reynolds number study has been presented by Joung et al. (2007)

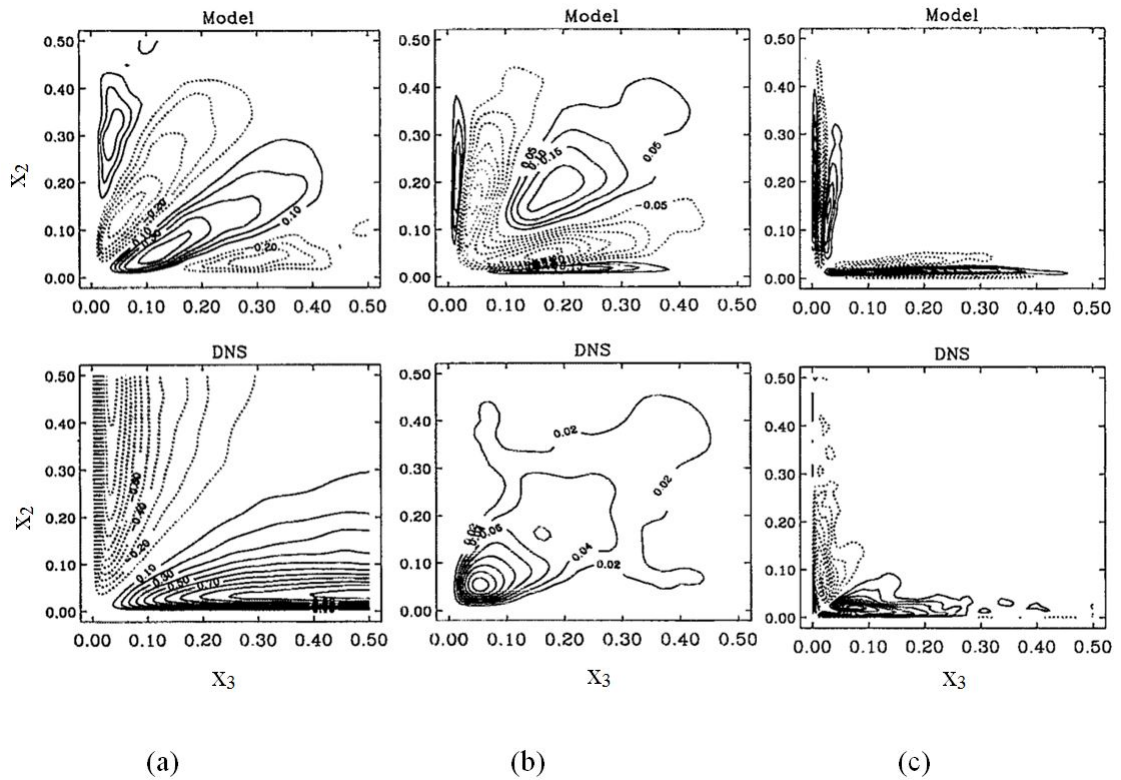


Figure 6.7: Comparison of Reynolds anisotropy terms from DNS (Huser and Biringen, 1993) and Nonlinear k-epsilon model (Speziale, 1987); (a) $u_2' u_3'$, (b)

$u_2'^2 - u_3'^2$; (c) source term in vorticity equation (6.18),

$$\left[-\frac{\partial^2}{\partial x_2 \partial x_3} (u_2'^2 - u_3'^2) + \left(\frac{\partial^2}{\partial x_2^2} - \frac{\partial^2}{\partial x_3^2} \right) u_2' u_3' \right]$$
 taken from Huser et al. (1994)

to illuminate the secondary flow mechanism from a quadrant analysis. They argued that the evolution of sweep and ejection events is strongly dependent of local wall shear stress maxima or minima respectively. The directional change of this ejection event gives rise to counter clockwise vortex which consequently generates secondary flow.

Realizing the lack of higher order turbulent statistics description from previous study, Zhu et al. (2009) reported a DNS study of turbulent flow in a square duct at a Reynolds number 600 based on friction velocity. Along with mean flow variable, the authors presented the root mean square, flatness and skewness factor of fluctuating components of velocities along the wall bisector.

Further DNS studies have been reported on turbulent flow in square duct considering sustenance of turbulence structure at marginal condition at low Reynolds number (Uhlmann et al., 2007), Reynolds number dependence of flow structure at low Reynolds number regime (Pinelli et al., 2010), mean flow and secondary flow structure through square annular duct (Xu, 2009), turbulent and buoyancy driven flow in heated horizontal square duct (Sekimoto et al., 2011),

6.5 Performance of Various Turbulence Model to Predict Secondary Flow in Square Ducts

The above review of the literature on secondary flows in non-circular ducts has highlighted several opportunities for further work. It has prompted us to investigate applicability of ranges of models of turbulence. For this purpose, we have used commercial CFD package FLUENT to simulate turbulent flows in a rectangular duct. The characteristics of the velocity contours, the secondary velocity profiles and the

Table 6.4: Parameters used to simulate turbulent flow in rectangular pipe

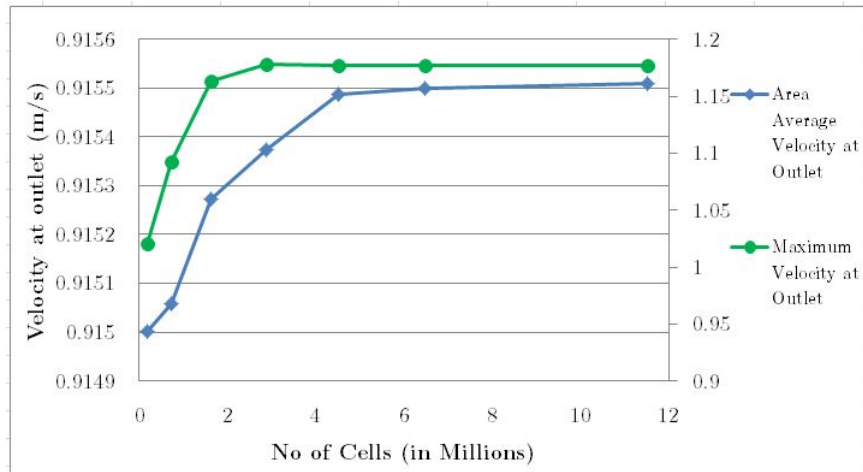
Variable	Parameters
Geometry (b×w×L)	4 cm×4.1cm ×223 cm
Number of mesh	2.01×10^6
L/D_h	55
Bulk velocity at inlet	0.915 m/s
Reynolds number, Re_b	42,000
Fluid	Water
Time (for transient solutions)	10 s

secondary velocity vectors were observed. Prior to performing the simulation, a grid sensitivity test was carried out to determine the number of grid points to be used in the simulation runs. Two parameters- the maximum and mean velocities at the outlet and the mean and maximum turbulent viscosity at the outlet, were chosen to compare their variation with grid refinement can be observed in Figure 6.8

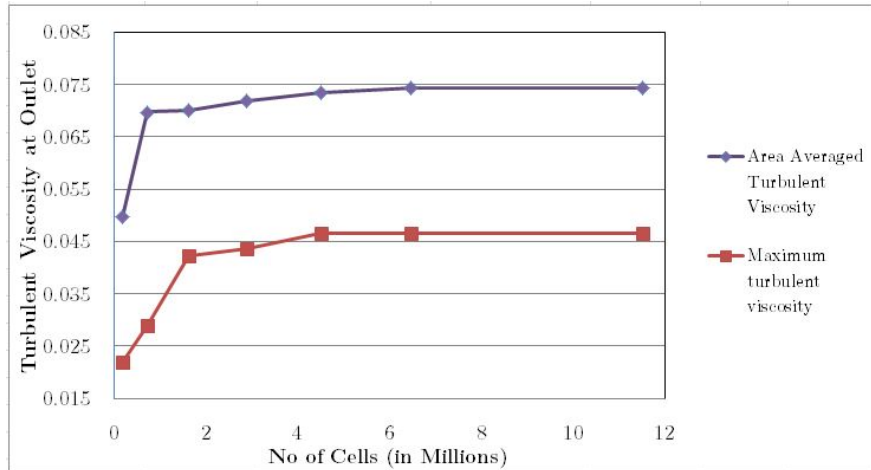
6.5.1 Flow Regime

The flow were setup for a rectangular duct to solve the three dimensional Navier Stokes equation using various turbulence models. The domain size and various parameters used in the simulation are presented in the following Table 6.4

Models used in the simulations were the standard k-epsilon model, Re-normalization Group (RNG) k-epsilon model, Scale Adaptive Simulation (SAS), Reynolds Stress Model (RSM) with Linear Pressure-Strain model (LPS), Quadratic Pressure-Strain (QPS) model and Stress Omega model for modelling Reynolds stress terms, Detached Eddy Simulation (DES) (with Spallart Allmaras (SA), SST k-omega and Realizable k-epsilon model as the RANS model) and Large Eddy Simulation (LES) with the Smogirinsky-Lilly (SL), Wall modelled LES (WMLES), and Kinetic-Energy Transport (KET) sub-grid scale models.



(a) Plot of area-averaged velocity and maximum velocity at the outlet of the duct



(b) Plot of maximum turbulent viscosity and area averaged turbulent viscosity at the outlet of the duct

Figure 6.8: Grid sensitivity test for the simulation of turbulent flow through rectangular ducts

6.5.2 Outlet Velocity Contours

As discussed in the earlier sections, due to the effect of secondary flow in the corners of the duct, one might expect velocity contours at the outlet to be distorted. This has been visualized by plotting the outlet velocity contour in Figure 6.9. A comparison of these simulation results can be made with the experimental results reported in Figure 6.3. It can be seen that the linear eddy viscosity models, such as the standard k-epsilon model and RNG k-epsilon model inevitably fail to predict the trace of secondary flow. The Scale Adaptive Simulation (SAS) and Detached Eddy Simulation (DES) model along with the SST k-omega and Realizable k-epsilon RANS model can predict the existence of secondary flow to some extent as observed in Figure 6.9 (c), (e) and (f), however along with the Spallart-Allmaras RANS model, DES model fails to identify the distortion of the isotach (Figure 6.9(d)).

The simulation results for the velocity contours at the outlet of a rectangular duct obtained by the Reynolds Stress Models (RSM) seem more promising in terms of capturing the secondary flow (Figure 6.10(g) - (i)). Particularly the Stress Omega model (Figure 6.10(i)) for Reynolds stress terms do very well in representing the isotach distortion. Moreover, the Large Eddy Simulation (LES) with various sub-grid scale filters anticipate the presence of secondary flow in fine details (Figure 6.10(j) - (l)). Nevertheless, the Kinetic Energy Transport sub-grid scale model in LES (Figure 6.10(l)) perhaps overestimates the distortion of the secondary flow.

6.5.3 Secondary Flow Velocity Contours

In order to compare the magnitude and the orientation pattern of the secondary flow, the contours of the secondary flow in the rectangular duct have been plotted in 6.11.

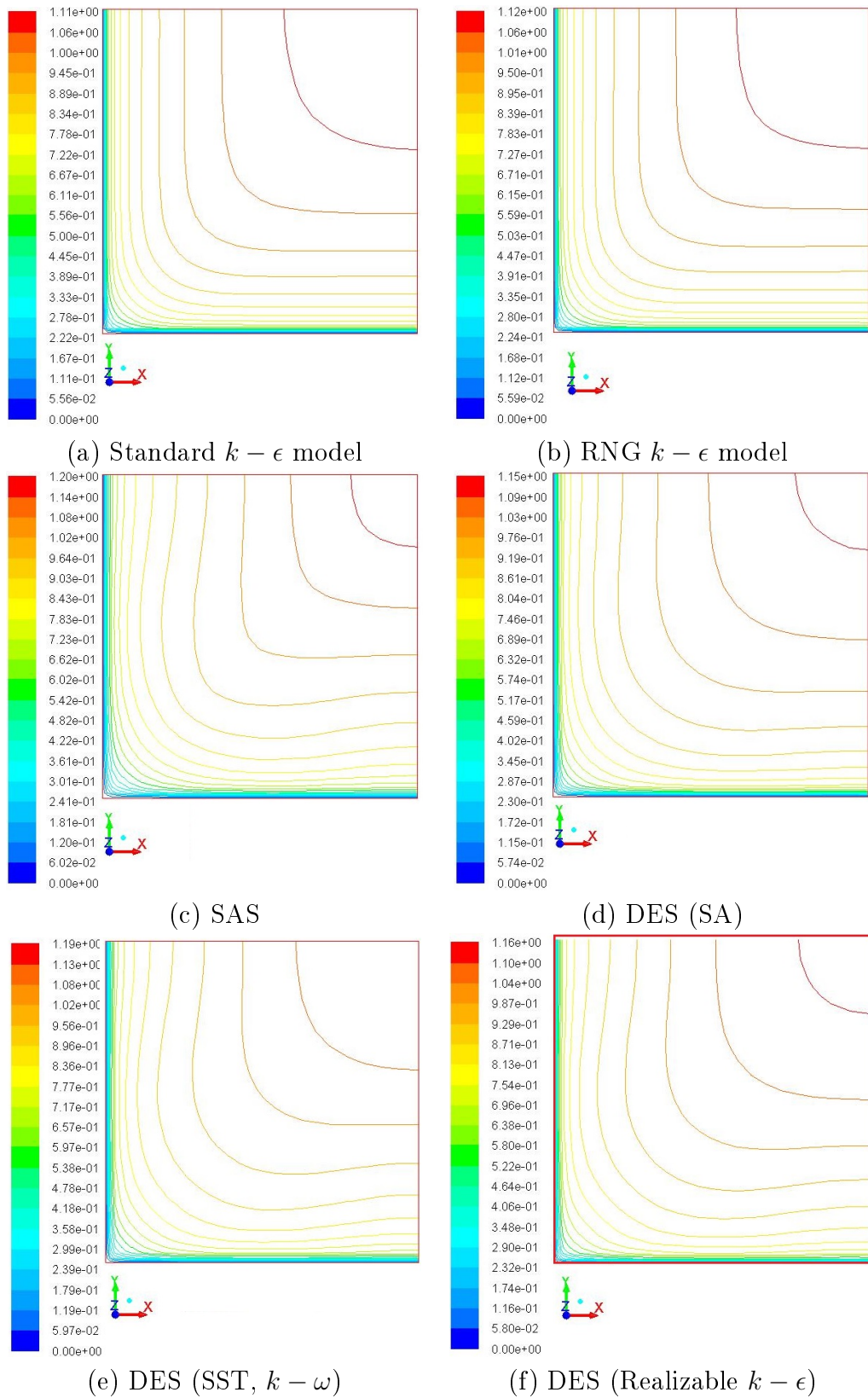


Figure 6.9: Simulation results of outlet velocity contour for turbulent flow in rectangular duct using various turbulent models

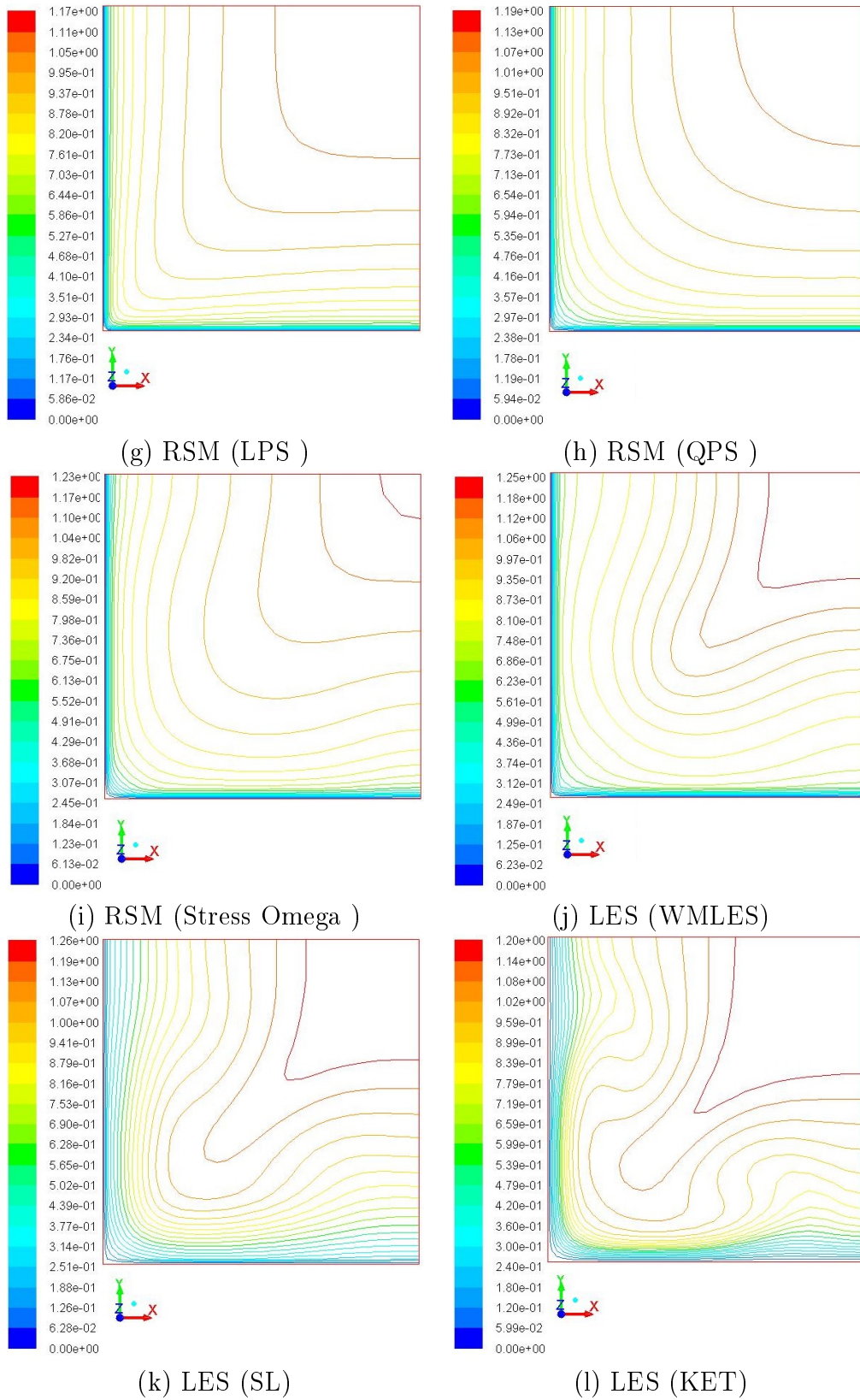


Figure 6.10: Simulation results of outlet velocity contour for turbulent flow in rectangular duct using various turbulent models

Simulation results for various turbulence models have been recorded. It can be noted that the magnitude of secondary flow calculated using linear viscosity model is almost negligible ($<0.000015\%$) whereas with other models reasonable approximations were obtained. From experimental data and DNS results, we find that the magnitude of the secondary flow would be 1-2% of the maximum axial flow velocity (Hoagland, 1960; Gavrilakis, 1992). The secondary flow patterns in the simulation results from SAS, DES and RSM models match closely with experimental results, however SAS and DES models seem to underestimate the magnitude the maximum secondary flow velocity (approximately 0.3-0.5% of the bulk velocity). Interestingly, RSM models seem to do very well in predicting the magnitude of the secondary motions. Apart from the Quadratic Pressure Strain (QPS) model for the Reynolds stress (which results in approximately 0.5% of the stream-wise flow), the Linear Pressure Strain (LPS) model and the Stress Omega model represents secondary motion approximately 1% of the axial centreline velocity.

It seems that the most accurate results for the flow pattern and the magnitude of the turbulent secondary motion among all models are obtained from the simulation results of LES turbulence model as can be observed in Figure 6.12. All sub-grid scale models capture the secondary flow. The Kinetic Energy Transport (KET) sub-grid scale model approximates to be 1% of the centreline velocity and it appears to be particularly promising.

6.5.4 Secondary Velocity Vector

The simulated velocity vectors of the secondary flows also shed some light on the efficacy of the turbulence models we have investigated. It can be observed from Figure 6.14 that no plausible vector pattern were obtained from the k-epsilon models.

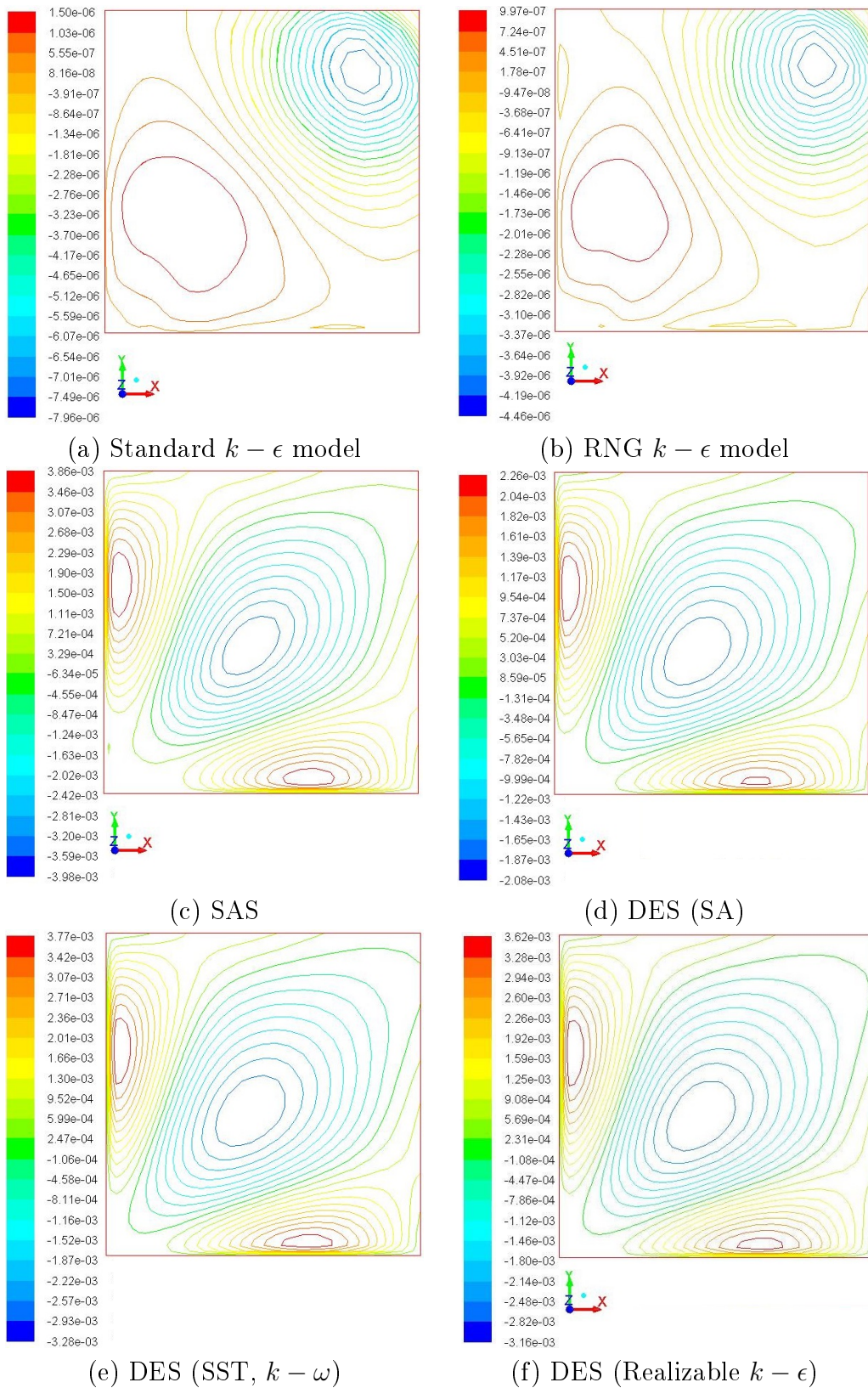


Figure 6.11: Simulation results of contour of secondary velocity at outlet of a rectangular duct in turbulent flow using various turbulent models

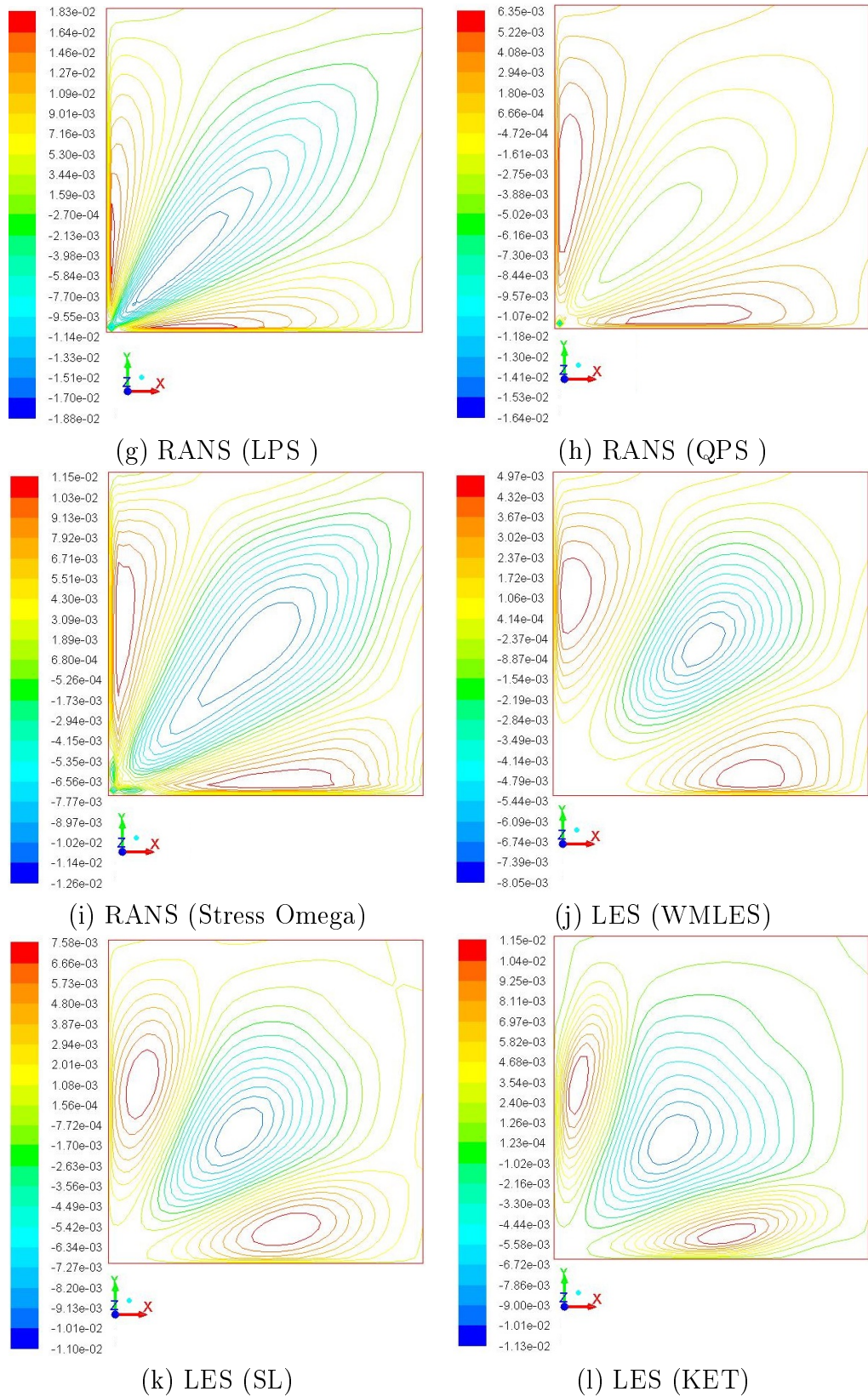


Figure 6.12: Simulation results of contour of secondary velocity at outlet of a rectangular duct in turbulent flow using various turbulent models

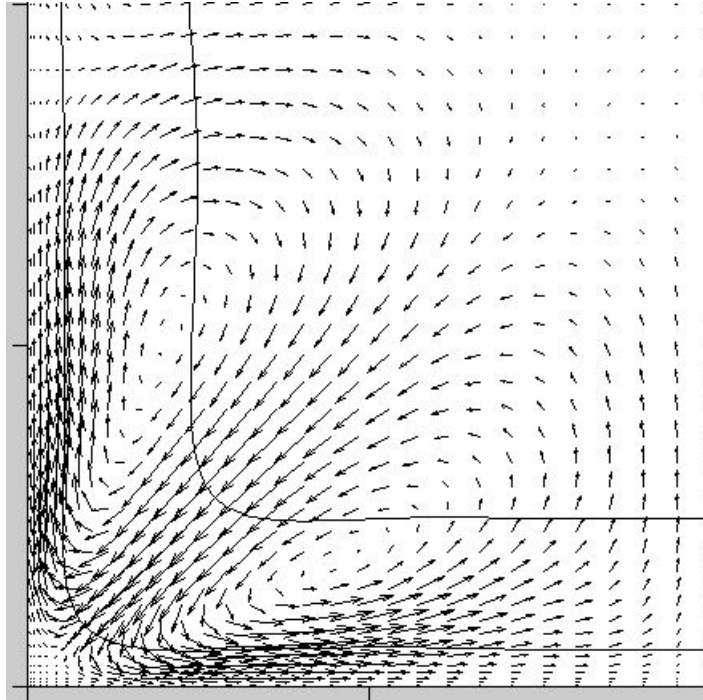


Figure 6.13: DNS results (Pinelli et al., 2010) for secondary flow vector in a square duct at $Re = 3500$

In contrast, the SAS, DES, RANS and LES models produce meaningful vector plots of the secondary flow which has been obtained from DNS results shown in Figure 6.13. Again among all these models the LES performs very well in predicting the secondary flow vector as might be expected.

6.6 Conclusions

A general review of the turbulent flow through non-circular ducts have been presented in which special attention has been given to the mechanisms of the generation of secondary flows normal to the axial flow. It is evident from the experimental results that, the magnitude of the secondary flow is small compared with that of the mean velocity; however in certain applications the effect is quite significant. Moreover, the mechanics of the generation of these secondary vortices remains somewhat obscure,

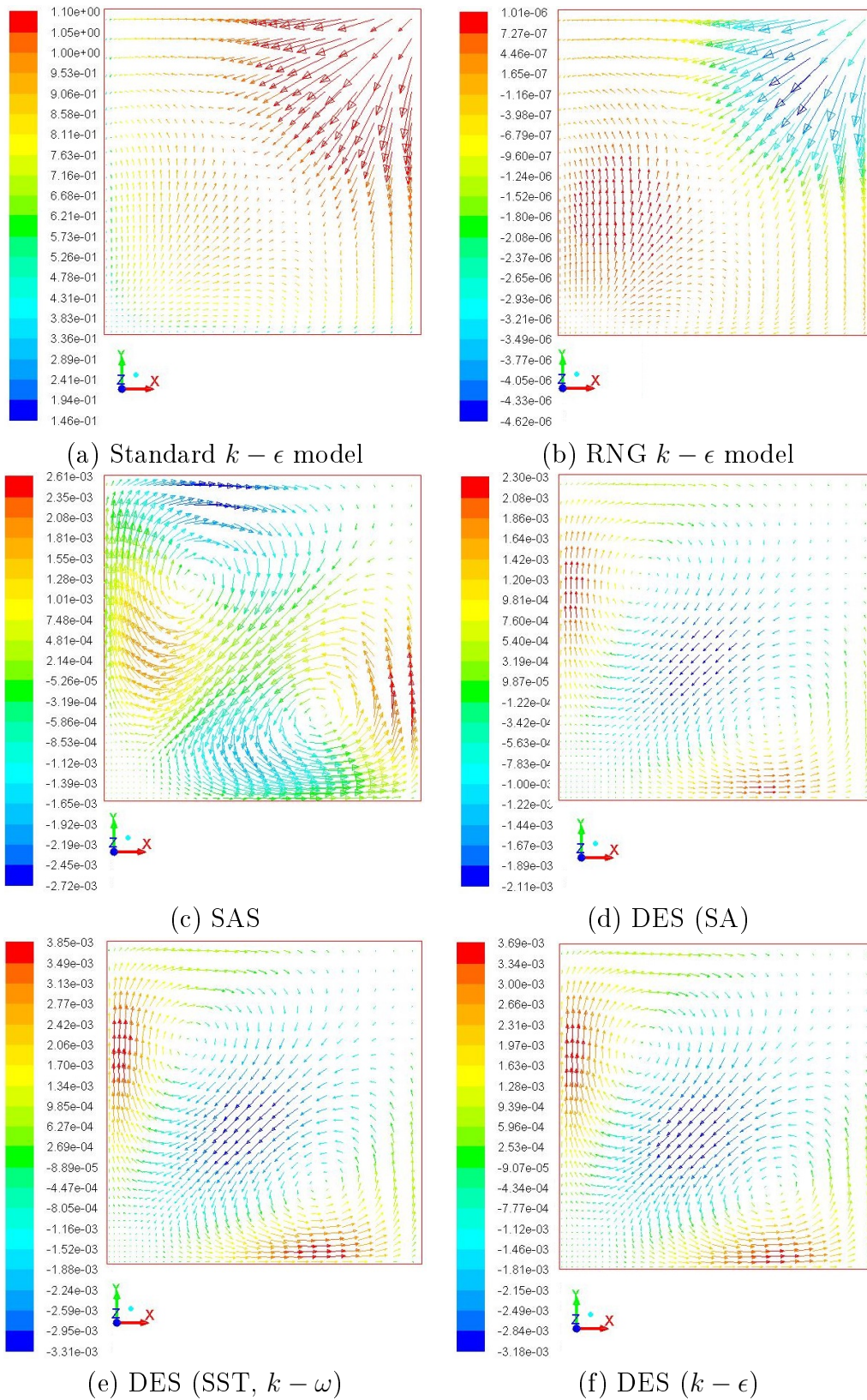


Figure 6.14: Simulation results of contour of secondary velocity at outlet of a rectangular duct in turbulent flow using various turbulent models

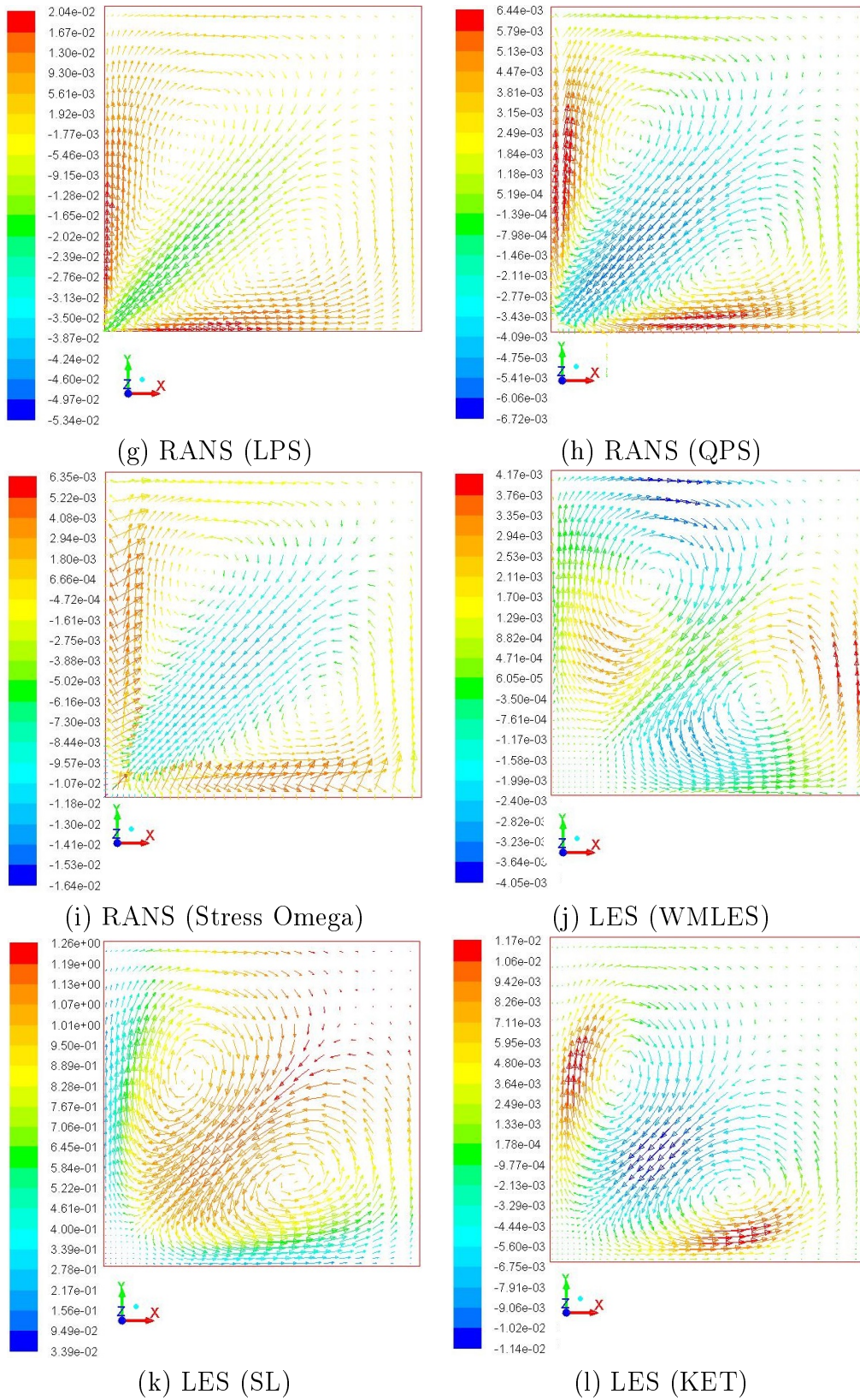


Figure 6.15: Simulation results of contour of secondary velocity at outlet of a rectangular duct in turbulent flow using various turbulent models,

particularly if one has only experimental data as a guide.. Therefore many mathematical models have been developed to describe and simulate the flow phenomena. There has been a long search to identify an appropriate model to simulate the turbulence driven secondary flow in non-circular ducts. As a consequence a wide range of models has been proposed and tested against experimental results to validate those models. The two equation model with a non-linear description of eddy viscosity model has gained increasing acceptance because of its relative simplicity and greater accuracy in determining the Reynolds stress components. Nevertheless, better approximations have been developed in last decade using high performance computing facilities. Methods such as large eddy simulation (LES) and Direct Numerical Simulation (DNS) illuminate details of the phenomena that occur in turbulent flows through non-circular ducts. Despite of the flows being limited to low Reynolds numbers due to high computational requirements, these results have laid the ground work for future research.

Furthermore, an investigation of the flow patterns of the primary and secondary flow velocity have been conducted as a part of this research project. Commercial software package FLUENT has been used to perform these simulation of turbulent flow through rectangular ducts using a number of turbulent models available in the package. The primary velocity contours, secondary flow velocity contours and secondary flow vectors obtained from the simulation using various turbulence models were compared with the experimental and DNS results. The outcome was as expected, linear turbulence models such as standard k epsilon model and RNG k-epsilon model fail completely to predict any secondary flow where as other non linear models such as Scale Adaptive Simulation (SAS), Detached Eddy Simulation (DES) with various RANS models, Reynolds Stress Models (RSM) with different models of the Reynolds stress term and Large Eddy Simulation (LES) with various sub-grid scale models

predict the flow pattern, secondary flow magnitude very well. Among these results, LES models appear to exhibit a superiority over the other turbulence models we have examined.

Chapter 7

Conclusions and Recommendations for Further Work

7.1 Summary of the Work

The spreading of a passive scalar in laminar or turbulent flows have many implications in natural as well as industrial systems. In this thesis, numerical techniques have been developed and implemented that simulate the rate of dispersion of a passive tracer in laminar and turbulent flows through circular and non-circular ducts. A major concern in numerical simulation is to avoid false diffusion in the solution. In this work, it has been addressed by developing higher order finite difference schemes in two and three-dimensional coordinate system.

A new scheme based on the QUICKEST scheme for one-dimension has been developed to simulate dispersion in laminar and turbulent flows through circular pipes in an axi-symmetric geometry. The performance of the new scheme in suppressing artificial diffusion has been demonstrated by analyzing the error propagation behavior in the

Fourier domain using the modified equation approach and von-Neumann stability analysis. It has been found that the numerical simulation using the scheme developed in this work is capable of predicting the spreading of solute in convection dominated flows as well as diffusion dominated flows. Moreover, the effective dispersion coefficient has been calculated from the local concentration distribution using method of moments and it is found satisfactory.

Furthermore, the modified QUICKEST scheme has been extended to simulate dispersion in rectangular ducts in three-dimensional coordinate systems. Such a scheme is reported for the first time, and the stability condition and error behavior have been analyzed both qualitatively and quantitatively. By estimating the amplification factor of the error terms using von-Neumann analysis, it has been found that the error will diminish if the scheme satisfies the CFL condition, i.e. Courant number less than 0.5. The spreading pattern of the solute in the dispersion process has been reported high and low Peclet numbers at early and later times after the solute is injected. Moreover it is found that the amount of dispersion is greater in square duct than in a circular duct.

Following the interest in developing high order finite difference schemes, a combined compact difference scheme has been developed to solve the convection diffusion equation in two and three dimension. This sixth order spatially accurate scheme extended to solve the solute dispersion process in three-dimensional rectangular coordinate system. The stability criteria and performance of the new scheme to eliminate artificial diffusion from the solution has been demonstrated using Fourier analysis. Furthermore numerical experiments performed to demonstrate the accuracy of the scheme developed in this work.

Dispersion in turbulent flow through circular pipes is highly dependent on the ve-

locity flow profile. Using the scheme developed for dispersion in laminar flow through circular pipes in conjunction with the velocity and turbulent viscosity simulated separately in FLUENT, the spreading of solute in turbulent flow through circular pipes has been calculated. The dispersion coefficients obtained from the simulated results have been found in nice agreement with some of the analytical solutions.

In rectangular ducts, dispersion is expected to be highly affected by the presence of the secondary flows when the fluid motion is turbulent. Therefore, a detailed investigation has been reported regarding the origin of the turbulent secondary flow in non-circular ducts. Moreover, the performance of various turbulence models in capturing the secondary flow has been evaluated by performing simulations for turbulent flow through rectangular duct. From a comparison study of velocity contour and secondary velocity vector with the experimental and direct numerical simulation data, it was found that the linear eddy viscosity models fail to capture the secondary flow whereas it is predicted by large eddy simulation and the Reynolds stress model.

7.2 Major Contributions

Numerical techniques have been used in physics-based modeling for over half a century. In the dispersion of a passive scalar in laminar and turbulent flow through circular and non-circular ducts, literature on numerical simulation techniques is quite exiguous. Very few works can be found for simulating dispersion in laminar flow through circular ducts. Even these works suffer the drawbacks of inclusion of artificial diffusion in the solution due to use of lower order difference scheme in the discretization process. In this work, we overcome these issues and we have presented two unique difference schemes for the numerical simulation of the solute dispersion process.

Furthermore, to the author's knowledge, no study on the simulation of dispersion in three-dimensional coordinates has been reported to date. We have developed the schemes and extended to three-dimensional coordinates for this purpose which opens up many avenues for utilizing these schemes in future research.

Finally a critical analysis of the turbulent flow through non-circular ducts has been reported by reviewing experimental and numerical works. Attention primarily focused on the origin of turbulent secondary flows which is believed to have significant influence in the dispersion process in flow through non-circular geometries. A comparison study of the simulation of turbulent secondary flow using different turbulence models has been reported for the first time which suggests new avenues for simulating turbulent flow through non-circular ducts.

In brief, the major contributions of this work are-

1. Development and implementation of third order modified QUICKEST scheme for simulation of dispersion in laminar and turbulent flow through circular pipes.
2. For the first time, development of a numerical scheme with third order accuracy for simulation of dispersion in laminar flow through rectangular geometry in three-dimensions.
3. Development of a novel compact combined difference scheme with sixth order accuracy to solve the convection diffusion equation in two and three-dimensions.
4. Implementation of the developed scheme to simulate solute dispersion in three-dimensional Cartesian coordinate system.
5. Reporting a critical review in the origin of turbulent secondary flow along with a comparison study for various turbulence models in simulating turbulent flow through rectangular duct

7.3 Scope, Limitations and Recommendations

The achievements of this thesis have the potential to impact on the field of computational fluid dynamics. Particularly, the sixth order accurate combined compact difference method for solving convection diffusion equation developed in this work may be applied to solve many practical problems. This research has laid the ground work towards the solution of many engineering problems where the outcome will be reliable and accurate. One such example could be combined heat and mass transfer through hygroscopic porous media, or more specially the estimation of heat and mass transfer in food grain storage system. This is just an single example whereas there could be many more cases where the outcome of this thesis can be utilized.

Although the schemes developed in this work are capable of minimizing artificial diffusion from the solution, they require additional computational effort. Particularly the CCD method developed to solve the convection diffusion equation and the solute dispersion in laminar and turbulent flow through rectangular ducts requires a considerable amount of computational power because of simultaneous solving of a large number of equations. An alternative approach, based on the original work proposed by G I Taylor has been described in appendix G. The methodology is derived to calculate the dispersion coefficient in turbulent flow through rectangular duct using the concept the shear velocity profile which can be utilized for both laminar and turbulent cases. Although this appears to be most promising, it is left for future work.

References

- Ahmed, S. and E. Brundrett (1971). Turbulent flow in non-circular ducts. part 1: Mean flow properties in the developing region of a square duct. *International Journal of Heat and Mass Transfer* 14(3), 365–375.
- Ajdari, A., N. Bontoux, and H. A. Stone (2006, Jan). Hydrodynamic dispersion in shallow microchannels: the effect of cross-sectional shape. *Analytical chemistry* 78(2), 387–92.
- Aly, A., A. Trupp, and A. Gerrard (1978). Measurements and prediction of fully developed turbulent flow in an equilateral triangular duct. *Journal of Fluid Mechanics* 85(01), 57–83.
- Ananthakrishnan, V., W. Gill, and A. J. Barduhn (1965). Laminar dispersion in capillaries: Part i. mathematical analysis. *AIChE Journal* 11(6), 1063–1072.
- Andersson, B. and T. Berglin (1981). Dispersion in laminar flow through a circular tube. In *Proceedings of the Royal Society of London A: Mathematical, Physical and Engineering Sciences*, Volume 377, pp. 251–268. The Royal Society.
- Apsley, D. D. and M. A. Leschziner (1998). A new low-reynolds-number nonlinear two-equation turbulence model for complex flows. *International journal of heat and fluid flow* 19(3), 209–222.

- Argyropoulos, C. and N. Markatos (2015). Recent advances on the numerical modelling of turbulent flows. *Applied Mathematical Modelling* 39(2), 693–732.
- Aris, R. (1956). On the dispersion of a solute in a fluid flowing through a tube. In *Proceedings of the Royal Society of London A: Mathematical, Physical and Engineering Sciences*, Volume 235, pp. 67–77. The Royal Society.
- Bailey, H. and W. Gogarty (1962). Numerical and experimental results on the dispersion of a solute in a fluid in laminar flow through a tube. In *Proceedings of the Royal Society of London A: Mathematical, Physical and Engineering Sciences*, Volume 269, pp. 352–367. The Royal Society.
- Beam, R. M. and R. F. Warming (1976). An implicit finite-difference algorithm for hyperbolic systems in conservation-law form. *Journal of computational physics* 22(1), 87–110.
- Berselli, L., T. Iliescu, and W. J. Layton (2005). *Mathematics of large eddy simulation of turbulent flows*. Springer Science & Business Media.
- Bird, R. B., W. E. Stewart, and E. N. Lightfoot (1960). Transport phenomena. 1960. *Madison, USA*.
- Boris, J. P. and D. L. Book (1973). Flux-corrected transport. i. shasta, a fluid transport algorithm that works. *Journal of computational physics* 11(1), 38–69.
- Bournia, A., J. Coull, and G. Houghton (1961). Dispersion of gases in laminar flow through a circular tube. In *Proceedings of the Royal Society of London A: Mathematical, Physical and Engineering Sciences*, Volume 261, pp. 227–236. The Royal Society.

- Bradshaw, P. (1987). Turbulent secondary flows. *Annual review of fluid mechanics* 19(1), 53–74.
- Breuer, M. and W. Rodi (1994). Large-eddy simulation of turbulent flow through a straight square duct and a 180 bend. In *Direct and large-eddy simulation I*, pp. 273–285.
- Brundrett, E. and W. Baines (1964). The production and diffusion of vorticity in duct flow. *Journal of Fluid Mechanics* 19(03), 375–394.
- Buleev, N., J. Cornish, and J. Woodrow (1963). *Theoretical model of the mechanism of turbulent exchange in fluid flows*. Atomic Energy Research Establishment.
- Carajilescov, P. and N. Todreas (1976). Experimental and analytical study of axial turbulent flows in an interior subchannel of a bare rod bundle. *Journal of Heat Transfer* 98(2), 262–268.
- Chatwin, P. and C. Allen (1985). Mathematical models of dispersion in rivers and estuaries. *Annual Review of Fluid Mechanics* 17(1), 119–149.
- Chatwin, P. and P. J. Sullivan (1982). The effect of aspect ratio on longitudinal diffusivity in rectangular channels. *Journal of Fluid Mechanics* 120, 347–358.
- Cheesewright, R., G. McGrath, and D. Petty (1990). Lda measurements of turbulent flow in a duct of square cross section at low reynolds number. *Aeronautical Engineering Dept. Rep. ER 1011*.
- Chikwendu, S. (1986). Calculation of longitudinal shear dispersivity using an n-zone model as n $\rightarrow \infty$. *Journal of Fluid Mechanics* 167, 19–30.

- Chu, P. C. and C. Fan (1998). A three-point combined compact difference scheme. *Journal of Computational Physics* 140(2), 370–399.
- Chung, T. (2010). *Computational fluid dynamics*. Cambridge university press.
- Cousteix, J. and D. Arnal (1982). Turbulent flow in unbounded streamwise corners. *ONERA, TP no. 1982-41, 1982. 27 p. Service Technique des Programmes Aeronautiques*.
- Craft, T. and B. Launder (1996). A reynolds stress closure designed for complex geometries. *International Journal of Heat and Fluid Flow* 17(3), 245–254.
- Daskopoulos, P. and A. Lenhoff (1988). Dispersion coefficient for laminar flow in curved tubes. *AIChE journal* 34(12), 2052–2058.
- Davidson, J., D. Farquharson, J. Picken, and D. Taylor (1955). Gas mixing in long pipelines. *Chemical Engineering Science* 4(5), 201–205.
- De Gance, A. and L. Johns (1978). On the dispersion coefficients for poiseuille flow in a circular cylinder. *Applied Scientific Research* 34(2-3), 227–258.
- Demuren, A. (1991). Calculation of turbulence-driven secondary motion in ducts with arbitrary cross section. *AIAA journal* 29(4), 531–537.
- Demuren, A. and W. Rodi (1984). Calculation of turbulence-driven secondary motion in non-circular ducts. *Journal of Fluid Mechanics* 140, 189–222.
- Demuren, A. and W. Rodi (1987). Three-dimensional calculation of turbulent duct flow with non-uniform inlet conditions. *Computers & fluids* 15(1), 47–57.

- Doshi, M. R., P. M. Daiya, and W. N. Gill (1978). Three dimensional laminar dispersion in open and closed rectangular conduits. *Chemical Engineering Science* 33(7), 795–804.
- Durbin, P. A. (1991). Near-wall turbulence closure modeling without "damping functions". *Theoretical and Computational Fluid Dynamics* 3(1), 1–13.
- Durst, F., J. Jovanovic, and J. Sender (1995). Lda measurements in the near-wall region of a turbulent pipe flow. *Journal of Fluid Mechanics* 295, 305–335.
- Dutta, D., A. Ramachandran, and D. T. Leighton Jr (2006). Effect of channel geometry on solute dispersion in pressure-driven microfluidic systems. *Microfluidics and Nanofluidics* 2(4), 275–290.
- Eichelbrenner, E. and N. Toan (1969). Concerning the secondary velocities in the turbulent boundary layer in the interior of a dihedron(secondary velocities analysis in turbulent boundary layer in dihedron interior based on turbulence anisotropy and effects on wall pressure gradient).
- Einstein, H. and H. Li (1958). Secondary currents in straight channels. *Eos, Transactions American Geophysical Union* 39(6), 1085–1088.
- Ekambara, K. and J. Joshi (2003). Axial mixing in pipe flows: turbulent and transition regions. *Chemical Engineering Science* 58(12), 2715–2724.
- Ekambara, K. and J. Joshi (2004). Axial mixing in laminar pipe flows. *Chemical Engineering Science* 59(18), 3929–3944.
- Emery, A., P. Neighbors, and F. Gessner (1979). Computational procedure for developing turbulent flow and heat transfer in a square duct. *Numerical Heat Transfer, Part A: Applications* 2(4), 399–416.

- Evans, E. and C. Kenney (1965). Gaseous dispersion in laminar flow through a circular tube. In *Proceedings of the Royal Society of London A: Mathematical, Physical and Engineering Sciences*, Volume 284, pp. 540–550. The Royal Society.
- Fischer, H. B. (1973). Longitudinal dispersion and turbulent mixing in open-channel flow. *Annual Review of Fluid Mechanics* 5(1), 59–78.
- Fischer, H. B., J. E. List, C. R. Koh, J. Imberger, and N. H. Brooks (2013). *Mixing in inland and coastal waters*. Elsevier.
- Flint, L. and P. Eisenklam (1969). Longitudinal gas dispersion in transitional and turbulent flow through a straight tube. *The Canadian Journal of Chemical Engineering* 47(2), 101–106.
- Fujita, H., M. Hirota, H. Yokosawa, M. Hasegawa, and I. Gotoh (1990). Fully developed turbulent flows through rectangular ducts with one roughened wall. *JSME international journal. Ser. 2, Fluids engineering, heat transfer, power, combustion, thermophysical properties* 33(4), 692–701.
- Fujita, H., H. Yokosawa, and M. Hirota (1989). Secondary flow of the second kind in rectangular ducts with one rough wall. *Experimental Thermal and Fluid Science* 2(1), 72–80.
- Gatski, T. and C. Rumsey (2002). Linear and nonlinear eddy viscosity models. *Closure strategies for turbulent and transitional flows*, 9–46.
- Gatski, T. and C. G. Speziale (1993). On explicit algebraic stress models for complex turbulent flows. *Journal of fluid Mechanics* 254, 59–78.
- Gavrilakis, S. (1992). Numerical simulation of low-reynolds-number turbulent flow through a straight square duct. *Journal of Fluid Mechanics* 244, 101–129.

- Ge, Y., Z. F. Tian, and J. Zhang (2013). An exponential high-order compact advection method for 3d unsteady convection–diffusion problems. *Numerical Methods for Partial Differential Equations* 29(1), 186–205.
- Gerard, R. (1978). Secondary flow in noncircular conduits. *Journal of the Hydraulics Division* 104(5), 755–773.
- Germano, M., U. Piomelli, P. Moin, and W. H. Cabot (1991). A dynamic subgrid-scale eddy viscosity model. *Physics of Fluids A: Fluid Dynamics (1989-1993)* 3(7), 1760–1765.
- Gessner, F. (1973). The origin of secondary flow in turbulent flow along a corner. *Journal of Fluid Mechanics* 58(01), 1–25.
- Gessner, F. and A. Emery (1976). A reynolds stress model for turbulent corner flows - part i: Development of the model. *Journal of Fluids Engineering* 98(2), 261–268.
- Gessner, F. and A. Emery (1977). A length-scale model for developing turbulent flow in a rectangular duct. *Journal of Fluids Engineering* 99(2), 347–356.
- Gessner, F. and A. Emery (1981). The numerical prediction of developing turbulent flow in rectangular ducts. *Journal of Fluids Engineering* 103(3), 445–453.
- Gessner, F. and J. Jones (1965). On some aspects of fully-developed turbulent flow in rectangular channels. *Journal of fluid mechanics* 23(04), 689–713.
- Gilbert, A. E. and N. C. Jorgenson (1960). Small bowel obstruction due to hemorrhage secondary to anticoagulant therapy. *The American Journal of Surgery* 99(6), 945–948.

- Gill, W. and R. Sankarasubramanian (1970). Exact analysis of unsteady convective diffusion. In *Proceedings of the Royal Society of London A: Mathematical, Physical and Engineering Sciences*, Volume 316, pp. 341–350. The Royal Society.
- Gill, W. and R. Sankarasubramanian (1971). Dispersion of a non-uniform slug in time-dependent flow. In *Proceedings of the Royal Society of London A: Mathematical, Physical and Engineering Sciences*, Volume 322, pp. 101–117. The Royal Society.
- Gill, W. N. and V. Ananthakrishnan (1967). Laminar dispersion in capillaries: Part iv. the slug stimulus. *AIChE Journal* 13(4), 801–807.
- Golay, M. J. and J. G. Atwood (1979). Early phases of the dispersion of a sample injected in poiseuille flow. *Journal of Chromatography A* 186, 353–370.
- Gosman, A. and C. Rapley (1978). A prediction method for fully-developed flow through non-circular passages. In *Numerical Methods in Laminar and Turbulent Flow*, Volume 1, pp. 271–285.
- Gosman, A. and C. Rapley (1980). Fully-developed flow in passages of arbitrary cross-section. *Recent Advances in Numerical Methods in Fluids* 1, 335–399.
- Gupta, M. M., R. P. Manohar, and J. W. Stephenson (1984). A single cell high order scheme for the convection-diffusion equation with variable coefficients. *International Journal for Numerical Methods in Fluids* 4(7), 641–651.
- Hanjalic, K. and B. Launder (1972). A reynolds stress model of turbulence and its application to thin shear flows. *Journal of fluid Mechanics* 52(04), 609–638.
- Hart, J., I. Guymer, A. Jones, and V. Stovin (2013). Longitudinal dispersion coefficients within turbulent and transitional pipe flow. In *Experimental and Computational Solutions of Hydraulic Problems*, pp. 133–145. Springer.

- Hinze, J. O. (1973). Experimental investigation on secondary currents in the turbulent flow through a straight conduit. *Applied Scientific Research* 28(1), 453–465.
- Hirsch, C. (2007). *Numerical Computation of Internal and External Flows: The Fundamentals of Computational Fluid Dynamics: The Fundamentals of Computational Fluid Dynamics*, Volume 1. Butterworth-Heinemann.
- Hoagland, L. C. (1960). Fully developed turbulent flow in straight rectangular ducts - secondary flow, its cause and effect on the primary flow (thesis). technical report no. 2. Technical report, Massachusetts Inst. of Tech., Cambridge.
- Holmes, D. and J. Vermeulen (1968). Velocity profiles in ducts with rectangular cross sections. *Chemical Engineering Science* 23(7), 717–722.
- Huser, A. and S. Biringen (1993). Direct numerical simulation of turbulent flow in a square duct. *Journal of Fluid Mechanics* 257, 65–95.
- Huser, A., S. Biringen, and F. F. Hatay (1994). Direct simulation of turbulent flow in a square duct: Reynolds-stress budgets. *Physics of Fluids (1994-present)* 6(9), 3144–3152.
- Johnson, R. W. (2016). *Handbook of fluid dynamics*. Crc Press.
- Joung, Y., S.-U. Choi, and J.-I. Choi (2007). Direct numerical simulation of turbulent flow in a square duct: analysis of secondary flows. *Journal of engineering mechanics* 133(2), 213–221.
- Kacker, S. (1973). Discussion of " prediction of flow and heat transfer in ducts of square cross-section,". *Proceedings of the Institution of Mechanical Engineers* 187, D147–D148.

- Kajishima, T. and Y. Miyake (1992). A discussion on eddy viscosity models on the basis of the large eddy simulation of turbulent flow in a square duct. *Computers & fluids* 21(2), 151–161.
- Karaa, S. (2006). A high-order compact adi method for solving three-dimensional unsteady convection-diffusion problems. *Numerical Methods for Partial Differential Equations* 22(4), 983–993.
- Karaa, S. (2010). A hybrid padé adi scheme of higher-order for convection–diffusion problems. *International Journal for Numerical Methods in Fluids* 64(5), 532–548.
- Karaa, S. and J. Zhang (2004). High order adi method for solving unsteady convection–diffusion problems. *Journal of Computational Physics* 198(1), 1–9.
- Korenaga, T., F. Shen, and T. Takahashi (1989). An experimental study of the dispersion in laminar tube flow. *AIChE journal* 35(8), 1395–1398.
- Launder, B., G. J. Reece, and W. Rodi (1975). Progress in the development of a reynolds-stress turbulence closure. *Journal of fluid mechanics* 68(03), 537–566.
- Launder, B. and B. Sharma (1974). Application of the energy-dissipation model of turbulence to the calculation of flow near a spinning disc. *Letters in heat and mass transfer* 1(2), 131–137.
- Launder, B. and W. Ying (1972). Secondary flows in ducts of square cross-section. *Journal of Fluid Mechanics* 54(02), 289–295.
- Leighton, D. T. and D. Dutta (2005). Hydrodynamic dispersion in microfluidic geometries: Causes and remedies (plenary). In *ASME 3rd International Conference on Microchannels and Minichannels*, pp. 153–161. American Society of Mechanical Engineers.

- Leonard, A. (1975). Energy cascade in large-eddy simulations of turbulent fluid flows. *Advances in geophysics* 18, 237–248.
- Leonard, B. P. (1979). A stable and accurate convective modelling procedure based on quadratic upstream interpolation. *Computer methods in applied mechanics and engineering* 19(1), 59–98.
- Leutheusser, H. J. (1963). Turbulent flow in rectangular ducts. *Journal of the Hydraulics Division* 89(3), 1–19.
- Levenspiel, O. (2011). *Tracer Technology: Modeling the Flow of Fluids*, Volume 96. Springer Science & Business Media.
- Liao, W. (2012). A compact high-order finite difference method for unsteady convection-diffusion equation. *International Journal for Computational Methods in Engineering Science and Mechanics* 13(3), 135–145.
- Liao, W., J. Zhu, and A. Q. Khaliq (2006). A fourth-order compact algorithm for nonlinear reaction-diffusion equations with neumann boundary conditions. *Numerical Methods for Partial Differential Equations* 22(3), 600–616.
- Lien, F. and P. Durbin (1996). Non-linear k-v2 modelling with application to high-lift. *Proceedings of the Summer Program Centre for Turbulence Research. Stanford University*, 5–22.
- Lighthill, M. (1966). Initial development of diffusion in poiseuille flow. *IMA Journal of Applied Mathematics* 2(1), 97–108.
- Lund, E. G. (1977). *Mean flow and turbulence characteristics in the near corner region of a square duct*. Ph. D. thesis.

- Madabhushi, R. K. and S. Vanka (1991). Large eddy simulation of turbulence-driven secondary flow in a square duct. *Physics of Fluids A: Fluid Dynamics (1989-1993)* 3(11), 2734–2745.
- Maeda, N., M. Hirota, and H. Fujita (2005). Turbulent flow in a rectangular duct with a smooth-to-rough step change in surface roughness. *Energy* 30(2), 129–148.
- Mansour, A. R. (1989). Dispersion of solute in laminar flow through a circular tube. *Separation Science and Technology* 24(15), 1437–1442.
- Mauri, R. and S. Haber (1991). Time-dependent dispersion of small particles in rectangular conduits. *SIAM Journal on Applied Mathematics* 51(6), 1538–1555.
- Mayock, K., J. Tarbell, and J. Duda (1980). Numerical simulation of solute dispersion in laminar tube flow. *Separation Science and Technology* 15(6), 1285–1296.
- Melling, A. and J. Whitelaw (1976). Turbulent flow in a rectangular duct. *Journal of Fluid Mechanics* 78(02), 289–315.
- Métais, O. and M. Lesieur (1992). Spectral large-eddy simulation of isotropic and stably stratified turbulence. *Journal of Fluid Mechanics* 239, 157–194.
- Miyake, Y. and T. Kajishima (1991). Explanation of the origin of the secondary flow in a straight square duct of the basis of les. In *Separated Flows and Jets*, pp. 149–152. Springer.
- Mompean, G., S. Gavrilakis, L. Machiels, and M. Deville (1996). On predicting the turbulence-induced secondary flows using nonlinear k-epsilon models. *Physics of Fluids (1994-present)* 8(7), 1856–1868.

- Myong, H. K. (1991). Numerical investigation of fully developed turbulent fluid flow and heat transfer in a square duct. *International journal of heat and fluid flow* 12(4), 344–352.
- Myong, H. K. and N. Kasagi (1990). A new approach to the improvement of k-epsilon turbulence model for wall-bounded shear flows. *JSME international journal. Ser. 2, Fluids engineering, heat transfer, power, combustion, thermophysical properties* 33(1), 63–72.
- Naimi, M. and F. Gessner (1995). A calculation method for developing turbulent flow in rectangular ducts of arbitrary aspect ratio. *Journal of fluids engineering* 117(2), 249–258.
- Nakayama, A. (1981). Three dimensional flow within conduits of arbitrary geometrical configurations.
- Nakayama, A. and W. Chow (1986). Turbulent flows within straight ducts. In *Encyclopedia of Fluid Mechanics. Volume 1*, Volume 1, pp. 638–674.
- Nakayama, A., W. Chow, and D. Sharma (1983). Calculation of fully developed turbulent flows in ducts of arbitrary cross-section. *Journal of Fluid Mechanics* 128, 199–217.
- Nakayama, A., W. Chow, and D. Sharma (1984). Three-dimensional developing turbulent flow in a square duct. *Bulletin of JSME* 27(229), 1438–1445.
- Naot, D. and W. Rodi (1982). Calculation of secondary currents in channel flow. *Journal of the Hydraulics Division* 108(8), 948–968.
- Naot, D., A. Savit, and M. Wolfshtin (1974). Numerical calculation of reynolds

- stresses in a square duct with secondary flow. *Wärme-und Stoffübertragung* 7(3), 151–161.
- Naot, D., A. Shavit, and M. Wolfshtein (1973). Two-point correlation model and the redistribution of reynolds stresses. *Physics of Fluids (1958-1988)* 16(6), 738–743.
- Neti, S. and R. Eichhorn (1979). Computations of developing turbulent flow in a square duct. In *Turbulent Boundary Layers: Forced, Incompressible, Non-Reacting*, pp. 179–186.
- Niederschulte, M., R. Adrian, and T. Hanratty (1990). Measurements of turbulent flow in a channel at low reynolds numbers. *Experiments in Fluids* 9(4), 222–230.
- Nikuradse, J. (1926). *Untersuchung über die Geschwindigkeitsverteilung in turbulenten Strömungen*. Vdi-verlag.
- Nisizima, S. (1990). A numerical study of turbulent square-duct flow using an anisotropic k-epsilon model. *Theoretical and Computational Fluid Dynamics* 2(1), 61–71.
- Nisizima, S. and A. Yoshizawa (1987). Turbulent channel and couette flows using an anisotropic k-epsilon model. *AIAA journal* 25(3), 414–420.
- Noye, B. and H. Tan (1989). Finite difference methods for solving the two-dimensional advection–diffusion equation. *International Journal for Numerical Methods in Fluids* 9(1), 75–98.
- Owen, W. (1954). Laminar to turbulent flow in a wide open channel. *Transactions of the American Society of Civil Engineers* 119(1), 1157–1164.

- Paine, M., R. Carbonell, and S. Whitaker (1983). Dispersion in pulsed systems heterogenous reaction and reversible adsorption in capillary tubes. *Chemical Engineering Science* 38(11), 1781–1793.
- Parks, M. L. and L. A. Romero (2007). Taylor–aris dispersion in high aspect ratio columns of nearly rectangular cross section. *Mathematical and computer modelling* 46(5), 699–717.
- Patankar, S. (1980). *Numerical heat transfer and fluid flow*. CRC press.
- Pattison, M. J., K. N. Premnath, and S. Banerjee (2009). Computation of turbulent flow and secondary motions in a square duct using a forced generalized lattice boltzmann equation. *Physical Review E* 79(2), 026704.
- Peaceman, D. W. and H. H. Rachford, Jr (1955). The numerical solution of parabolic and elliptic differential equations. *Journal of the Society for Industrial and Applied Mathematics* 3(1), 28–41.
- Pecnik, R. and G. Iaccarino (2007). Predictions of turbulent secondary flows using the v^2 -f model. *Center for Turbulence Research, Annual Research Briefs, Stanford University*, 333–343.
- Perkins, H. (1970). The formation of streamwise vorticity in turbulent flow. *Journal of Fluid Mechanics* 44(04), 721–740.
- Phillips, C. and S. Kaye (1997). The initial transient of concentration during the development of taylor dispersion. In *Proceedings of the Royal Society of London A: Mathematical, Physical and Engineering Sciences*, Volume 453, pp. 2669–2688. The Royal Society.

- Pinelli, A., M. Uhlmann, A. Sekimoto, and G. Kawahara (2010). Reynolds number dependence of mean flow structure in square duct turbulence. *Journal of Fluid Mechanics* 644, 107–122.
- Piomelli, U., J. FERZIGER, and P. Moin (1988). Model consistency in large eddy simulation of turbulent channel flows. *Physics of Fluids* 31(7), 1884.
- Po, J. K.-o. (1975). *Developing turbulent flow in the entrance region of a square duct*.
- Pope, S. (1975). A more general effective-viscosity hypothesis. *Journal of Fluid Mechanics* 72(02), 331–340.
- Pope, S. B. (2001). *Turbulent flows*.
- Prandtl, L. (1926). Über die ausgebildete turbulenz. In *Kongress Techn. Mech., Zürich*, pp. 62–75.
- Ramachandra, V. (1979). The numerical prediction of flow and heat transfer in rod-bundle geometries.
- Rapley, C. and A. Gosman (1984). The prediction of turbulent flow and heat transfer in a narrow isosceles triangular duct. *International journal of heat and mass transfer* 27(2), 253–262.
- Reece, G. J. (1977). *A generalized Reynolds-stress model of turbulence*. University of London.
- Reejhsinghani, N. S., W. N. Gill, and A. J. Barduhn (1966). Laminar dispersion in capillaries: Part iii. experiments in horizontal tubes including observations on natural convection effects. *AIChE Journal* 12(5), 916–921.

- Reif, B. A. P. and M. Mortensen (2011). A nonlinear eddy-viscosity model for near-wall turbulence. In *Progress in Wall Turbulence: Understanding and Modeling*, pp. 269–276. Springer.
- Reif, B. A. P., M. Mortensen, and C. A. Langer (2009). Towards sensitizing the nonlinear v^2 -f model to turbulence structures. *Flow, Turbulence and Combustion* 83(2), 185–203.
- Reif, B. P. and H. Andersson (2002). Prediction of turbulence-generated secondary mean flow in a square duct. *Flow, turbulence and combustion* 68(1), 41–61.
- Reynolds, O. (1883). An experimental investigation of the circumstances which determine whether the motion of water shall be direct or sinuous, and of the law of resistance in parallel channels. *Proceedings of the royal society of London* 35(224-226), 84–99.
- Roache, P. J. (1972). On artificial viscosity. *Journal of Computational Physics* 10(2), 169–184.
- Rokni, M. and T. B. Gatski (2001). Predicting turbulent convective heat transfer in fully developed duct flows. *International journal of heat and fluid flow* 22(4), 381–392.
- Rokni, M., C.-O. Olsson, and B. Sundén (1998). Numerical and experimental investigation of turbulent flow in a rectangular duct. *International journal for numerical methods in fluids* 28(2), 225–242.
- Romero-Gomez, P. and C. Y. Choi (2011). Axial dispersion coefficients in laminar flows of water-distribution systems. *Journal of Hydraulic Engineering* 137(11), 1500–1508.

- Rubinstein, R. and J. M. Barton (1990). Nonlinear reynolds stress models and the renormalization group. *Physics of Fluids A: Fluid Dynamics (1989-1993)* 2(8), 1472–1476.
- Schumann, U. (1975). Subgrid scale model for finite difference simulations of turbulent flows in plane channels and annuli. *Journal of computational physics* 18(4), 376–404.
- Seibold, B. (2008). A compact and fast matlab code solving the incompressible navier-stokes equations on rectangular domains mit18086 navierstokes. m. *Massachusetts Institute of Technology*.
- Sekimoto, A., G. Kawahara, K. Sekiyama, M. Uhlmann, and A. Pinelli (2011). Turbulence-and buoyancy-driven secondary flow in a horizontal square duct heated from below. *Physics of Fluids (1994-present)* 23(7), 075103.
- Shankar, A. and A. Lenhoff (1989). Dispersion in laminar flow in short tubes. *AICHE journal* 35(12), 2048–2052.
- Shih, T.-H., J. Zhu, and J. L. Lumley (1993). A realizable reynolds stress algebraic equation model.
- Shir, C. (1973). A preliminary numerical study of atmospheric turbulent flows in the idealized planetary boundary layer. *Journal of the Atmospheric Sciences* 30(7), 1327–1339.
- Sittel Jr, C., W. Threadgill, and K. Schnelle Jr (1968). Longitudinal dispersion for turbulent flow in pipes. *Industrial & Engineering Chemistry Fundamentals* 7(1), 39–43.

- Smagorinsky, J. (1963). General circulation experiments with the primitive equations: I. the basic experiment*. *Monthly weather review* 91(3), 99–164.
- Speziale, C. G. (1980). Closure relations for the pressure-strain correlation of turbulence. *Physics of Fluids (1958-1988)* 23(3), 459–463.
- Speziale, C. G. (1982). On turbulent secondary flows in pipes of noncircular cross-section. *International Journal of Engineering Science* 20(7), 863–872.
- Speziale, C. G. (1987). On nonlinear kl and k-epsilon models of turbulence. *Journal of Fluid Mechanics* 178, 459–475.
- Speziale, C. G. (1990). Analytical methods for the development of reynolds stress closures in turbulence. Technical report, DTIC Document.
- Spiga, M. and G. Morino (1994). A symmetric solution for velocity profile in laminar flow through rectangular ducts. *International communications in heat and mass transfer* 21(4), 469–475.
- Spotz, W. and G. Carey (2001). Extension of high-order compact schemes to time-dependent problems. *Numerical Methods for Partial Differential Equations* 17(6), 657–672.
- Straub, L. G., E. Silberman, and H. C. Nelson (1958). Open-channel flow at small reynolds numbers. *Transactions of the American Society of Civil Engineers* 123(1), 685–706.
- Su, M. and R. Friedrich (1993). Turbulent secondary flow in a straight duct. *Zeitschrift Angewandte Mathematik und Mechanik* 73, 563.

- Sun, H.-W. and L. Z. Li (2014). A ccd-adi method for unsteady convection-diffusion equations. *Computer Physics Communications* 185(3), 790-797.
- Takahashi, T. and W. N. GILL (1980). Hydrodynamic chromatography: three dimensional laminar dispersion in rectangular conduits with transverse flow. *Chemical Engineering Communications* 5(5-6), 367-385.
- Takahashi, T., T. Korenaga, and F. Shen (1990). A numerical solution for the dispersion in laminar flow through a circular tube. *The Canadian Journal of Chemical Engineering* 68(2), 191-196.
- Tannehill, J., D. Anderson, and R. Pletcher (1997). Computational fluid mechanics and heat transfer. *Series in computational and physical processes in mechanics and thermal sciences Show all parts in this series.*
- Tatchell, D. G. (1975). *Convection processes in confined three-dimensional boundary layers*. Ph. D. thesis, University of London.
- Taylor, G. (1953). Dispersion of soluble matter in solvent flowing slowly through a tube. *Proceedings of the Royal Society of London. Series A. Mathematical and Physical Sciences* 219(1137), 186-203.
- Taylor, G. (1954a). Conditions under which dispersion of a solute in a stream of solvent can be used to measure molecular diffusion. In *Proceedings of the Royal Society of London A: Mathematical, Physical and Engineering Sciences*, Volume 225, pp. 473-477. The Royal Society.
- Taylor, G. (1954b). The dispersion of matter in turbulent flow through a pipe. In *Proceedings of the Royal Society of London A: Mathematical, Physical and Engineering Sciences*, Volume 223, pp. 446-468. The Royal Society.

- Tian, Z. and S. Dai (2007). High-order compact exponential finite difference methods for convection–diffusion type problems. *Journal of Computational Physics* 220(2), 952–974.
- Tian, Z. and Y. Ge (2007). A fourth-order compact adi method for solving two-dimensional unsteady convection–diffusion problems. *Journal of Computational and Applied Mathematics* 198(1), 268–286.
- Tian, Z. F. and P. Yu (2011). A high-order exponential scheme for solving 1d unsteady convection–diffusion equations. *Journal of computational and applied mathematics* 235(8), 2477–2491.
- Tichacek, L., C. Barkelew, and T. Baron (1957). Axial mixing in pipes. *AIChE Journal* 3(4), 439–442.
- Townsend, A. A. (1980). *The structure of turbulent shear flow*. Cambridge university press.
- Tseng, C. and R. Besant (1970). Dispersion of a solute in a fully developed laminar tube flow. In *Proceedings of the Royal Society of London A: Mathematical, Physical and Engineering Sciences*, Volume 317, pp. 91–99. The Royal Society.
- Uhlmann, M., A. Pinelli, G. Kawahara, and A. Sekimoto (2007). Marginally turbulent flow in a square duct. *Journal of fluid mechanics* 588, 153–162.
- Vázquez, M. S. and O. Métais (2002). Large-eddy simulation of the turbulent flow through a heated square duct. *Journal of Fluid Mechanics* 453, 201–238.
- Vrentas, J. and C. Vrentas (1988). Dispersion in laminar tube flow at low pecelet numbers or short times. *AIChE journal* 34(9), 1423–1430.

- Vrentas, J. and C. Vrentas (2000). Asymptotic solutions for laminar dispersion in circular tubes. *Chemical engineering science* 55(4), 849–855.
- Wallin, S. and A. V. Johansson (2000). An explicit algebraic reynolds stress model for incompressible and compressible turbulent flows. *Journal of Fluid Mechanics* 403, 89–132.
- Wang, F., Y. Chew, B. Khoo, and K. Yeo (1994). Computation of turbulent flow in a square duct: aspects of the secondary flow and its origin. *Computers & fluids* 23(1), 157–176.
- Wang, X.-H., Z.-F. Liu, and X.-X. Lu (2011). Derivation of a second-order model for reynolds stress using renormalization group analysis and the two-scale expansion technique. *Acta Mechanica Sinica* 27(5), 649–659.
- Wilcox, D. C. et al. (1998). *Turbulence modeling for CFD*, Volume 2. DCW industries La Canada, CA.
- Wu, Y. and R. A. Falconer (2000). A mass conservative 3-d numerical model for predicting solute fluxes in estuarine waters. *Advances in water resources* 23(5), 531–543.
- Xu, H. (2009). Direct numerical simulation of turbulence in a square annular duct. *Journal of Fluid Mechanics* 621, 23–57.
- Xu, H. and A. Pollard (2001). Large eddy simulation of turbulent flow in a square annular duct. *Physics of Fluids (1994-present)* 13(11), 3321–3337.
- You, D. (2006). A high-order padé adi method for unsteady convection–diffusion equations. *Journal of Computational Physics* 214(1), 1–11.

- Younis, B. (1993). Prediction of turbulent flows in rotating rectangular ducts. *Journal of fluids engineering* 115(4), 646–652.
- Yu, J. (1976). An approximate analysis of laminar dispersion in circular tubes. *Journal of Applied Mechanics* 43(4), 537–542.
- Yu, J. (1979). On laminar dispersion for flow through round tubes. *Journal of Applied Mechanics* 46(4), 750–756.
- Yu, J. (1981). Dispersion in laminar flow through tubes by simultaneous diffusion and convection. *Journal of Applied Mechanics* 48(2), 217–223.
- Zhao, H. and H. H. Bau (2007). Effect of secondary flows on Taylor-Aris dispersion. *Analytical chemistry* 79(20), 7792–7798.
- Zhu, Z.-j., H.-x. YANG, and T.-y. CHEN (2009). Direct numerical simulation of turbulent flow in a straight square duct at Reynolds number 600. *Journal of Hydrodynamics, Ser. B* 21(5), 600–607.

Appendix A

Artificial Diffusion in Numerical Schemes

A.1 Preamble

Much of this thesis is concerned with dispersion. We have noted in the Chapter 2 that it is essential that the result of our analysis are not compromised or contaminated by numerical dispersion. Since the avoidance of numerical dispersion is central to our mission, in this appendix, we demonstrate how it arises in a simple case. In order to discretize governing equations into various grid points, many schemes have been devised in the last few decades. However, satisfactory numerical modelling of fluid flow phenomena have always posed dilemmas to researchers. The development of artificial numerical diffusion during convection of a sharp axial discontinuity (Roache 1972) brings a great challenge to the solution of the governing equation. Particularly, the use of lower order discretization scheme such as first order upwind, central difference, hybrid differencing, Lax-Wendroff etc give rise to unwanted diffusion in

the solution. The initial condition is a pulse of solute across the cross-section having sharp axial concentration. Even, with a Gaussian pulse, it is quite common in lower order discretization schemes to introduce false diffusion in the solution. In order to calculate the actual spreading rate, it is very important that one should be most careful to avoid any artificial dispersion so that it does not overestimate the actual dispersion.

The order of a discretization scheme (which, in a sense, represents its order of accuracy) is the lowest power of the variable in truncation error. Truncation error evolves as a result of approximation of derivatives from a polynomial expansion. For a discretization scheme, it is the largest truncation error of each individual derivative term in the differential equation that is being discretized. Although truncation errors give an idea of accuracy of any discretization method, it does not represent how much error included in the solution; rather it tells about how fast the error is decrease over mesh refinement.

A.2 Finite Difference Method

Leonard Euler first proposed the idea of approximating derivatives by means of Taylor's series expansion (Tannehill et al. 1997). It is one of the simplest methods to formulate and apply but works on only structured mesh. Such method always introduces errors which are called truncation errors. For a function $\phi(x)$, the Taylors series expansion can be expressed near x as

$$\begin{aligned} \phi(x) = \phi(x_i) + (x - x_i) \left. \frac{\partial \phi}{\partial x} \right|_i + \frac{(x - x_i)^2}{2!} \left. \frac{\partial^2 \phi}{\partial x^2} \right|_i + \dots \\ + \frac{(x - x_i)^n}{n!} \left. \frac{\partial^n \phi}{\partial x^n} \right|_i + \dots \end{aligned} \quad (\text{A.1})$$

Replacing x by x_{i+1} and x_{i-1} we obtain,

$$\begin{aligned} \phi(x_{i+1}) = \phi(x_i) + (x_{i+1} - x_i) \left. \frac{\partial \phi}{\partial x} \right|_i + \frac{(x_{i+1} - x_i)^2}{2!} \left. \frac{\partial^2 \phi}{\partial x^2} \right|_i + \dots \\ + \frac{(x_{i+1} - x_i)^n}{n!} \left. \frac{\partial^n \phi}{\partial x^n} \right|_i + \dots \end{aligned} \quad (\text{A.2})$$

and

$$\begin{aligned} \phi(x_{i-1}) = \phi(x_i) - (x_i - x_{i-1}) \left. \frac{\partial \phi}{\partial x} \right|_i + \frac{(x_i - x_{i-1})^2}{2!} \left. \frac{\partial^2 \phi}{\partial x^2} \right|_i - \dots \\ + (-1)^n \frac{(x_i - x_{i-1})^n}{n!} \left. \frac{\partial^n \phi}{\partial x^n} \right|_i + \dots \end{aligned} \quad (\text{A.3})$$

Subtracting Equation (A.3) from equation (A.2). and dividing by $(x_i - x_{i-1})$ gives the backward differencing formulation of the first derivative $\left. \frac{\partial \phi}{\partial x} \right|_i$ at point i

$$\frac{\phi(x_i) - \phi(x_{i-1})}{(x_i - x_{i-1})} = \left. \frac{\partial \phi}{\partial x} \right|_i + \frac{(x_i - x_{i-1})}{2!} \left. \frac{\partial^2 \phi}{\partial x^2} \right|_i + HOT \quad (\text{A.4})$$

Here *HOT* refers to higher order terms of $(x_i - x_{i-1})$ which approach zero as $(x_i - x_{i-1})$ tends to zero. Likewise the forward difference can be obtained as

$$\frac{\phi(x_{i+1}) - \phi(x_i)}{(x_{i+1} - x_i)} = \frac{\partial\phi}{\partial x}\Big|_i + \frac{(x_{i+1} - x_i)}{2!} \frac{\partial^2\phi}{\partial x^2}\Big|_i + HOT \quad (\text{A.5})$$

For a uniform mesh size, $x_{i+1} - x_i = x_i - x_{i-1} = \Delta x$, we can write equations (A.4) and (A.5) as

$$\frac{\partial\phi}{\partial x}\Big|_i = \frac{\phi(x_i) - \phi(x_{i-1})}{\Delta x} + \mathcal{O}(\Delta x) \quad (\text{A.6})$$

and

$$\frac{\partial\phi}{\partial x}\Big|_i = \frac{\phi(x_{i+1}) - \phi(x_i)}{\Delta x} + \mathcal{O}(\Delta x) \quad (\text{A.7})$$

Equations (A.6) and (A.7) are called first order upwind difference schemes because they account for one-sided differences in the approximation. Here $\mathcal{O}(\Delta x)$ refers to the truncation error which also indicates the order of the scheme considered from the highest power of Δx .

In the following section, we demonstrate the source of artificial diffusion from numerical schemes. Furthermore, to represent a quantitative analysis, the amount of diffusion generated by the first order upwind scheme is calculated by Fourier analysis.

A.3 Numerical Diffusion in Linear Convection Equation

To demonstrate the fact that lower order differencing schemes suffer from artificial diffusion arising from the numerical scheme, we consider a linear unsteady convection equation in one dimension

$$\frac{\partial \phi}{\partial t} + u \frac{\partial \phi}{\partial x} = 0 \quad (\text{A.8})$$

Discretising the equation A.8 using FTBS (forward in time and backward in space) which is a first order upwind scheme,

$$\frac{\phi_i^{n+1} - \phi_i^n}{\Delta t} + u \frac{\phi_i^n - \phi_{i-1}^n}{\Delta x} = 0 \quad (\text{A.9})$$

Equation (A.9) is the numerical approximation of the partial differential equation (A.8) and it involves a truncation error. A detailed analysis of this truncation error enables us to understand the behaviour of the scheme, as well as the numerical diffusion associated in the scheme qualitatively and quantitatively. The qualitative analysis is performed by rewriting the partial differential equation in terms of its equivalent differential equation or the modified equation. A quantitative estimation of the numerical dispersion arising from the differencing scheme can be obtained by decomposing the variable into Fourier domain. This method is known as Von Neumann stability analysis. In the following sections, we will discuss these two approaches.

A.3.1 Modified Equation

The behaviour of the numerical solution can be predicted in great detail by studying the truncation error involved in the numerical scheme. The method involves rewriting the numerical scheme with a truncation error in a form which is known as a modified equation. Two types of error are observed namely dispersion error and dissipation error. The former occurs when the leading terms in the truncation error have odd-order derivatives and are usually characterized by oscillations or small

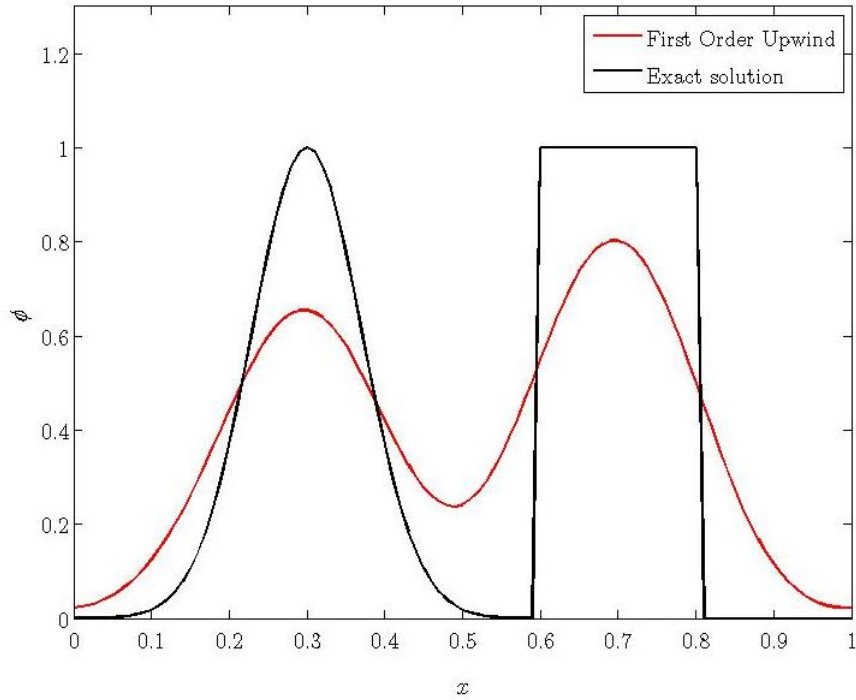


Figure A.1: Illustration of artificial diffusion generated by the first order upwind scheme

moving wave perturbations in the solution. It is also referred as phase error cause waves of different wavelength moves at different speed in the numerical solution because of approximation causing a phase difference or dispersion of waves in the frequency domain. The second type of error usually evolves when the leading term in the truncation error contains even-order derivatives and quantified as loss in wave amplitude. This is often called as amplitude error or artificial viscosity effect of numerical solution. The combined effect of dispersion and dissipation error in a numerical solution is often referred to as artificial diffusion .(Tannehill et al., 1997)

An example has been illustrated for representing the fact of induced high amount of artificial diffusion in the numerical solution of linear convection equation in Figure A.1

In order to observe the artificial diffusion arising from the discretization scheme described in equation ,(A.9) we develop a modified equation of equation (A.8) by

expanding terms ϕ_i^{n+1} and ϕ_{i-1}^n by means of Taylor's series

$$\phi_i^{n+1} = \phi_i^n + \Delta t \left. \frac{\partial \phi}{\partial t} \right|_i^n + \frac{(\Delta t)^2}{2} \left. \frac{\partial^2 \phi}{\partial t^2} \right|_i^n + \frac{(\Delta t)^3}{6} \left. \frac{\partial^3 \phi}{\partial t^3} \right|_i^n + \text{HOT} \quad (\text{A.10})$$

$$\phi_{i-1}^n = \phi_i^n - \Delta x \left. \frac{\partial \phi}{\partial x} \right|_i^n + \frac{(\Delta x)^2}{2} \left. \frac{\partial^2 \phi}{\partial x^2} \right|_i^n - \frac{(\Delta x)^3}{6} \left. \frac{\partial^3 \phi}{\partial x^3} \right|_i^n + \text{HOT} \quad (\text{A.11})$$

Rearranging and subtracting equations (A.10) and (A.11) results in

$$\frac{\phi_i^{n+1} - \phi_i^n}{\Delta t} = \left. \frac{\partial \phi}{\partial t} \right|_i^n + \frac{\Delta t}{2} \left. \frac{\partial^2 \phi}{\partial t^2} \right|_i^n + \frac{(\Delta t)^2}{6} \left. \frac{\partial^3 \phi}{\partial t^3} \right|_i^n + \text{HOT} \quad (\text{A.12})$$

and

$$\frac{\phi_{i-1}^n - \phi_i^n}{\Delta x} = - \left. \frac{\partial \phi}{\partial x} \right|_i^n + \frac{\Delta x}{2} \left. \frac{\partial^2 \phi}{\partial x^2} \right|_i^n - \frac{(\Delta x)^2}{6} \left. \frac{\partial^3 \phi}{\partial x^3} \right|_i^n + \text{HOT} \quad (\text{A.13})$$

Subtracting the product of u and equation (A.13) from equation (A.12) gives

$$\begin{aligned} \frac{\phi_i^{n+1} - \phi_i^n}{\Delta t} + u \frac{\phi_i^n - \phi_{i-1}^n}{\Delta x} = \\ \left(\left. \frac{\partial \phi}{\partial t} \right|_i^n + u \left. \frac{\partial \phi}{\partial x} \right|_i^n \right) + \left(\frac{\Delta t}{2} \left. \frac{\partial^2 \phi}{\partial t^2} \right|_i^n - \frac{\Delta x}{2} \left. \frac{\partial^2 \phi}{\partial x^2} \right|_i^n + \mathcal{O}((\Delta t)^2, (\Delta x)^2) \right) \end{aligned} \quad (\text{A.14})$$

Let us denote $\mathcal{D}(\phi) = 0$ refers to the equation that we want to solve numerically; i.e. (A.8). Also $\mathcal{N}(\phi_i^n) = 0$ refers to the numerical scheme; i.e. equation (A.9). Therefore, from equation (A.14) we get

$$\mathcal{N}(\phi_i^n) - \mathcal{D}(\phi_i^n) = TE \quad (\text{A.15})$$

Where TE is the truncation error defined as

$$TE = \frac{\Delta t}{2} \left. \frac{\partial^2 \phi}{\partial t^2} \right|_i^n - \frac{\Delta x}{2} \left. \frac{\partial^2 \phi}{\partial x^2} \right|_i^n + \mathcal{O}((\Delta t)^2, (\Delta x)^2) \quad (\text{A.16})$$

Furthermore, let us consider the exact solution of the numerical scheme is $\overline{\phi}_i^n$ which satisfies the modified differential equation. Hence it gives

$$\frac{\overline{\phi}_i^{n+1} - \overline{\phi}_i^n}{\Delta t} + u \frac{\overline{\phi}_i^n - \overline{\phi}_{i-1}^n}{\Delta x} \equiv 0 \quad (\text{A.17})$$

Rewrite equation (A.14) for the exact solution of the discretized equation

$$\begin{aligned} \frac{\overline{\phi}_i^{n+1} - \overline{\phi}_i^n}{\Delta t} + u \frac{\overline{\phi}_i^n - \overline{\phi}_{i-1}^n}{\Delta x} &= \left(\left. \frac{\partial \overline{\phi}}{\partial t} \right|_i^n + u \left. \frac{\partial \overline{\phi}}{\partial x} \right|_i^n \right) \\ &+ \left(\frac{\Delta t}{2} \left. \frac{\partial^2 \overline{\phi}}{\partial t^2} \right|_i^n - \frac{\Delta x}{2} \left. \frac{\partial^2 \overline{\phi}}{\partial x^2} \right|_i^n + \mathcal{O}((\Delta t)^2, (\Delta x)^2) \right) \end{aligned} \quad (\text{A.18})$$

Denote $\frac{\partial \overline{\phi}}{\partial t}$ as $\overline{\phi}_t$ and $\frac{\partial \overline{\phi}}{\partial x}$ as $\overline{\phi}_x$ equation (A.18) together with equation (A.17) becomes

$$(\overline{\phi}_t)_i^n = -u (\overline{\phi}_x)_i^n + \mathcal{O}(\Delta t, \Delta x) \quad (\text{A.19})$$

Taking time derivation of the above equation gives

$$(\overline{\phi}_{tt})_i^n = -u ([\overline{\phi}_x]_t)_i^n + \mathcal{O}(\Delta t, \Delta x) \quad (\text{A.20})$$

It can also be written as

$$(\overline{\phi}_{tt})_i^n = -u ([\overline{\phi}_t]_x)_i^n + \mathcal{O}(\Delta t, \Delta x) \quad (\text{A.21})$$

Incorporating equation (A.19) into (A.21)

$$\left(\overline{\phi_{tt}}\right)_i^n = -u^2 \left(\overline{\phi_{xx}}\right)_i^n + \mathcal{O}(\Delta t, \Delta x) \quad (\text{A.22})$$

Replacing $\left(\overline{\phi_{tt}}\right)_i^n$ in equation (A.16) using expression from equation (A.22)

$$TE = -u^2 \frac{\Delta t}{2} \left(\overline{\phi_{xx}}\right)_i^n + u \frac{\Delta t}{2} \left(\overline{\phi_{xx}}\right)_i^n + HOT \quad (\text{A.23})$$

or,

$$TE = u \frac{\Delta t}{2} \left(1 - u \frac{\Delta t}{\Delta x}\right) \left.\frac{\partial^2 \phi}{\partial x^2}\right|_i^n + HOT \quad (\text{A.24})$$

Therefore, the exact solution of the numerical scheme should satisfy

$$\mathcal{D} \left(\overline{\phi}_i^n\right) = TE \quad (\text{A.25})$$

$$\left(\left.\frac{\partial \overline{\phi}}{\partial t}\right|_i^n + u \left.\frac{\partial \overline{\phi}}{\partial x}\right|_i^n\right) = u \frac{\Delta t}{2} \left(1 - u \frac{\Delta t}{\Delta x}\right) \left.\frac{\partial^2 \overline{\phi}}{\partial x^2}\right|_i^n + HOT \quad (\text{A.26})$$

This is equation is the modified differential equation of the linear convection equation. Although the governing equation is a purely convection equation, the modified equation consists of both convection and diffusion terms as the leading term in the truncation error contains an even-order derivative; which confirms the diffusive nature of the first order upwind scheme. This is a qualitative assessment that tells us about the presence of numerical dispersion in the scheme. However we cannot estimate how much false diffusion will arise as the solution marched through time. Nevertheless, the stability condition can be determined from the coefficient of the diffusion term in the truncation error. For example, it can be noted that it order

to ensure the scheme stable (i.e. error term to be damped out) for the first order upwind scheme, it must satisfy following condition

$$0 \leq u \frac{\Delta t}{\Delta x} \leq 1 \quad \text{and} \quad u \geq 0 \quad (\text{A.27})$$

For the two-dimensional case, it can be readily concluded that the stability condition requires

$$0 \leq \left(u \frac{\Delta t}{\Delta x} + v \frac{\Delta t}{\Delta y} \right) \leq \frac{1}{2} \quad \text{and} \quad u, v \geq 0 \quad (\text{A.28})$$

A.3.2 Von-Neumann Stability Analysis

The modified equation representation of the partial differential equation gives us a qualitative appreciation of the origin of artificial diffusion in a differencing scheme. To estimate the degree of artificial diffusion arising within the differencing scheme, it is required to look at the behaviour of the solution in its frequency domain. This is achieved by expanding the solution variable or the error term by Fourier analysis. An amplification factor is examined for decay of growth which identifies the stability of the numerical algorithm. This method is referred as von Neumann stability analysis .(Chung, 2010) Generally in Fourier analysis, a periodic boundary is assumed. If we consider a periodic boundary between $-L$ to L with mesh spacing $\Delta x = \frac{L}{N}$ where N is total number of mesh points then the shortest and largest wavelength that can be resolved in the domain is $\lambda_{min} = 2\Delta x$ and $\lambda_{max} = 2L$ respectively. It corresponds to the maximum and minimum number of wave number ($\kappa = \frac{2\pi}{\lambda}$) being equal to $\kappa_{max} = \frac{2\pi}{2\Delta x} = \frac{\pi}{\Delta x}$ and $\kappa_{min} = \frac{2\pi}{2L} = \frac{\pi}{L}$. Therefore, the harmonic of a finite difference mesh is

$$\kappa_j = j\kappa_{min} = j\frac{\pi}{L} = j\frac{\pi}{N\Delta x} \quad (\text{A.29})$$

with $j = 0, 1, 2, \dots, N$

It can be readily proven that for any numerical scheme, the error satisfies the same equation as the numerical solution .(Hirsch, 2007) Hence either the numerical solution or the error term can be checked for von Neumann stability analysis. Assuming a Fourier expression in space of the function $\phi_i^n (= \phi(x_i, t_n))$ as

$$\phi_i^n = \sum_{j=-N}^N (\Phi_j^n \exp(\iota \kappa_j x_i)) \quad (\text{A.30})$$

$$\phi_i^n = \sum_{j=-N}^N \left(\Phi_j^n \exp \left(\iota \left(j \frac{\pi}{N\Delta x} \right) (i\Delta x) \right) \right) \quad (\text{A.31})$$

$$\phi_i^n = \sum_{j=-N}^N \left(\Phi_j^n \exp \left(\iota \left(ij \frac{\pi}{N} \right) \right) \right) \quad (\text{A.32})$$

With the imaginary number $\iota = \sqrt{-1}$, Φ_j^n being the amplitude of the j^{th} harmonic and phase angle defied as

$$\varphi = k_j \Delta x = j \frac{\pi}{N} \quad (\text{A.33})$$

For any numerical scheme to be stable, the amplitude of any harmonic must not grow indefinitely in time as $n \rightarrow \infty$. That means the amplification factor must remain less than unity.

$$|\mathcal{G}| = \left| \frac{\Phi_j^{n+1}}{\Phi_j^n} \right| \leq 1 \quad (\text{A.34})$$

This is known as von Neumann stability condition. It is worthwhile noting that the amplification factor \mathcal{G} is a function of phase angle φ , but not function of time level n .

Now we represent terms in first order upwind scheme for a single harmonic in equation (A.9) as

$$\phi_i^n = \Phi_j^n \exp(i\varphi) \quad (\text{A.35})$$

$$\phi_{i-1}^n = \Phi_j^n \exp(i(i-1)\varphi) \quad (\text{A.36})$$

$$\phi_i^{n+1} = \Phi_j^{n+1} \exp(i\varphi) \quad (\text{A.37})$$

Using these values in equation (A.9) to find the amplification factor \mathcal{G}

$$\frac{(\Phi_j^{n+1} - \Phi_j^n)}{\Delta t} \exp(i\varphi) + \frac{u}{\Delta x} \Phi_j^n (\exp(i\varphi) - \exp(i(i-1)\varphi)) = 0 \quad (\text{A.38})$$

Rearranging terms gives

$$\frac{\Phi_j^{n+1}}{\Phi_j^n} = 1 - \frac{u\Delta t}{\Delta x} (1 - \exp(i\varphi)) \quad (\text{A.39})$$

Writing the Courant number, $C_r = \frac{u\Delta t}{\Delta x}$ and expanding the exponential, we obtain

$$\begin{aligned} \mathcal{G} &= \frac{\Phi_j^{n+1}}{\Phi_j^n} = (1 - C_r + C_r \cos\varphi) - iC_r \sin\varphi \\ &= 1 - 2C_r \sin^2 \frac{\varphi}{2} - iC_r \sin\varphi \end{aligned} \quad (\text{A.40})$$

Separating real and imaginary parts of the amplification factor \mathcal{G}

$$\begin{aligned}\operatorname{Re}(\mathcal{G}) &= 1 - C_r + C_r \cos \varphi \\ &= 1 - 2C_r \sin^2 \frac{\varphi}{2} \\ \operatorname{Im}(\mathcal{G}) &= -C_r \sin \varphi\end{aligned}\tag{A.41}$$

The modulus of the amplification factor can be obtained as

$$\begin{aligned}|\mathcal{G}| &= \sqrt{\operatorname{Re}(\mathcal{G})^2 + \operatorname{Im}(\mathcal{G})^2} \\ &= \left[(1 - C_r + C_r \cos \varphi)^2 + C_r^2 \sin^2 \varphi \right]^{\frac{1}{2}} \\ |\mathcal{G}| &= \left[\left(1 - 4C_r(1 - C_r) \sin^2 \frac{\varphi}{2} \right) \right]^{\frac{1}{2}}\end{aligned}\tag{A.42}$$

Since the amplification factor is a complex number equation (A.40) can be expressed in exponential form $\mathcal{G} = |\mathcal{G}| \exp(i\psi)$

where ψ is the phase angle of the amplification factor defined by

$$\begin{aligned}\psi &= \tan^{-1} \left[\frac{\operatorname{Im}(\mathcal{G})}{\operatorname{Re}(\mathcal{G})} \right] \\ &= \tan^{-1} \left[\frac{-C_r \sin \varphi}{1 - C_r + C_r \cos \varphi} \right]\end{aligned}$$

It can be readily shown that the modulus of the amplification factor ($|\mathcal{G}|$) and phase shift (ψ_e) for the exact solution for linear convection equation would be 1 and $(-C_r \varphi)$ respectively. Hence the total diffusion error in the numerical solution resulting from

first order upwind scheme for N time steps can be quantified by

$$\epsilon_{diffusion} = \left(1 - |\mathcal{G}|^N\right) \Phi_0 \quad (\text{A.43})$$

Where, Φ_0 is the initial amplitude of the wave. Likewise, the total dispersion or phase error can be expressed as

$$\epsilon_{dispersion} = N (\psi_e - \psi) \quad (\text{A.44})$$

The relative phase shift of the numerical solution from the exact solution in one time step is given by

$$\frac{\psi}{\psi_e} = \frac{\tan^{-1} \left[\frac{-C_r \sin \phi}{1 - C_r + C_r \cos \phi} \right]}{-C_r \phi} \quad (\text{A.45})$$

From the nomenclature we defined at the beginning of this section, it can be noted that the highest frequency that can be obtained in the mesh corresponds to the shortest wavelength (which is $\lambda = 2\Delta x$). This corresponds to the phase angle, $\phi = \pi$. Therefore, we designate regions in Figure A.2 around $\phi = 0$ as the low frequency region and $\phi = \pi$ as the high frequency region in Figure A.2. For the purpose of estimating the amount of dispersion involved in the scheme, we present an enlarged view of the diffusion error in the low frequency region of Figure A.3.

For estimating the amount of diffusion arise in the FOU scheme, we run simulation for the convection of a sinusoidal pulse with lowest phase angle $\phi = \pi/15 = 12^\circ$ and the simulation was run with Courant number $C_r = 0.3$. The profile of the solution after a complete cycle in the periodic domain has been presented in Figure 10 along with the exact solution. It required n=333 time steps to complete the full cycle simulation. Referring to Figure A.3, we can find that for phase angle 12° and $C_r = 0.3$,

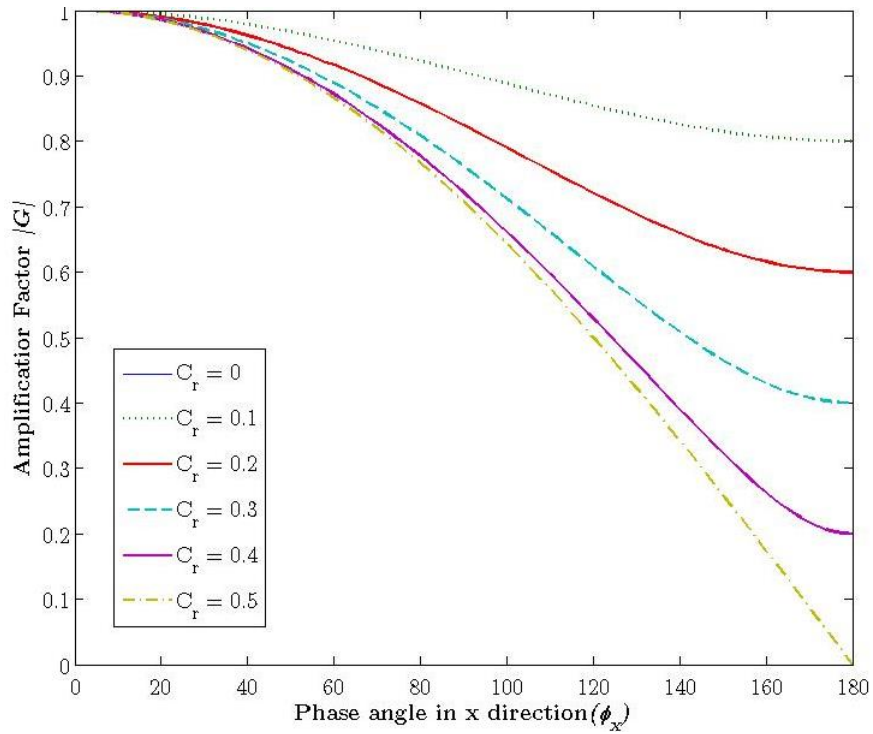


Figure A.2: Diffusion error for a first order upwind scheme for the linear convection equation

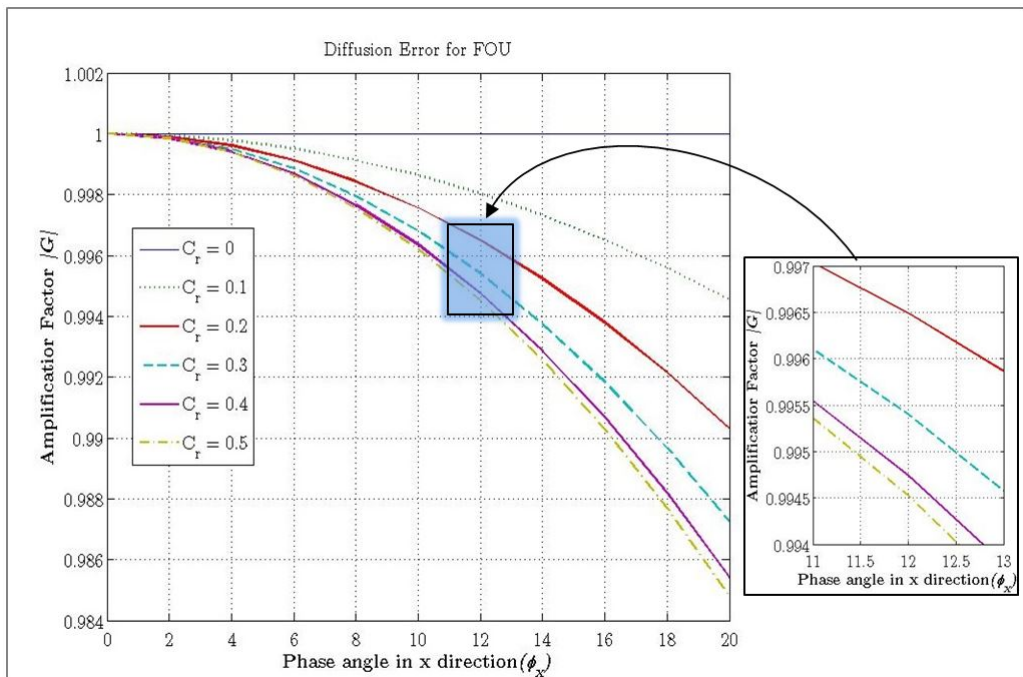


Figure A.3: Enlarged view of diffusion error for a first order upwind scheme for the linear convection equation in low frequency region

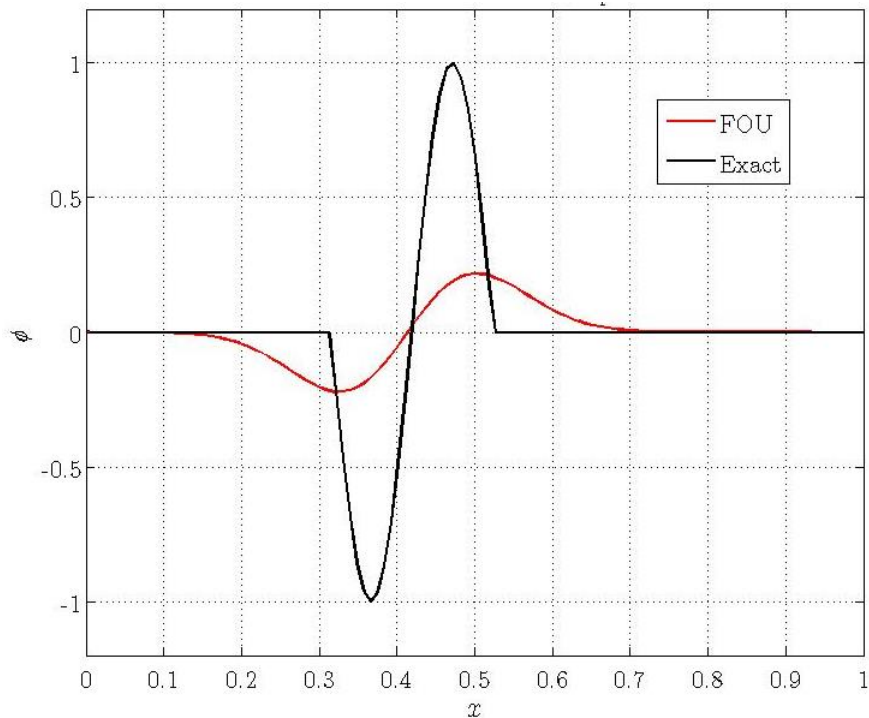


Figure A.4: Artificial diffusion in the first order upwind Scheme for convection of a pulse with $\phi = \pi/15$, simulation carried out with $C_r = 0.3$

the amplification factor $|\mathcal{G}| = 0.9954$. The amplitude of the pulse should diffuse down to $|\mathcal{G}|^n = (0.9954)^{333} = 0.215$; which is also observed in Figure A.4 Hence we can see that according the (A.42), the amount of diffusion induced from the first order upwind scheme is $1 - 0.215 = 0.785 = 78.5\%$ of the initial pulse.

References

Chung, T., 2010. *Computational fluid dynamics*, Cambridge university press.

Hirsch, C., 2007. *Numerical Computation of Internal and External Flows: The Fundamentals of Computational Fluid Dynamics*, Butterworth-Heinemann.

Roache, P.J., 1972. On artificial viscosity. *Journal of Computational Physics*, 10(2), pp.169–184.

Tannehill, J., Anderson, D. & Pletcher, R., 1997. *Computational fluid mechanics*

and heat transfer. Series in computational and physical processes in mechanics

Appendix B

A Matlab Script for Simulation of Laminar Dispersion Flow through Pipes

B.1 Main Program

```
% Simulation of dimensionless convection diffusion equation,  
% dimensionless parameters are defined as follows  
% Pe = R*u0/D  
% X = (x-0.5u0*t),      according to Vrentas(2000)  
% t = time*D/R^2;      which is basically 'tau'  
% -----%  
  
clear all,  
  
clc
```

```

Pe = 1e1;      u0 = Pe;      t = 0.02;      D = 1;

L = 6*u0*t;

nX = 201;      dX = L/(nX-1);      X = ((0:dX:L)-6*u0*t/2);
ny = 81;      dy = 1/(ny-1);      r = (0:dy:1);
dt = 2e-6;    nt = int32(t/dt);    tau = dt:dt:t;

u = u0*(.5-r.^2);

% Dimensionless numbers to check the stability of numerical scheme must
% be less than 0.5
gamma_x = D*dt/dX^2;
gamma_r = D*dt/dy^2;
Cr = u*dt/dX;

% Initial Condition Preallocation
Cold = zeros(nX,ny);
Ct=zeros(nt,1);
for i=1:nX,
    if X(i)==0,          % pulse input
        Cold(i,:) = 1;
    end;
end
Cnew = Cold;
Ci = Cold;

% Check initial condition

```

```

plot(2*X/(Pe*t),area_average(Cold,r),'k','linewidth',2);

%%

for kk=1:nt

% Check solution as it runs....

%     X = (x-0.5*u0*time(kk))/(R);

%     h= plot(2*X/(t*Pe),area_average(Cnew,r),'k','linewidth',2);

%     h=contourf(X,y,Cnew');

%     refreshdata (h), pause(0.001);

for j=1:ny-1

    for i=2:nX-2

        if u(j)>=0, % care for velocity direction

            A1=gamma_x*Cr(j)+Cr(j)/6*(Cr(j)^2-1);

            B1=gamma_x*(1-3*Cr(j))-Cr(j)/2*(Cr(j)^2-Cr(j)-2);

            C1=-gamma_x*(2-3*Cr(j))+Cr(j)/2*(Cr(j)^2-2*Cr(j)-1);

            D1=gamma_x*(1-Cr(j))-Cr(j)/6*(Cr(j)^2-3*Cr(j)+2);

            Cnew(i,j)=Cold(i,j)+A1*Cold(i-2,j)+B1*Cold(i-1,j)...

                +C1*Cold(i,j)+D1*Cold(i+1,j);

        end;

    if u(j)<0,

        A1=-gamma_x*Cr(j)-Cr(j)/6*(Cr(j)^2-1);

        B1=gamma_x*(1+3*Cr(j))+Cr(j)/2*(Cr(j)^2+Cr(j)-2);

        C1=-gamma_x*(2+3*Cr(j))-Cr(j)/2*(Cr(j)^2+2*Cr(j)-1);

```

```

D1=gamma_x*(1+Cr(j))+Cr(j)/6*(Cr(j)^2+3*Cr(j)+2);
Cnew(i,j)=Cold(i,j)+A1*Cold(i+2,j)+B1*Cold(i+1,j)...
                +C1*Cold(i,j)+D1*Cold(i-1,j);
end;

if j==1,      % Radial diffusion at center line
    Cnew(i,j) = Cnew(i,j)+2*gamma_r*(Cold(i,2)-Cold(i,1));
else
    Cnew(i,j) = Cnew(i,j)+D*dt/(2*r(j)*dy)*(Cold(i,j+1)...
        -Cold(i,j-1))+gamma_r*(Cold(i,j-1)-2*Cold(i,j)...
        +Cold(i,j+1));

end

end

end

end

% Impose boundary conditions
Cnew(:,ny) = Cnew(:,ny-1); % at the wall
Cnew(2,:) = Cnew(1,:);    % at the inlet

% Outlet BC
% first order accurate
Cnew(nX,:) = Cnew(nX-1,:);

% second order b.c
% Cnew(nx,:) = (4*Cnew(nx-1,:)-Cnew(nx-2,:))/3;

% third order b.c
% Cnew(nX,:) = (18*Cnew(nX-1,:)-9*Cnew(nX-2,:)+2*Cnew(nX-1,:))/11;

```

```

% update solution every timestep
Cold = Cnew;

% Record area average concentration profile at every time step
Ct(nx, kk)=area_average(Cnew(nx,:), r);

% display counter
iteration_remaining = nt-kk

end

% Compare mass balance
totalci= sum(area_average(Ci, r))
totalc = sum(area_average(Cnew, r))

% plot the result for axial mean concentration profile
plot((2*X/(Pe*t)), area_average(Cnew, r)/(Pe*t), 'k', 'linewidth', 2);
grid on

% Calculate Effective Dispersion Coefficient
time = tau*R^2/D; % convert from dimensionless time
D_effective = dispersion_coeff(Ct, time, u0, L)

```

B.2 Function area_average.m

```
function Cmean = area_average(Cnew, r)

% Calculate the mean concentration along the length of the pipe

[nx,ny] = size(Cnew);

R = max(r);

Cmean(nx)=0;

for i=1:nx
    sumc=0.0;
    for j=1:ny-1
        sumc=sumc+0.5*(Cnew(i,j)+Cnew(i,j+1))*(r(j+1)^2-r(j)^2)/R^2;
    end
    Cmean(i)=sumc;
end

end
```

B.3 Function dispersion_coeff.m

```
function [ D, t_bar ] = dispersion_coeff( C, time, u0, L )

% A function to calculate effective dispersion coefficient from the local
% concentration profile of a solute flowing through ducts
```

```

% It will return the Effective dispersion coefficient, D and the resident
% mean time, t_bar
Ct = C.*time;

CtSq = C.*time.^2;

t_bar = sum(Ct)/sum(C);

sigmaSq = sum(CtSq)/sum(C)-t_bar^2;

sigma_thetaSq = sigmaSq/t_bar^2;

% Easier Approach for Effective Dispersion Coefficient
D =(u0*L/2)*sigma_thetaSq;

% Accurate Approach for Effective Dispersion Coefficient
% sym alpha
% D = u0*L*solve(sigma_thetaSq==2*alpha-2*alpha^2*(1-exp(-1/alpha)));
end

```

Appendix C

High order Non-periodic Boundary Condition for CCD Method

C.1 Preamble

In order to solve the simultaneous system of linear equations for a dependent variable and its first and second derivatives with sixth order accuracy by a three point compact combined difference scheme, it is necessary to develop pair of high order compact equations at the boundaries to close the system of equations. The idea is to expand the function of dependent variable at the boundary by a Taylor's series. This will result a pair of equations at the boundaries with higher order accuracy.

C.2 Development of the Boundary Equations

In the development of the scheme, we consider a uniform grid spacing of $\Delta x = h$. If x_1 be the left boundary point and x_2 and x_3 is the first two neighboring nodes then expanding the dependent variable ϕ and its derivatives in a Taylor series gives

$$\begin{aligned} \phi(x_1) = \phi(x_2) - h\phi'(x_2) + \frac{h^2}{2}\phi''(x_2) - \frac{h^3}{6}\phi'''(x_2) + \frac{h^4}{24}\phi^{(4)}(x_2) \\ - \frac{h^5}{120}\phi^{(5)}(x_2) + \frac{h^6}{720}\phi^{(6)}(x_2) + \mathcal{O}(h^7) \quad (\text{C.1}) \end{aligned}$$

$$\begin{aligned}\phi(x_3) = \phi(x_2) + h\phi'(x_2) + \frac{h^2}{2}\phi''(x_2) + \frac{h^3}{6}\phi'''(x_2) + \frac{h^4}{24}\phi^{(4)}(x_2) \\ + \frac{h^5}{120}\phi^{(5)}(x_2) + \frac{h^6}{720}\phi^{(6)}(x_2) + \mathcal{O}(h^7) \quad (\text{C.2})\end{aligned}$$

$$\begin{aligned}\phi'(x_1) = \phi'(x_2) - h\phi''(x_2) + \frac{h^2}{2}\phi'''(x_2) - \frac{h^3}{6}\phi^{(4)}(x_2) + \frac{h^4}{24}\phi^{(5)}(x_2) \\ - \frac{h^5}{120}\phi^{(6)}(x_2) + \mathcal{O}(h^6) \quad (\text{C.3})\end{aligned}$$

$$\begin{aligned}\phi''(x_1) = \phi''(x_2) - h\phi'''(x_2) + \frac{h^2}{2}\phi^{(4)}(x_2) - \frac{h^3}{6}\phi^{(5)}(x_2) + \frac{h^4}{24}\phi^{(6)}(x_2) \\ + \mathcal{O}(h^5) \quad (\text{C.4})\end{aligned}$$

Algebraic manipulation of the above equation leads to the following equation

$$\begin{aligned}14\phi'(x_1) + 16\phi'(x_2) + 2h\phi''(x_1) - 4h\phi''(x_2) + \frac{1}{h}(31\phi(x_1) - 32\phi(x_2) + \phi(x_3)) = \\ \frac{h^5}{90}\phi^{(6)}(x_2) + \mathcal{O}(h^6) \quad (\text{C.5})\end{aligned}$$

By writing $\phi(x_i) = \phi_i$ and dropping the truncation error, the non-periodic boundary condition becomes

$$14\phi'(x_1) + 16\phi'(x_2) + 2h\phi''(x_1) - 4h\phi''(x_2) + \frac{1}{h}(31\phi(x_1) - 32\phi(x_2) + \phi(x_3)) = 0 \quad (\text{C.6})$$

With fifth order accuracy ($\mathcal{O}(h^5)$)

Following similar procedure at the last node of the boundary will give following boundary equation at x_N with fifth order accuracy

$$14\phi'(x_N) + 16\phi'(x_{N-1}) - 2h\phi''(x_N) + 4h\phi''(x_{N-1}) - \frac{1}{h}(31\phi(x_N) - 32\phi(x_{N-1}) + \phi(x_{N-2})) = 0 \quad (\text{C.7})$$

C.3 Conclusions and Scope

In order to maintain higher order accuracy of the solution at the boundary, it is important to develop one sided boundary equations at the first and last grid point. In this section, we have developed fifth order accurate boundary equations for the combined compact difference scheme that has been used to solve the convection diffusion equation with higher order accuracy.

Appendix D

Solving a Twin-Tridiagonal Matrix

D.1 Solving Algorithm

Twin tridiagonal matrices usually arise when it is desired to calculate the first and second derivatives for higher order schemes developed from the higher order expansion of Taylor series. The resulting scheme consists of $2N$ simultaneous equations with an equal number of variables. It can be efficiently solved by a modified version of Thomas algorithm, which involves twin forward elimination of the entire matrix to transform the twin tridiagonal matrix into twin diagonal matrix until the last two rows of the matrix. These two rows correspond to the boundary node which gives two simultaneous equations with two unknowns and can be readily found by a linear solver. After that, these known values are substituted in reverse order to get the values of the unknowns at respective grid points. To demonstrate the calculation procedure, a test example consists of 5 node points which corresponds to 10 equations with 10 unknown variables is presented here. The augmented matrix is as follows

$$\begin{pmatrix}
b_1 & c_1 & 0 & 0 & 0 & B_1 & C_1 & 0 & 0 & 0 \\
e_1 & f_1 & 0 & 0 & 0 & E_1 & F_1 & 0 & 0 & 0 \\
a_2 & b_2 & c_2 & 0 & 0 & A_2 & B_2 & C_2 & 0 & 0 \\
d_2 & e_2 & f_2 & 0 & 0 & D_2 & E_2 & F_2 & 0 & 0 \\
0 & a_3 & b_3 & c_3 & 0 & 0 & A_3 & B_3 & C_3 & 0 \\
0 & d_3 & e_3 & f_3 & 0 & 0 & D_3 & E_3 & F_3 & 0 \\
0 & 0 & a_4 & b_4 & c_4 & 0 & 0 & A_4 & B_4 & C_4 \\
0 & 0 & d_4 & e_4 & f_4 & 0 & 0 & D_4 & E_4 & F_4 \\
0 & 0 & 0 & a_5 & b_5 & 0 & 0 & 0 & A_5 & B_5 \\
0 & 0 & 0 & d_5 & e_5 & 0 & 0 & 0 & D_5 & E_5
\end{pmatrix}
\begin{pmatrix}
x_1 \\
x_2 \\
x_3 \\
x_4 \\
x_5 \\
y_1 \\
y_2 \\
y_3 \\
y_4 \\
y_5
\end{pmatrix}
=
\begin{pmatrix}
s_1 \\
t_1 \\
s_2 \\
t_2 \\
s_3 \\
t_3 \\
s_4 \\
t_4 \\
s_5 \\
t_5
\end{pmatrix}
\tag{D.1}$$

Stage 1: Twin-forward Elimination

Step 1: Make first element of Row 1 unity

$$\text{Row 1 } b_1x_1 + c_1x_2 + B_1y_1 + C_1y_2 = s_1$$

$$\text{Rewrite } \psi_1x_1 + c_1x_2 + \xi_1y_1 + C_1y_2 = ss_1$$

For the first loop, write $\psi_1 = b_1, \quad \xi_1 = B_1, \quad ss_1 = s_1;$

Divide by ψ_1

$$x_1 + \frac{c_1}{\psi_1}x_2 + \frac{\xi_1}{\psi_1}y_1 + \frac{C_1}{\psi_1}y_2 = \frac{ss_1}{\psi_1}
\tag{D.2}$$

Rewrite, $x_1 + \alpha_1x_2 + \beta_1y_1 + \gamma_1y_2 = \rho_1$

Where, $\alpha_1 = \frac{c_1}{\psi_1}$, $\rho_1 = \frac{ss_1}{\psi_1}$, $\beta_1 = \frac{\xi_1}{\psi_1}$, $\gamma_1 = \frac{C_1}{\psi_1}$,

$$\begin{pmatrix} 1 & \alpha_1 & 0 & 0 & 0 & \beta_1 & \gamma_1 & 0 & 0 & 0 \\ e_1 & f_1 & 0 & 0 & 0 & E_1 & F_1 & 0 & 0 & 0 \\ a_2 & b_2 & c_2 & 0 & 0 & A_2 & B_2 & C_2 & 0 & 0 \\ d_2 & e_2 & f_2 & 0 & 0 & D_2 & E_2 & F_2 & 0 & 0 \\ 0 & a_3 & b_3 & c_3 & 0 & 0 & A_3 & B_3 & C_3 & 0 \\ 0 & d_3 & e_3 & f_3 & 0 & 0 & D_3 & E_3 & F_3 & 0 \\ 0 & 0 & a_4 & b_4 & c_4 & 0 & 0 & A_4 & B_4 & C_4 \\ 0 & 0 & d_4 & e_4 & f_4 & 0 & 0 & D_4 & E_4 & F_4 \\ 0 & 0 & 0 & a_5 & b_5 & 0 & 0 & 0 & A_5 & B_5 \\ 0 & 0 & 0 & d_5 & e_5 & 0 & 0 & 0 & D_5 & E_5 \end{pmatrix} \begin{pmatrix} x_1 \\ x_2 \\ x_3 \\ x_4 \\ x_5 \\ y_1 \\ y_2 \\ y_3 \\ y_4 \\ y_5 \end{pmatrix} = \begin{pmatrix} \rho_1 \\ t_1 \\ s_2 \\ t_2 \\ s_3 \\ t_3 \\ s_4 \\ t_4 \\ s_5 \\ t_5 \end{pmatrix} \quad (\text{D.3})$$

Step 2: Use Row 1 to eliminate all first elements from rows 2, 3 and 4

Row 2: $e_1x_1 + f_1x_2 + E_1y_1 + F_1y_2 = t_1$

For the first loop, write $\nu_1 = e_1$, $\chi_1 = E_1$, $tt_1 = t_1$;

$$\nu_1x_1 + f_1x_2 + \chi_1y_1 + F_1y_2 = tt_1 \quad (\text{D.4})$$

Use ν_1 times row 1 to eliminate first term of above equation,

Row 2	$\nu_1x_1 + f_1x_2 + \chi_1y_1 + F_1y_2 = tt_1$
$\nu_1 \times$ Row 1	$\nu_1x_1 + \nu_1\alpha_1x_2 + \nu_1\beta_1y_1 + \nu_1\gamma_1y_2 = \nu_1\rho_1$
New Row 2	$(f_1 - e_1\alpha_1)x_2 + (\chi_1 - \nu_1\beta_1)y_1 + (F_1 - \nu_1\gamma_1)y_2 = tt_1 - \nu_1\rho_1$

Rewrite, $\pi_1x_2 + \sigma_1y_1 + \theta_1y_2 = \Delta_1$

Where, $\pi_1 = f_1 - \nu_1\alpha_1$, $\sigma_1 = \chi_1 - \nu_1\beta_1$, $\theta_1 = F_1 - \nu_1\gamma_1$, $\Delta_1 = tt_1 - \nu_1\rho_1$

Row 3: $a_2x_1 + b_2x_2 + c_2x_3 + A_2y_1 + B_2y_2 + C_2y_3 = s_2$

Use a_2 times row 1 to eliminate first term of above equation,

Row 3	$a_2x_1 + b_2x_2 + c_2x_3 +$	$A_2y_1 +$	$B_2y_2 + C_2y_3 = s_2$
$a_2 \times$ Row 1	$a_2x_1 + a_2\alpha_1x_2 +$	$a_2\beta_1y_1 +$	$a_2\gamma_1y_2 = a_2\rho_1$
New Row 3	$(b_2 - a_2\alpha_1)x_2 + c_2x_3 +$	$(A_2 - a_2\beta_1)y_1 + (B_2 - a_2\gamma_1)y_2 + C_2y_3 =$	$s_2 - a_2\rho_1$

Rewrite, $\Delta_1x_2 + c_2x_3 + \lambda_1y_1 + \zeta_1y_2 + C_2y_3 = S_1$

Where, $\Delta_1 = b_2 - a_2\alpha_1$, $\lambda_1 = A_2 - a_2\beta_1$, $\zeta_1 = B_2 - a_2\gamma_1$, $S_1 = s_2 - a_2\rho_1$

Row 4: $d_2x_1 + e_2x_2 + f_2x_3 + D_2y_1 + E_2y_2 + F_2y_3 = t_2$

Use d_2 times row 1 to eliminate first term of the above equation,

Row 3	$d_2x_1 + e_2x_2 + f_2x_3 +$	$D_2y_1 +$	$E_2y_2 + F_2y_3 = t_2$
$d_2 \times$ Row 1	$d_2x_1 + d_2\alpha_1x_2 +$	$d_2\beta_1y_1 +$	$d_2\gamma_1y_2 = d_2\rho_1$
New Row 3	$(e_2 - d_2\alpha_1)x_2 + f_2x_3 + (D_2 - d_2\beta_1)y_1 + (E_2 - d_2\gamma_1)y_2 + F_2y_3 =$	$t_2 - d_2\rho_1$	

Rewrite, $\mu_1x_2 + f_2x_3 + \phi_1y_1 + \omega_1y_2 + F_2y_3 = T_1$

Where, $\mu_1 = e_2 - d_2\alpha_1$, $\phi_1 = D_2 - d_2\beta_1$, $\omega_1 = E_2 - d_2\gamma_1$, $T_1 = t_2 - d_2\rho_1$

$$\begin{pmatrix} 1 & \alpha_1 & 0 & 0 & 0 & \beta_1 & \gamma_1 & 0 & 0 & 0 \\ 0 & \pi_1 & 0 & 0 & 0 & \sigma_1 & \theta_1 & 0 & 0 & 0 \\ 0 & \Delta_1 & c_2 & 0 & 0 & \lambda_1 & \zeta_1 & C_2 & 0 & 0 \\ 0 & \mu_1 & f_2 & 0 & 0 & \phi_1 & \omega_1 & F_2 & 0 & 0 \\ 0 & a_3 & b_3 & c_3 & 0 & 0 & A_3 & B_3 & C_3 & 0 \\ 0 & d_3 & e_3 & f_3 & 0 & 0 & D_3 & E_3 & F_3 & 0 \\ 0 & 0 & a_4 & b_4 & c_4 & 0 & 0 & A_4 & B_4 & C_4 \\ 0 & 0 & d_4 & e_4 & f_4 & 0 & 0 & D_4 & E_4 & F_4 \\ 0 & 0 & 0 & a_5 & b_5 & 0 & 0 & 0 & A_5 & B_5 \\ 0 & 0 & 0 & d_5 & e_5 & 0 & 0 & 0 & D_5 & E_5 \end{pmatrix} \begin{pmatrix} x_1 \\ x_2 \\ x_3 \\ x_4 \\ x_5 \\ y_1 \\ y_2 \\ y_3 \\ y_4 \\ y_5 \end{pmatrix} = \begin{pmatrix} \rho_1 \\ \Delta_1 \\ S_1 \\ T_1 \\ s_3 \\ t_3 \\ s_4 \\ t_4 \\ s_5 \\ t_5 \end{pmatrix} \quad (\text{D.5})$$

Step 3: Make the third element of Row 2 unity (first element associated with y)

Row 2: $\pi_1x_2 + \sigma_1y_1 + \theta_1y_2 = \Delta_1$

Divide by σ_1

$$\frac{\pi_1}{\sigma_1}x_2 + y_1 + \frac{\theta_1}{\sigma_1}y_2 = \frac{\Delta_1}{\sigma_1} \quad (\text{D.6})$$

Rewrite, $\epsilon_1 x_2 + y_1 + \eta_1 y_2 = \tau_1$,

Where, $\epsilon_1 = \frac{\pi_1}{\sigma_1}$, $\eta_1 = \frac{\theta_1}{\sigma_1}$, $\tau_1 = \frac{\Delta_1}{\sigma_1}$

$$\begin{pmatrix} 1 & \alpha_1 & 0 & 0 & 0 & \beta_1 & \gamma_1 & 0 & 0 & 0 \\ 0 & \epsilon_1 & 0 & 0 & 0 & 1 & \eta_1 & 0 & 0 & 0 \\ 0 & \Delta_1 & c_2 & 0 & 0 & \lambda_1 & \zeta_1 & C_2 & 0 & 0 \\ 0 & \mu_1 & f_2 & 0 & 0 & \phi_1 & \omega_1 & F_2 & 0 & 0 \\ 0 & a_3 & b_3 & c_3 & 0 & 0 & A_3 & B_3 & C_3 & 0 \\ 0 & d_3 & e_3 & f_3 & 0 & 0 & D_3 & E_3 & F_3 & 0 \\ 0 & 0 & a_4 & b_4 & c_4 & 0 & 0 & A_4 & B_4 & C_4 \\ 0 & 0 & d_4 & e_4 & f_4 & 0 & 0 & D_4 & E_4 & F_4 \\ 0 & 0 & 0 & a_5 & b_5 & 0 & 0 & 0 & A_5 & B_5 \\ 0 & 0 & 0 & d_5 & e_5 & 0 & 0 & 0 & D_5 & E_5 \end{pmatrix} \begin{pmatrix} x_1 \\ x_2 \\ x_3 \\ x_4 \\ x_5 \\ y_1 \\ y_2 \\ y_3 \\ y_4 \\ y_5 \end{pmatrix} = \begin{pmatrix} \rho_1 \\ \tau_1 \\ S_1 \\ T_1 \\ s_3 \\ t_3 \\ s_4 \\ t_4 \\ s_5 \\ t_5 \end{pmatrix} \quad (\text{D.7})$$

Step 4: Use Row 2 to eliminate all first elements associated with y from rows 3 and 4

Row 3: $\Delta_1 x_2 + c_2 x_3 + \lambda_1 y_1 + \zeta_1 y_2 + C_2 y_3 = S_1$

Use λ_1 times row 2 to eliminate the term associated with y_1 of the above equation,

Row 3	$\Delta_1 x_2 + c_2 x_3 + \lambda_1 y_1 + \zeta_1 y_2 + C_2 y_3 = S_1$
$\lambda_1 \times \text{Row 2}$	$\lambda_1 \epsilon_1 x_2 + \lambda_1 y_1 + \lambda_1 \eta_1 y_2 = \lambda_1 \tau_1$
New Row 3	$(\Delta_1 - \lambda_1 \epsilon_1) x_2 + c_2 x_3 + (\zeta_1 - \lambda_1 \eta_1) y_2 + C_2 y_3 = S_1 - \lambda_1 \tau_1$

Rewrite, $\psi_2 x_2 + c_2 x_3 + \xi_2 y_2 + C_2 y_3 = s s_2$

$$\psi_2 = \Delta_1 - \lambda_1 \epsilon_1, \quad \xi_2 = \zeta_1 - \lambda_1 \eta_1, \quad s s_2 = S_1 - \lambda_1 \tau_1 \quad (\text{D.8})$$

Row 4: $\mu_1 x_2 + f_2 x_3 + \phi_1 y_1 + \omega_1 y_2 + F_2 y_3 = T_1$

Use ϕ_1 times row 2 to eliminate the term associated with y_1 of the above equation,

Row 4	$\mu_1 x_2 + f_2 x_3 + \phi_1 y_1 +$	$\omega_1 y_2 + F_2 y_3 = T_1$
$\phi_1 \times$ Row 2	$\phi_1 \epsilon_1 x_2 + \phi_1 y_1 + \phi_1 \eta_1 y_2$	$= \phi_1 \tau_1$
New Row 3	$(\mu_1 - \phi_1 \epsilon_1) x_2 + f_2 x_3 +$	$(\omega_1 - \phi_1 \eta_1) y_2 + F_2 y_3 = T - \phi_1 \tau_1$

Rewrite, $\nu_2 x_2 + c_2 x_3 + \chi_2 y_2 + F_2 y_3 = tt_2$

Where, $\nu_2 = \mu_1 - \phi_1 \epsilon_1$, $\chi_2 = \omega_1 - \phi_1 \eta_1$, $tt_2 = T_1 - \phi_1 \tau_1$

$$\begin{pmatrix} 1 & \alpha_1 & 0 & 0 & 0 & \beta_1 & \gamma_1 & 0 & 0 & 0 \\ 0 & \epsilon_1 & 0 & 0 & 0 & 1 & \eta_1 & 0 & 0 & 0 \\ 0 & \psi_2 & c_2 & 0 & 0 & 0 & \xi_2 & C_2 & 0 & 0 \\ 0 & \nu_2 & f_2 & 0 & 0 & 0 & \chi_2 & F_2 & 0 & 0 \\ 0 & a_3 & b_3 & c_3 & 0 & 0 & A_3 & B_3 & C_3 & 0 \\ 0 & d_3 & e_3 & f_3 & 0 & 0 & D_3 & E_3 & F_3 & 0 \\ 0 & 0 & a_4 & b_4 & c_4 & 0 & 0 & A_4 & B_4 & C_4 \\ 0 & 0 & d_4 & e_4 & f_4 & 0 & 0 & D_4 & E_4 & F_4 \\ 0 & 0 & 0 & a_5 & b_5 & 0 & 0 & 0 & A_5 & B_5 \\ 0 & 0 & 0 & d_5 & e_5 & 0 & 0 & 0 & D_5 & E_5 \end{pmatrix} \begin{pmatrix} x_1 \\ x_2 \\ x_3 \\ x_4 \\ x_5 \\ y_1 \\ y_2 \\ y_3 \\ y_4 \\ y_5 \end{pmatrix} = \begin{pmatrix} \rho_1 \\ \tau_1 \\ ss_2 \\ tt_2 \\ s_3 \\ t_3 \\ s_4 \\ t_4 \\ s_5 \\ t_5 \end{pmatrix} \quad (\text{D.9})$$

Step 1: Make the first element of Row 3 to unity

Row 3: $\psi_2 x_2 + c_2 x_3 + \xi_2 y_2 + C_2 y_3 = ss_2$

Divide by ψ_2

$$x_2 + \frac{c_2}{\psi_2} x_3 + \frac{\xi_2}{\psi_2} y_2 + \frac{C_2}{\psi_2} y_3 = \frac{ss_2}{\psi_2} \quad (\text{D.10})$$

Rewrite $x_2 + \alpha_2 x_3 + \beta_2 y_2 + \gamma_2 y_3 = \rho_2$,

Where, $\alpha_2 = \frac{c_2}{\psi_2}$, $\rho_2 = \frac{ss_2}{\psi_2}$, $\beta_2 = \frac{\xi_2}{\psi_2}$, $\gamma_2 = \frac{C_2}{\psi_2}$

$$\begin{pmatrix} 1 & \alpha_1 & 0 & 0 & 0 & \beta_1 & \gamma_1 & 0 & 0 & 0 \\ 0 & \epsilon_1 & 0 & 0 & 0 & 1 & \eta_1 & 0 & 0 & 0 \\ 0 & 1 & \alpha_2 & 0 & 0 & 0 & \beta_2 & \gamma_2 & 0 & 0 \\ 0 & \nu_2 & f_2 & 0 & 0 & 0 & \chi_2 & F_2 & 0 & 0 \\ 0 & a_3 & b_3 & c_3 & 0 & 0 & A_3 & B_3 & C_3 & 0 \\ 0 & d_3 & e_3 & f_3 & 0 & 0 & D_3 & E_3 & F_3 & 0 \\ 0 & 0 & a_4 & b_4 & c_4 & 0 & 0 & A_4 & B_4 & C_4 \\ 0 & 0 & d_4 & e_4 & f_4 & 0 & 0 & D_4 & E_4 & F_4 \\ 0 & 0 & 0 & a_5 & b_5 & 0 & 0 & 0 & A_5 & B_5 \\ 0 & 0 & 0 & d_5 & e_5 & 0 & 0 & 0 & D_5 & E_5 \end{pmatrix} \begin{pmatrix} x_1 \\ x_2 \\ x_3 \\ x_4 \\ x_5 \\ y_1 \\ y_2 \\ y_3 \\ y_4 \\ y_5 \end{pmatrix} = \begin{pmatrix} \rho_1 \\ \tau_1 \\ \rho_2 \\ tt_2 \\ s_3 \\ t_3 \\ s_4 \\ t_4 \\ s_5 \\ t_5 \end{pmatrix} \quad (\text{D.11})$$

Step 2: Use Row 3 to eliminate all first elements from rows 4, 5 and 6

Row 4: $\nu_2 x_2 + c_2 x_3 + \chi_2 y_2 + C_2 y_3 = tt_2$

Use ν_2 times row 3 to eliminate term associated with x_2 of above equation,

Row 4	$\nu_2 x_2 +$	$f_2 x_3 +$	$\chi_2 y_2 +$	$F_2 y_3 = tt_2$
$\nu_2 \times$ Row 3	$\nu_2 x_2 +$	$\nu_2 \alpha_2 x_3 +$	$\nu_2 \beta_2 y_2 +$	$\nu_2 \gamma_2 y_3 = \nu_2 \rho_2$
New Row 4	$(f_2 - \nu_2 \alpha_2) x_3 + (\chi_2 - \nu_2 \beta_2) y_2 + (F_2 - \nu_2 \gamma_2) y_3 = (tt_2 - \nu_2 \rho_2)$			

Rewrite, $\pi_2 x_3 + \sigma_2 y_2 + \theta_2 y_3 = \Delta_2$

Where, $\pi_2 = f_2 - \nu_2 \alpha_2$, $\sigma_2 = \chi_2 - \nu_2 \beta_2$, $\theta_2 = F_2 - \nu_2 \gamma_2$, $\Delta_2 = tt_2 - \nu_2 \rho_2$

Row 5: $a_3 x_2 + b_3 x_3 + c_3 x_4 + A_3 y_2 + B_3 y_3 + C_3 y_4 = s_3$

Use a_3 times row 1 to eliminate first term of above equation,

Row 5	$a_3 x_2 +$	$b_3 x_3 + c_3 x_4 +$	$A_3 y_2 +$	$B_3 y_3 + C_3 y_4 = s_3$
$a_3 \times$ Row 1	$a_3 x_2 +$	$a_3 \alpha_2 x_3 +$	$a_3 \beta_2 y_2 +$	$a_3 \gamma_2 y_3 = a_3 \rho_3$
New Row 3	$(b_2 - a_2 \alpha_1) x_3 + c_3 x_4 + (A_3 - a_3 \beta_2) y_2 + (B_3 - a_3 \gamma_2) y_3 + C_3 y_4 = s_3 - a_3 \rho_3$			

Rewrite, $\Delta_2 x_3 + c_3 x_4 + \lambda_2 y_2 + \zeta_2 y_3 + C_3 y_4 = S_2$

Where, $\Delta_2 = b_3 - a_3\alpha_2$, $\lambda_2 = A_3 - a_3\beta_2$, $\zeta_2 = B_3 - a_3\gamma_2$, $S_2 = s_3 - a_3\rho_3$

Row 6: $d_3x_2 + e_3x_3 + f_3x_4 + D_3y_2 + E_3y_3 + F_3y_4 = t_3$

Use d_3 times row 1 to eliminate first term of above equation,

Row 6	$d_3x_2 +$	$e_3x_3 + f_3x_4 +$	$D_3y_2 +$	$E_3y_3 + F_3y_4 = t_3$
$d_3 \times$ Row 3	$d_3x_2 +$	$d_3\alpha_2x_3 +$	$d_3\beta_2y_2 +$	$d_3\gamma_2y_3 = d_3\rho_3$
New Row 6	$(e_3 - d_3\alpha_2)x_3 + f_3x_4 + (D_3 - d_3\beta_2)y_2 + (E_3 - d_3\gamma_2)y_3 + F_3y_4 = t_3 - d_3\rho_3$			

Rewrite, $\mu_2x_3 + f_2x_4 + \phi_2y_2 + \omega_2y_3 + F_3y_4 = T_2$

Where, $\mu_2 = e_3 - d_3\alpha_2$, $\phi_2 = D_3 - d_3\beta_2$, $\omega_2 = E_3 - d_3\gamma_2$, $T_2 = t_3 - d_3\rho_3$

$$\begin{pmatrix} 1 & \alpha_1 & 0 & 0 & 0 & \beta_1 & \gamma_1 & 0 & 0 & 0 \\ 0 & \epsilon_1 & 0 & 0 & 0 & 1 & \eta_1 & 0 & 0 & 0 \\ 0 & 1 & \alpha_2 & 0 & 0 & 0 & \beta_2 & \gamma_2 & 0 & 0 \\ 0 & 0 & \pi_2 & 0 & 0 & 0 & \sigma_2 & \theta_2 & 0 & 0 \\ 0 & 0 & \Delta_2 & c_3 & 0 & 0 & \lambda_2 & \zeta_2 & C_3 & 0 \\ 0 & 0 & \mu_2 & f_3 & 0 & 0 & \phi_2 & \omega_2 & F_3 & 0 \\ 0 & 0 & a_4 & b_4 & c_4 & 0 & 0 & A_4 & B_4 & C_4 \\ 0 & 0 & d_4 & e_4 & f_4 & 0 & 0 & D_4 & E_4 & F_4 \\ 0 & 0 & 0 & a_5 & b_5 & 0 & 0 & 0 & A_5 & B_5 \\ 0 & 0 & 0 & d_5 & e_5 & 0 & 0 & 0 & D_5 & E_5 \end{pmatrix} \begin{pmatrix} x_1 \\ x_2 \\ x_3 \\ x_4 \\ x_5 \\ y_1 \\ y_2 \\ y_3 \\ y_4 \\ y_5 \end{pmatrix} = \begin{pmatrix} \rho_1 \\ \tau_1 \\ \rho_2 \\ \Delta_2 \\ S_2 \\ T_2 \\ s_4 \\ t_4 \\ s_5 \\ t_5 \end{pmatrix} \quad (\text{D.12})$$

Step 3: Make the third element of Row 2 to unity (first element associated with 'y')

Row 4: $\pi_2x_3 + \sigma_2y_2 + \theta_2y_3 = \Delta_2$

Divide by σ_2

$$\frac{\pi_2}{\sigma_2}x_3 + y_2 + \frac{\theta_2}{\sigma_2}y_3 = \frac{\Delta_2}{\sigma_2} \quad (\text{D.13})$$

Rewrite, $\epsilon_2x_3 + y_2 + \eta_2y_3 = \tau_2$,

Where, $\epsilon_2 = \frac{\pi_2}{\sigma_2}$, $\eta_2 = \frac{\theta_2}{\sigma_2}$, $\tau_2 = \frac{\Delta_2}{\pi_2}$

$$\begin{pmatrix} 1 & \alpha_1 & 0 & 0 & 0 & \beta_1 & \gamma_1 & 0 & 0 & 0 \\ 0 & \epsilon_1 & 0 & 0 & 0 & 1 & \eta_1 & 0 & 0 & 0 \\ 0 & 1 & \alpha_2 & 0 & 0 & 0 & \beta_2 & \gamma_2 & 0 & 0 \\ 0 & 0 & \epsilon_2 & 0 & 0 & 0 & 1 & \eta_2 & 0 & 0 \\ 0 & 0 & \Delta_2 & c_3 & 0 & 0 & \lambda_2 & \zeta_2 & C_3 & 0 \\ 0 & 0 & \mu_2 & f_3 & 0 & 0 & \phi_2 & \omega_2 & F_3 & 0 \\ 0 & 0 & a_4 & b_4 & c_4 & 0 & 0 & A_4 & B_4 & C_4 \\ 0 & 0 & d_4 & e_4 & f_4 & 0 & 0 & D_4 & E_4 & F_4 \\ 0 & 0 & 0 & a_5 & b_5 & 0 & 0 & 0 & A_5 & B_5 \\ 0 & 0 & 0 & d_5 & e_5 & 0 & 0 & 0 & D_5 & E_5 \end{pmatrix} \begin{pmatrix} x_1 \\ x_2 \\ x_3 \\ x_4 \\ x_5 \\ y_1 \\ y_2 \\ y_3 \\ y_4 \\ y_5 \end{pmatrix} = \begin{pmatrix} \rho_1 \\ \tau_1 \\ \rho_2 \\ \tau_2 \\ S_2 \\ T_2 \\ s_4 \\ t_4 \\ s_5 \\ t_5 \end{pmatrix} \quad (\text{D.14})$$

Step 4: Use Row 2 to eliminate all first elements associated with ‘y’ from row 5 and 6

$$\text{Row 5: } \Delta_2 x_3 + c_3 x_4 + \lambda_2 y_2 + \zeta_2 y_3 + C_3 y_4 = S_2$$

Use λ_2 times row 4 to eliminate term the associated with y_2 of the above equation,

Row 5	$\Delta_2 x_3 + c_3 x_4 + \lambda_2 y_2 +$	$\zeta_2 y_3 + C_3 y_4 = S_2$
$\lambda_2 \times \text{Row 4}$	$\lambda_2 \epsilon_2 x_3 +$	$\lambda_2 y_2 + \lambda_2 \eta_2 y_3 = \lambda_2 \tau_2$
New Row 3	$(\Delta_2 - \lambda_2 \epsilon_2) x_3 + c_3 x_4 +$	$(\zeta_2 - \lambda_2 \eta_2) y_3 + C_3 y_4 = S_2 - \lambda_2 \tau_2$

Rewrite, $\psi_3 x_3 + c_3 x_4 + \xi_3 y_3 + C_3 y_4 = s s_3$

$$\psi_3 = \Delta_2 - \lambda_2 \epsilon_2, \quad \xi_3 = \zeta_2 - \lambda_2 \eta_2, \quad s s_3 = S_2 - \lambda_2 \tau_2 \quad (\text{D.15})$$

$$\text{Row 6: } \mu_2 x_3 + f_3 x_4 + \phi_2 y_2 + \omega_2 y_3 + F_3 y_4 = T_2$$

Use ϕ_2 times row 2 to eliminate the term associated with y_1 of the above equation,

Row 4	$\mu_2 x_3 + f_3 x_4 + \phi_2 y_2 +$	$\omega_2 y_3 + F_3 y_4 = T_2$
$\phi_2 \times$ Row 2	$\phi_2 \epsilon_2 x_3 + \quad \phi_2 y_2 + \quad \phi_2 \eta_2 y_3$	$= \phi_2 \tau_2$
New Row 3	$(\mu_2 - \phi_2 \epsilon_2) x_3 + f_3 x_3 +$	$(\omega_2 - \phi_2 \eta_2) y_3 + F_3 y_4 = T_2 - \phi_2 \tau_2$

Rewrite, $\nu_3 x_3 + c_3 x_4 + \chi_3 y_3 + F_3 y_4 = tt_3$

Where, $\nu_3 = \mu_2 - \phi_2 \epsilon_2$, $\chi_3 = \omega_2 - \phi_2 \eta_2$, $tt_3 = T_2 - \phi_2 \tau_2$

$$\begin{pmatrix} 1 & \alpha_1 & 0 & 0 & 0 & \beta_1 & \gamma_1 & 0 & 0 & 0 \\ 0 & \epsilon_1 & 0 & 0 & 0 & 1 & \eta_1 & 0 & 0 & 0 \\ 0 & 1 & \alpha_2 & 0 & 0 & 0 & \beta_2 & \gamma_2 & 0 & 0 \\ 0 & 0 & \epsilon_2 & 0 & 0 & 0 & 1 & \eta_2 & 0 & 0 \\ 0 & 0 & \psi_3 & c_3 & 0 & 0 & 0 & \xi_3 & C_3 & 0 \\ 0 & 0 & \nu_3 & f_3 & 0 & 0 & 0 & \chi_3 & F_3 & 0 \\ 0 & 0 & a_4 & b_4 & c_4 & 0 & 0 & A_4 & B_4 & C_4 \\ 0 & 0 & d_4 & e_4 & f_4 & 0 & 0 & D_4 & E_4 & F_4 \\ 0 & 0 & 0 & a_5 & b_5 & 0 & 0 & 0 & A_5 & B_5 \\ 0 & 0 & 0 & d_5 & e_5 & 0 & 0 & 0 & D_5 & E_5 \end{pmatrix} \begin{pmatrix} x_1 \\ x_2 \\ x_3 \\ x_4 \\ x_5 \\ y_1 \\ y_2 \\ y_3 \\ y_4 \\ y_5 \end{pmatrix} = \begin{pmatrix} \rho_1 \\ \tau_1 \\ \rho_2 \\ \tau_2 \\ ss_3 \\ tt_3 \\ s_4 \\ t_4 \\ s_5 \\ t_5 \end{pmatrix} \quad (\text{D.16})$$

$$\begin{pmatrix}
1 & \alpha_1 & 0 & 0 & 0 & \beta_1 & \gamma_1 & 0 & 0 & 0 \\
0 & \epsilon_1 & 0 & 0 & 0 & 1 & \eta_1 & 0 & 0 & 0 \\
0 & 1 & \alpha_2 & 0 & 0 & 0 & \beta_2 & \gamma_2 & 0 & 0 \\
0 & 0 & \epsilon_2 & 0 & 0 & 0 & 1 & \eta_2 & 0 & 0 \\
0 & 0 & 1 & \alpha_3 & 0 & 0 & 0 & \beta_3 & \gamma_3 & 0 \\
0 & 0 & 0 & \epsilon_3 & 0 & 0 & 0 & 1 & \eta_3 & 0 \\
0 & 0 & 0 & \psi_4 & c_4 & 0 & 0 & 0 & \xi_4 & C_4 \\
0 & 0 & 0 & \nu_4 & f_4 & 0 & 0 & 0 & \chi_4 & F_4 \\
0 & 0 & 0 & a_5 & b_5 & 0 & 0 & 0 & A_5 & B_5 \\
0 & 0 & 0 & d_5 & e_5 & 0 & 0 & 0 & D_5 & E_5
\end{pmatrix}
\begin{pmatrix}
x_1 \\
x_2 \\
x_3 \\
x_4 \\
x_5 \\
y_1 \\
y_2 \\
y_3 \\
y_4 \\
y_5
\end{pmatrix}
=
\begin{pmatrix}
\rho_1 \\
\tau_1 \\
\rho_2 \\
\tau_2 \\
\rho_3 \\
\tau_3 \\
ss_4 \\
tt_4 \\
s_5 \\
t_5
\end{pmatrix}
\tag{D.17}$$

And again.....

$$\begin{pmatrix}
1 & \alpha_1 & 0 & 0 & 0 & \beta_1 & \gamma_1 & 0 & 0 & 0 \\
0 & \epsilon_1 & 0 & 0 & 0 & 1 & \eta_1 & 0 & 0 & 0 \\
0 & 1 & \alpha_2 & 0 & 0 & 0 & \beta_2 & \gamma_2 & 0 & 0 \\
0 & 0 & \epsilon_2 & 0 & 0 & 0 & 1 & \eta_2 & 0 & 0 \\
0 & 0 & 1 & \alpha_3 & 0 & 0 & 0 & \beta_3 & \gamma_3 & 0 \\
0 & 0 & 0 & \epsilon_3 & 0 & 0 & 0 & 1 & \eta_3 & 0 \\
0 & 0 & 0 & 1 & \alpha_4 & 0 & 0 & 0 & \beta_4 & \gamma_4 \\
0 & 0 & 0 & 0 & \epsilon_4 & 0 & 0 & 0 & 1 & \eta_4 \\
0 & 0 & 0 & 0 & \psi_5 & 0 & 0 & 0 & 0 & \xi_5 \\
0 & 0 & 0 & 0 & \nu_5 & 0 & 0 & 0 & 0 & \chi_5
\end{pmatrix}
\begin{pmatrix}
x_1 \\
x_2 \\
x_3 \\
x_4 \\
x_5 \\
y_1 \\
y_2 \\
y_3 \\
y_4 \\
y_5
\end{pmatrix}
=
\begin{pmatrix}
\rho_1 \\
\tau_1 \\
\rho_2 \\
\tau_2 \\
\rho_3 \\
\tau_3 \\
\rho_4 \\
\tau_4 \\
ss_5 \\
tt_5
\end{pmatrix}
\tag{D.18}$$

This process continues until last two rows are partially calculated. This is done by

stopping the loop before it starts manipulating the coefficients associated with next level values, i.e. Δ , λ , θ , and Δ (notice the break command in the code). After that we end up with following two equations-

$$\text{Row 9 and 10: } \psi_5 x_5 + \xi_5 y_5 = ss_5$$

$$\nu_5 x_5 + \chi_5 y_5 = tt_5 \tag{D.19}$$

This system of linear equation can be solved by “*linsolve*” function in MATLAB or by elementary algebra to obtain the values of x_5 and y_5

Stage 2: Back Substitution:

Use the obtained values of x_5 and y_5 reversely to obtain x_4, x_3, x_2, x_1 and y_4, y_3, y_2, y_1

$$\text{Row 8: } \epsilon_4 x_5 + y_4 + \eta_4 y_5 = \tau_4$$

$$\text{Gives, } y_4 = \tau_4 - \epsilon_4 x_5 - \eta_4 y_5$$

$$\text{Row 7: } x_4 + \alpha_4 x_5 + \beta_4 y_4 + \gamma_4 y_5 = \rho_4$$

$$\text{Gives, } x_4 = \rho_4 - (\alpha_4 x_5 + \beta_4 y_4 + \gamma_4 y_5)$$

Repeat.....

$$\text{Row 6: } \epsilon_3 x_4 + y_3 + \eta_3 y_4 = \tau_3$$

$$\text{Gives, } y_3 = \tau_3 - \epsilon_3 x_4 - \eta_3 y_4$$

$$\text{Row 5: } x_3 + \alpha_3 x_4 + \beta_3 y_3 + \gamma_3 y_4 = \rho_3$$

$$\text{Gives, } x_3 = \rho_3 - (\alpha_3 x_4 + \beta_3 y_3 + \gamma_3 y_4)$$

Repeat.....

$$\text{Row 4: } \epsilon_2 x_3 + y_2 + \eta_2 y_3 = \tau_2$$

$$\text{Gives, } y_2 = \tau_2 - \epsilon_2 x_3 - \eta_2 y_3$$

$$\text{Row 3: } x_2 + \alpha_2 x_3 + \beta_2 y_2 + \gamma_2 y_3 = \rho_2$$

$$\text{Gives, } x_2 = \rho_2 - (\alpha_2 x_3 + \beta_2 y_2 + \gamma_2 y_3)$$

Repeat.....

$$\text{Row 2: } \epsilon_1 x_2 + y_1 + \eta_1 y_2 = \tau_1$$

$$\text{Gives, } y_1 = \tau_1 - \epsilon_1 x_2 - \eta_1 y_2$$

$$\text{Row 1: } x_1 + \alpha_1 x_2 + \beta_1 y_1 + \gamma_1 y_2 = \rho_1$$

$$\text{Gives, } x_1 = \rho_1 - (\alpha_1 x_2 + \beta_1 y_1 + \gamma_1 y_2)$$

D.2 Conclusions and Scope

The twin tridiagonal matrix is a special type of sparse matrix where the elements are mostly in the diagonal indices. Solving such systems by a linear solver is inefficient as many arithmetic operations are redundant. Hence an algorithm is required which will involve operations only on non-zero elements. In this work this is achieved by twin forward elimination and twin back substitution. The performance of the algorithm can be observed by solving system of twin tridiagonal matrix by this algorithm and linear solver such as Gaussian elimination. Finally this algorithm can be extended to triple tridiagonal matrix system by following the same procedure where one can efficiently solve for $3N$ variables from $3N$ simultaneous equation.

Appendix E

A Twin Tridiagonal Matrix Solver in MATLAB

E.1 Main Program

The following program solves a twin-tridiagonal matrix efficiently using an algorithm based on Thomas algorithm. The functionality of the solver can be extended to solve a triple tridiagonal matrix. A triple tridiagonal matrix is required to solve in the CCD method to obtain solution for second derivative, first derivative and the variable simultaneously from a system of equations.

```

% Solve 2n x 2n twin-tridiagonal system for x and y: %
% %
%[ b(1) c(1) B(1) C(1) ][ x(1) ] [ s(1)]%
%[ e(1) f(1) E(1) F(1) ][ x(2) ] [ t(1)]%
%[ a(2) b(2) c(2) A(2) B(2) C(2) ][ x(3) ] [ s(2)]%
%[ d(2) e(2) f(2) D(2) E(2) F(2) ][ ... ] [ t(2)]%
%[ a(3) b(3) c(3) A(3) B(3) C(3) ][ ... ] [ ]%
%[ d(3) e(3) f(3) D(3) E(3) F(3) ][ x(n) ] [ ]%
%[ ... ... ... ... ][ y(1) ] = ... ]%
%[ ... ... ... ... ][ y(2) ] [ ... ]%
%[ ... ... ... ... ][ ... ] [ ]%
%[ ... ... ... ... ][ ... ] [ ]%
%[ a(n-1) b(n-1) c(n-1) A(n-1) B(n-1) C(n-1)][y(n-1)] [ s(n)]%
%[ d(n-1) e(n-1) f(n-1) D(n-1) E(n-1) F(n-1)][y(n-1)] [ s(n)]%
%[ a(n) b(n) A(n) B(n) ][ y(n) ] [ (n) ]%
%[ d(n) e(n) D(n) E(n) ][ y(n) ] [ (n) ]%

```

```
% f must be a vector (row or column) of length n %
% a, b, c, A, B, C, d, e, f, D, E, F must be vectors of length n (note that a(1) and c(n) are not used) %
%
%           Developed by %
%           Mohammad Mahmudur Rahman, %
%           Victoria University, %
%           Novermber 2015 %
```

```

function [x,y]=twin_tridiag(a,b,c,A,B,C,s, d,e,f,D,E,F,t,n)

% preallocation
alpha= zeros(n,1); beta = alpha; gamma = zeros(n,1); rho = zeros(n,1);
pi   = alpha;      sigma= alpha; theta = alpha;      Delta= alpha;
delta= alpha;      lamda= alpha; zita  = alpha;      S     = alpha;
mu    = alpha;     phi   = alpha; omega = alpha;     T     = alpha;
eps   = alpha;     eta   = alpha; tau    = alpha;
psi   = alpha;     Xi    = alpha; ss    = alpha;
nu    = alpha;     chi   = alpha; tt    = alpha;

% allocate initial values of the coefficeints
psi(1)= b(1);
Xi(1) = B(1);
ss(1) = s(1);

nu(1) = e(1);
chi(1)= E(1);
tt(1) = t(1);

for i=1:n;
% Calculate coefficients in first row-make first coefficient unity
alpha(i)= c(i) /psi(i);

```

```
beta(i) = Xi(i)/psi(i);
```

```
gamma(i)= C(i) /psi(i);
```

```
rho(i) = ss(i) /psi(i);
```

```
% eliminate first coefficients from second, third, and fourth row of
```

```
% first tridiagonal matrix
```

```
% Calculate coefficients in second row
```

```
pi(i) = f(i) -nu(i)*alpha(i);
```

```
sigma(i) = chi(i)-nu(i)*beta(i);
```

```
theta(i) = F(i) -nu(i)*gamma(i);
```

```
Delta(i) = tt(i) -nu(i)*rho(i);
```

```
if i==n
```

```
    break
```

```
end
```

```
% Calculate coefficients in third row
```

```
delta(i) = b(i+1)-a(i+1)*alpha(i);
```

```
lamda(i) = A(i+1)-a(i+1)*beta(i);
```

```
zita(i) = B(i+1)-a(i+1)*gamma(i);
```

```
S(i) = s(i+1)-a(i+1)*rho(i);
```

```
% Calculate coefficients in fourth row
```

```
mu(i) = e(i+1)-d(i+1)*alpha(i);
```

```
phi(i) = D(i+1)-d(i+1)*beta(i);
```

```

omega(i)= E(i+1)-d(i+1)*gamma(i);
T(i)      = t(i+1)-d(i+1)*rho(i);

% Calculate coefficients in second row-make second coefficient unity
eps(i) = pi(i)    /sigma(i);
eta(i) = theta(i)/sigma(i);
tau(i) = Delta(i)/sigma(i);

% Eliminate first coefficients from third and fourth row of second
% tridiagonal matrix

% Calculate coefficients in third row
psi(i+1)= delta(i)-eps(i)*lamda(i);
Xi(i+1)= zita(i) -eta(i)*lamda(i);
ss(i+1) = S(i)    -tau(i)*lamda(i);

% Calculate coefficients in fourth row
nu(i+1)= mu(i)    -eps(i)*phi(i);
chi(i+1)= omega(i)-eta(i)*phi(i);
tt(i+1) = T(i)    -tau(i)*phi(i);

end

xy=linsolve([psi(n),Xi(n);nu(n),chi(n)], [ss(n);tt(n)]);

```

```
x(n)=xy(1,1); y(n)=xy(2,1);
```

```
% Back substitution
```

```
for jk=n-1:-1:1;
```

```
    y(jk) = tau(jk)-eps(jk)*x(jk+1)-eta(jk)*y(jk+1);
```

```
    x(jk) = rho(jk)-beta(jk)*y(jk)-gamma(jk)*y(jk+1)-alpha(jk)*x(jk+1);
```

```
end
```

Appendix F

A MATLAB Script to Solve 3D Convection Diffusion Equation by CCD-ADI Method

F.1 Main Program

```
% This program is developed to solve the convection diffusion equation in
% three dimensional rectangular duct to find the scalar concentration
% distribution and the effective disperison rate due to non-uniform
% velocity in the duct.

clear all

clc

Lx = 1;      Ly = 0.01;   Lz = 0.01;   % channel geometry
dx = 0.01;   dy = 0.001; dz = 0.001; % space
u0 = 1;      q  = 0;      r  = 0;      % u0 is the centerline z-velocity
aa = 1e-5;   bb = 1e-5;   cc = 1e-5;   % diffusion coefficients, D in cm^2/s
rho= 1;      mu = 1e-5;   % Density and viscosity
```

```

T = 0.05; dt = 0.001; nt = T/dt; % Total time and time increment
Pe = u0*dx/aa % Cell Peclet number
Re = rho*Ly*u0/mu
gamma_x=aa*dt/dx^2; gamma_y=bb*dt/dy^2; gamma_z=cc*dt/dz^2;

% Spatial and Temporal mesh
x = 0:dx:Lx; y = 0:dy:Ly; z=0:dz:Lz;
nx = length(x); ny = length(y); nz=length(z);

% Calculate the fully developed velocity profile in x-y plane, the
% analytical expression has been documented in the thesis.
p = Velocity_profile(Ly,Lz,ny,nz,mu,u0);

% preallocation
C_old(nx,ny,nz) = 0; Cx_old(nx,ny,nz) = 0; Cxx_old(nx,ny,nz) = 0;
Cstar_y(nx,ny,nz) = 0; Cstar_yy(nx,ny,nz) = 0;
C2star_z(nx,ny,nz)= 0; C2star_zz(nx,ny,nz)= 0;
g(nx,ny,nz) = 0; gy(nx,ny,nz) = 0; gyy(nx,ny,nz) = 0;
hz(nx,ny,nz)= 0; hzz(nx,ny,nz)= 0;

% initial condition, at t=0;
% C_old(2:12,,:) = 1;
% for i=2:4,C_old(i,,:) = 1-(i-2)/2; end
for i=1:nx,
    if (x(i)>=0.1 && x(i)<=0.3),

```

```

        C_old(i, :, :) = exp(-500*(x(i)-0.2)^2);
    end;
end

% plot(x, area_average(C_old, Ly, Lz, dy, dz))
C2star=C_old; Cstar=C_old; C_new=C_old; C_in=C_old;

%(1)Compute u_y_0 and u_yy_0 for all x points using eq.(15)-(18)&(24)-(25)
% The equation numbers refere to the original CCD-ADI aritcle by Sun & Li

% call twin_tridiag function to calculate du/dy and d2u/dy2 at t=0;
for j=1:ny;
    for k=1:nz
        [a,b,c,A,B,C,s,d,e,f,D,E,F,t] = coefficients3D_x(C_old,dx,j,k,nx);
        [Cx_old(:,j,k),Cxx_old(:,j,k)]=twin_tridiag(a,b,c,A,B,C,s(:,j,k),...
                                                    d,e,f,D,E,F,t(:,j,k),nx);
    end
end

% Update
Cx_new=Cx_old; Cxx_new=Cxx_old;

%% (2) time marching
time=dt:dt:T;
for kk=1:nt
% plot result every time step

```

```

%      h=plot(x,area_average(C_new,Ly,Lz,dy,dz),'r','linewidth',2);
%      refreshdata(h); pause(0.001);
%% (a) compute the RHS of Eq (22) for all mesh points

%      step (i)- calculate gn(i,j,k), here r=0 hence no issue with index
for j=1:ny
    for k=1:nz
        g(1:nx,j,k) = C_new(1:nx,j,k) + dt*(aa*Cxx_new(1:nx,j,k)...
                                -p(j,k)*Cx_new(1:nx,j,k))/2;
    end
end

%      step (ii)- calculate dg/dy & d2g/dy2 using
[a,b,c,A,B,C,s,d,e,f,D,E,F,t] = coefficients3D_y(g,dy,1:nx,1:nz,ny);

%      call twin_tridiag function to calculate dg/dy & d2g/dy2
for i=1:nx
    for k=1:nz
        [gy(i,:,k),gyy(i,:,k)]=twin_tridiag(a,b,c,A,B,C,s(i,:,k),...
                                d,e,f,D,E,F,t(i,:,k),ny);
    end
end

%      step (i)- calculate hn(i,j,k), here q=0 hence no issue with index
h = g + dt*(bb*gyy-q*gy)/2;

```

```

% step (ii)- calculate hx and hxx

[a,b,c,A,B,C,s,d,e,f,D,E,F,t] = coefficients3D_z(h,dx,1:nx,1:ny,nz);
% call twin_tridiag function to calculate dg/dx & d2g/dx2
for i=1:nx
    for j=1:ny
        [hz(i,j,:),hzz(i,j,:)] = twin_tridiag(a,b,c,A,B,C,s(i,j,:),...
            d,e,f,D,E,F,t(i,j,:),nz);
    end
end
end
% step (iii)- calculate ff, here p = p(y,z) therefore need
% careful attention in indexing
ff = h + dt*(cc*hzz-r*hz)/2;

%% (d) solve for u** using ff(22)

zero = zeros(nx,ny,nz);
for i=1:nx
    for j=1:ny
        % get coefficients for incorporating into triple tridiagonal matrix
        % note that p (convection velocity) is a array cause p = p(y,z);
        % that's why the coefficients function inside the for loop unlike
        % other two in the following sections
        [ax,bx,cx,ay,by,cy,az,bz,cz,Dx,ex,fx,Dy,ey,fy,Dz,ez,fz,px,qx,rx,...
            py,qy,ry,pz,qz,rz] = coefficients_triple_Neumann4(dz,cc,r,dt,nz);
    end
end

```

```

[C2star(i,j,:),C2star_z(i,j,:),C2star_zz(i,j,:)] = ...
    triple_tridiag(ax,bx,cx,ay,by,cy,az,bz,cz,zero(i,j,:),...
    Dx,ex,fx,Dy,ey,fy,Dz,ez,fz,zero(i,j,:),...
    px,qx,rx,py,qy,ry,pz,qz,rz,ff(i,j,:),nz);

end

end

%% (e) solve for u* using u**
[ax,bx,cx,ay,by,cy,az,bz,cz,Dx,ex,fx,Dy,ey,fy,Dz,ez,fz,px,qx,rx,...
    py,qy,ry,pz,qz,rz] = coefficients_triple_Neumann4(dy,bb,q,dt,ny);

for i=1:nx
    for k=1:nz
        [Cstar(i,:,k),Cstar_y(i,:,k),Cstar_yy(i,:,k)] = ...
            triple_tridiag(ax,bx,cx,ay,by,cy,az,bz,cz,zero(i,:,k),...
            Dx,ex,fx,Dy,ey,fy,Dz,ez,fz,zero(i,:,k),px,qx,rx,...
            py,qy,ry,pz,qz,rz,C2star(i,:,k),ny);

        end
    end

end

%% (f) solve for u_new
for j=1:ny
    for k=1:nz

% get coefficients for incorporating into triple tridiagonal matrix

```

```

[ax,bx,cx,ay,by,cy,az,bz,cz,Dx,ex,fx,Dy,ey,fy,Dz,ez,fz,px,qx,rx,...
py,qy,ry,pz,qz,rz] =coefficients_triple_Neumann4(dx,aa,p(j,k),dt,nx-1);

[C_new(2:nx,j,k),Cx_new(2:nx,j,k),Cxx_new(2:nx,j,k)] =...
    triple_tridiag(ax,bx,...
    cx,ay,by,cy,az,bz,cz,zero(2:nx,j,k),...
    Dx,ex,fx,Dy,ey,fy,Dz,ez,fz,zero(2:nx,j,k),...
    px,qx,rx,py,qy,ry,pz,qz,rz,Cstar(2:nx,j,k),nx-1);

    end

end

Cnew_mean=area_average(C_new,Ly,Lz,dy,dz);
% plot(x,Cnew_mean)
% refreshdata
% pause(0.02)
%% update value in every time step

C_old   = C_new;
Cx_old  = Cx_new;
Cxx_old = Cxx_new;

% Record axial distribution of area averaged concentration at alocation
loc = (nx-1)/2; % Location of the sensor to record concentration
s=0;

for j=1:ny-1,

```

```

    for k=1:nz-1
        s=s+0.25*(C_new(loc,j,k)+C_new(loc,j+1,k)+C_new(loc,j,k+1)...
                +C_new(loc,j+1,k+1))*dy*dz/(Ly*Lz);
    end;
end;

Cend(kk)=s;

% plot result every timeteps
% plot(time,Cend,'b','linewidth',2);

timestep_remaining = nt-kk

end

plot(x,area_average(C_new,Ly,Lz,dy,dz),'b','linewidth',2);

% check with mass balance

totalci = sum(area_average(C_new,Ly,Lz,dy,dz))
totalc  = sum(area_average(C_in,Ly,Lz,dy,dz))

% Calculate Dispersion Coefficeint
D = dispersion_coeff(Cend,time, u0, Lx);

```

F.2 Function `area_average_rect.m`

```

function [ Cm ] = area_average_rect( C,Ly,Lz,dy,dz )

% This fucntion will calculate the area averaged quantity

```

```
% in three dimensional cartesian coordinate
```

```
N=size(C);  
nx=N(1); ny=N(2); nz=N(3);  
Cm(nx)=0;  
for i=1:nx  
    s=0;  
    for j=1:ny-1,  
        for k=1:nz-1  
            s=s+0.25*(C(i,j,k)+C(i,j+1,k)+C(i,j,k+1)...  
                    +C(i,j+1,k+1))*dy*dz/(Ly*Lz);  
        end  
    end  
    Cm(i)=s;  
end  
  
end
```

F.3 Function coefficients_triple.m

```
function [ax,bx,cx,ay,by,cy,az,bz,cz,dx,ex,fx,dy,ey,fy,dz,...  
        ez,fz,px,qx,rx,py,qy,ry,pz,qz,rz] = ...  
        coefficients_triple(h, diff_coeff, convect_vel, dt,n)
```

```

% This function is to calculate the coefficeints for the triple
% tridiagonal matrix at different nodes

% boundary condition at 1st node
ax(1)= 0;    bx(1)= 12/h;    cx(1)=-12/h;
ay(1)= 0;    by(1)= 6;      cy(1)= 6;
az(1)= 0;    bz(1)= h;      cz(1)= -h;

dx(1)= 0;    ex(1)= 1;      fx(1)= 0;
dy(1)= 0;    ey(1)= 0;      fy(1)= 0;
dz(1)= 0;    ez(1)= 0;      fz(1)= 0;

% boundary value of p,q,r are included in the governing equation

% interior nodes
ax(2:n-1)= 15/(16*h); bx(2:n-1)= 0;    cx(2:n-1)= -15/(16*h);
ay(2:n-1)= 7/16;      by(2:n-1)= 1;    cy(2:n-1)= 7/16;
az(2:n-1)= h/16;      bz(2:n-1)= 0;    cz(2:n-1)= -h/16;

dx(2:n-1)=-3/h^2;    ex(2:n-1)=6/h^2; fx(2:n-1)=-3/h^2;
dy(2:n-1)=-9/(8*h); ey(2:n-1)= 0;    fy(2:n-1)= 9/(8*h);
dz(2:n-1)=-1/8;     ez(2:n-1) = 1;    fz(2:n-1)=-1/8;

% this corresponds to the differential equation, here equation (19)

```

```
px(1:n)= 0;      qx(1:n)= 1;      rx(1:n)= 0;
py(1:n)= 0;      qy(1:n)= convect_vel*dt/2; ry(1:n)= 0;
pz(1:n)= 0;      qz(1:n)=-diff_coeff*dt/2;  rz(1:n) = 0;
```

```
% boundary condition at last node
```

```
ax(n)= -12/h; bx(n)=-12/h;  cx(n)= 0;
ay(n)= -6;   by(n)= -6;   cy(n)= 0;
az(n)= -h;   bz(n)=h;     cz(n)= 0;
```

```
% Dirichlet boundary, prescribed value at boundary
```

```
dx(n)= 0;      ex(n)= 1;      fx(n)= 0;
dy(n)= 0;      ey(n)= 0;      fy(n)= 0;
dz(n)= 0;      ez(n)= 0;      fz(n)= 0;
```

```
% boundary value of p,q,r are included in the governing equation
```

Appendix G

Dispersion of a Solute in a Square Conduit in Which the Flow is Turbulent

G.1 Background

It is well established that solutes being conveyed by turbulently flowing fluids in circular pipes disperse. The rate of dispersion mimics the Fickian law of diffusion. The value of the longitudinal dispersion coefficient depends on the Reynolds number and the diameter of the pipe.

We anticipate that fluids flowing in a square duct will also give rise to dispersion. Interestingly the magnitude of the dispersion coefficient decreases with increasing turbulent viscosity because concentration gradients normal to the direction of flow are reduced. It is hypothesized that secondary flows that occur in fluids that are

flowing turbulently in ducts may further reduce the rate of dispersion in square duct. In this appendix we elucidate an analytical approach to calculate the dispersion for turbulent flow through non-circular ducts.

G.2 Mathematical Formulation of Flow System

A mass balance on an element of domain in which fluid flows may be expressed as

$$\frac{\partial \mathcal{C}}{\partial t} + \frac{\partial(u_i \mathcal{C})}{\partial x_i} = \nabla(D_{eff} \nabla \mathcal{C}) \quad (\text{G.1})$$

Here

$$D_{eff} = \frac{\nu_t}{Sc} + D_m \quad (\text{G.2})$$

In the above equations, ν_t is the turbulent viscosity, D_m is the molecular diffusivity and Sc is an empirically determined Schmidt number. \mathcal{C} is the concentration of solute and u_i represents velocity in each spatial directions. Einstein summation convention applies to repeated indices.

If we expand the second term of equation (G.1) gives

$$\frac{\partial(u_i \mathcal{C})}{\partial x_i} = u_i \frac{\partial \mathcal{C}}{\partial x_i} + \mathcal{C} \frac{\partial u_i}{\partial x_i} \quad (\text{G.3})$$

However, by continuity we have

$$\frac{\partial u_i}{\partial x_i} = 0 \quad (\text{G.4})$$

Therefore above equation becomes

$$\frac{\partial(u_i \mathcal{C})}{\partial x_i} = u_i \frac{\partial \mathcal{C}}{\partial x_i} \quad (\text{G.5})$$

Equation (G.1) can be rewritten by expanding the gradient term in the right hand side and incorporating equation (G.5)

$$\frac{\partial \mathcal{C}}{\partial t} + u_i \frac{\partial \mathcal{C}}{\partial x_i} = \frac{\partial}{\partial x_i} (D_{eff} \frac{\partial \mathcal{C}}{\partial x_i}) \quad (\text{G.6})$$

In turbulent flow, the velocity and convection terms can be decomposed into the mean and fluctuating components as follows:

$$u_i = \bar{u}_i + u'_i; \quad \mathcal{C} = \bar{\mathcal{C}} + \mathcal{C}' \quad (\text{G.7})$$

Rewrite equation (G.6) incorporating the above values

$$\frac{\partial(\bar{\mathcal{C}} + \mathcal{C}')}{\partial t} + (\bar{u}_i + u'_i) \frac{\partial(\bar{\mathcal{C}} + \mathcal{C}')}{\partial x_i} = \frac{\partial}{\partial x_i} (D_{eff} \frac{\partial(\bar{\mathcal{C}} + \mathcal{C}')}{\partial x_i}) \quad (\text{G.8})$$

At this stage we shall express the terms with indices into all spatial directions for our convenience of analysis in upcoming steps

$$\begin{aligned} \frac{\partial(\bar{\mathcal{C}} + \mathcal{C}')}{\partial t} + (\bar{u}_1 + u'_1) \frac{\partial(\bar{\mathcal{C}} + \mathcal{C}')}{\partial x_1} + (\bar{u}_2 + u'_2) \frac{\partial(\bar{\mathcal{C}} + \mathcal{C}')}{\partial x_2} + (\bar{u}_3 + u'_3) \frac{\partial(\bar{\mathcal{C}} + \mathcal{C}')}{\partial x_3} = \\ \frac{\partial}{\partial x_1} (D_{eff} \frac{\partial(\bar{\mathcal{C}} + \mathcal{C}')}{\partial x_1}) + \frac{\partial}{\partial x_2} (D_{eff} \frac{\partial(\bar{\mathcal{C}} + \mathcal{C}')}{\partial x_2}) + \frac{\partial}{\partial x_3} (D_{eff} \frac{\partial(\bar{\mathcal{C}} + \mathcal{C}')}{\partial x_3}) \end{aligned} \quad (\text{G.9})$$

The analysis becomes somewhat simpler if we choose to work in a frame of reference that moves in the axial direction with the mean axial velocity, \bar{u}_1 of the flow. This was Taylor's strategy and it has been made a little more rigorous and

transparent by adapting the flowing coordinate transformations

$$\xi = x_1 - \bar{u}_1 t \quad (\text{G.10})$$

$$\tau = t \quad (\text{G.11})$$

$$y = x_2 \quad (\text{G.12})$$

$$z = x_3 \quad (\text{G.13})$$

By applying the chain rule to the derivatives,

$$\frac{\partial}{\partial x_1} = \frac{\partial}{\partial \xi} \frac{\partial \zeta}{\partial x_1} + \frac{\partial}{\partial \tau} \frac{\partial \tau}{\partial x_1} + \frac{\partial}{\partial y} \frac{\partial y}{\partial x_1} + \frac{\partial}{\partial z} \frac{\partial z}{\partial x_1} = \frac{\partial}{\partial \xi} \quad (\text{G.14})$$

$$\frac{\partial}{\partial x_2} = \frac{\partial}{\partial \xi} \frac{\partial \zeta}{\partial x_2} + \frac{\partial}{\partial \tau} \frac{\partial \tau}{\partial x_2} + \frac{\partial}{\partial y} \frac{\partial y}{\partial x_2} + \frac{\partial}{\partial z} \frac{\partial z}{\partial x_2} = \frac{\partial}{\partial y} \quad (\text{G.15})$$

$$\frac{\partial}{\partial x_3} = \frac{\partial}{\partial \xi} \frac{\partial \zeta}{\partial x_3} + \frac{\partial}{\partial \tau} \frac{\partial \tau}{\partial x_3} + \frac{\partial}{\partial y} \frac{\partial y}{\partial x_3} + \frac{\partial}{\partial z} \frac{\partial z}{\partial x_3} = \frac{\partial}{\partial z} \quad (\text{G.16})$$

$$\frac{\partial}{\partial t} = \frac{\partial}{\partial \xi} \frac{\partial \zeta}{\partial t} + \frac{\partial}{\partial \tau} \frac{\partial \tau}{\partial t} + \frac{\partial}{\partial y} \frac{\partial y}{\partial t} + \frac{\partial}{\partial z} \frac{\partial z}{\partial t} = \frac{\partial}{\partial \tau} - \bar{u}_1 \frac{\partial}{\partial \xi} \quad (\text{G.17})$$

Our task is to simplify equation (G.8) rewrite it in terms of the new coordinate system expressed by equations (G.10) - (G.13). Firstly we note that \bar{C} is a function of one spatial coordinate only ξ , because it is an area averaged concentration. Moreover,

empirical evidence obtained from studies on dispersion in circular pipes suggests that the term $\frac{\partial}{\partial x_1}(D_{eff}\frac{\partial(\bar{C}+C')}{\partial x_1})$ has negligible effect on the longitudinal dispersion and it will therefore not be considered at this stage. However, if it is regarded as being important it can be added to the overall dispersion calculated as a result of this analysis.

Hence equation (G.8) becomes

$$\begin{aligned} \frac{\partial(\bar{C}+C')}{\partial \tau} - \bar{u}_1 \frac{\partial(\bar{C}+C')}{\partial \xi} + (\bar{u}_1 + u'_1) \frac{\partial(\bar{C}+C')}{\partial \xi} \\ + (\bar{u}_2 + u'_2) \frac{\partial C'}{\partial y} + (\bar{u}_3 + u'_3) \frac{\partial C'}{\partial z} = \\ \frac{\partial}{\partial y}(D_{eff} \frac{\partial(\bar{C}+C')}{\partial y}) + \frac{\partial}{\partial z}(D_{eff} \frac{\partial(\bar{C}+C')}{\partial z}) \end{aligned} \quad (G.18)$$

With the benefit of six decades of hindsight we are now aware that the magnitude of axial dispersion is determined to a large extent by the rate at which concentrations in the direction normal to the flow are made more uniform. The rate at which this evening out of concentration happens depends on the magnitudes of variation of C from the mean, i.e. C' and the values of D_{eff} in the direction y and z . Bearing this in mind we seek an equation for C' . This is obtained by formally defining the area averaged value \bar{C}

$$\bar{C} = \frac{1}{L_y L_z} \int_0^y \int_0^z C dy dz \quad (G.19)$$

And we shall see that some the terms in equation (G.18) are eliminated. Take average in equation (G.7) for concentration

$$\bar{c} = \bar{\bar{c}} + \bar{c}' \quad (\text{G.20})$$

Where $\bar{\bar{c}}$ represents the average of an average, but since it is independent of y and z therefore

$$\bar{\bar{c}} = \frac{1}{L_y L_z} \int_0^y \int_0^z \bar{c} dy dz = \bar{c} \quad (\text{G.21})$$

Now, from equations (G.20) and (G.21)

$$\bar{c}' = 0 \quad (\text{G.22})$$

A similar argument is used to demonstrate that

$$\bar{u}' = 0 \quad (\text{G.23})$$

We may obtain the following expressions

$$\overline{\frac{\partial \bar{c}}{\partial \tau}} = \frac{1}{L_y L_z} \int_0^y \int_0^z \frac{\partial \bar{c}}{\partial \tau} dy dz \quad (\text{G.24})$$

Since τ is independent of y and z , therefore we can place the derivative outside the integral

$$\overline{\frac{\partial \bar{c}}{\partial \tau}} = \frac{1}{L_y L_z} \frac{\partial}{\partial \tau} \int_0^y \int_0^z \bar{c} dy dz = \frac{\partial \bar{c}}{\partial \tau} \quad (\text{G.25})$$

By use of a similar argument and equation (G.22) we obtain

$$\overline{\frac{\partial \bar{c}'}{\partial \tau}} = \frac{1}{L_y L_z} \frac{\partial}{\partial \tau} \int_0^y \int_0^z \bar{c}' dy dz = 0 \quad (\text{G.26})$$

Similarly

$$\overline{u'_1 \frac{\partial \bar{\mathcal{C}}}{\partial \xi}} = 0 \quad (\text{G.27})$$

$$\overline{\bar{\mathcal{C}} \frac{\partial u_1}{\partial \xi}} = 0 \quad (\text{G.28})$$

However, we note that

$$\overline{u'_1 \frac{\partial \mathcal{C}'}{\partial \xi}} = \frac{1}{L_y L_z} \frac{\partial}{\partial \xi} \int_0^y \int u'_1 \mathcal{C}' dy dz \neq 0 \quad (\text{G.29})$$

The reason for the result given by equation (G.29) is that both u'_1 and \mathcal{C}' are unknown function of y and z and therefore we can say little about therefore product.

Similarly we have

$$\overline{\mathcal{C}' \frac{\partial u'_1}{\partial \xi}} \neq 0 \quad (\text{G.30})$$

$$\overline{(\bar{u}_2 + u'_2) \frac{\partial \mathcal{C}'}{\partial y}} \neq 0 \quad (\text{G.31})$$

$$\overline{(\bar{u}_3 + u'_3) \frac{\partial \mathcal{C}'}{\partial z}} \neq 0 \quad (\text{G.32})$$

Furthermore,

$$\begin{aligned} \overline{\frac{\partial}{\partial y} \left(D \frac{\partial \mathcal{C}'}{\partial y} \right)} &= \frac{1}{L_y L_z} \int_0^Y \int_0^Z \frac{\partial}{\partial y} (D_{eff} \frac{\partial \mathcal{C}}{\partial y}) dy dz \\ &= \frac{1}{L_y L_z} \int_0^Z ((D \frac{\partial \mathcal{C}}{\partial y})|_Y - (D_{eff} \frac{\partial \mathcal{C}}{\partial y})|_0) dz \end{aligned} \quad (\text{G.33})$$

At the centre of the square conduit, because of symmetry

$$\left(\frac{\partial \mathcal{C}}{\partial y}\right)_0 = \left(\frac{\partial \bar{\mathcal{C}}}{\partial y}\right)_0 + \left(\frac{\partial \mathcal{C}'}{\partial y}\right)_0 = 0 \quad (\text{G.34})$$

Moreover, at the wall, there is also no mass flux, hence

$$\left(\frac{\partial \mathcal{C}}{\partial y}\right)_y = 0 \quad (\text{G.35})$$

Since $\bar{\mathcal{C}}$ is constant on plane normal to the flow, we therefore have

$$\overline{\frac{\partial}{\partial y} \left(D_{eff} \frac{\partial \mathcal{C}'}{\partial y} \right)} = 0 \quad (\text{G.36})$$

Similar reasoning leads to

$$\overline{\frac{\partial}{\partial z} \left(D_{eff} \frac{\partial \mathcal{C}'}{\partial z} \right)} = 0 \quad (\text{G.37})$$

Now equation (G.18) can be simplified by

$$\begin{aligned} \frac{\partial(\bar{\mathcal{C}} + \mathcal{C}')}{\partial \tau} + u'_1 \frac{\partial(\bar{\mathcal{C}} + \mathcal{C}')}{\partial \xi} + (\bar{u}_2 + u'_2) \frac{\partial \mathcal{C}'}{\partial y} + (\bar{u}_2 + u'_3) \frac{\partial \mathcal{C}'}{\partial z} = \\ \frac{\partial}{\partial y} (D_{eff} \frac{\partial \mathcal{C}'}{\partial y}) + \frac{\partial}{\partial z} (D_{eff} \frac{\partial \mathcal{C}'}{\partial z}) \end{aligned} \quad (\text{G.38})$$

Taking the area average of equation (G.38) results

$$\frac{\partial \bar{\mathcal{C}}}{\partial \tau} + \frac{\partial(u'_1 \mathcal{C}')}{\partial \xi} + \overline{(\bar{u}_2 + u'_2) \frac{\partial \mathcal{C}'}{\partial y}} + \overline{(\bar{u}_3 + u'_3) \frac{\partial \mathcal{C}'}{\partial z}} = 0 \quad (\text{G.39})$$

Subtracting equation (G.39) from equation (G.38) results

$$\begin{aligned} \frac{\partial \mathcal{C}'}{\partial \tau} + u'_1 \frac{\partial \bar{\mathcal{C}}}{\partial \xi} + u'_1 \frac{\partial \mathcal{C}'}{\partial \zeta} + (\bar{u}_2 + u'_2) \frac{\partial \mathcal{C}'}{\partial y} + (\bar{u}_3 + u'_3) \frac{\partial \mathcal{C}'}{\partial z} = \\ \frac{\partial}{\partial y} (D_{eff} \frac{\partial \mathcal{C}}{\partial y}) + \frac{\partial}{\partial z} (D_{eff} \frac{\partial \mathcal{C}'}{\partial z}) + \overline{(\bar{u}_2 + u'_2) \frac{\partial \mathcal{C}'}{\partial y}} + \overline{(\bar{u}_3 + u'_3) \frac{\partial \mathcal{C}'}{\partial z}} \end{aligned}$$

After a sufficiently long time we expect that the cross section concentration profile may exhibit the form of particular note that the concentration of the solute in a plane to the flow becomes almost uniform, hence

$$c' \ll \bar{c} \quad (\text{G.40})$$

and

$$u'_i \frac{\partial \mathcal{C}'}{\partial \xi} \ll u'_i \frac{\partial \bar{\mathcal{C}}}{\partial \zeta} \quad (\text{G.41})$$

Similarly

$$\frac{\partial (\overline{u'_i \mathcal{C}'})}{\partial \xi} \ll u'_i \frac{\partial \bar{\mathcal{C}}}{\partial \zeta} \quad (\text{G.42})$$

The dispersion of the solute never reaches a steady state - the further downstream a slug of solute is conveyed, the more it disperses. However empirical evidence suggests that after a sufficiently long time

$$\frac{\partial \mathcal{C}'}{\partial \tau} \ll u' \frac{\partial \bar{\mathcal{C}}}{\partial \xi} \quad (\text{G.43})$$

The transport equation for the solute may be ultimately expressed as

$$u_1' \frac{\partial \bar{\mathcal{C}}}{\partial \xi} + u_2 \frac{\partial \mathcal{C}'}{\partial y} + u_3 \frac{\partial \mathcal{C}'}{\partial z} = \frac{\partial}{\partial y} \left(D_{eff} \frac{\partial \mathcal{C}'}{\partial y} \right) + \frac{\partial}{\partial z} \left(D_{eff} \frac{\partial \mathcal{C}'}{\partial z} \right) + \overline{u_2 \mathcal{C}'} + \overline{u_3 \mathcal{C}'} \quad (\text{G.44})$$

This is the equation that governs \mathcal{C} and as intimated above, it is subjected to the flowing boundary condition

$$\frac{\partial \mathcal{C}'}{\partial y} = 0 \text{ at } y = 0 \text{ and } y = L_y \quad (\text{G.45})$$

$$\frac{\partial \mathcal{C}'}{\partial z} = 0 \text{ at } z = 0 \text{ and } z = L_z \quad (\text{G.46})$$

Now average mass flux q_m is given by

$$\begin{aligned} q_m &= \frac{1}{L_y L_z} \int_0^Y \int_0^Z u_1' (\bar{\mathcal{C}} + \mathcal{C}') dy dz \\ &= \frac{1}{L_y L_z} \int_0^Y \int_0^Z u_1' \mathcal{C}' dy dz \end{aligned} \quad (\text{G.47})$$

We realize this because $\overline{u_1' \bar{\mathcal{C}}} = 0$. If we can assume that an equation analogous to Fick's law of diffusion holds

$$q_m = -D_L \frac{\partial \bar{\mathcal{C}}}{\partial \xi} \quad (\text{G.48})$$

Hence,

$$D_L = -\frac{1}{L_y L_z} \frac{1}{\frac{\partial \bar{\mathcal{C}}}{\partial \xi}} \int_0^{L_y} \int_0^{L_y} u_1' \mathcal{C}' dy dz \quad (\text{G.49})$$

Where C' is obtained by numerically solving equation (G.44) for a fixed value of $\frac{\partial \bar{C}}{\partial \xi} = 1$

The dispersion coefficient of a passive scalar flowing through turbulent flow in a three-dimensional Cartesian coordinate can be evaluated from (G.49) by knowing the turbulent velocity profile in the duct. Also note that the source terms $u_2 \frac{\partial C'}{\partial y}$ and $u_3 \frac{\partial C'}{\partial z}$ are initially unknown hence they must be updated as the solution progresses.

G.3 Conclusion

The analytical procedure to calculate the dispersion coefficient for a solute flowing in turbulent flow through a non-circular duct has been outlined in this chapter. After the turbulent flow profile in the non-circular duct is obtained from simulation, the longitudinal dispersion coefficient can be calculated from the analytical expression derived in this appendix. The quantitative estimation of the magnitude of the influence of the secondary flows on the the dispersion coefficient in turbulent flow through non-circular ducts is a topic for future investigation.